IMPACT OF TURBINE MODULATION ON VARIABLE-CYCLE ENGINE PERFORMANCE. PHASE IV. ADDITIONAL HARDWARE DESIGN AND FABRICATION, ENGINE MODIFICATION, AND ALTITUDE TEST. PART IIIB

W. R. Davenport, et al

AiResearch Manufacturing Company of Arizona

Prepared for:

Air Force Aero Propulsion Laboratory

December 1974

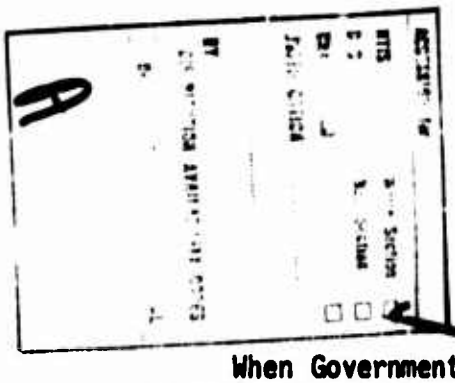

NOTICE

When Government drawings, specifications, or other data are used for any purpose other than in connection with a definitely related Government procurement operation, the United States Government thereby incurs no responsibility nor any obligation whatsoever; and the fact that the Government may have formulated, furnished, or in any way supplied the said drawings, specifications, or other data, is not to be regarded by implication or otherwise as in any manner licensing the holder or any other person or corporation, or conveying any rights or permission to manufacture, use, or sell any patented invention that may in any way be related thereto.

This final report was submitted by AiResearch Manufacturing Company of Arizona, under Contract F33615-71-C-1625. The effort was sponsored by the Air Force Aero Propulsion Laboratory, Air Force Systems Command, Wright-Patterson AFB, Ohio under Project 3066, Task 306606, and Work Unit 30660618 with Lt. Richard F. Topping, AFAPL/TBC, as Project Engineer. Mr. W. R. Davenport of AiResearch Manufacturing Company of Arizona was technically responsible for the work.

This report has been reviewed by the Information Office (ASD/OIP) and is releasable to the National Technical Information Service (NTIS). At NTIS, it will be available to the general public, including foreign nations.

This technical report has been reviewed and is approved for publication.

RICHARD F. TOPPING, 1/Lt, USAF
Project Engineer

FOR THE COMMANDER

JAMES L. RADLOFF, Major, USAF
Tech Area Manager, Turbines

Copies of this report should not be returned unless return is required by security considerations, contractual obligations, or notice on a specific document.

Unclassified

SECURITY CLASSIFICATION OF THIS PAGE (When Data Entered)

REPORT DOCUMENTATION PAGE		READ INSTRUCTIONS BEFORE COMPLETING FORM
1. REPORT NUMBER AFAPL-TR-74-109	2. GOVT ACCESSION NO.	3. RECIPIENT'S CATALOG NUMBER AD/A-000576
4. TITLE (and Subtitle) IMPACT OF TURBINE MODULATION ON VARIABLE-CYCLE-ENGINE PERFORMANCE		5. TYPE OF REPORT & PERIOD COVERED Tech. Report (Final) 17 May 71 - 31 Dec 74 6. PERFORMING ORG. REPORT NUMBER 73-210173
7. W.R. Davenport, G.J. Dixon, A. Fischer, K.R. Fledderjohn, J.R. Shearer, M.A. Steele, D.W. Stephenson, F. Weber		8. CONTRACT OR GRANT NUMBER(s) F33615-71-C-1625
9. PERFORMING ORGANIZATION NAME AND ADDRESS AiResearch Manufacturing Company of Arizona, 402 South 36th Street, Phoenix, Arizona 85034		10. PROGRAM ELEMENT, PROJECT, TASK AREA & WORK UNIT NUMBERS Proj. 3066 Task 306606 W. U. 30660618
11. CONTROLLING OFFICE NAME AND ADDRESS Air Force Aero Propulsion Laboratory Air Force Systems Command, Wright-Patterson Air Force Base, Ohio 45433		12. REPORT DATE December 1974 13. NUMBER OF PAGES 369
14. MONITORING AGENCY NAME & ADDRESS(if different from Controlling Office) Air Force Aero Propulsion Lab. (TBC) Wright-Patterson Air Force Base, Ohio 45433		15. SECURITY CLASS. (of this report) Unclassified 15a. DECLASSIFICATION/DOWNGRADING SCHEDULE

16. DISTRIBUTION STATEMENT (of this Report)

Approved for public release; distribution unlimited

17. DISTRIBUTION STATEMENT (of the abstract entered in Block 20, if different from Report)

18. SUPPLEMENTARY NOTES

Part I of this report documents the analysis, design, and rig tests conducted in Phases I and II. Part II reports the engine work and sea-level tests completed in Phase III. Parts IIIA and IIIB document the altitude tests conducted in Phase IV

19. KEY WORDS (Continue on reverse side if necessary and identify by block number)

Engine performance	Turbofan
Variable geometry	Turbine modulation
Variable-cycle engine	Variable turbine stator
Gas turbine	Installed engine performance

20. ABSTRACT (Continue on reverse side if necessary and identify by block number)

This program was conducted to determine the impact of variable geometry compressor, turbine, and exhaust-nozzle components on turbofan engine performance. An AiResearch Model TFE731-2 Turbofan Engine was modified to incorporate production-type variable-geometry hardware and tested to determine the effects of turbine modulation at both sea-level static and simulated high-altitude flight conditions at subsonic and supersonic flight Mach numbers. The program was conducted in four discrete phases which consisted of:

DD FORM 1 JAN 73 1473 EDITION OF 1 NOV 65 IS OBSOLETE

Unclassified

SECURITY CLASSIFICATION OF THIS PAGE (When Data Entered)

Phase I: Design of variable-geometry aerodynamic components and actuation mechanisms, and aerothermodynamic analyses of variable-cycle engine performance
Phase II: Fabrication or modification of hardware and rig testing of the low-pressure (LP) compressor and combustor
Phase III: Engine tests conducted at sea-level static conditions, over a range of variable-geometry settings with two different sizes of fixed fan and primary exhaust nozzles
Phase IV: Design and fabrication of a remotely variable exhaust-nozzle system and engine test support equipment, rebuild and reinstrumentation of the engine, and engine performance testing throughout a wide range of altitudes, flight Mach numbers, and ambient temperatures at the USAF Arnold Engineering Development Center (AEDC)

Significant conclusions based on the overall results of the program are:

(1) Minimal change in base-line engine performance resulted from the introduction of variable geometry components.

(2) LP turbine variable geometry was effective in increasing LP compressor surge margin at all rotor speeds. When compared to a fixed-cycle engine in a multimission aircraft, this surge margin increase will provide additional (a) inlet distortion tolerance, and (b) available thrust and/or improve SFC under virtually all flight conditions. Another potential benefit of this variable surge margin control is the ability to inexpensively compensate for unexpected stability problems frequently encountered in new flight installations.

(3) The variable LP turbine and primary exhaust-nozzle area allowed control of the turbine work splits, which resulted in independent control of rotor speeds and turbine temperature. Increased thrust is thereby provided at flight conditions where a single limit (speed or temperature) would be encountered in a fixed-cycle engine.

(4) The ability to modulate net thrust while maintaining a constant engine inlet airflow and a constant operating point on the LP compressor was demonstrated. This will reduce inlet spillage drag and exhaust-system drag losses during cruise.

(5) Bleed-effects testing confirmed the ability of variable-geometry modulation to recover part of the net thrust loss due to bleed-air extraction. Airframe concepts that use large bleed quantities (jet flap, etc.) may become more practical with a variable-cycle engine.

(6) High mechanical reliability was shown for the variable-geometry components.

The TFE731, modified to include variable geometry, proved to be an inexpensive, effective vehicle for development of variable-cycle engine concepts.

CONTENTS

PART IIIB

CONTENTS

PART IIIB (Contd)

LIST OF ILLUSTRATIONS

PART IIIB

LIST OF ILLUSTRATIONS

PART IIIB (Contd)

LIST OF ILLUSTRATIONS

PART IIIB

LIST OF TABLES

PART IIIB

LIST OF TABLES

PART IIIB (Contd)

SECTION II
TECHNICAL DISCUSSION

4.4.7 PHASE IV

4.4.7 Increased Climb Thrust and Airflow

4.4.7.1 Objective

At typical climb conditions, the engine referred LP rotor speed is below its design-point value. Therefore, by speeding up the LP rotor with the use of variable geometry, the engine inlet airflow and net thrust may be increased. Increased airflow may also be beneficial to engine inlet matching for some applications because, for a fixed inlet sized for a Mach-2-plus design point, spillage drag losses may be significant under typical climb conditions.

The objective of this series of tests was to demonstrate that the net thrust and airflow of the TFE731 Engine may be increased at Mach 0.6, 20,000 feet, standard atmosphere with the use of variable geometry that tends to increase the LP rotor speed or the engine airflow at a constant LP rotor speed.

4.4.7.2 Results

The test results are presented in Figures 532 through 540. Table 64 lists the parameters presented in these curves. Overall results corrected to a constant turbine inlet temperature of 1760°F are summarized for comparison in Table 65.

The test results indicate that a combination of 110 percent LP turbine nozzle area, 110-square-inch primary exhaust-nozzle area, and minus 5 degrees LP compressor IGV setting increased the LP rotor speed by 3.9 percent, the total airflow by 4.9 percent, and the net thrust by 7.2 percent. The specific fuel consumption was decreased by approximately 0.6 percent.

TABLE 64. INCREASED CLIMB THRUST AND AIRFLOW, MACH 0.6, 20,000 FEET, STANDARD ATM

Figure No.	Parameters Presented
532	Thrust specific fuel consumption versus net thrust
533	Net thrust versus turbine inlet total temperature
534	LP rotor speed versus turbine inlet total temperature
535	Total airflow versus turbine inlet total temperature
536	Bypass ratio versus turbine inlet total temperature
537	LP compressor inlet airflow versus turbine inlet total temperature
538	Bypass airflow versus turbine inlet total temperature
539	Fan tip pressure ratio versus total fan referred inlet airflow
540	Fan hub pressure ratio versus total fan referred inlet airflow

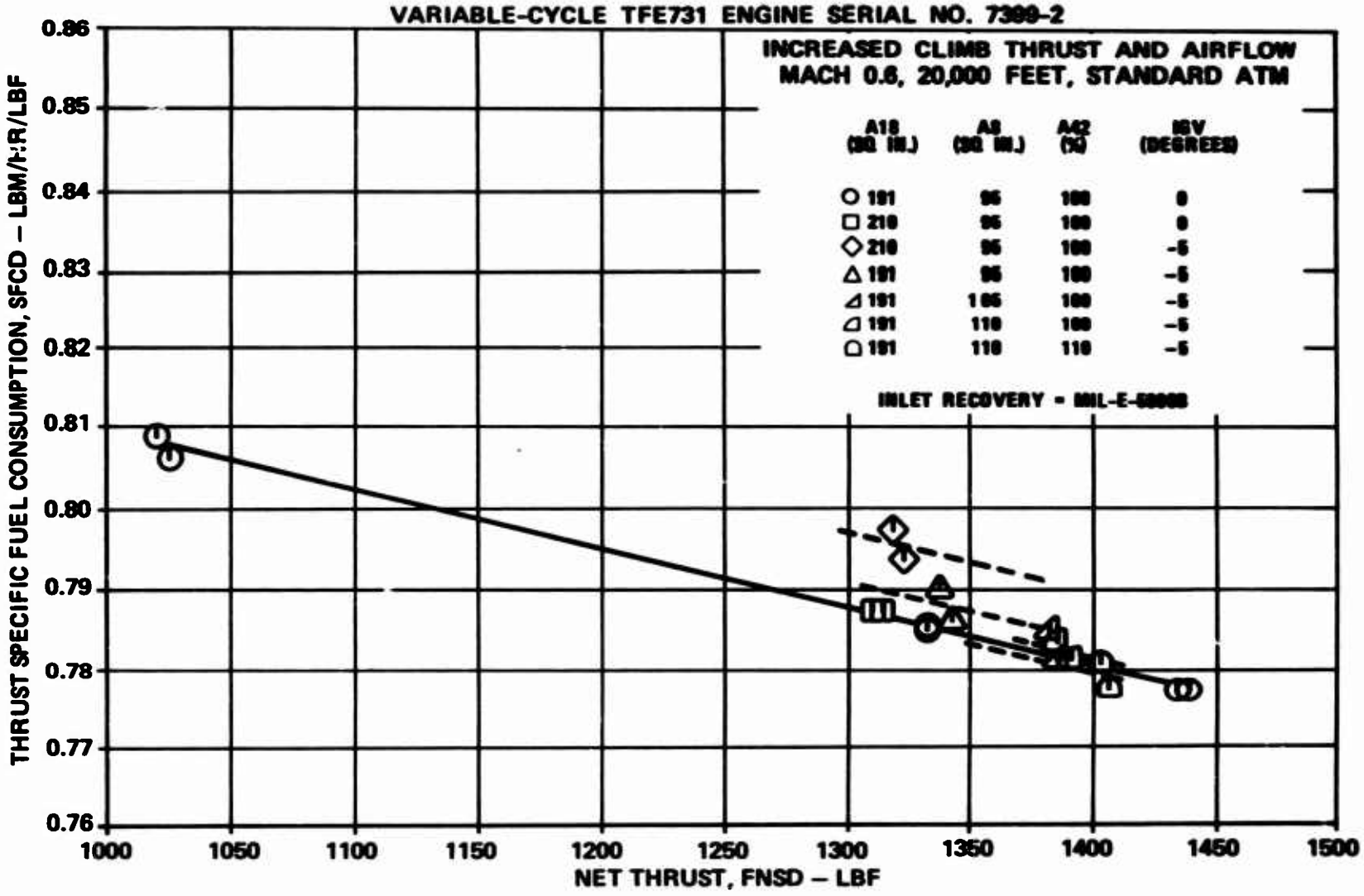

Figure 532. Increased Climb Thrust and Airflow at Mach 0.6, 20,000 Feet, Thrust Specific Fuel Consumption Versus Net Thrust.

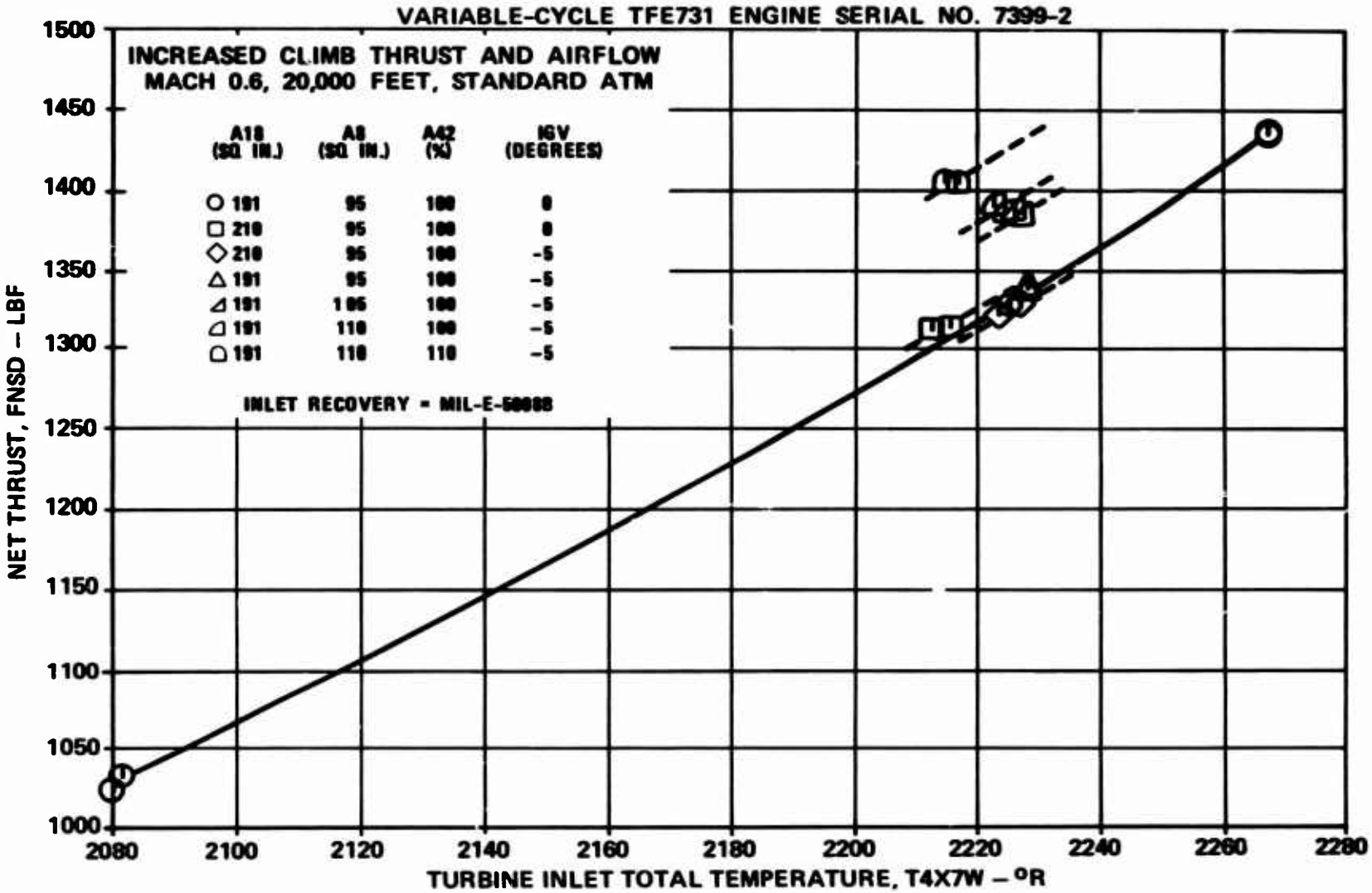

Figure 533. Increased Climb Thrust and Airflow at Mach 0.6, 20,000 Feet, Net Thrust Versus Turbine Inlet Total Temperature.

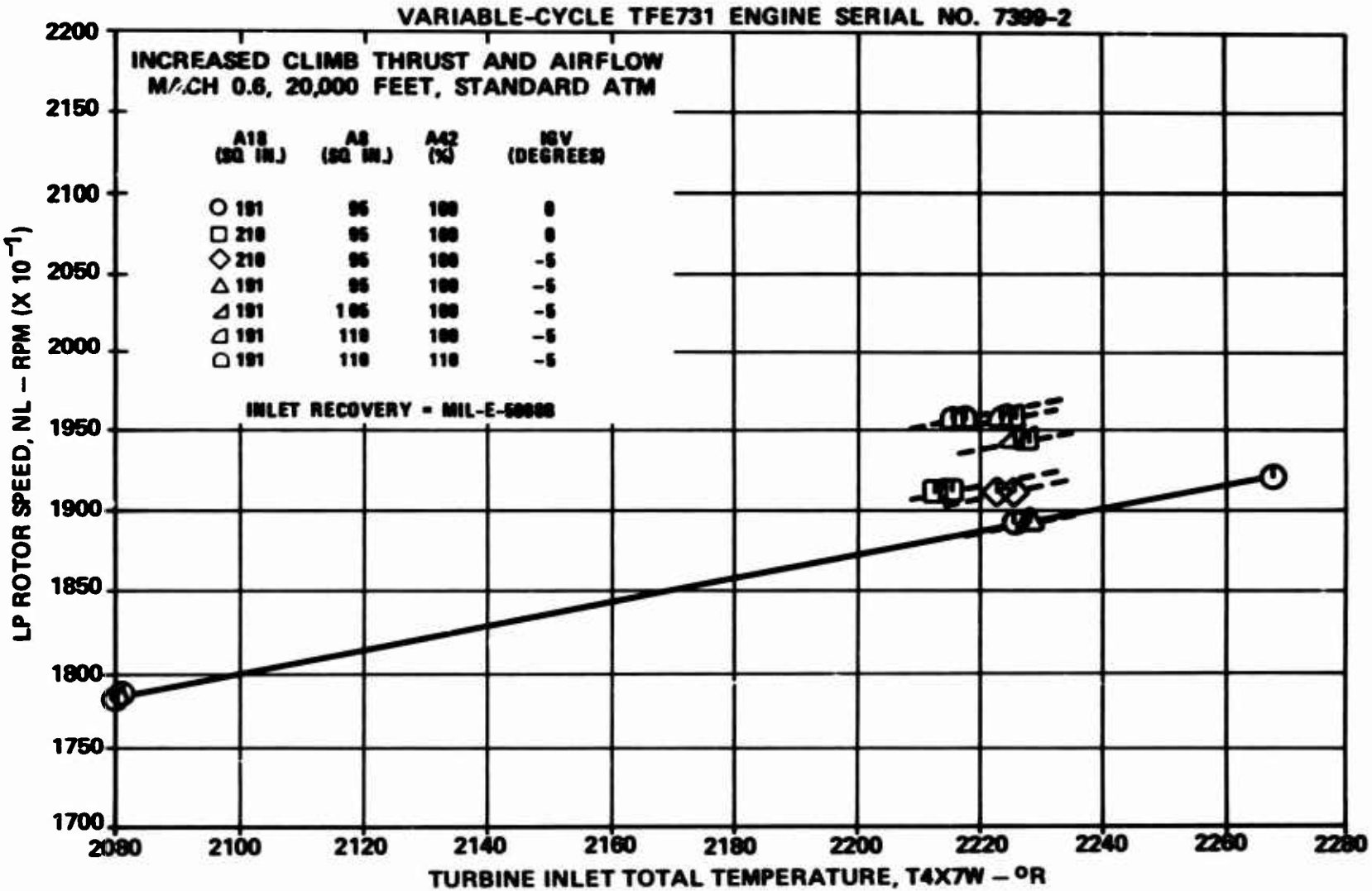

Figure 534. Increased Climb Thrust and Airflow at Mach 0.6, 20,000 Feet, LP Rotor Speed Versus Turbine Inlet Total Temperature.

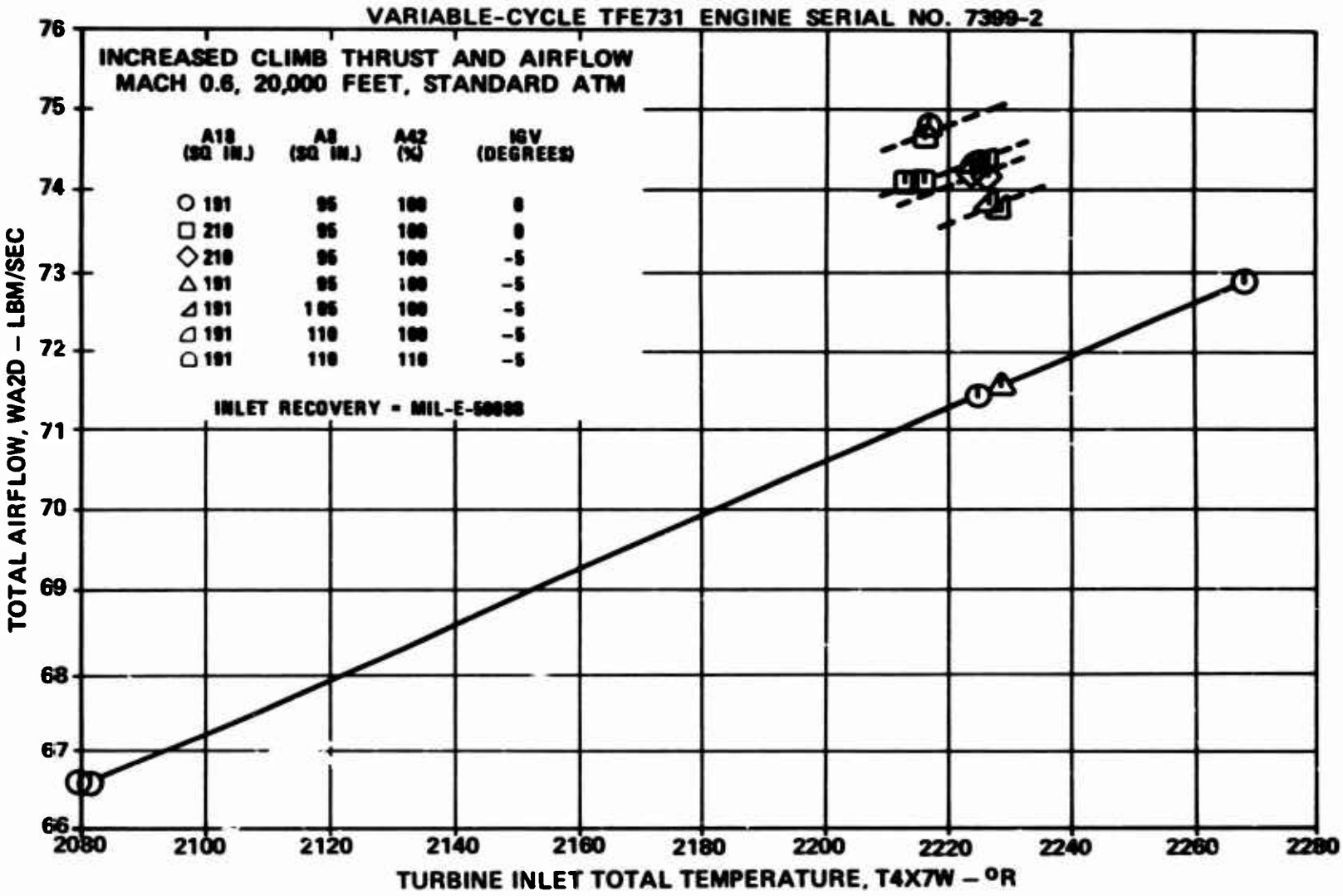

Figure 535. Increased Climb Thrust and Airflow at Mach 0.6, 20,000 Feet, Total Airflow Versus Turbine Inlet Total Temperature.

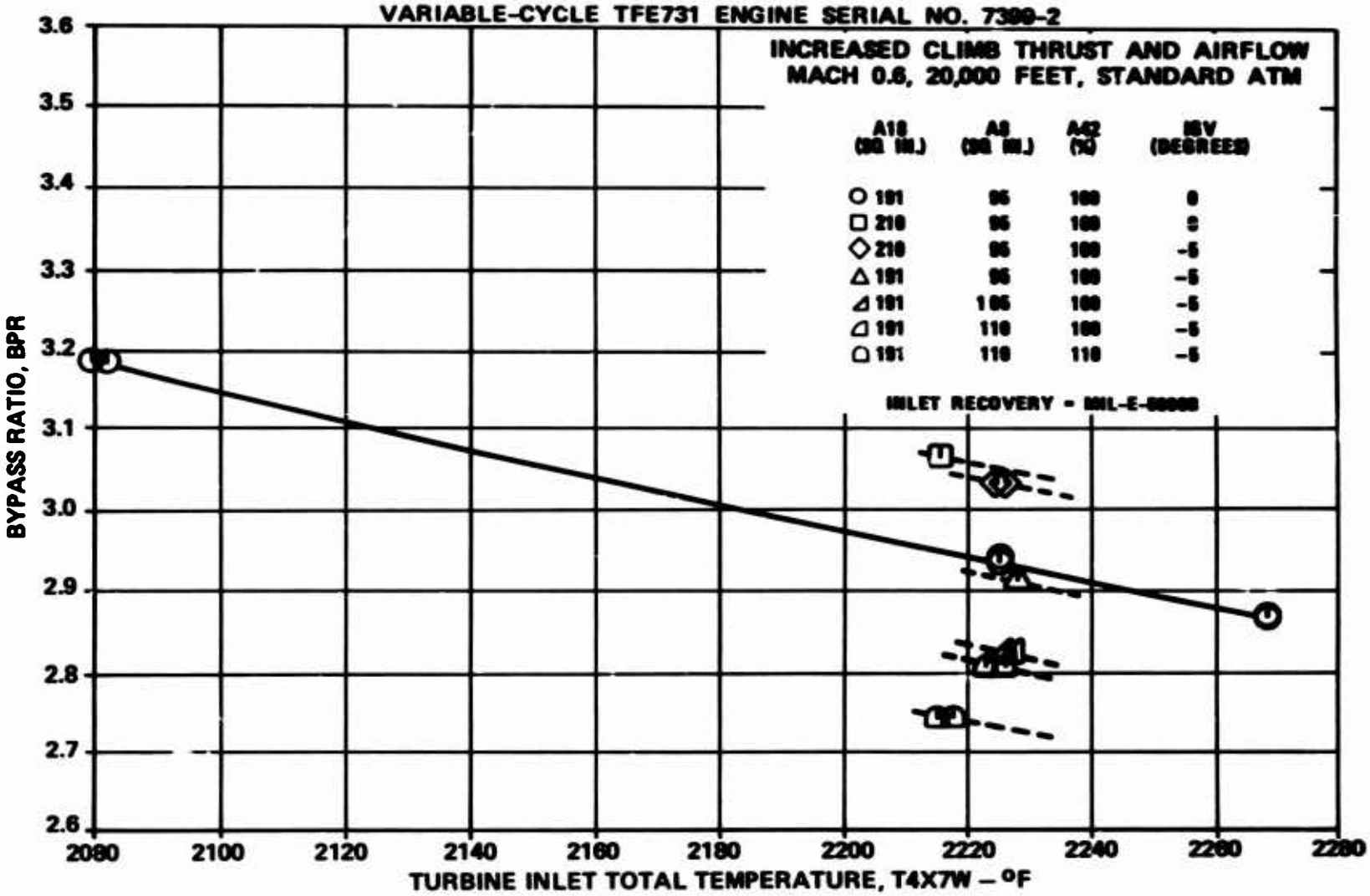

Figure 536. Increased Climb Thrust and Airflow at Mach 0.6, 20,000 Feet, Bypass Ratio Versus Turbine Inlet Total Temperature.

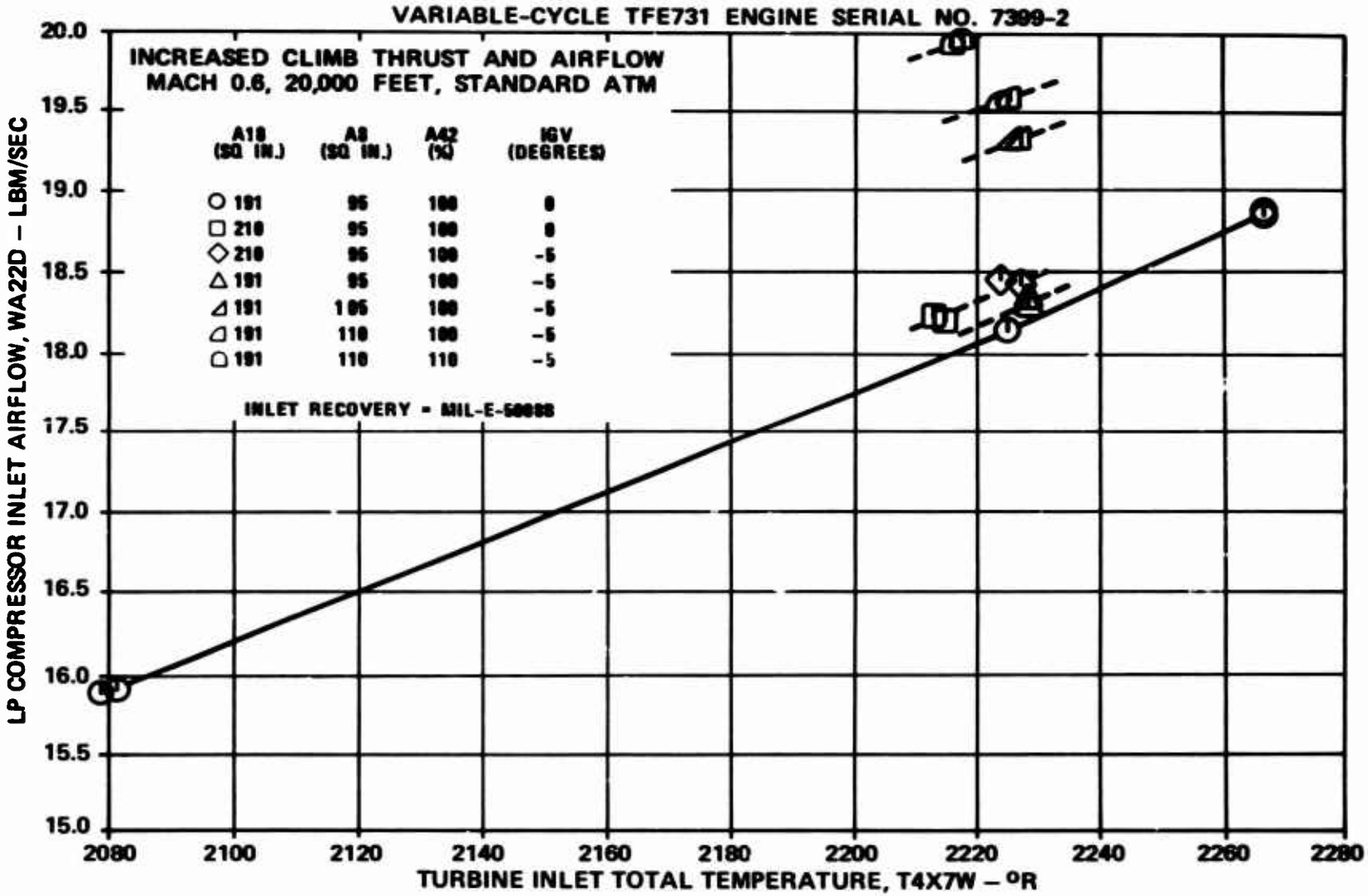

Figure 537. Increased Climb Thrust and Airflow at Mach 0.6, 20,000 Feet, LP Compressor Inlet Airflow Versus Turbine Inlet Total Temperature.

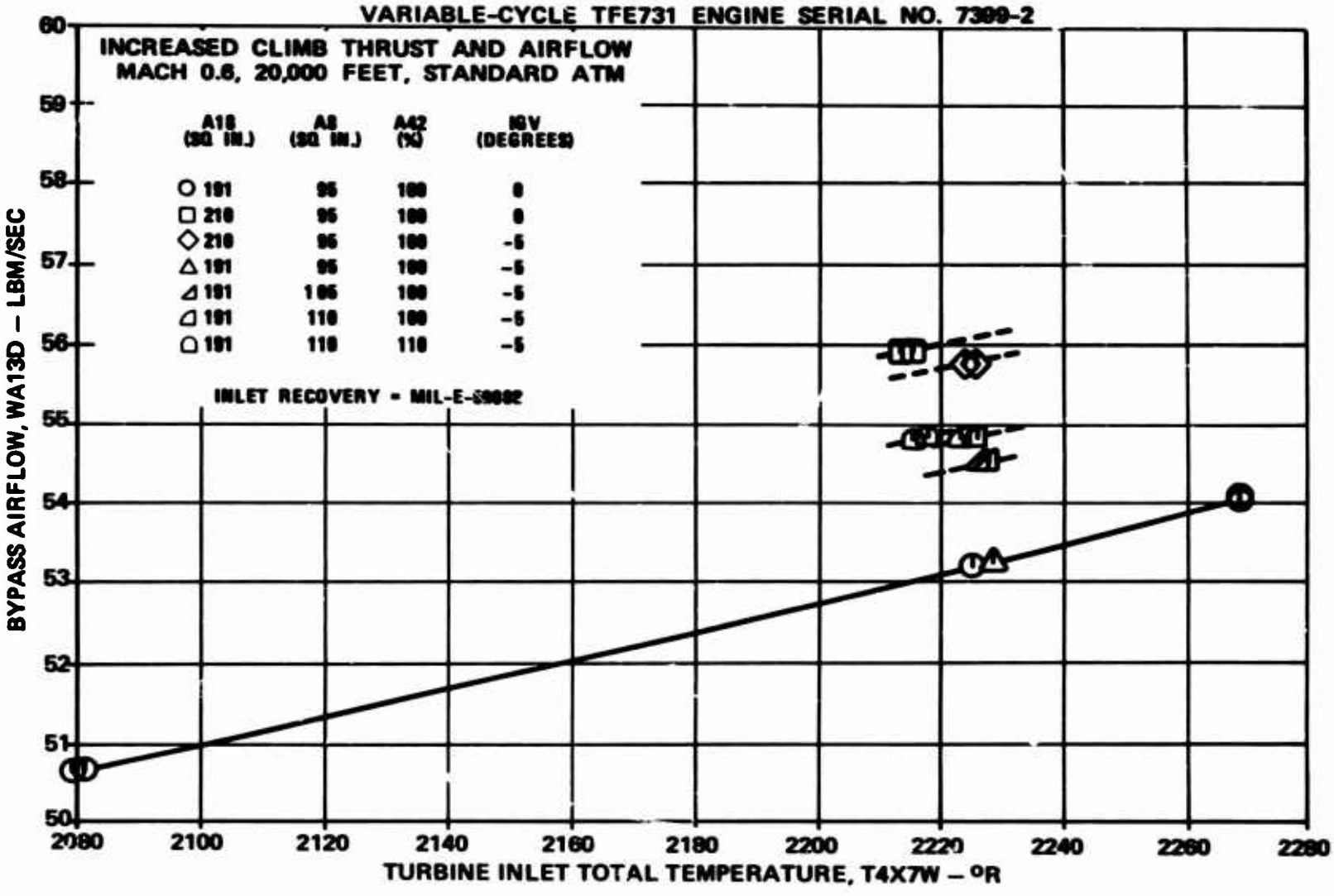

Figure 538. Increased Climb Thrust and Airflow at Mach 0.6, 20,000 Feet, Bypass Airflow Versus Turbine Inlet Total Temperature.

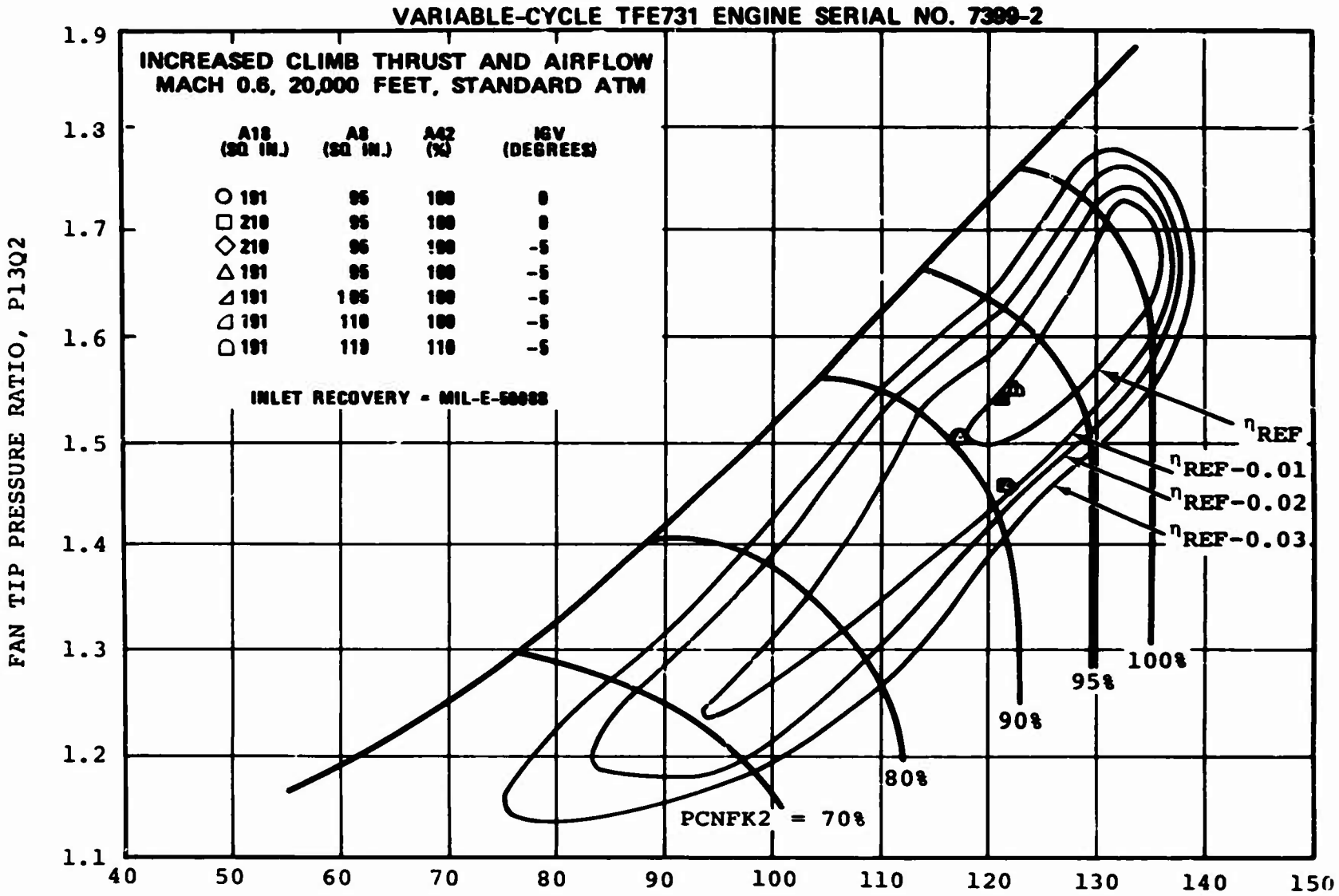

Figure 539. Component Operating Points at Mach 0.6, 20,000 Feet, Superimposed on Fan Tip Map.

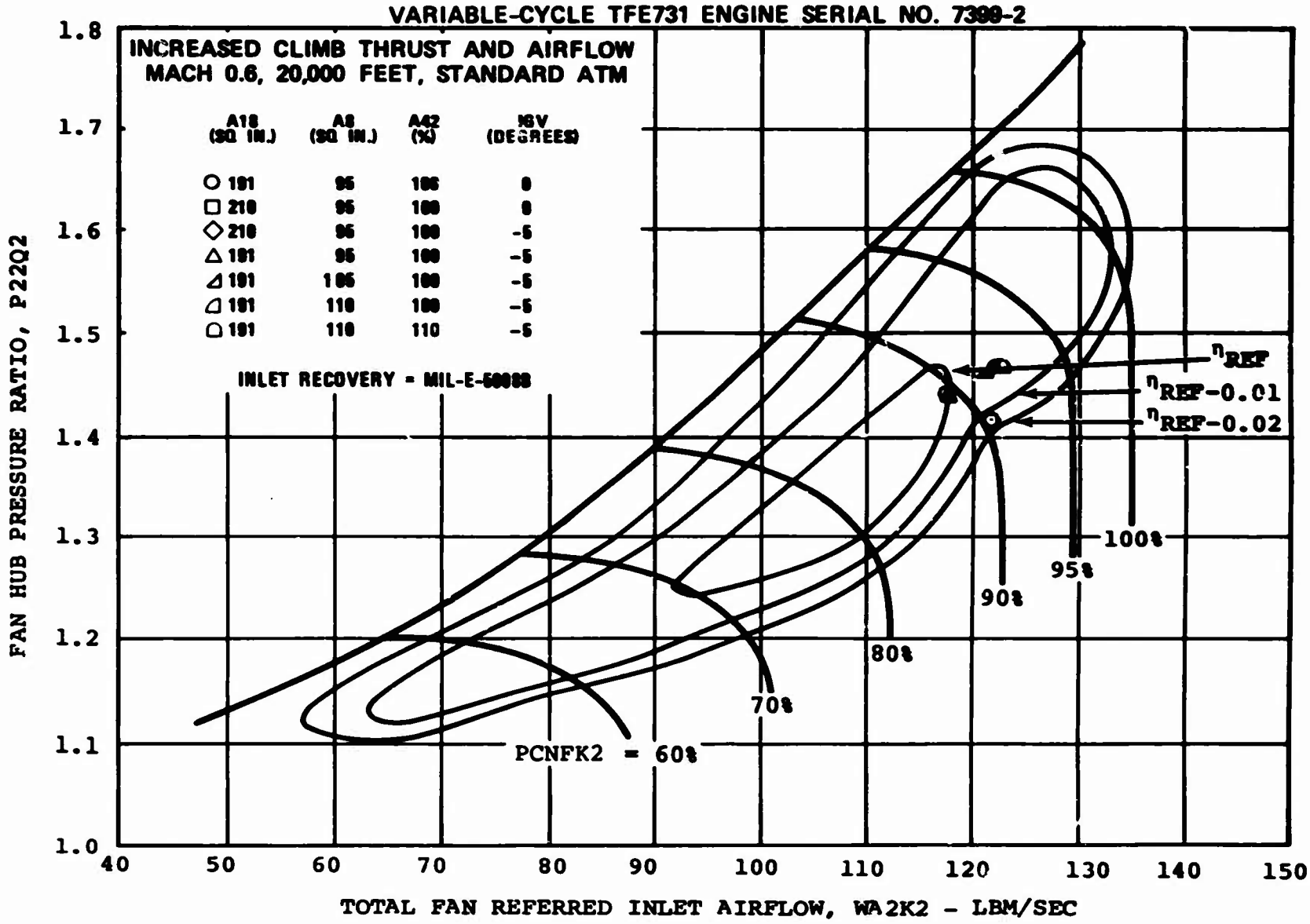

Figure 540. Component Operating Points at Mach 0.6, 20,000 Feet, Superimposed on Fan Hub Map.

TABLE 65. VARIABLE-GEOMETRY EFFECTS ON CLIMB NET THRUST, 20,000 FEET, MACH 0.6, STANDARD ATM AT A TURBINE INLET TOTAL TEMPERATURE OF 1760°F

A18 (sq in.)	A8 (sq in.)	A42 (%)	IGV (deg.)	LP Rotor Speed (rpm)	Total Airflow (lbm/sec)	Bypass Ratio	LPC Inlet Airflow (lbm/sec)	Bypass Airflow (lbm/sec)	Net Thrust (lbf)	SFC $\frac{\text{lbm/hr}}{\text{lbf}}$
191	95	100	0	18860	71.3	2.94	18.1	53.2	1320	0.787
210	95	100	0	19170	74.3	3.06	18.3	55.7	1315	0.786
210	95	100	-5	19080	74.0	3.04	18.3	55.7	1315	0.797
191	95	100	-5	18850	71.3	2.93	18.1	53.2	1322	0.790
191	105	100	-5	19380	73.6	2.84	19.2	54.4	1370	0.784
191	110	100	-5	19540	74.3	2.82	19.5	54.8	1380	0.783
191	110	110	-5	19600	74.8	2.74	20.0	54.8	1415	0.782

Surge bleed valve closed.

All of the improvement is attributed to the use of the increased primary exhaust-nozzle area and increased LP turbine nozzle area, since the minus-5-degree LP compressor IGV setting did not, by itself, improve the performance. This may be seen by comparing line one of Table 65 with line four for a 191-square-inch fan nozzle area and line two with line three for a 210-square-inch fan nozzle area. The test data indicates that the minus-5-degree IGV angle tended to increase the LP compressor airflow slightly, but the LP compressor efficiency was reduced by approximately 0.5 percent, which caused the LP rotor speed to decrease to a level where the LP compressor airflow was the same as that with the zero-degree IGV position.

The use of a fan exhaust-nozzle area increase from 191 square inches to 210 square inches caused the LP rotor speed to increase by 1.6 percent, the total airflow to increase by 4.2 percent, and the net thrust to increase by 0.4 percent when the LP compressor IGV angle was zero degrees. When the LP compressor IGV angle was set at minus 5 degrees, the corresponding changes were a 1.2-percent increase in LP rotor speed, a 3.8-percent increase in total airflow, and a 0.5-percent decrease in net thrust. Little change in net thrust occurred with the increased fan nozzle area because the total airflow and bypass ratio improvements were offset by reduced fan tip and hub efficiencies. The tested operating points superimposed on the analytical model fan map in Figures 539 and 540 support an expected decrease in fan tip and hub efficiencies with the increased fan nozzle area.

The trend of increased LP rotor speed, airflow, and net thrust with increases in primary exhaust-nozzle area and LP turbine nozzle area are in agreement with the results of the exhaust nozzle and turbine nozzle rematching tests discussed in Paragraphs 4.4.4 and 4.4.5. An analysis of the component performance contained in 4.4.4 and 4.4.5 explains why these trends occur.

4.4.8 Bleed Effects

The bleed effects tests were conducted to confirm predictions that part of the performance loss due to the effects of bleed-air extraction may be restored by the use of variable geometry. Testing was conducted at the following four operating conditions to determine their influence on engine performance:

(a) 40,000 feet, Mach 0.8, standard atmosphere
(b) 50,000 feet, Mach 0.8, standard atmosphere
(c) 50,000 feet, Mach 1.2, standard atmosphere
(d) 20,000 feet, Mach 0.6, standard atmosphere

The engine was initially operated as a fixed-cycle engine--first with the LP compressor surge bleed valve closed, and then with the surge bleed valve in the open position. With the bleed valve maintained in the open position, different elements of variable geometry or combinations of variable geometry were changed to determine their effects on engine performance. Testing was conducted at an approximately constant turbine inlet temperature. All data was corrected for any observed variation from a constant value.

Since all of the variable-geometry changes resulted in changes in bleed flow, a dashed line has been drawn on the performance curves connecting the zero bleed point and the base-line bleed point. All data was then corrected to the base-line bleed flow with use of the slope of the dashed line so that the variable-geometry effects could be evaluated at the constant bleed-airflow rate. The discussion that follows is organized by operating condition. It is succeeded by a discussion of overall results of all four operating conditions.

4.4.8.1 40,000 Feet, Mach 0.8

The results of the bleed testing at 40,000 feet, Mach 0.8, standard atmosphere are presented in Figures 541 through 554. The parameters presented in these curves are listed in Table 66. All parameters have been corrected to a turbine inlet temperature of 1805°F. The component operating points have been superimposed on the component maps used in the variable-cycle analytical model to help explain trends obtained. These maps are presented in Figures 555 through 559. Table 67 lists the maps presented.

After the engine was run in a nominal configuration with the bleed valve closed, the bleed valve was opened in order to obtain a base-line point. The opening of the valve bled off approximately 11 percent of the primary engine flow. The results of opening the valve were to decrease the LP rotor speed by approximately 810 rpm (4.2 percent), to reduce the net thrust by 115 pounds (15.9 percent), and with the exception of the fan hub, to move the compressor operating points away from their peak efficiency islands. After the bleed valve was opened, the LP turbine nozzle area was reduced to 90 percent in an effort to shift the LP compressor to an operating point nearer the peak efficiency island. It can be seen from Figure 557 that this was successfully accomplished and the HP compressor was also matched to a more efficient operating point. However, the engine net thrust was reduced. This was because of the sharp decrease in LP turbine efficiency as the LP turbine nozzle area was reduced below the nominal value (see Paragraph 4.4.5.1).

The next geometry change consisted of increasing the primary exhaust-nozzle area to 105 square inches while maintaining the turbine nozzle area at 90 percent. The increased primary exhaust-nozzle area resulted in an increase of 519 rpm in LP rotor speed (2.8 percent) and an increase of 21 pounds in net thrust (3.5 percent). The fan and compressors all remained on

TABLE 66. BLEED EFFECTS, 40,000 FEET, MACH 0.8, STANDARD ATM

Figure No.	Parameters Presented
541	Turbine inlet temperature versus LP bleed flow
542	Thrust specific fuel consumption versus LP bleed flow
543	Net thrust versus LP bleed flow
544	Fuel flow versus LP bleed flow
545	Interturbine temperature versus LP bleed flow
546	LP rotor speed versus LP bleed flow
547	HP rotor speed versus LP bleed flow
548	Engine total airflow versus LP bleed flow
549	Fan tip pressure ratio versus LP bleed flow
550	Fan hub pressure ratio versus LP bleed flow
551	Cycle pressure ratio versus LP bleed flow
552	Bypass ratio versus LP bleed flow
553	Engine pressure ratio versus LP bleed flow
554	LP compressor inlet airflow versus LP bleed flow

TABLE 67. COMPONENT OPERATING POINTS, 40,000 FEET, MACH 0.8, STANDARD ATM

Figure No.	Component Maps
555	Fan Tip Map
556	Fan Hub Map
557	LP Compressor Map
558	HP Compressor Map
559	HP Turbine Map

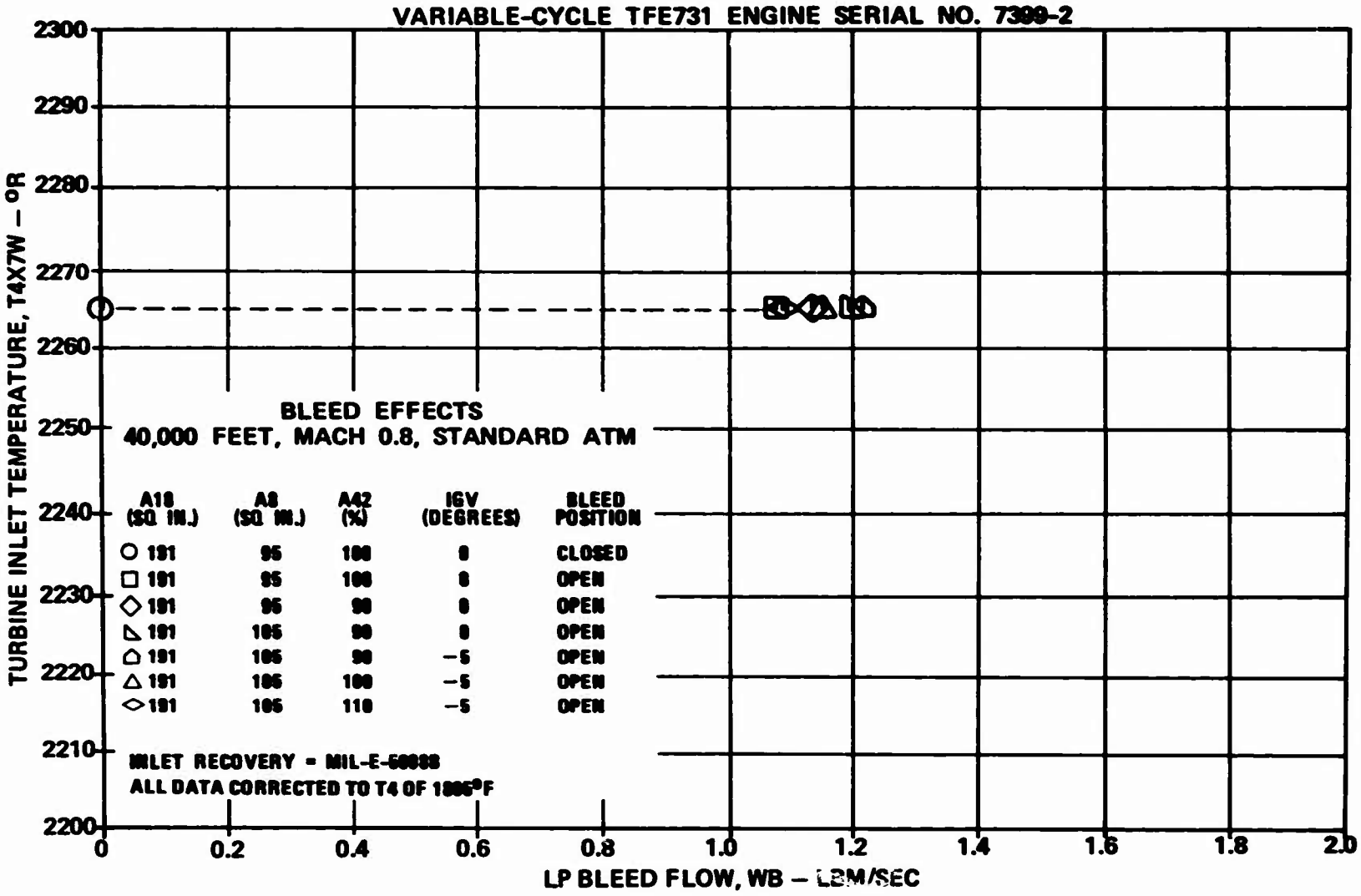

Figure 541. Bleed Effects at Mach 0.8, 40,000 Feet, Turbine Inlet Temperature Versus LP Bleed Flow.

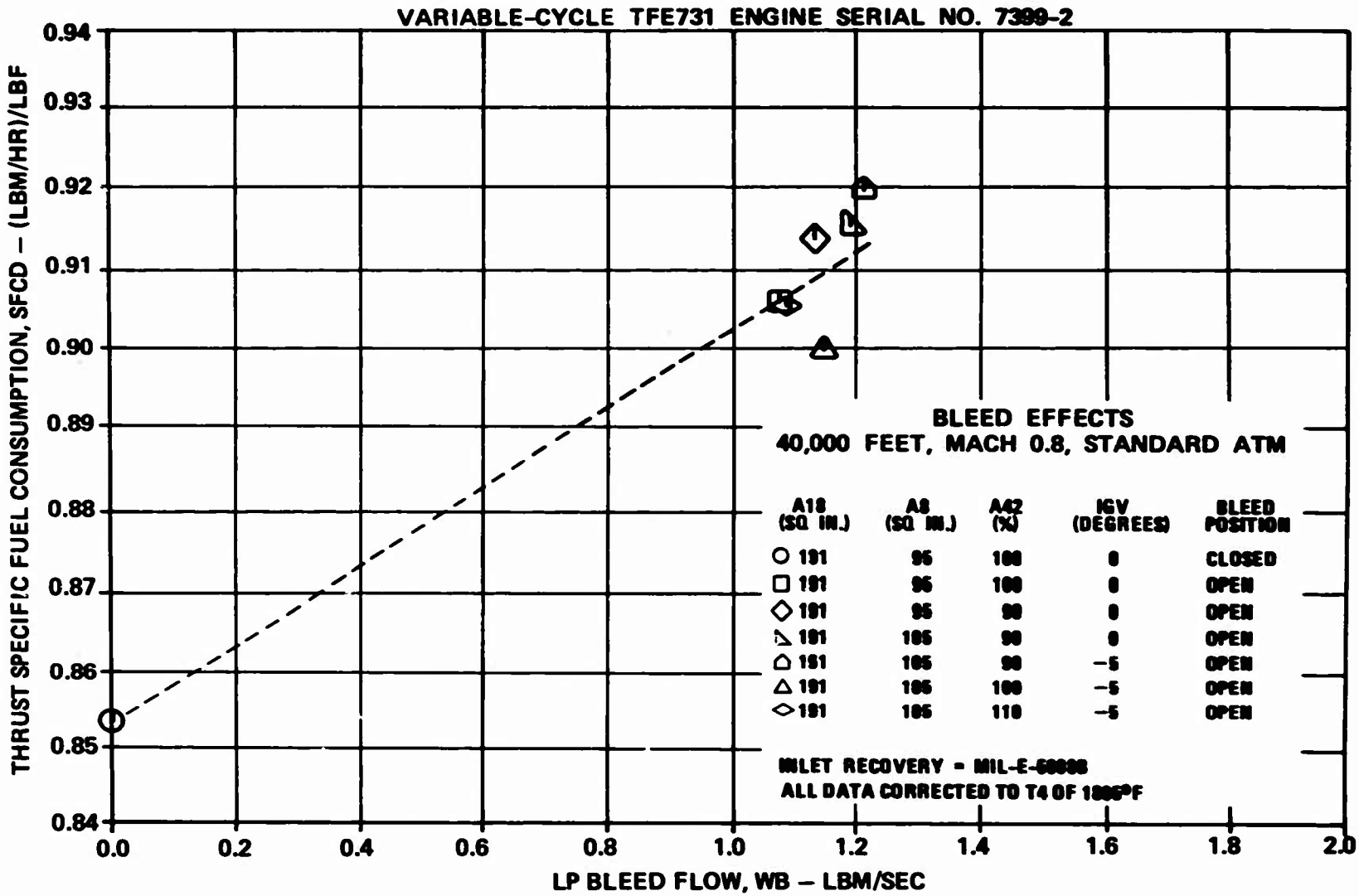

Figure 542. Bleed Effects at Mach 0.8, 40,000 Feet, Thrust Specific Fuel Consumption Versus LP Bleed Flow.

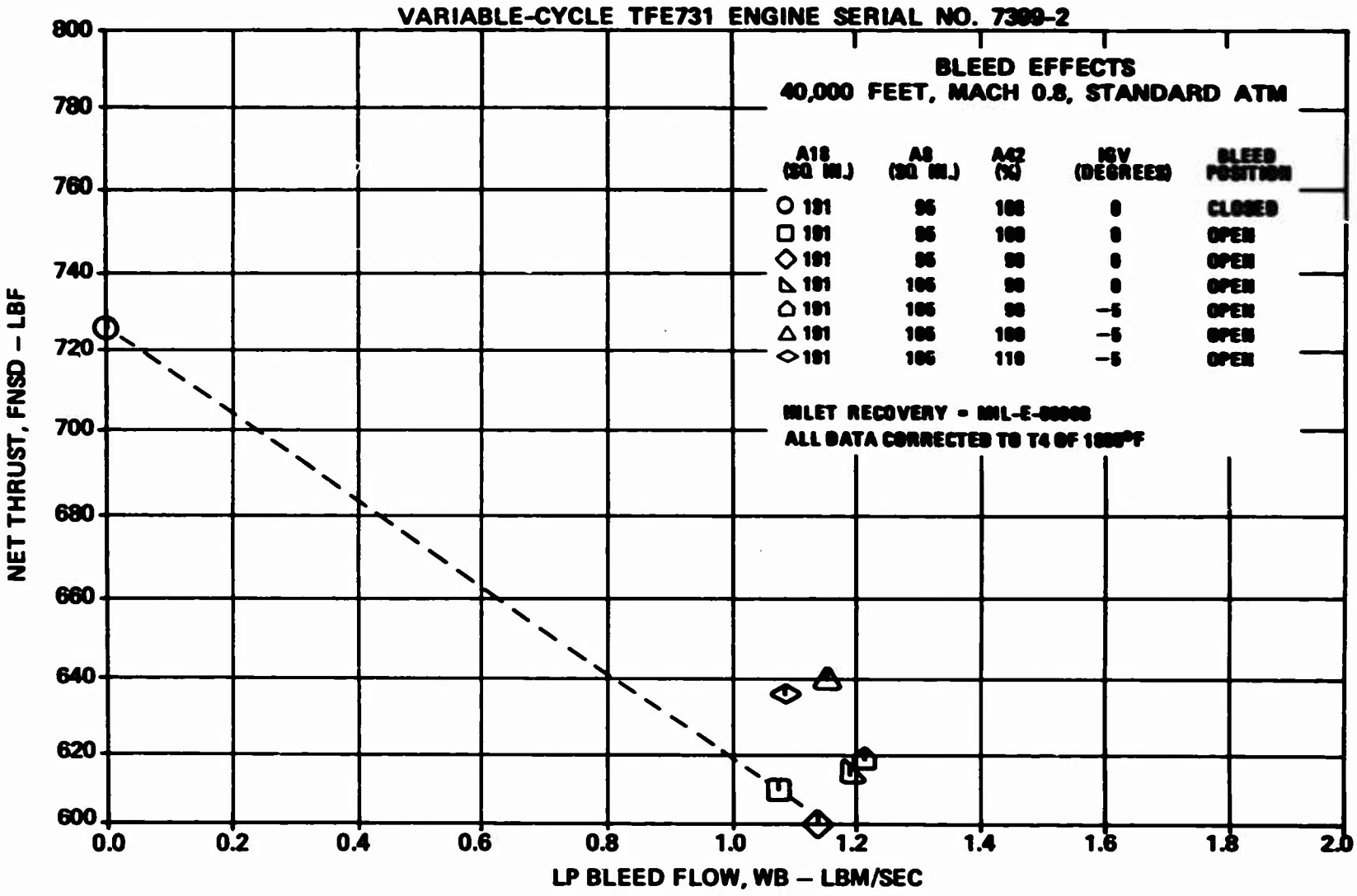

Figure 543. Bleed Effects at Mach 0.8, 40,000 Feet, Net Thrust Versus LP Bleed Flow.

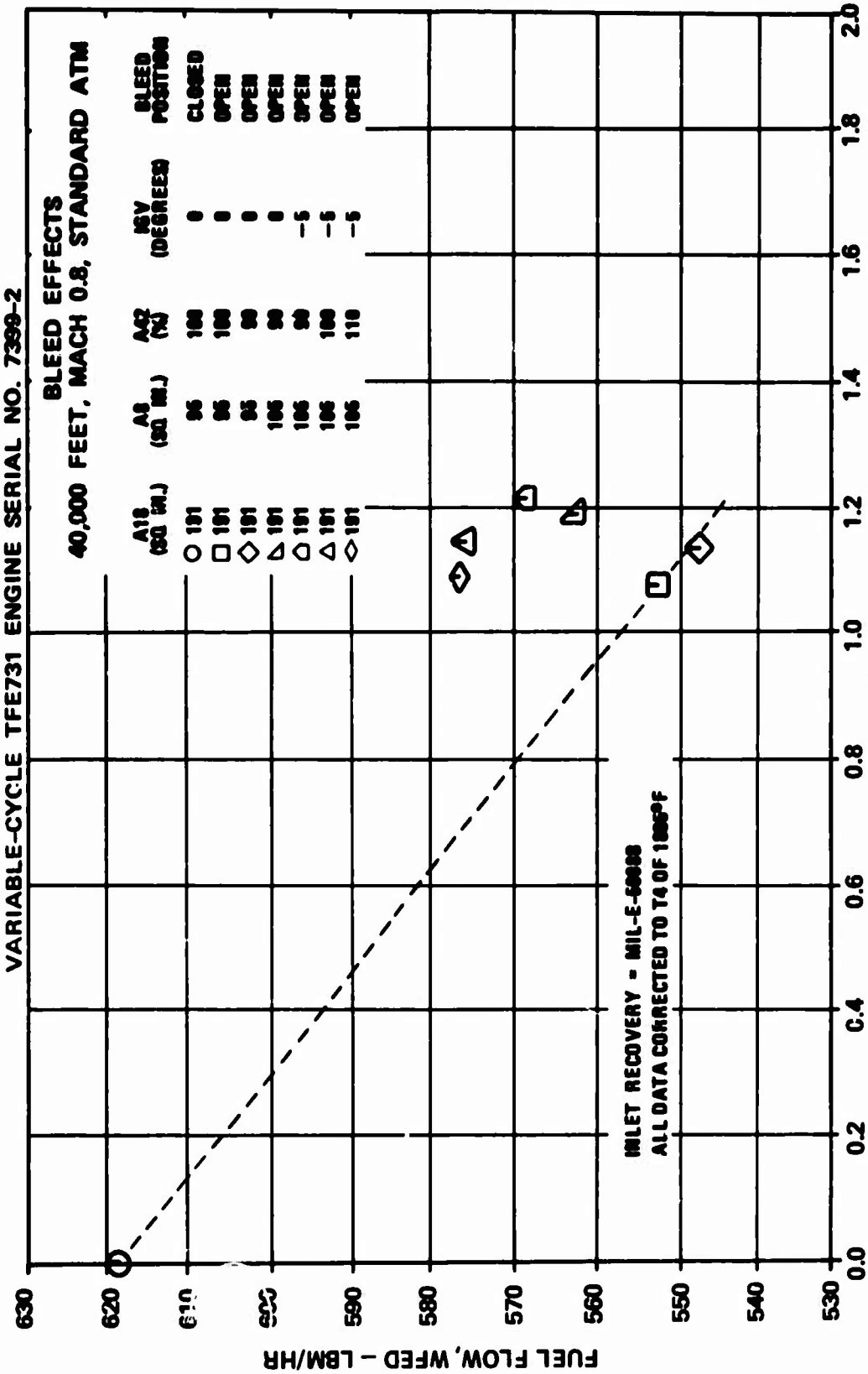

Figure 544. Bleed Effects at Mach 0.8, 40,000 Feet, Fuel Flow Versus LP Bleed Flow.

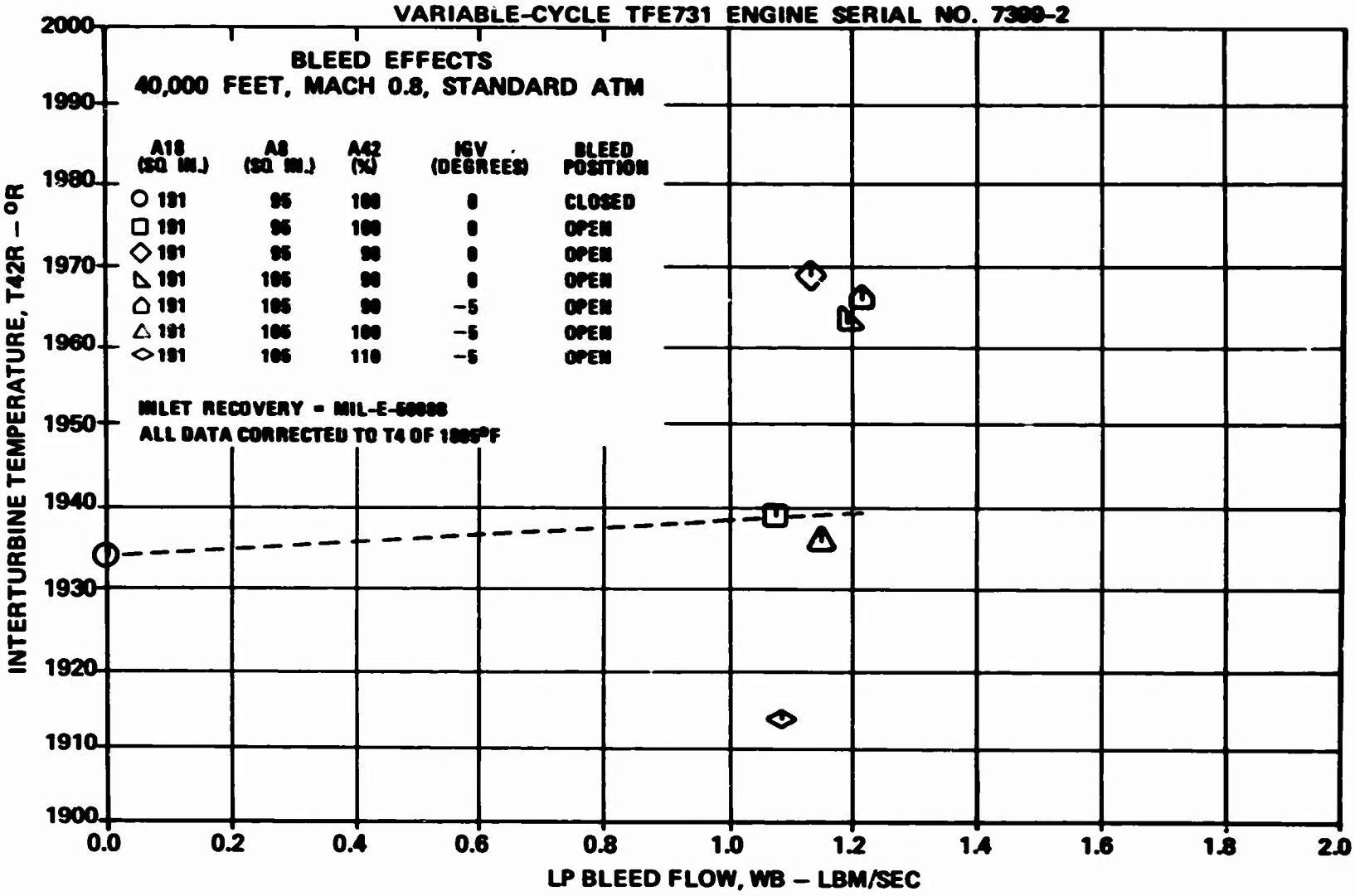

Figure 545. Bleed Effects at Mach 0.8, 40,000 Feet, Interturbine Temperature Versus LP Bleed Flow.

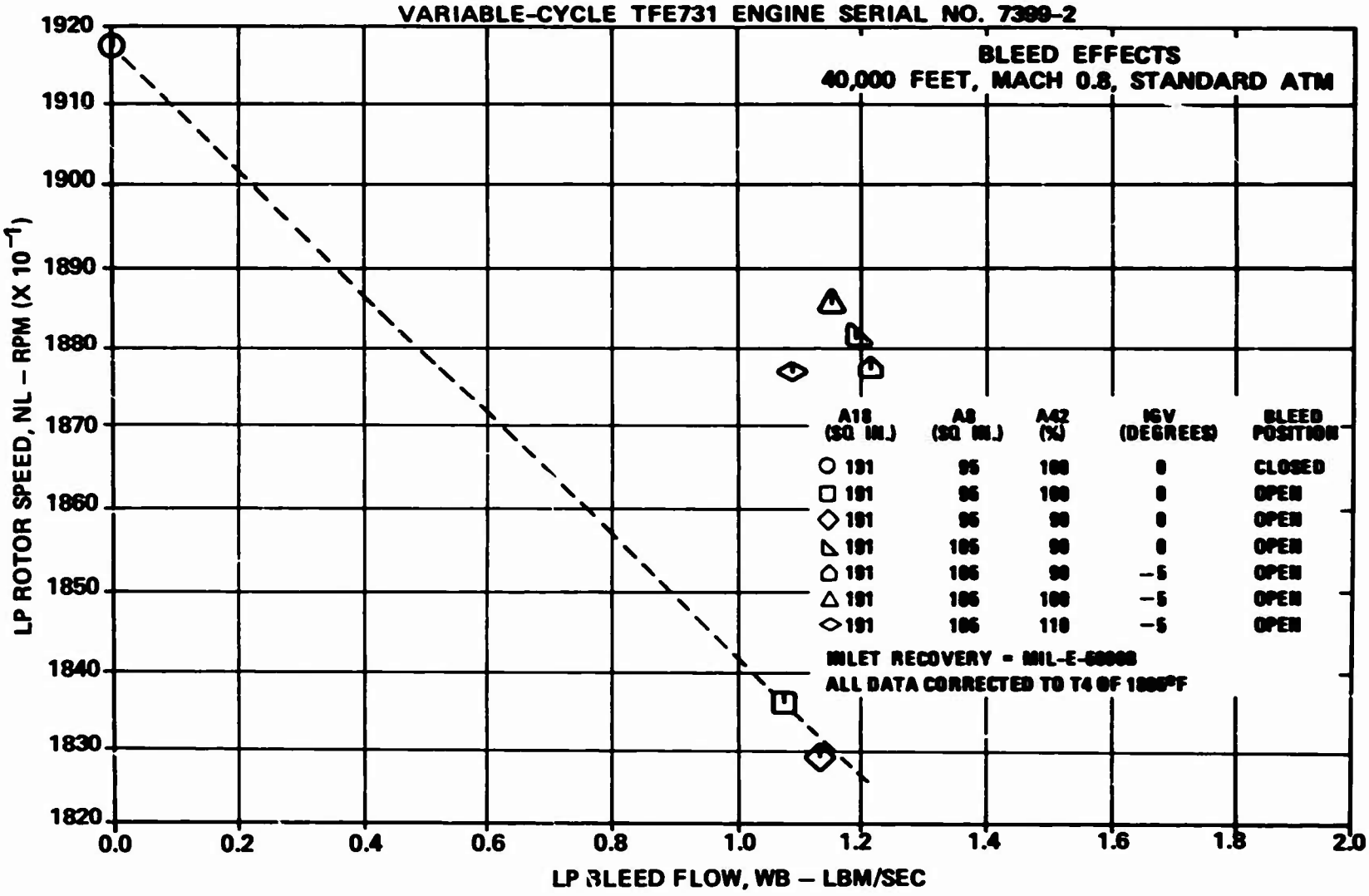

Figure 546. Bleed Effects at Mach 0.8, 40,000 Feet, LP Rotor Speed Versus LP Bleed Flow.

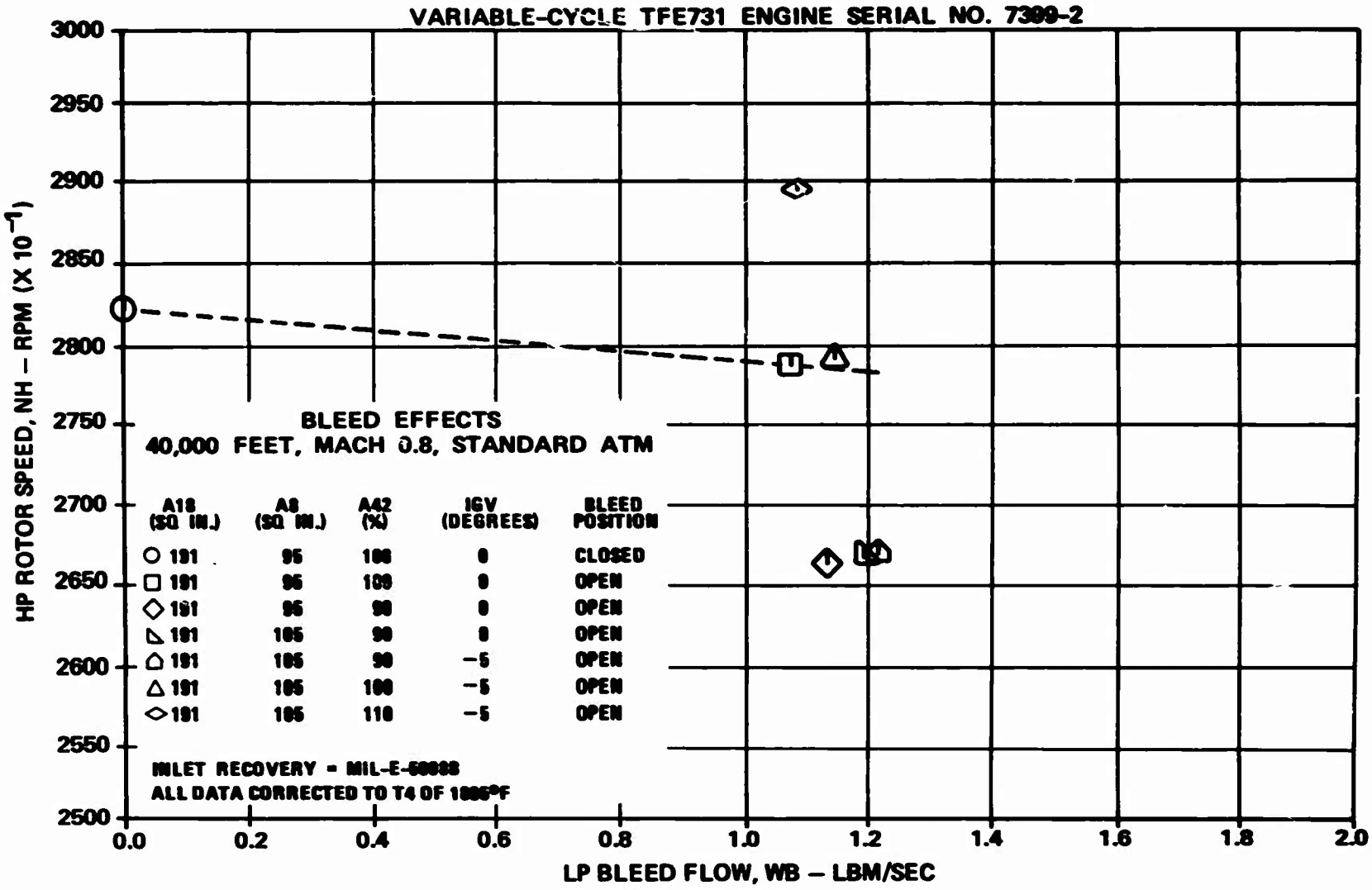

Figure 547. Bleed Effects at Mach 0.8, 40,000 Feet, HP Rotor Speed Versus LP Bleed Flow.

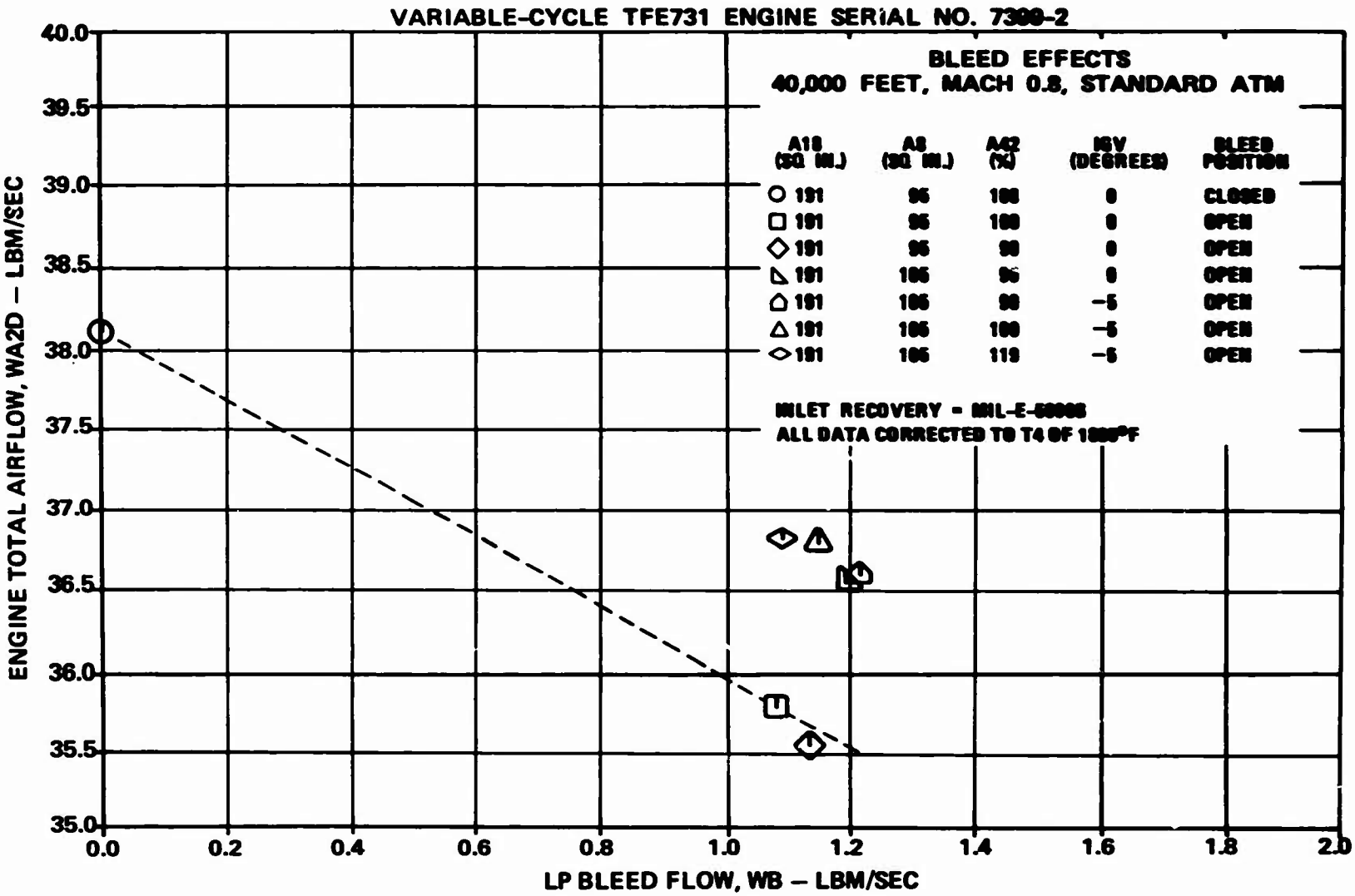

Figure 548. Bleed Effects at Mach 0.8, 40,000 Feet, Engine Total Airflow Versus LP Bleed Flow.

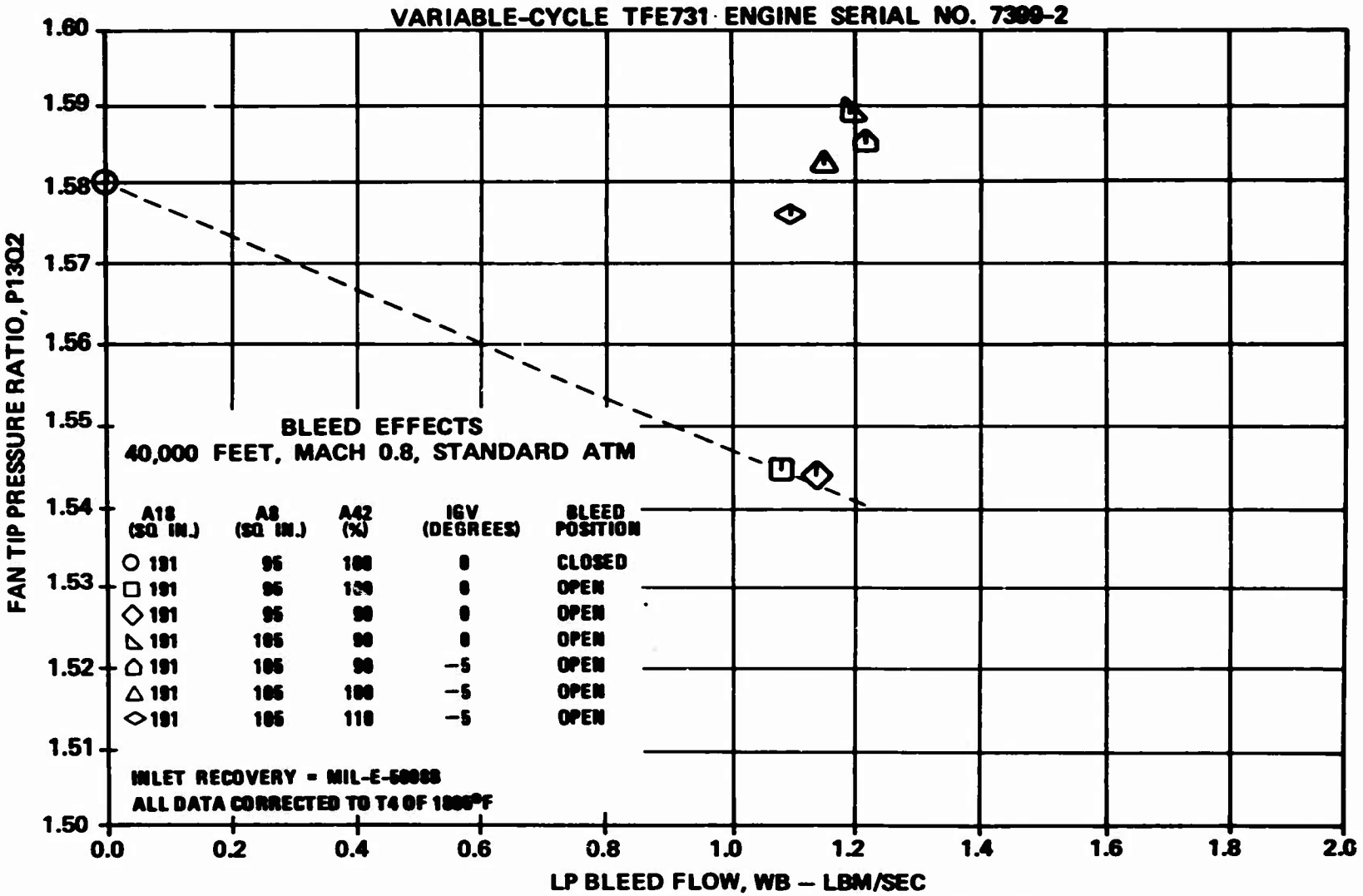

Figure 549. Bleed Effects at Mach 0.8, 40,000 Feet, Fan Tip Pressure Ratio Versus LP Bleed Flow.

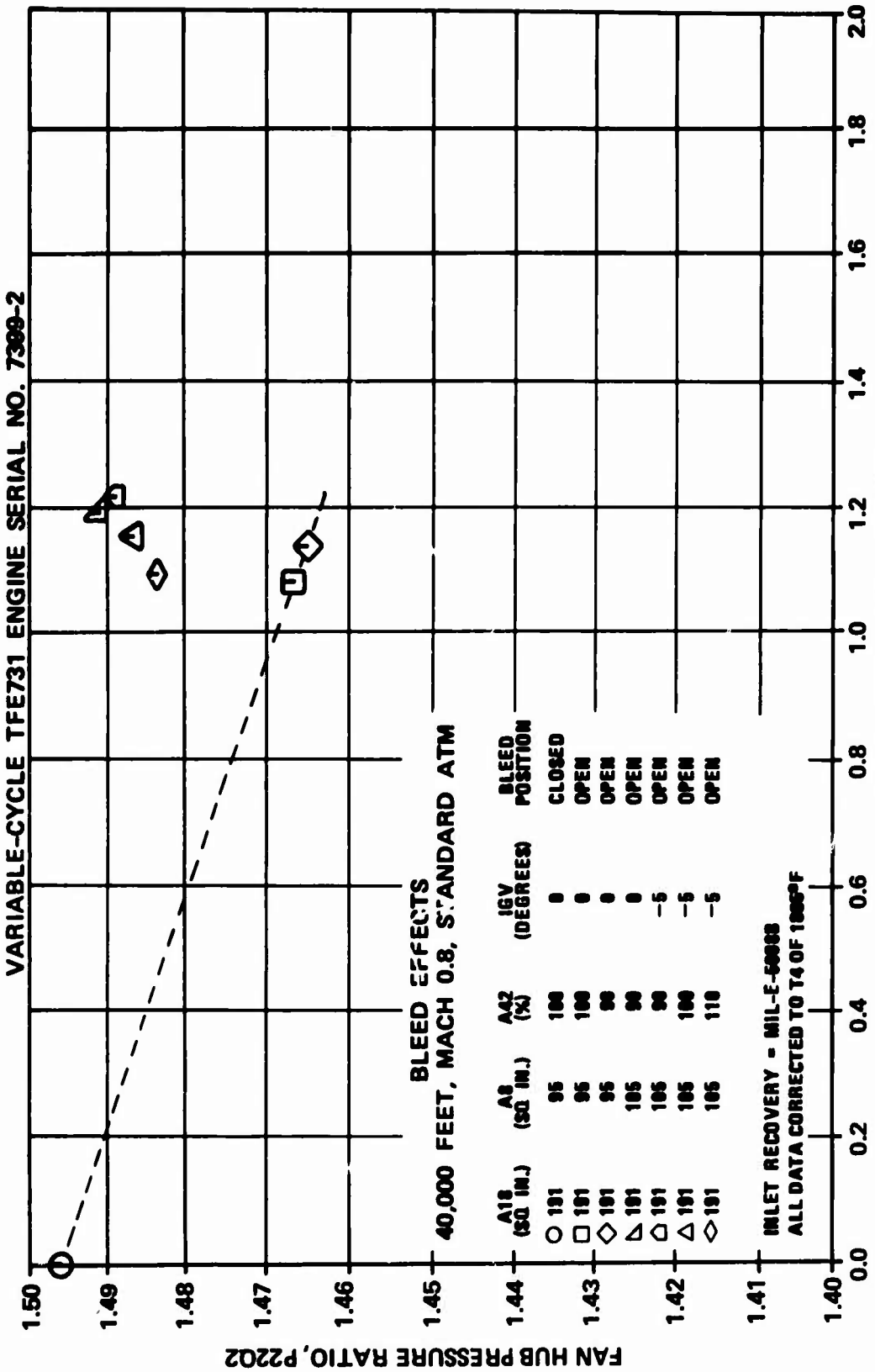

Figure 550. Bleed Effects at Mach 0.8, 40,000 Feet, Fan Hub Pressure Ratio Versus LP Bleed Flow.

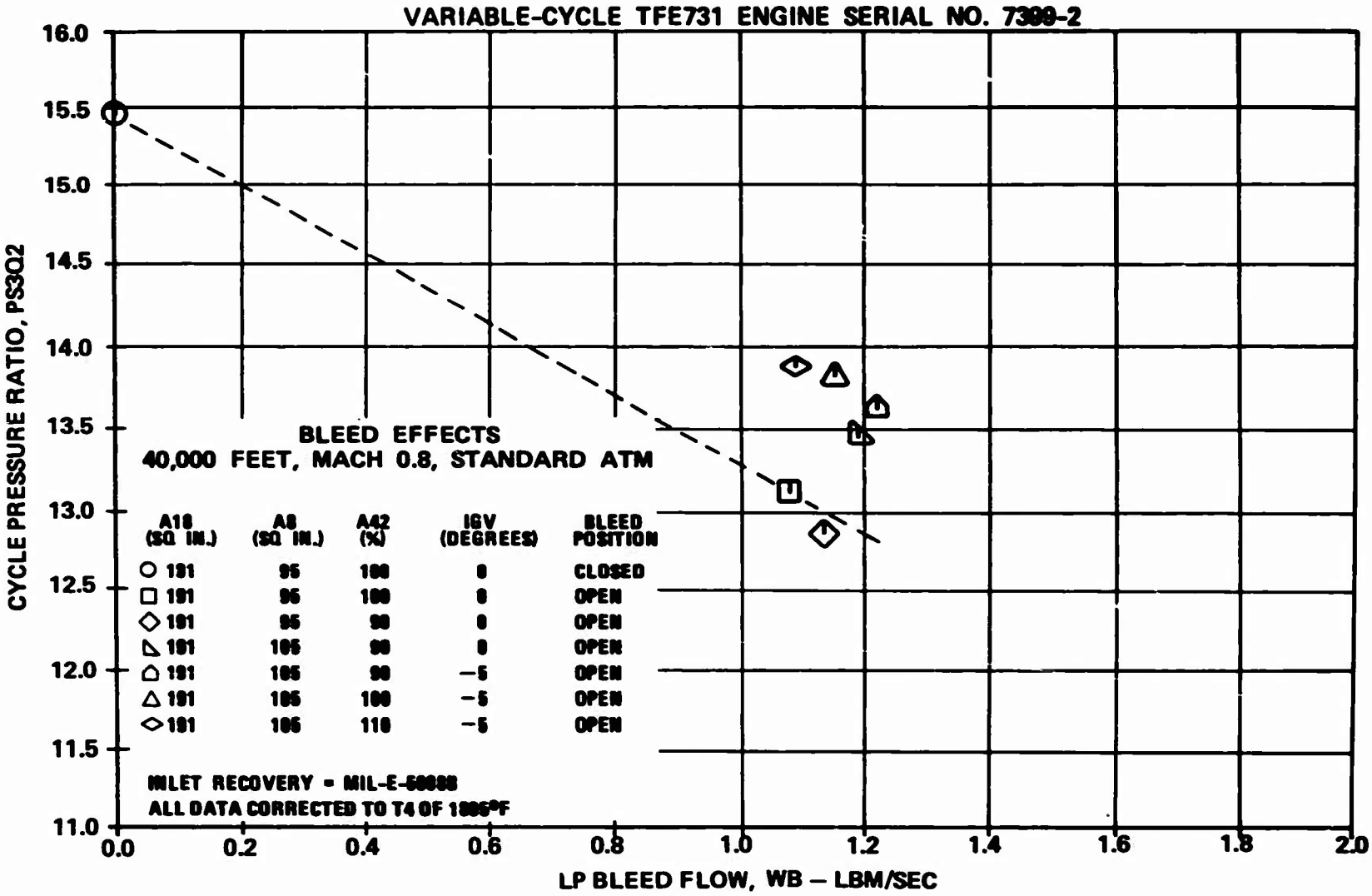

Figure 551. Bleed Effects at Mach 0.8, 40,000 Feet, Cycle Pressure Ratio Versus LP Bleed Flow.

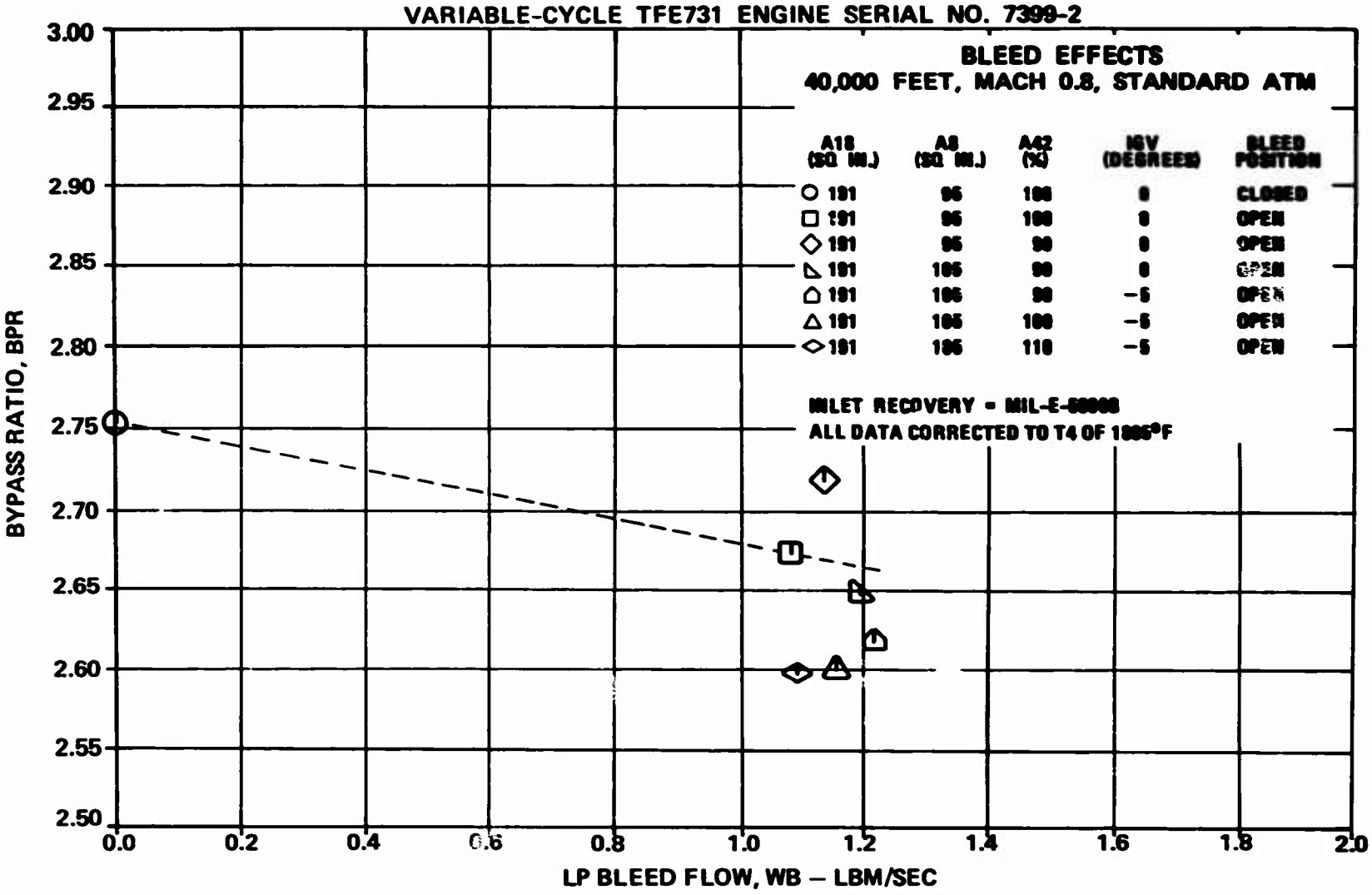

Figure 552. Bleed Effects at Mach 0.8, 40,000 Feet, Bypass Ratio Versus LP Bleed Flow.

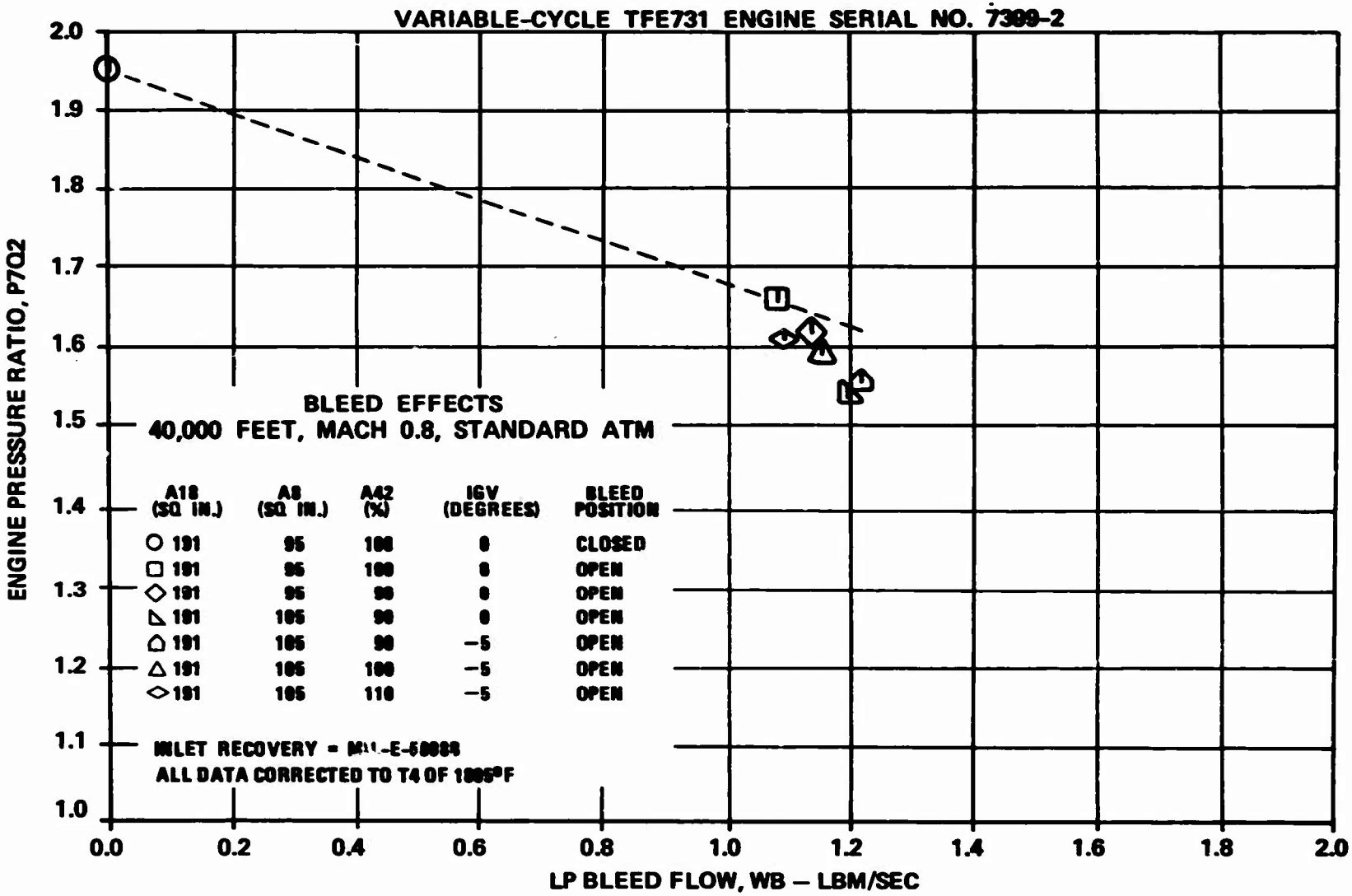

Figure 553. Bleed Effects at Mach 0.8, 40,000 Feet, Engine Pressure Ratio Versus LP Bleed Flow.

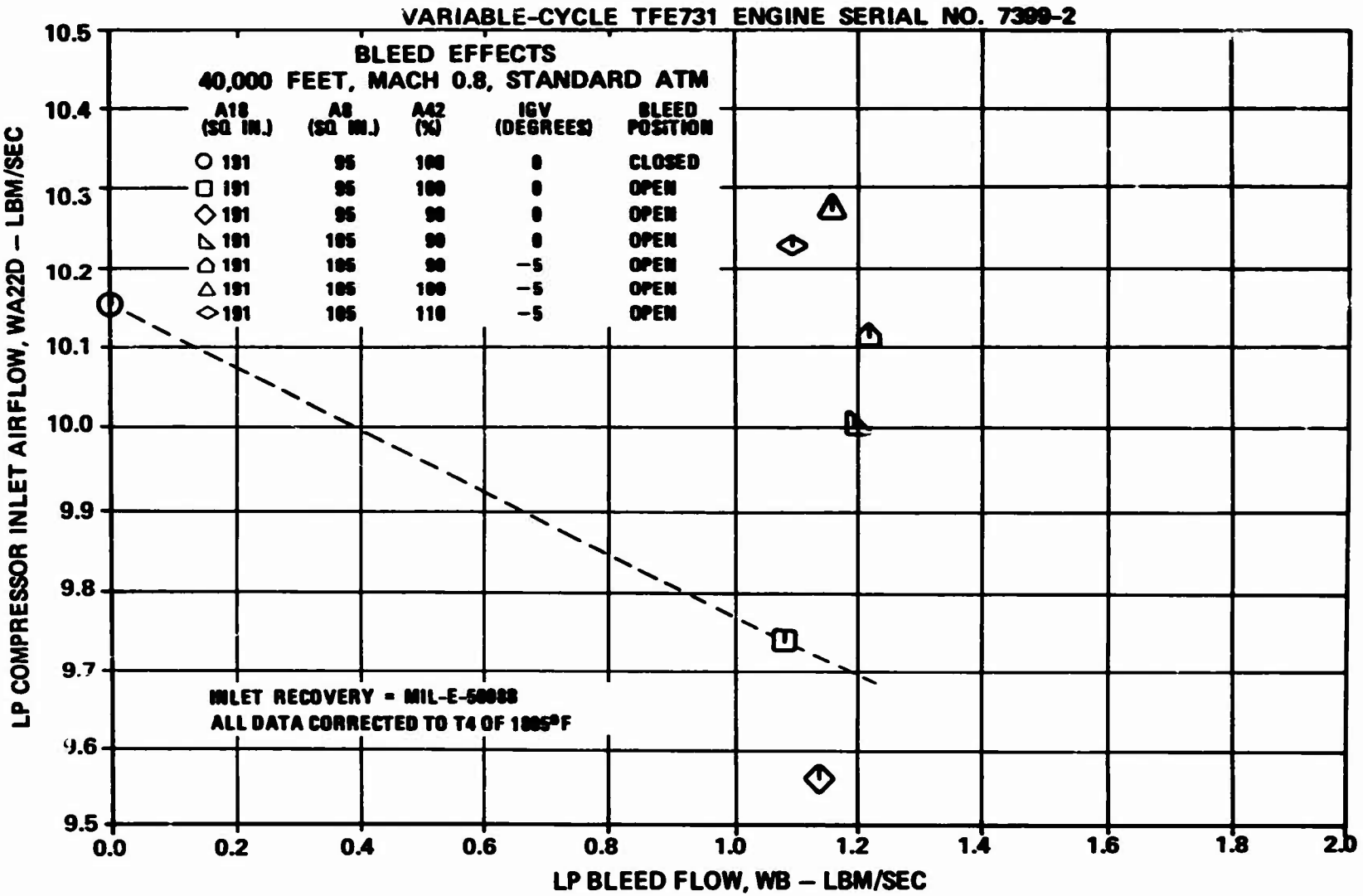

Figure 554. Bleed Effects at Mach 0.8, 40,000 Feet, LP Compressor Inlet Airflow Versus LP Bleed Flow.

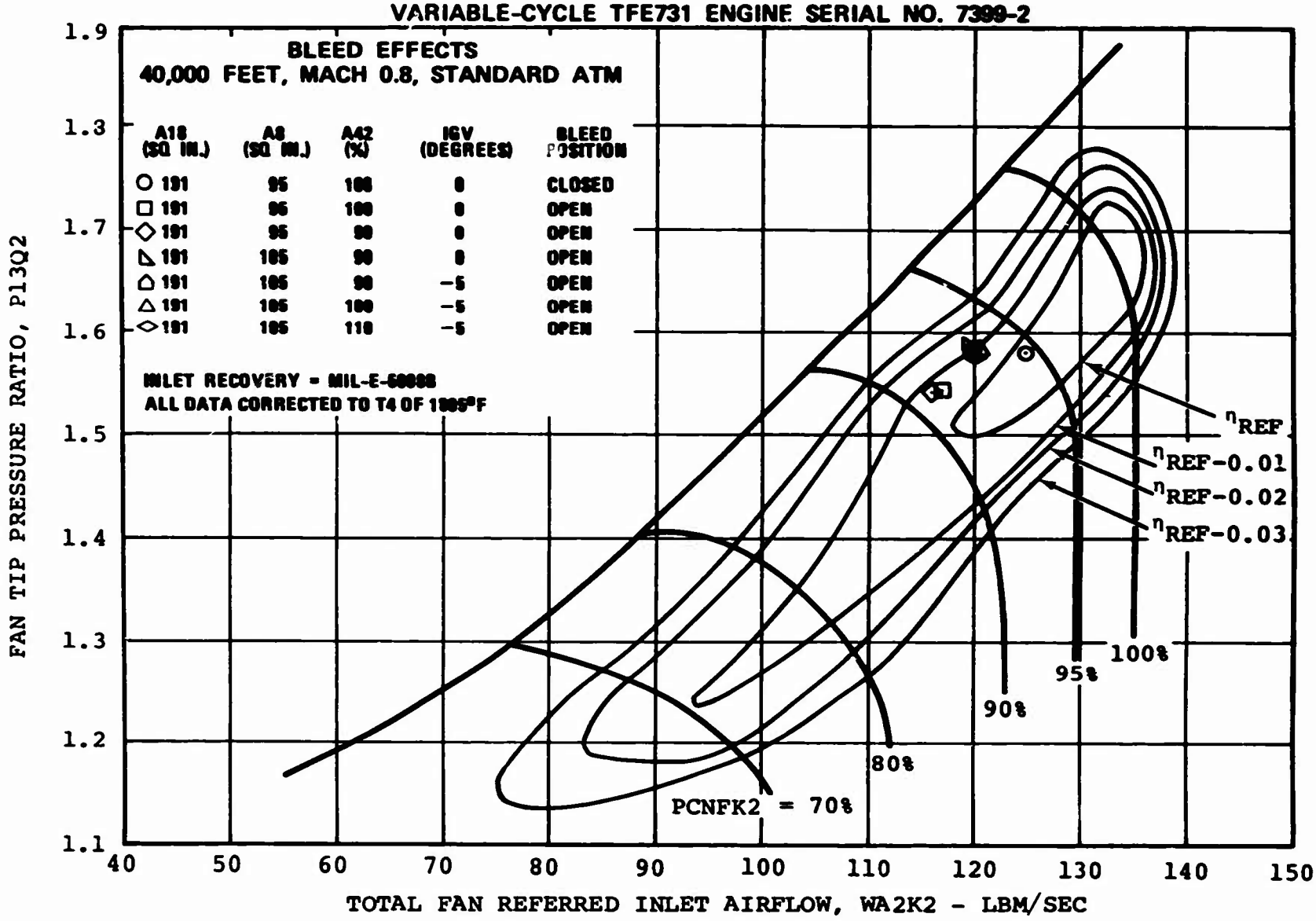

Figure 555. Component Operating Points at Mach 0.8, 40,000 Feet, Superimposed on Fan Tip Map.

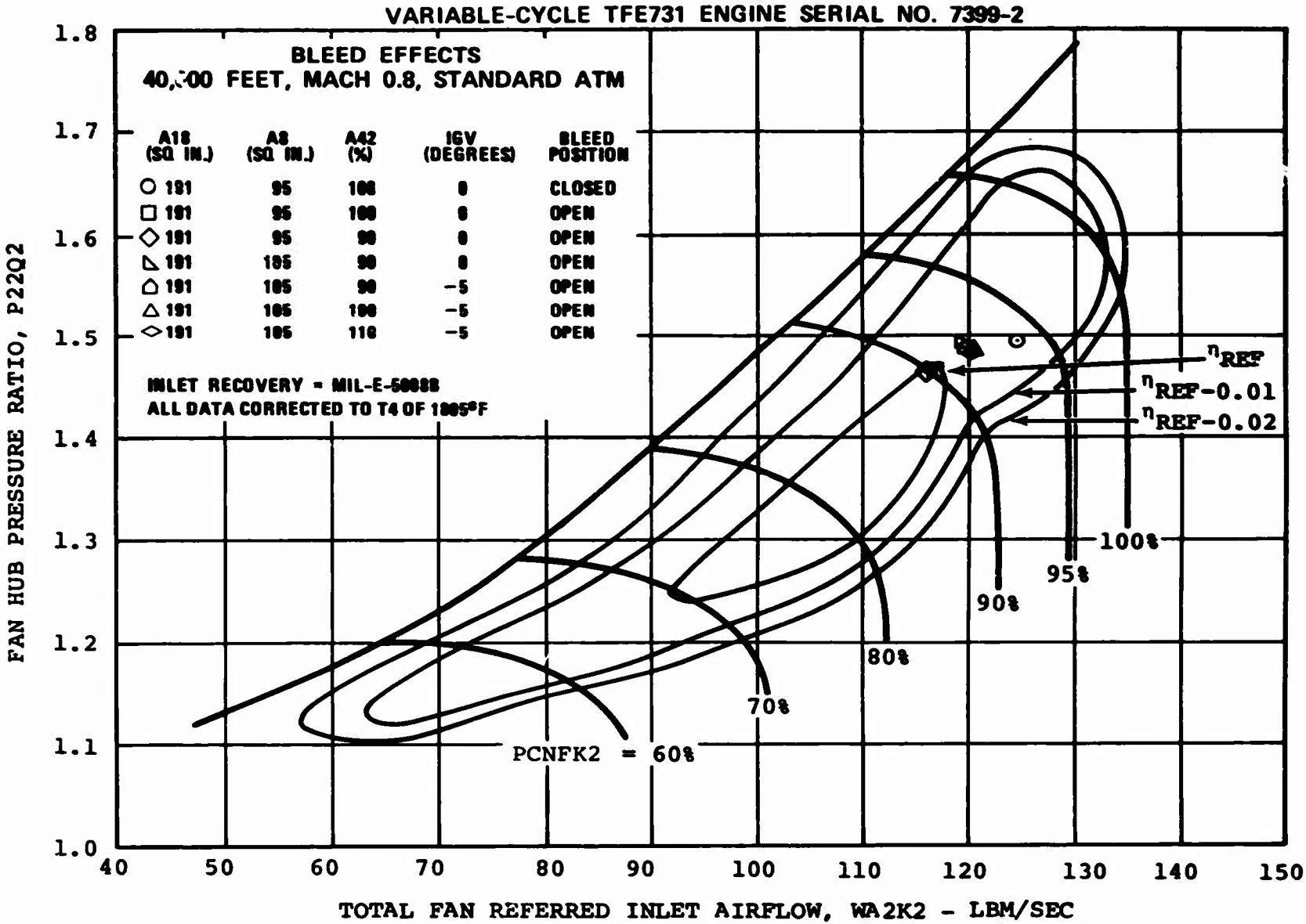

Figure 556. Component Operating Points at Mach 0.8, 40,000 Feet, Superimposed on Fan Hub Map.

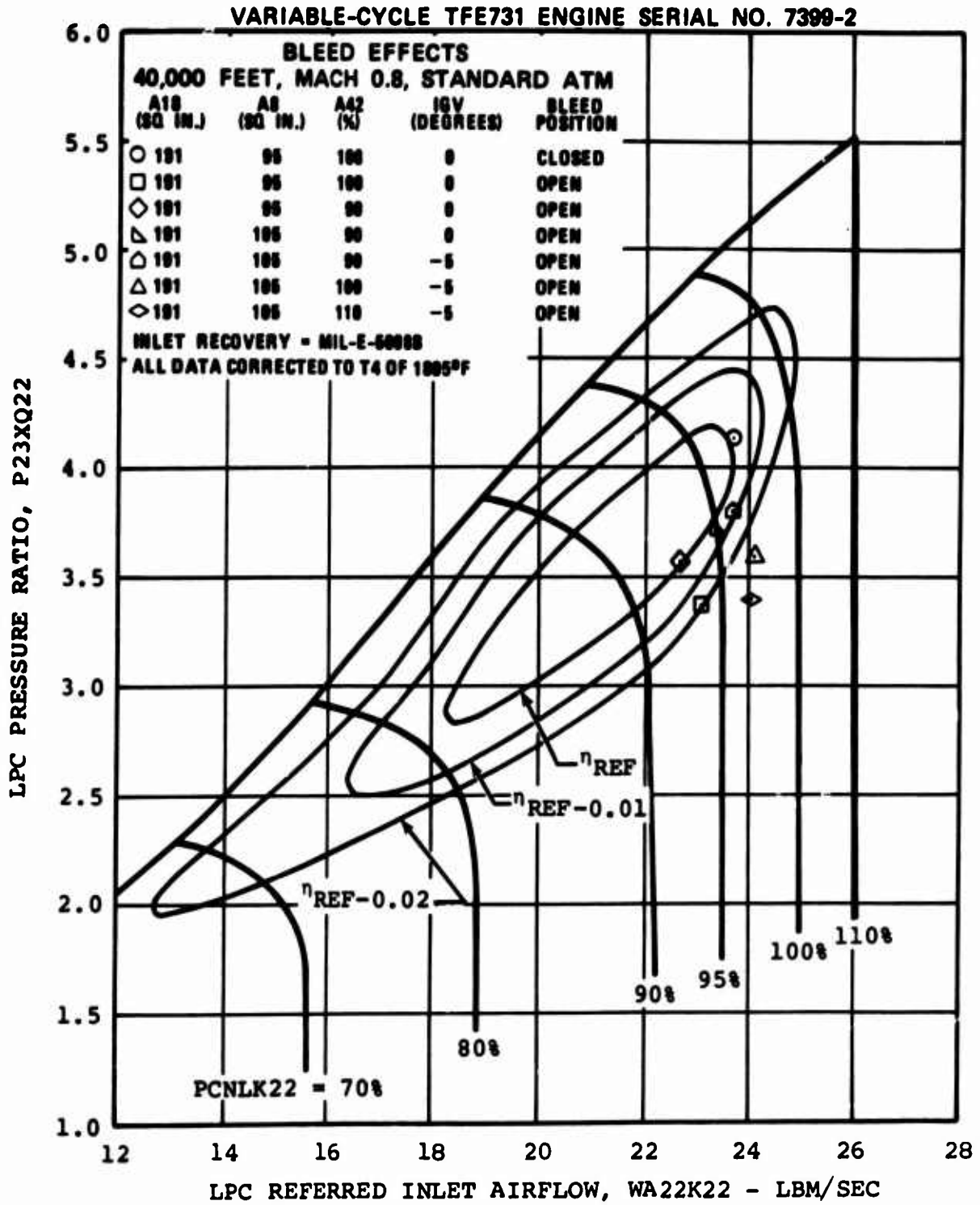

Figure 557. Component Operating Points at Mach 0.8, 40,000 Feet, Superimposed on LP Compressor Map.

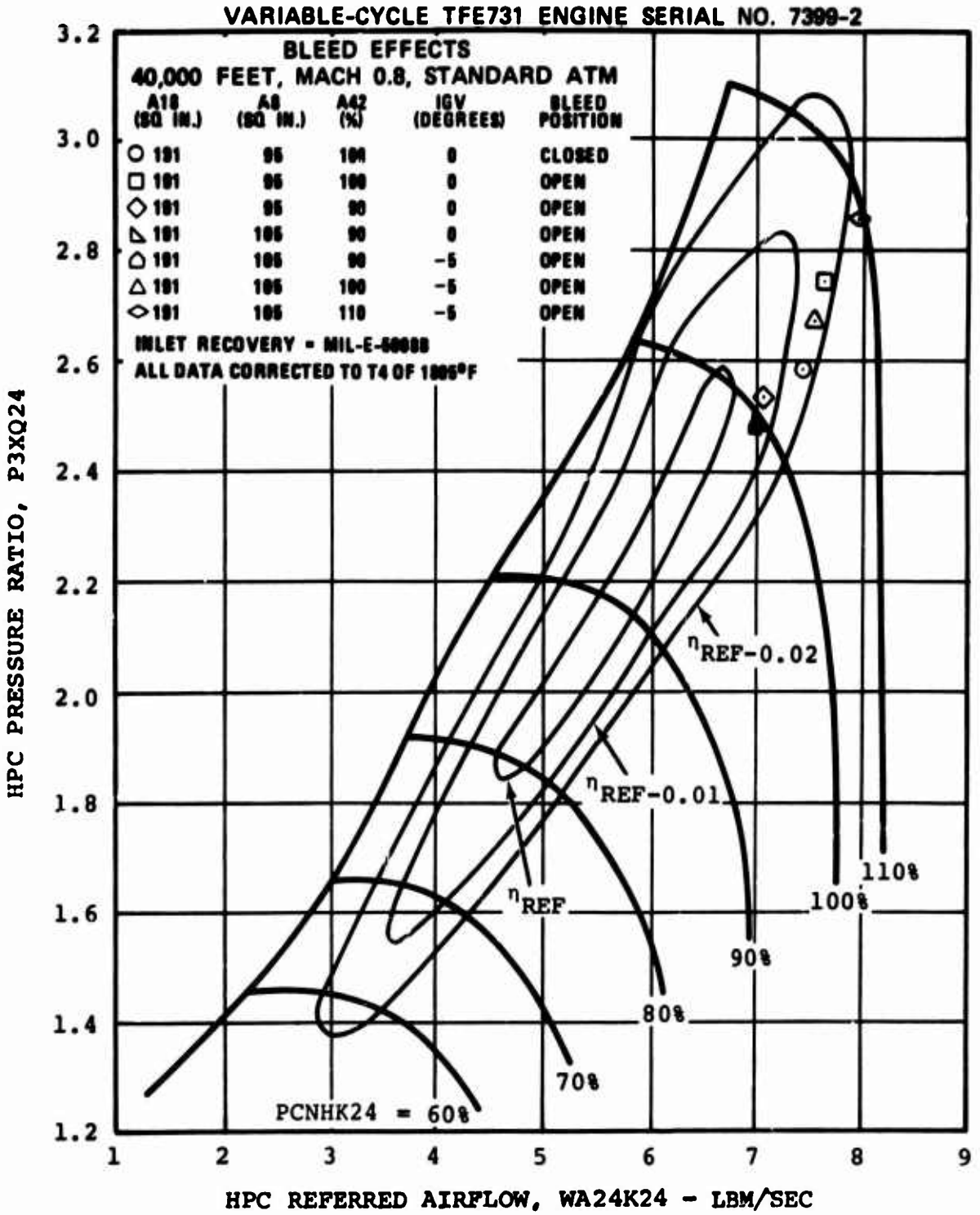

Figure 558. Component Operating Points at Mach 0.8, 40,000 Feet, Superimposed on HP Compressor Map.

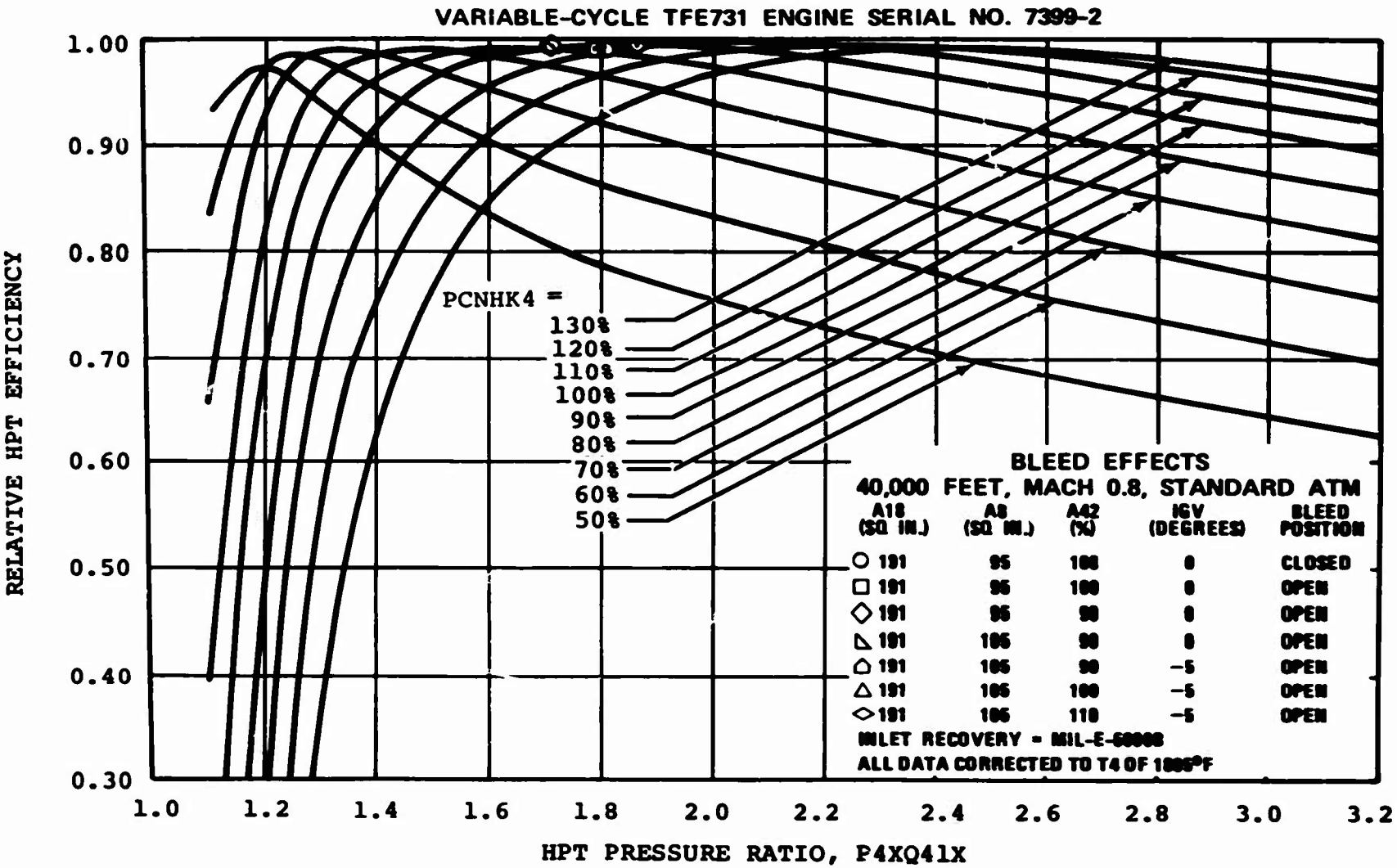

Figure 559. Component Operating Points at Mach 0.8, 40,000 Feet, Superimposed on HP Turbine Map.

essentially the same efficiency islands as those obtained with the previous geometry settings (see Figures 555 through 559).

After increasing the primary exhaust-nozzle area, the LP compressor IGV's were changed to minus 5 degrees. This resulted in an increase in net thrust of 8 pounds (1.3 percent). The minus-5-degree LP compressor operating points are shown in Figure 557 and indicate an increase in airflow and a slight decrease in efficiency. Although these points are plotted on a nominal IGV map, the test data confirms the general order of magnitude of decrease in efficiency indicated on this map.

Following the setting of the IGV's to minus 5 degrees, the LP turbine nozzle area was returned to its nominal value, and a net thrust increase of 13 pounds (2.1 percent) resulted. Returning the LP turbine nozzle area to the nominal value rematched both the LP and the HP compressors away from their peak efficiency islands, while the fan performance was not significantly affected. The increase in LP turbine efficiency gained by returning to the nominal LP turbine nozzle area more than offset the compressor losses to produce the gain in net thrust. This configuration (A18 = 191 square inches, A8 = 105 square inches, A42 = 100 percent, and a -5-degree IGV angle) produced the maximum net thrust while extracting bleed airflow at this flight condition. This net thrust of 647 pounds represents a 6.1-percent increase over the initial bleed condition and a recovery of 32 percent of the net thrust loss due to the bleed-air extraction.

The final configuration entailed an increase in the LP turbine nozzle area to 110 percent. This resulted in further matching the LP and the HP compressors away from their peak efficiencies, while the rate of turbine efficiency increase declined to the extent that the LP turbine efficiency increase was not sufficient to offset the compressor losses. The net thrust decreased by 9 pounds (-1.4 percent). A summary of the bleed test effects at 40,000 feet, Mach 0.8 is presented in Table 68.

TABLE 68. BLEED EFFECTS AT 40,000 FEET, MACH 0.8, STANDARD ATM, AT AN HP TURBINE INLET TEMPERATURE OF 1805°F.

A18 (sq in.)	A8 (sq in.)	A42 (%)	LPC (degrees)	Net Thrust (lbf)	LPC Bleed Rate (lbm/sec)
191	95	100	0	725	0
191	95	100	0	610	1.081
191	95	90	0	605	1.081
191	105	90	0	626	1.081
191	105	90	-5	634	1.081
191	105	100	-5	647	1.081
191	105	110	-5	638	1.081

4.4.8.2 50,000 Feet, Mach 0.8

The results of the bleed testing at 50,000 feet, Mach 0.8, standard atmosphere, are presented in Figures 560 through 573. The parameters presented in these curves are listed in Table 69. All parameters have been corrected to a turbine inlet temperature of 1805°F.

The results of the bleed testing at 50,000 feet, Mach 0.8, show essentially the same trends as those evidenced at 40,000 feet, Mach 0.8. There was, however, one anomaly noted. When the primary exhaust-nozzle area was increased to 105 square inches, the data showed a slight decrease in net thrust and, when the IGV's were changed to minus 5 degrees, there was an increase in net thrust that was larger than expected. This result was not found at the three other bleed test flight conditions. At those conditions, an increase in primary exhaust-nozzle area produced significant net thrust increases, while changing the IGV's to minus 5 degrees produced only slight increases or, in one case, a slight decrease in net thrust. Because of those conflicting results, it is believed that the slight thrust decrease noted with increased primary exhaust-nozzle area at 50,000 feet, Mach 0.8, may be in error.

At this test condition, the maximum net thrust increase over that of the base bleed point was 26 pounds (7.2 percent), which represents a recovery of 42 percent of the net thrust loss due to the bleed-air extraction.

During the bleed testing at 50,000 feet, Mach 0.8, an LP compressor IGV setting of minus 10 degrees and a fan exhaust nozzle area of 200 square inches were also tested. Neither of these configurations improved engine performance. A summary of the results of the 50,000 feet, Mach 0.8 bleed testing is presented in Table 70.

TABLE 69. BLEED EFFECTS, 50,000 FEET, MACH 0.8, STANDARD ATM

Figure No.	Parameters Presented
560	Turbine inlet temperature versus LP bleed flow
561	Thrust specific fuel consumption versus LP bleed flow
562	Net thrust versus LP bleed flow
563	Fuel flow versus LP bleed flow
564	Interturbine temperature versus LP bleed flow
565	LP rotor speed versus LP bleed flow
566	HP rotor speed versus LP bleed flow
567	Engine total airflow versus LP bleed flow
568	Fan tip pressure ratio versus LP bleed flow
569	Fan hub pressure ratio versus LP bleed flow
570	Cycle pressure ratio versus LP bleed flow
571	Bypass ratio versus lP bleed flow
572	Engine pressure ratio versus LP bleed flow
573	LP compressor inlet airflow versus LP bleed flow

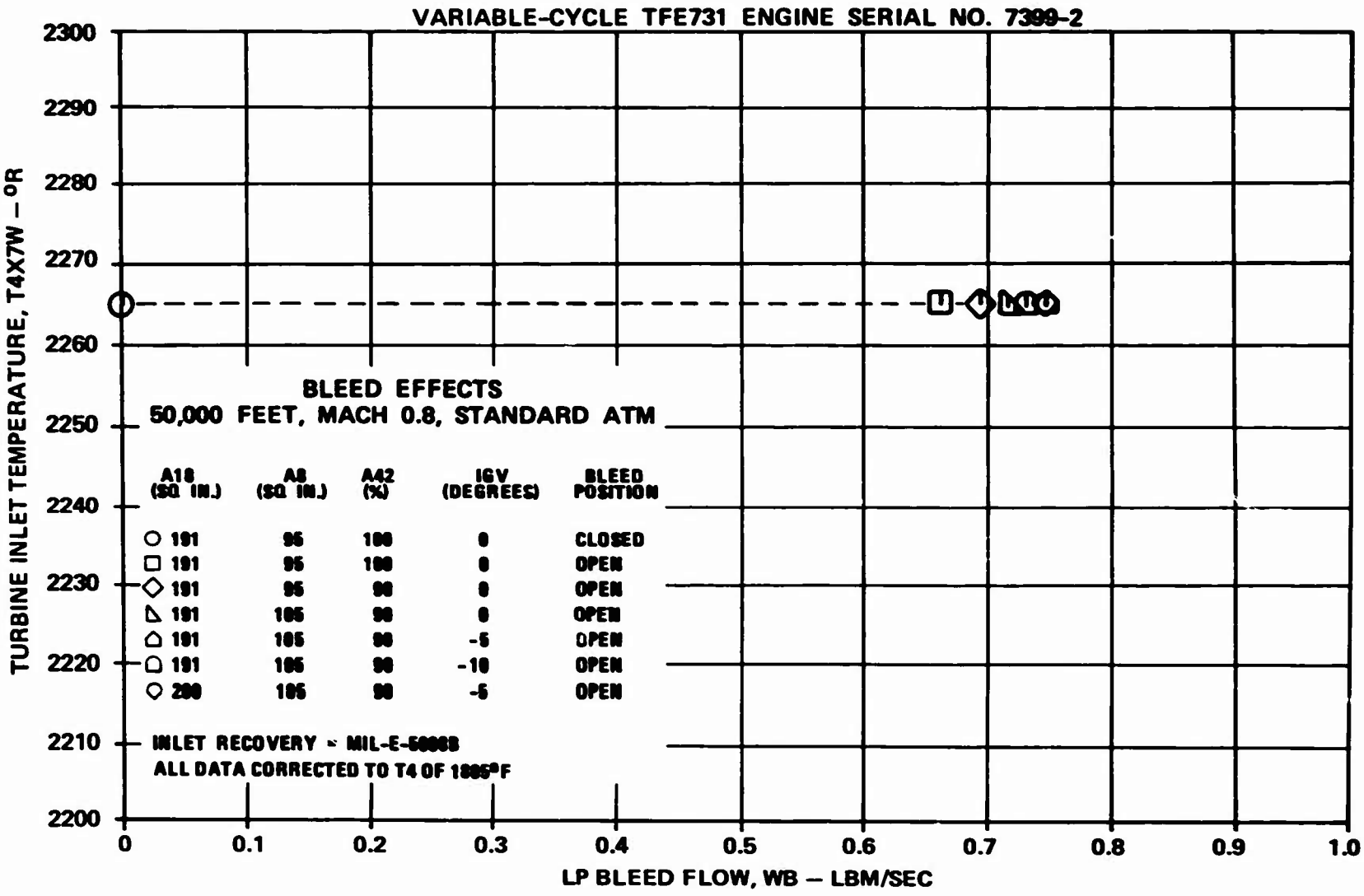

Figure 560. Bleed Effects at Mach 0.8, 50,000 Feet, Turbine Inlet Temperature Versus LP Bleed Flow.

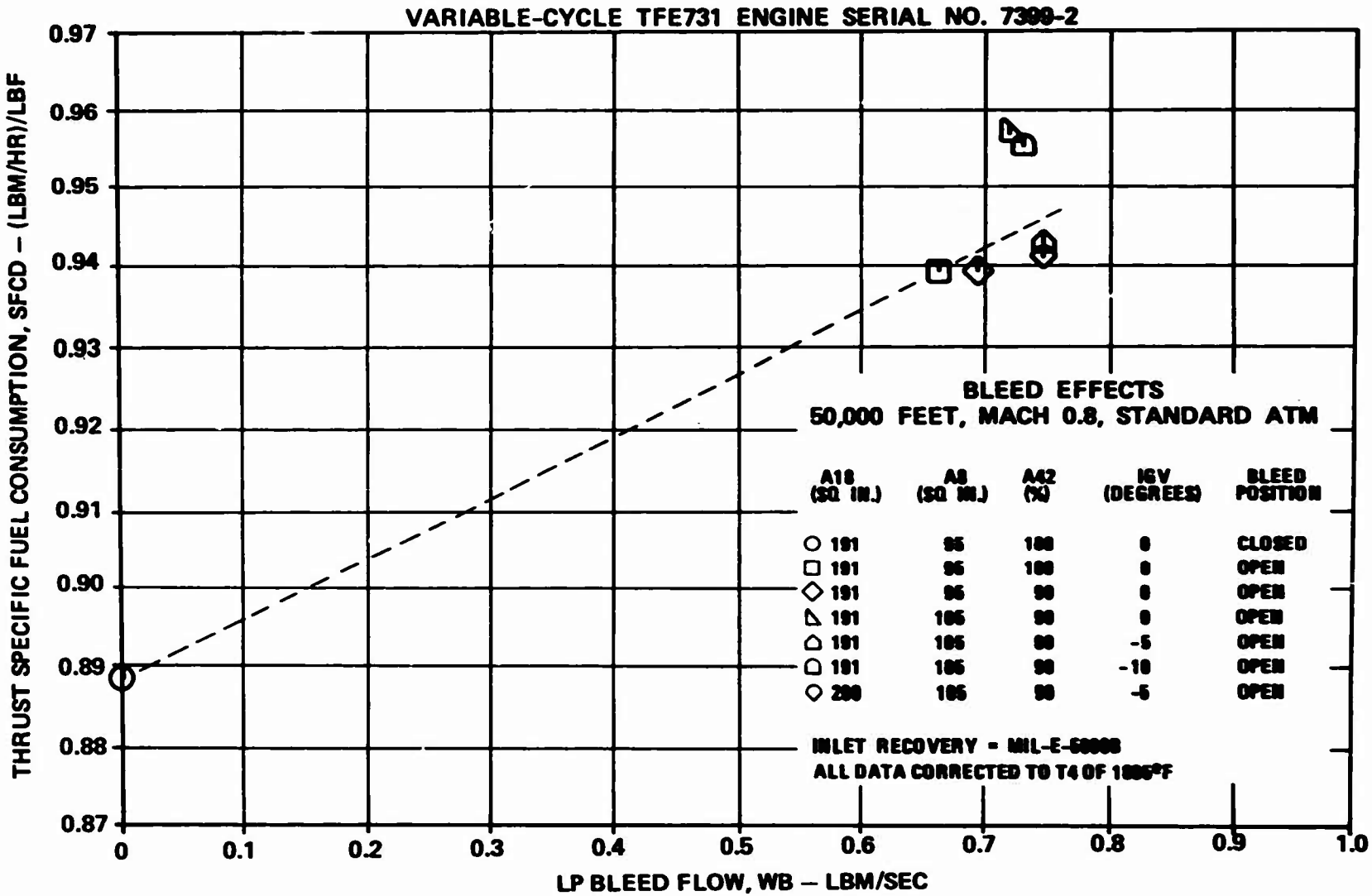

Figure 561. Bleed Effects at Mach 0.8, 50,000 Feet, Thrust Specific Fuel Consumption Versus LP Bleed Flow.

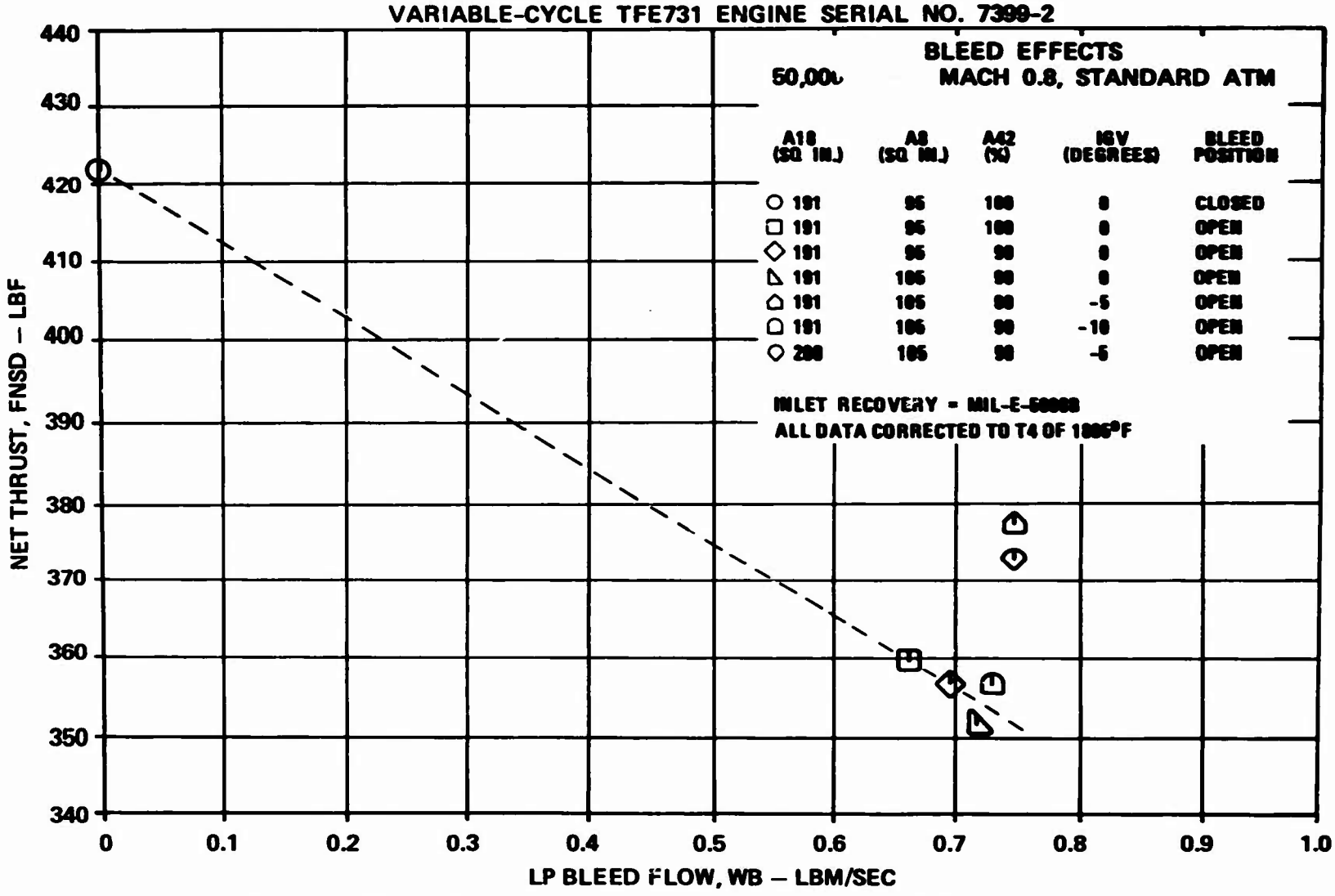

Figure 562. Bleed Effects at Mach 0.8, 50,000 Feet, Net Thrust Versus LP Bleed Flow.

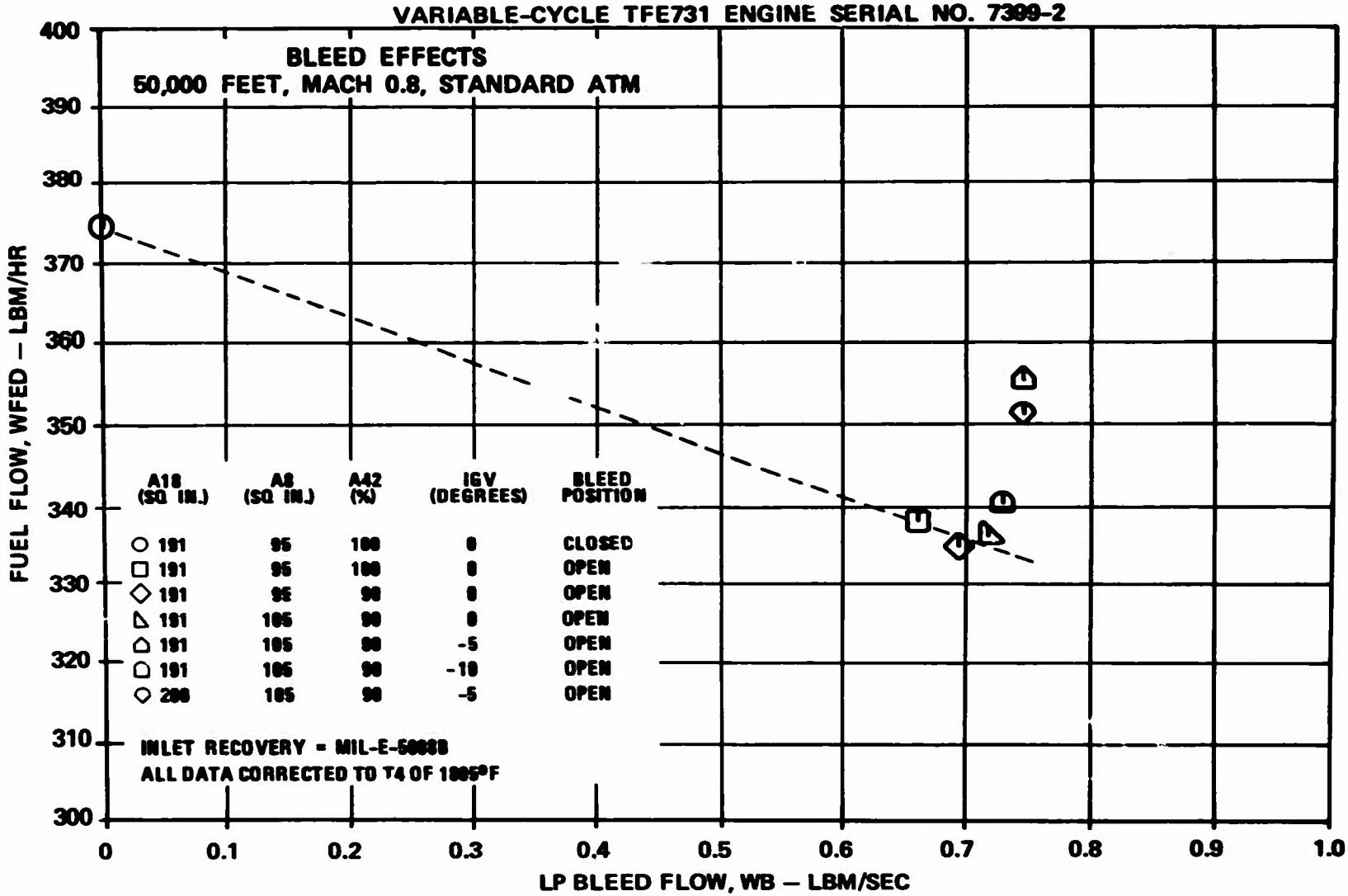

Figure 563. Bleed Effects at Mach 0.8, 50,000 Feet, Fuel Flow Versus LP Bleed Flow.

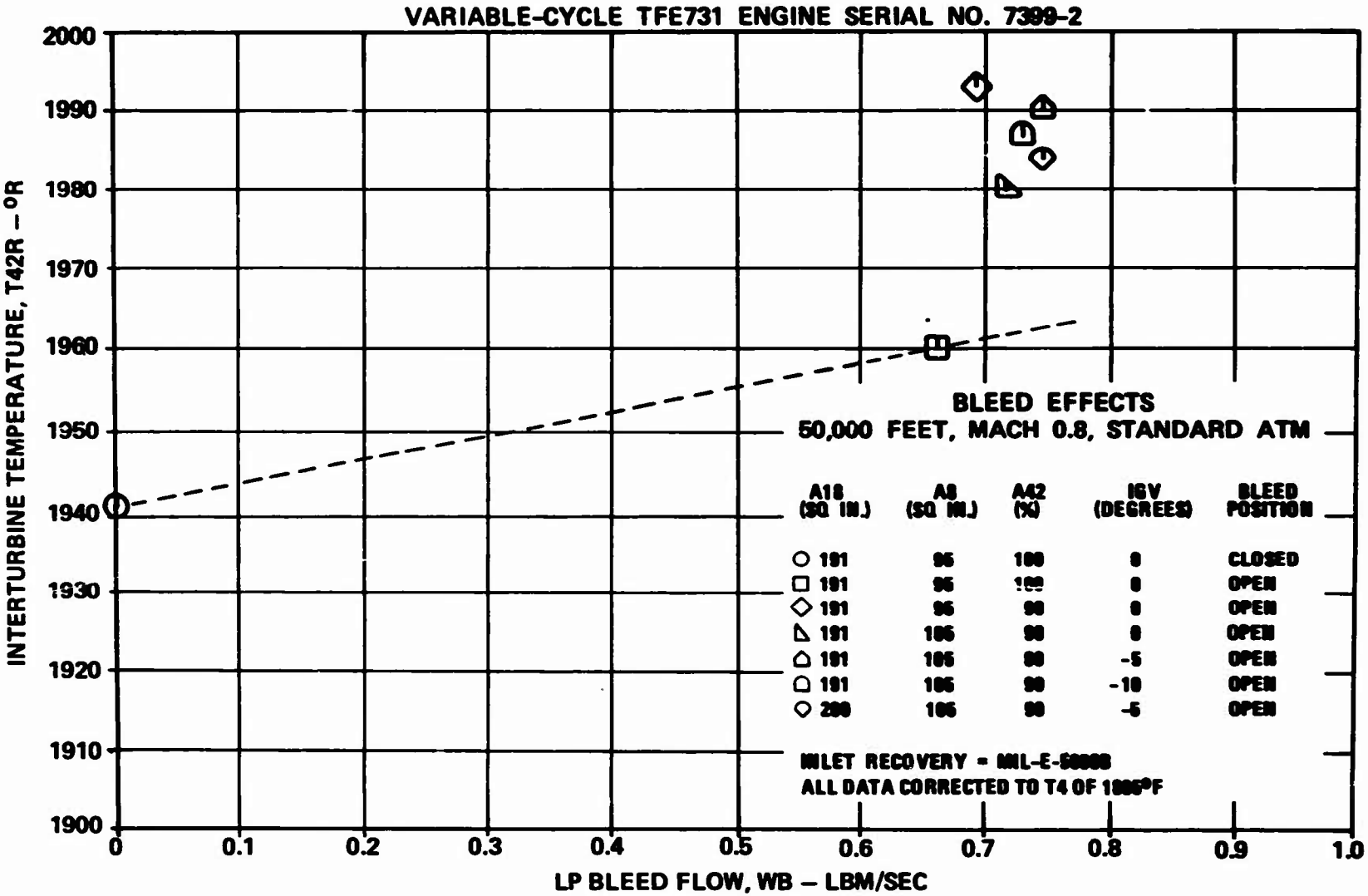

Figure 564. Bleed Effects at Mach 0.8, 50,000 Feet, Interturbine Temperature Versus LP Bleed Flow.

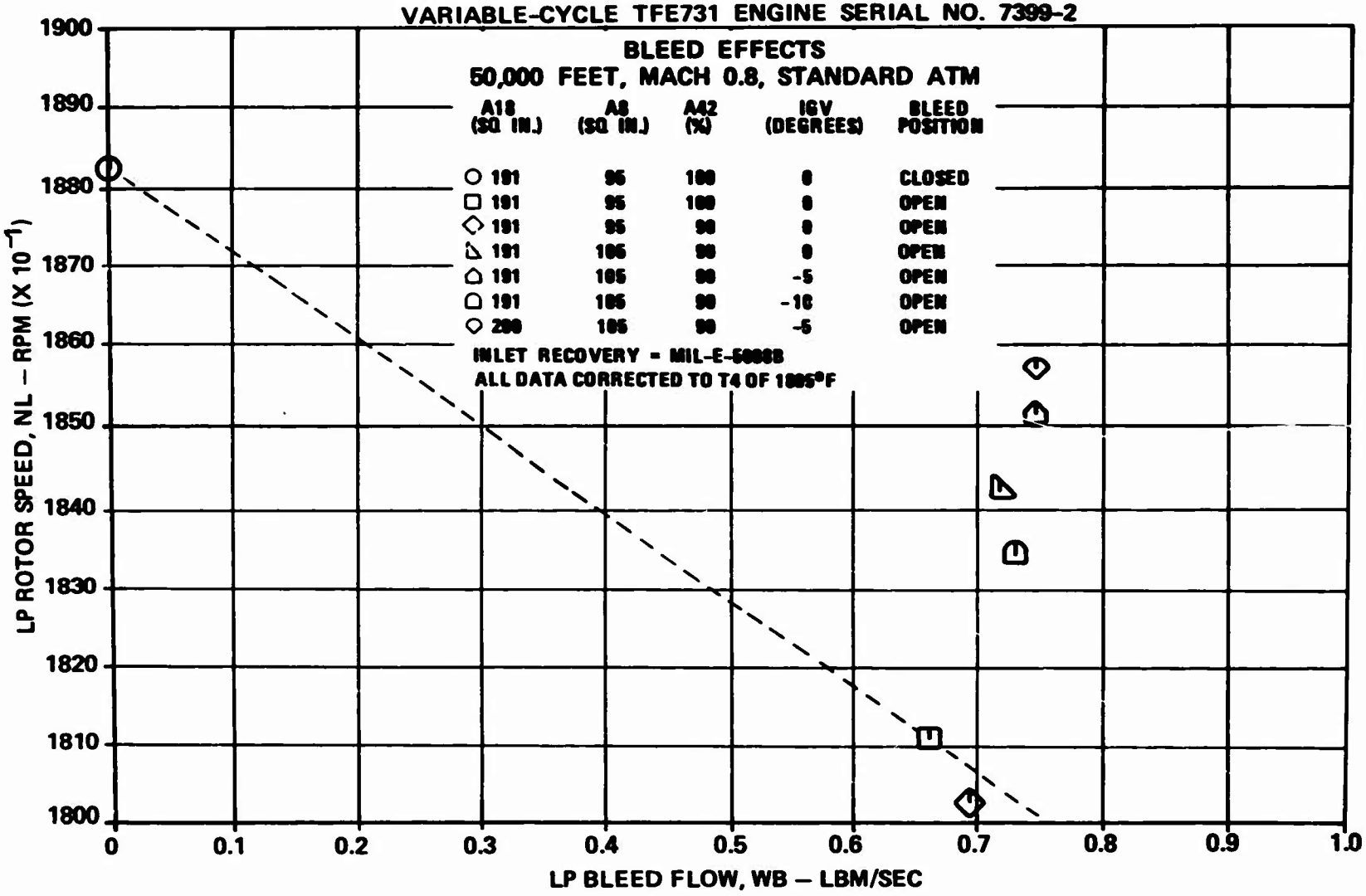

Figure 565. Bleed Effects at Mach 0.8, 50,000 Feet, LP Rotor Speed Versus LP Bleed Flow.

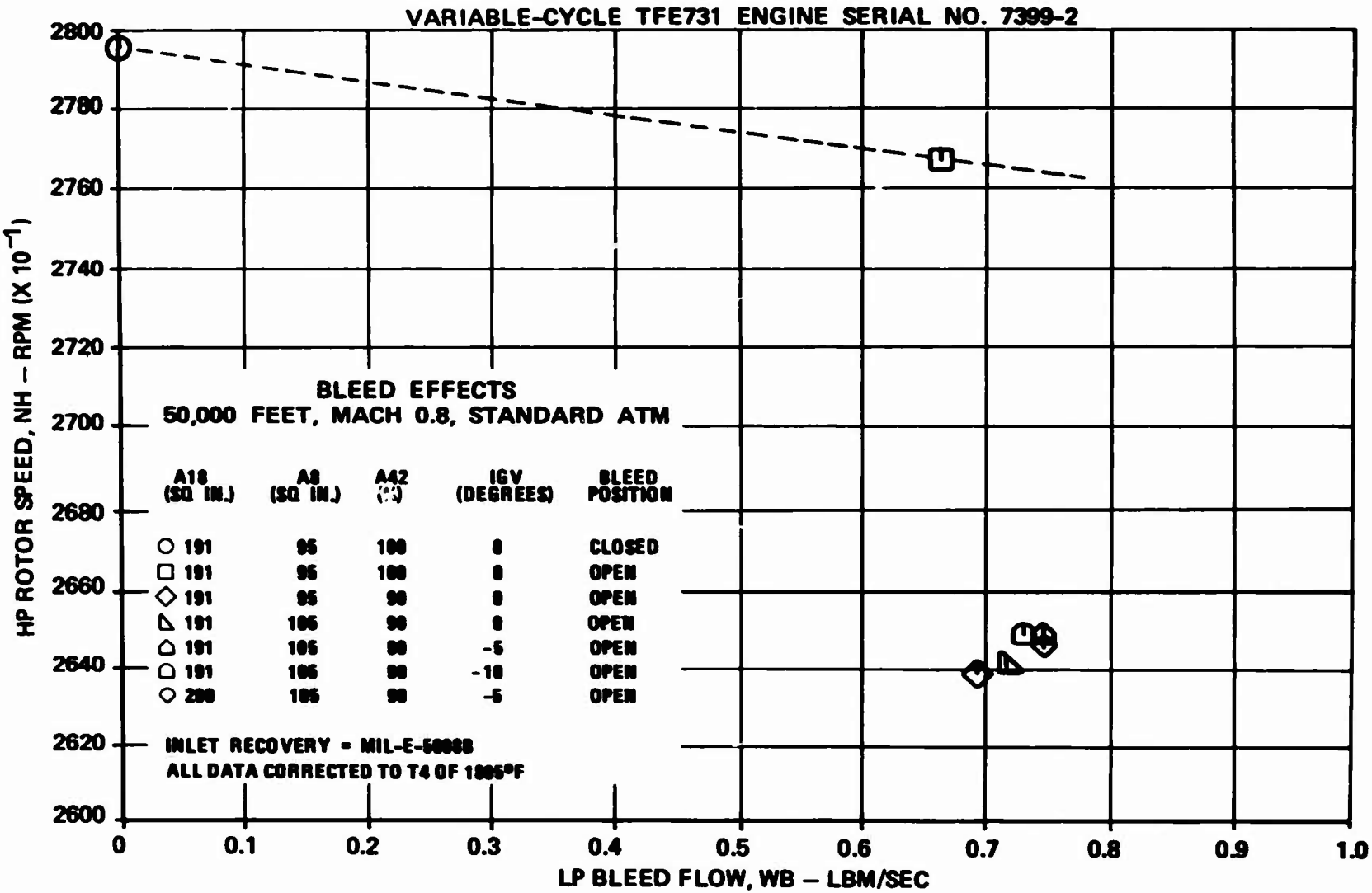

Figure 566. Bleed Effects at Mach 0.8, 50,000 Feet, HP Rotor Speed Versus LP Bleed Flow.

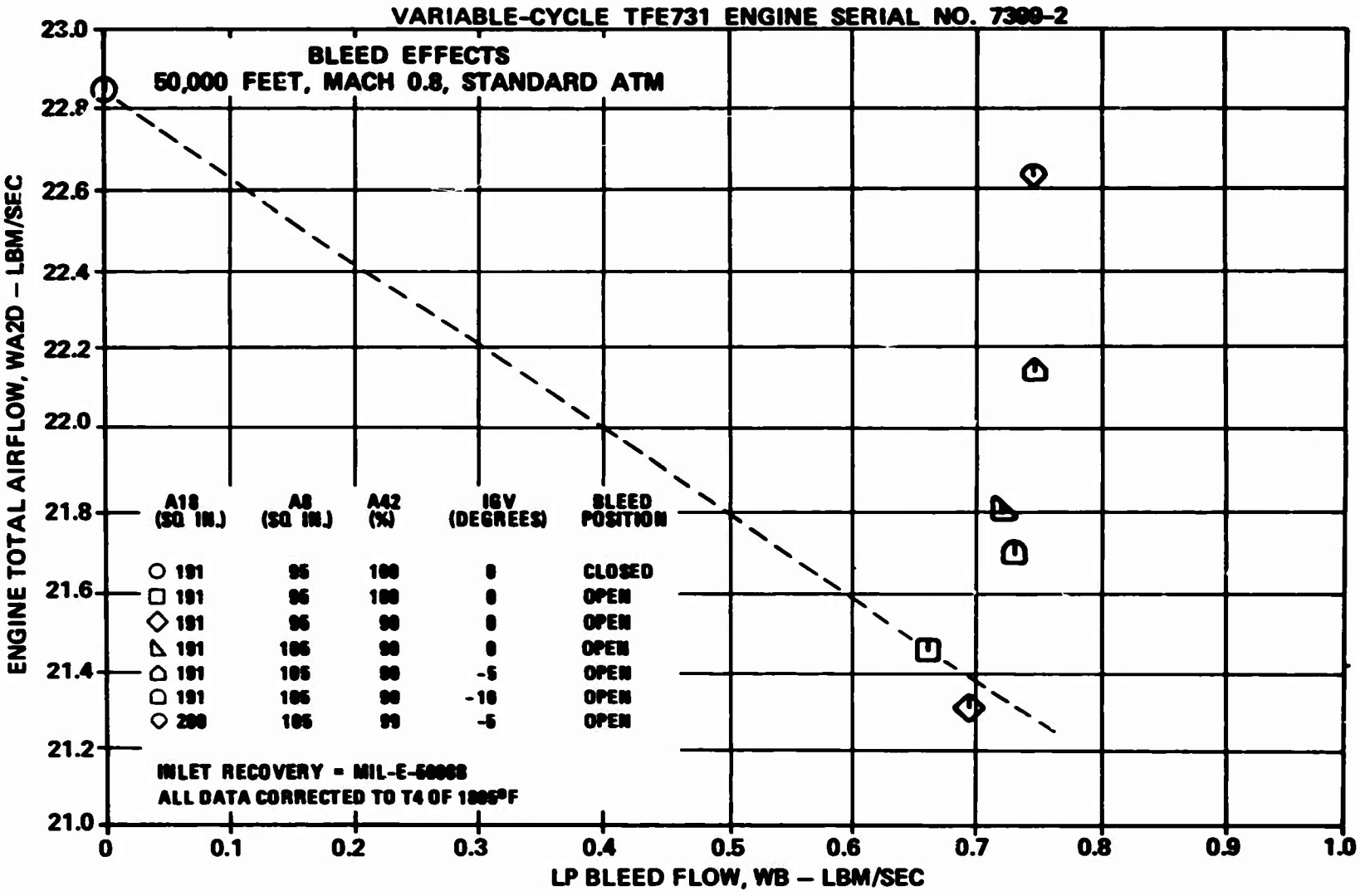

Figure 567. Bleed Effects at Mach 0.8, 50,000 Feet, Engine Total Airflow Versus LP Bleed Flow.

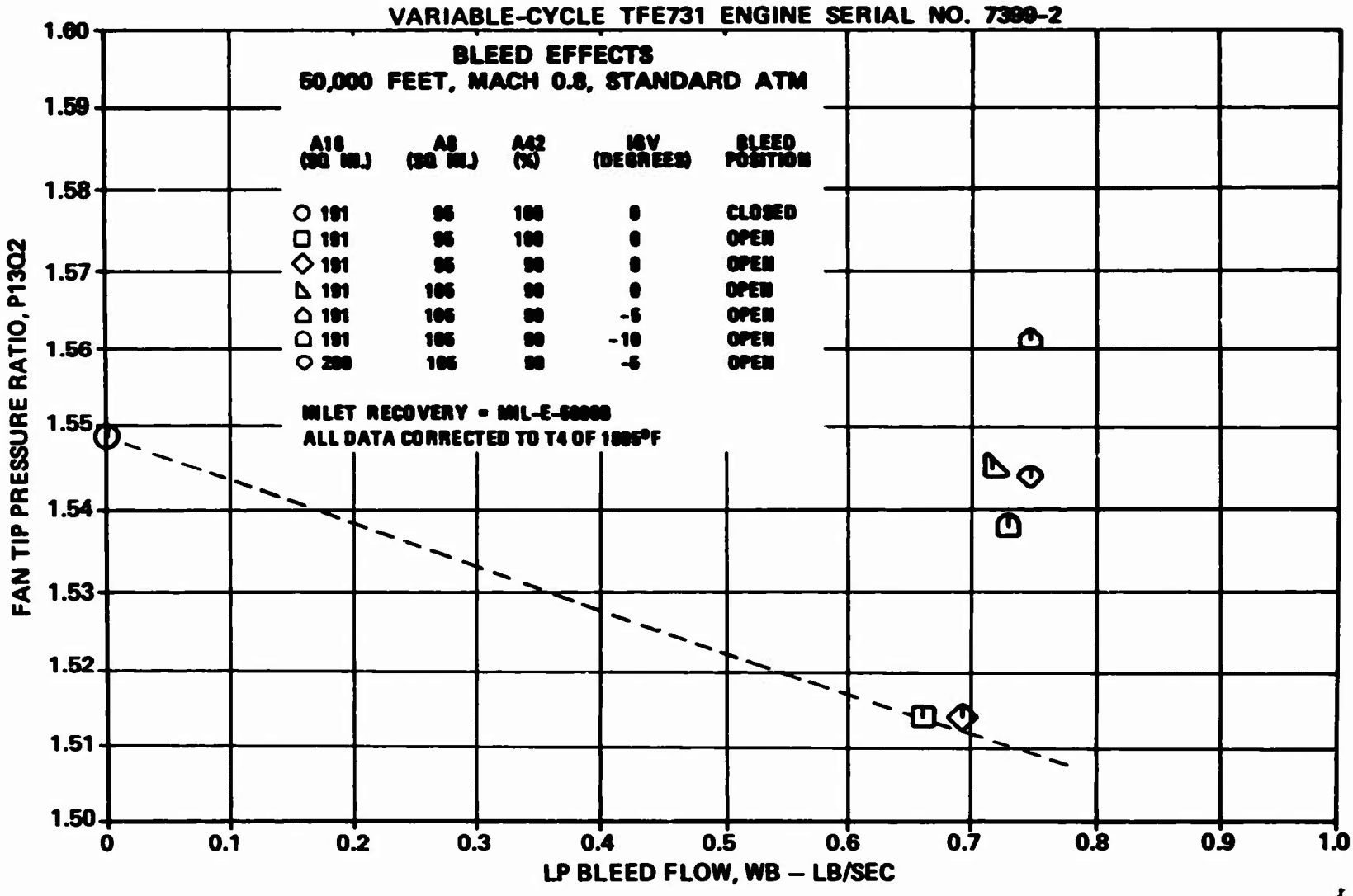

Figure 568. Bleed Effects at Mach 0.8, 50,000 Feet, Fan Tip Pressure Ratio Versus LP Bleed Flow.

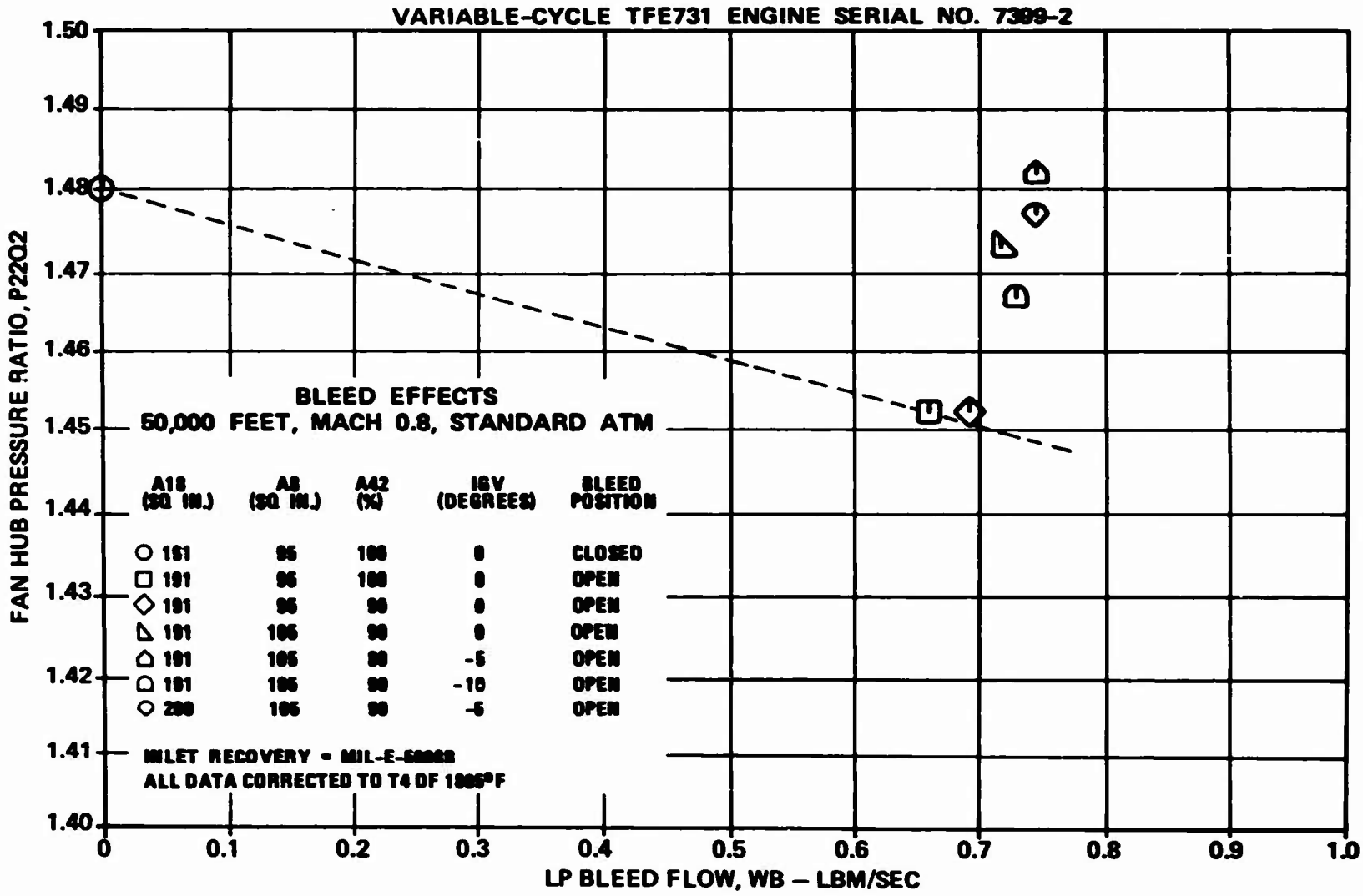

Figure 569. Bleed Effects at Mach 0.8, 50,000 Feet, Fan Hub Pressure Ratio Versus LP Bleed Flow.

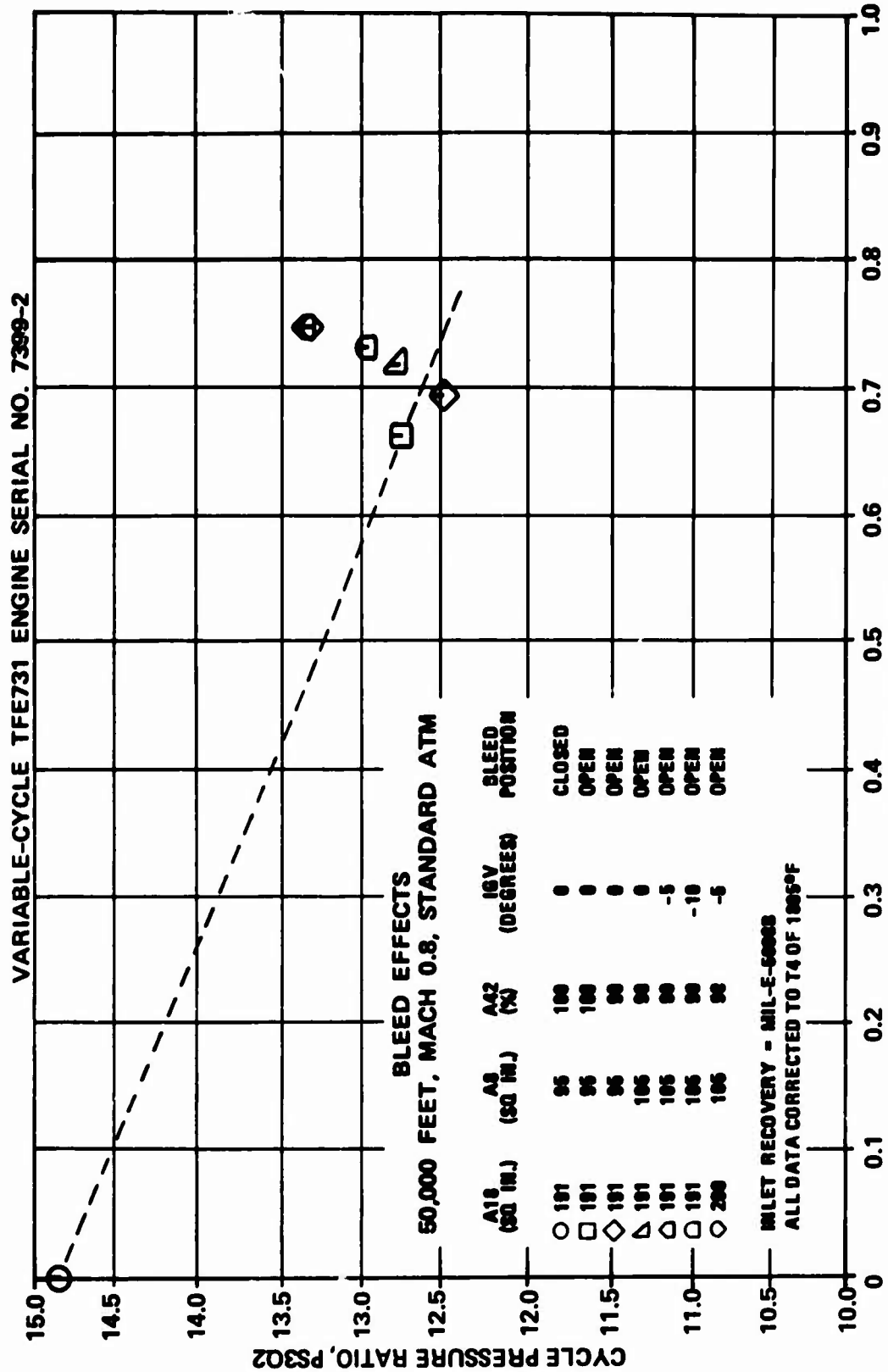

Figure 570. Bleed Effects at Mach 0.8, 50,000 Feet, Cycle Pressure Ratio Versus LP Bleed Flow.

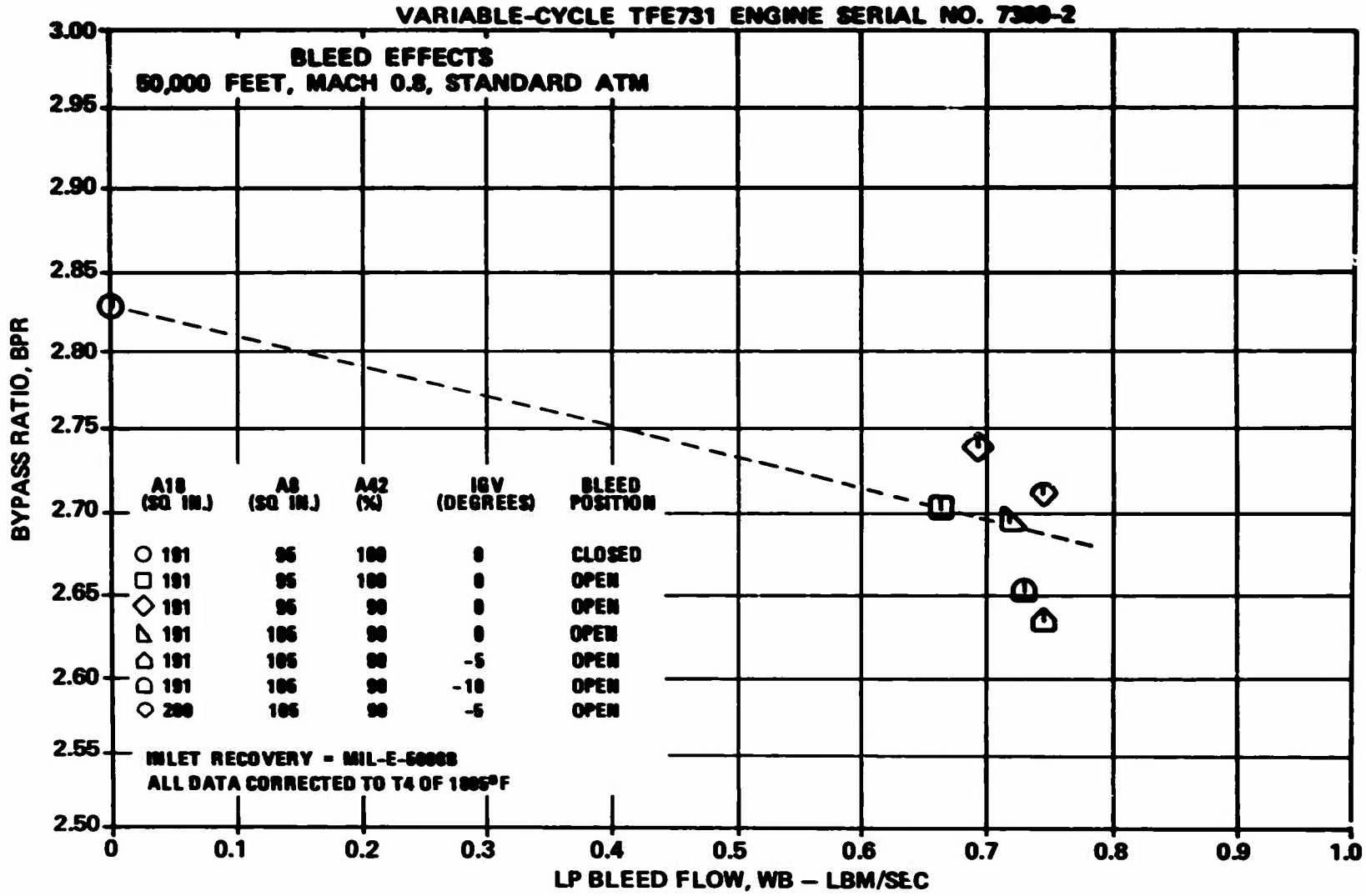

Figure 571. Bleed Effects at Mach 0.8, 50,000 Feet, Bypass Ratio Versus LP Bleed Flow.

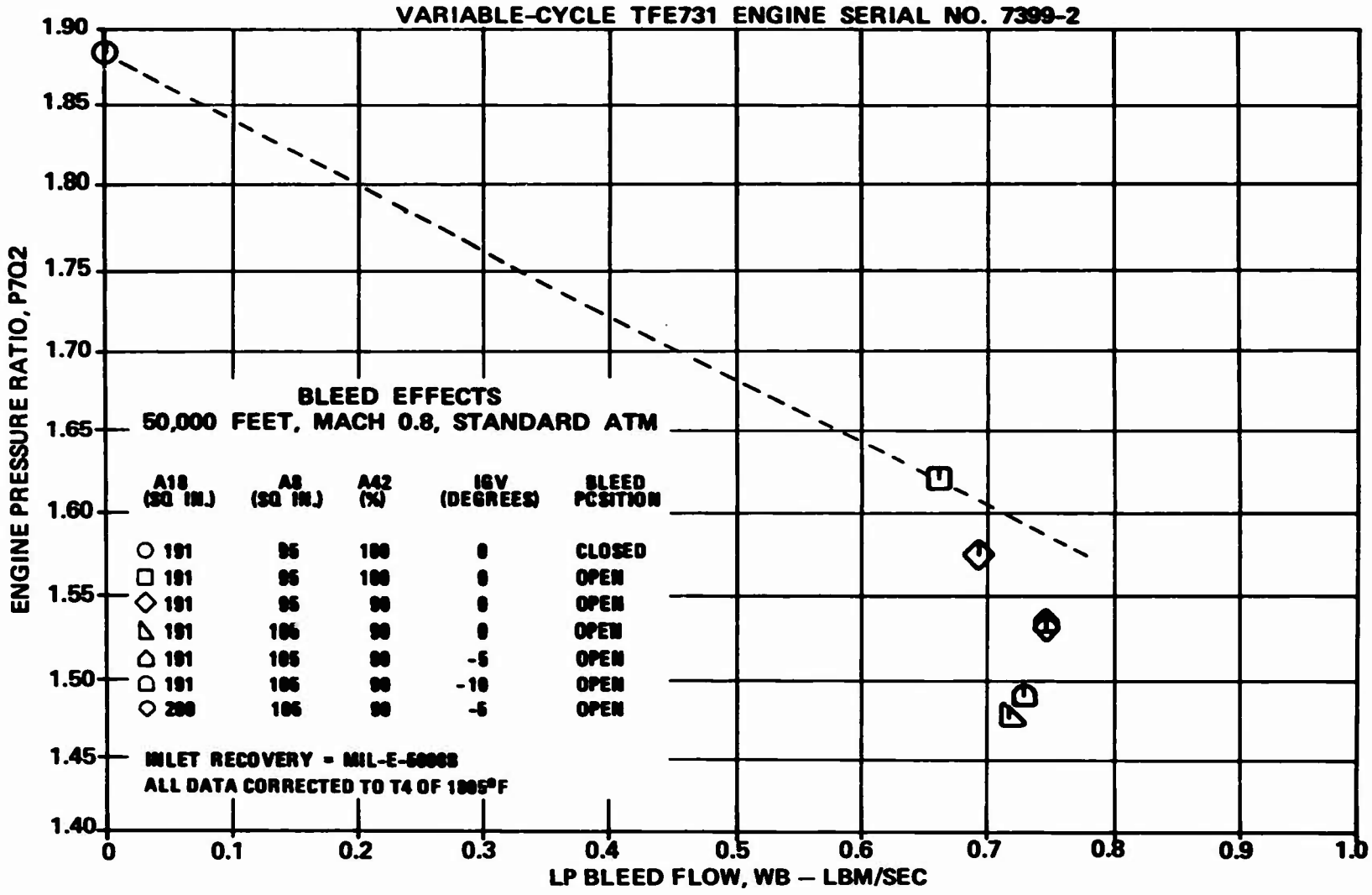

Figure 572. Bleed Effects at Mach 0.8, 50,000 Feet, Engine Pressure Ratio Versus LP Bleed Flow.

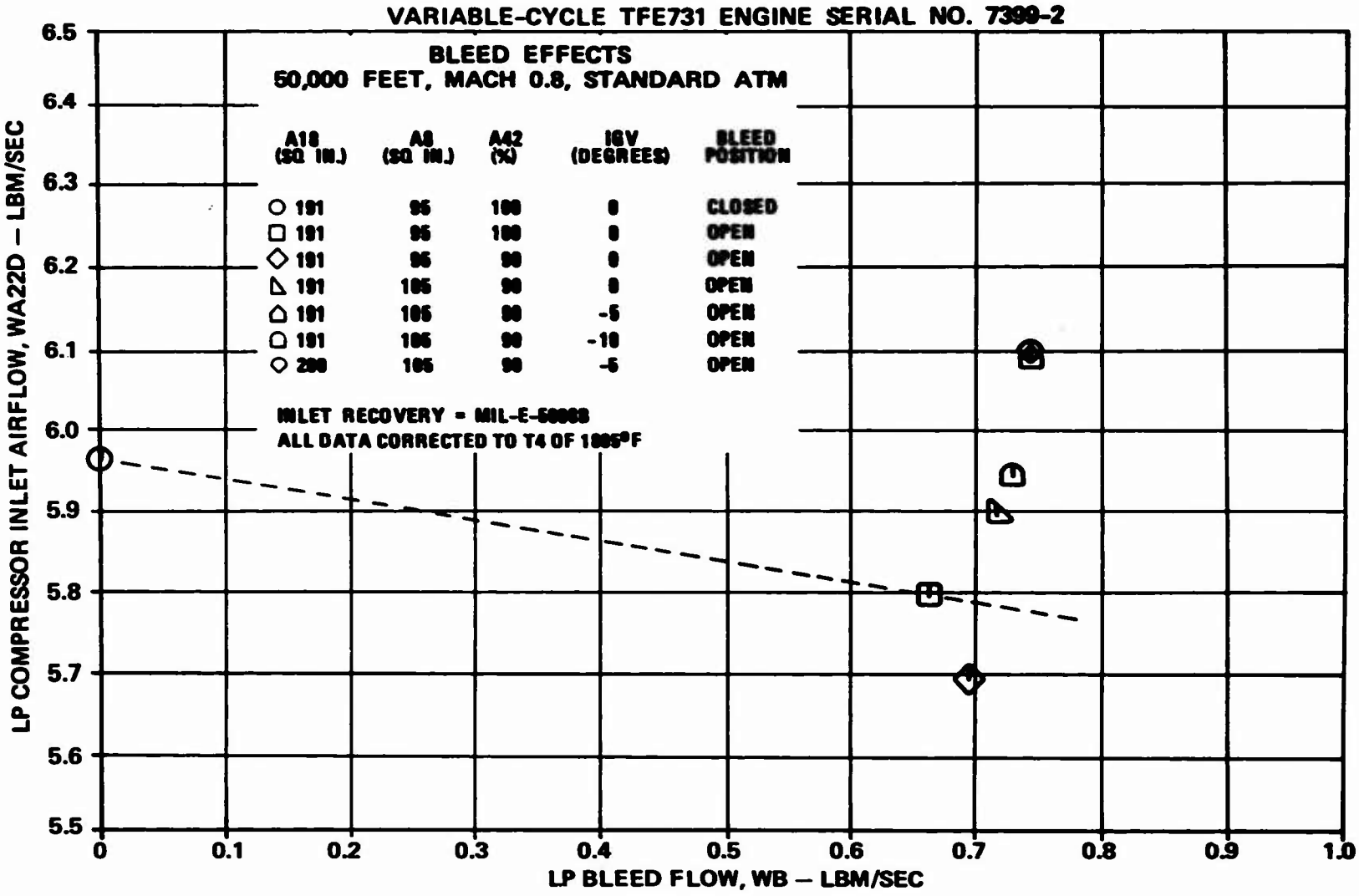

Figure 573. Bleed Effects at Mach 0.8, 50,000 Feet, LP Compressor Inlet Airflow Versus LP Bleed Flow.

TABLE 70. BLEED EFFECTS, 50,000 FEET, MACH 0.8, STANDARD ATM, AT AN HP TURBINE INLET TEMPERATURE OF 1805°F.

A18 (sq in.)	A8 (sq in.)	A42 (%)	LPC (degrees)	Net Thrust (lbf)	LPC Bleed Rate (lbm/sec)
191	95	100	0	422	0
191	95	100	0	360	0.6613
191	95	90	0	360	0.6613
191	105	90	0	357	0.6613
191	105	90	-5	386	0.6613
191	105	90	-10	363	0.6613
200	105	90	-5	382	0.6613

4.4.8.3 50,000 Feet, Mach 1.2

The results of the bleed testing at 50,000 feet, Mach 1.2, standard atmosphere, are presented in Figures 574 through 587. The parameters presented in the curves are listed in Table 71. All parameters have been corrected to a turbine inlet temperature of 1805°F.

The results of the bleed testing at 50,000 feet, Mach 1.2, show the same general trends exhibited at the previous conditions discussed. During the 50,000 feet, Mach 1.2 testing, the maximum net thrust increase over that of the base bleed point was 27 pounds (7.3 percent), which represents a recovery of 47 percent of the net thrust lost due to the LP compressor bleed.

During the bleed testing at this flight condition, the effect of an LP turbine nozzle area of 105 percent was determined. This LP turbine nozzle area did produce a small net thrust increase and is near the maximum A42 value that will produce a net thrust increase. From the net thrust increase, it can be seen that, at 105 percent A42, the increase in turbine efficiency still offsets the loss in compressor efficiency, but at 110 percent LP turbine nozzle area the compressor efficiency loss more than offsets the LP turbine efficiency increase. As discussed earlier in Paragraph 4.4.8.1, use of a 110-percent LP turbine nozzle area reduces net thrust due to the losses in compressor efficiency.

A summary of the 50,000-feet, Mach 1.2 bleed testing is presented in Table 72.

TABLE 71. BLEED EFFECTS, 50,000 FEET, MACH 1.2, STANDARD ATM

Figure No.	Parameters Presented
574	Turbine inlet temperature versus LP bleed flow
575	Thrust specific fuel consumption versus LP bleed flow
576	Net thrust versus LP bleed flow
577	Fuel flow versus LP bleed flow
578	Interturbine temperature versus LP bleed flow
579	LP rotor speed versus LP bleed flow
580	HP rotor speed versus LP bleed flow
581	Engine total airflow versus LP bleed flow
582	Fan tip pressure ratio versus LP bleed flow
583	Fan hub pressure ratio versus LP bleed flow
584	Cycle pressure ratio versus LP bleed flow
585	Bypass ratio versus LP bleed flow
586	Engine pressure ratio versus LP bleed flow
587	LP compressor inlet airflow versus LP bleed flow

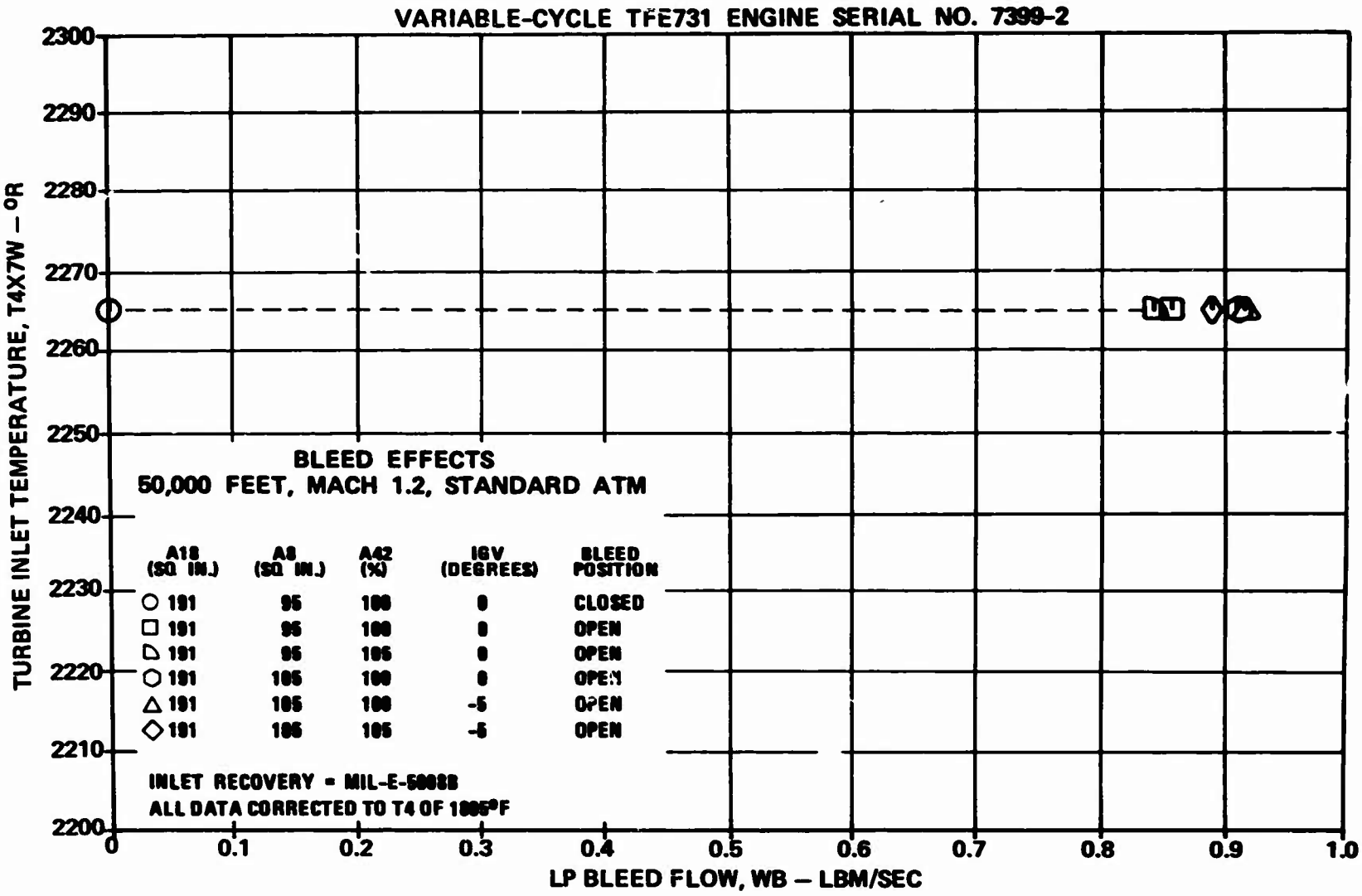

Figure 574. Bleed Effects at Mach 1.2, 50,000 Feet, Turbine Inlet Temperature Versus LP Bleed Flow.

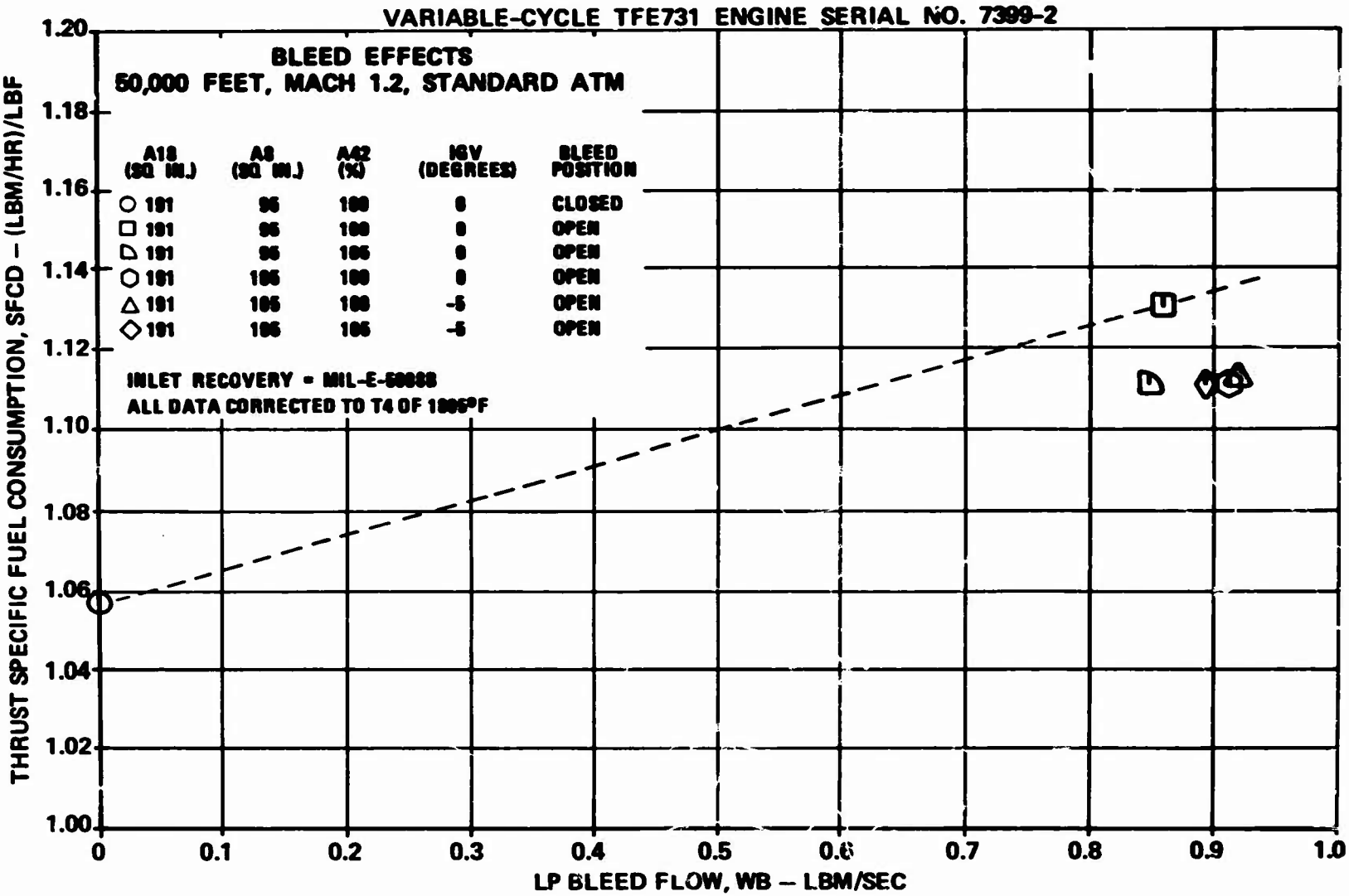

Figure 575. Bleed Effects at Mach 1.2, 50,000 Feet, Thrust Specific Fuel Consumption Versus LP Bleed Flow.

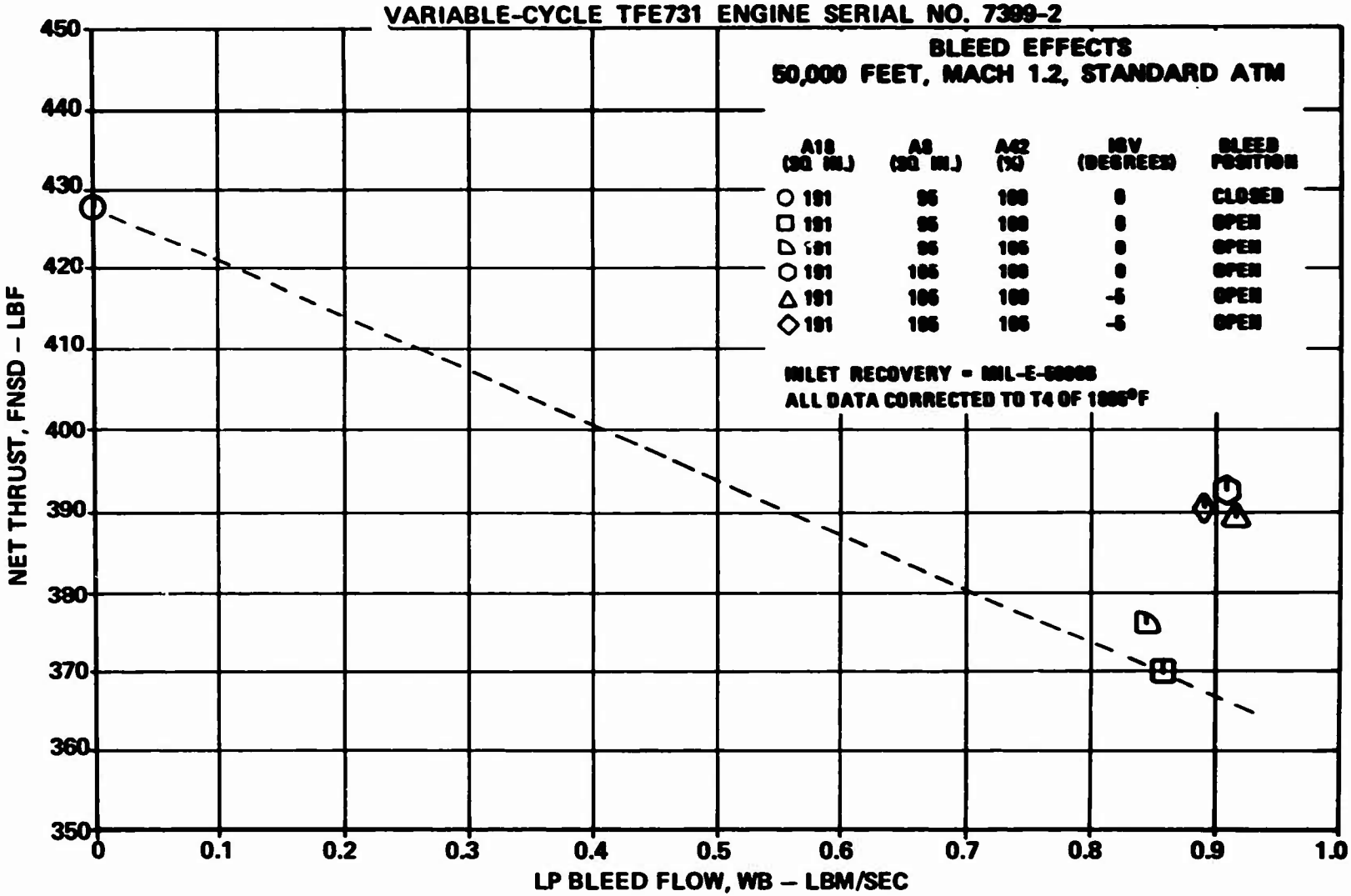

Figure 576. Bleed Effects at Mach 1.2, 50,000 Feet, Net Thrust Versus LP Bleed Flow.

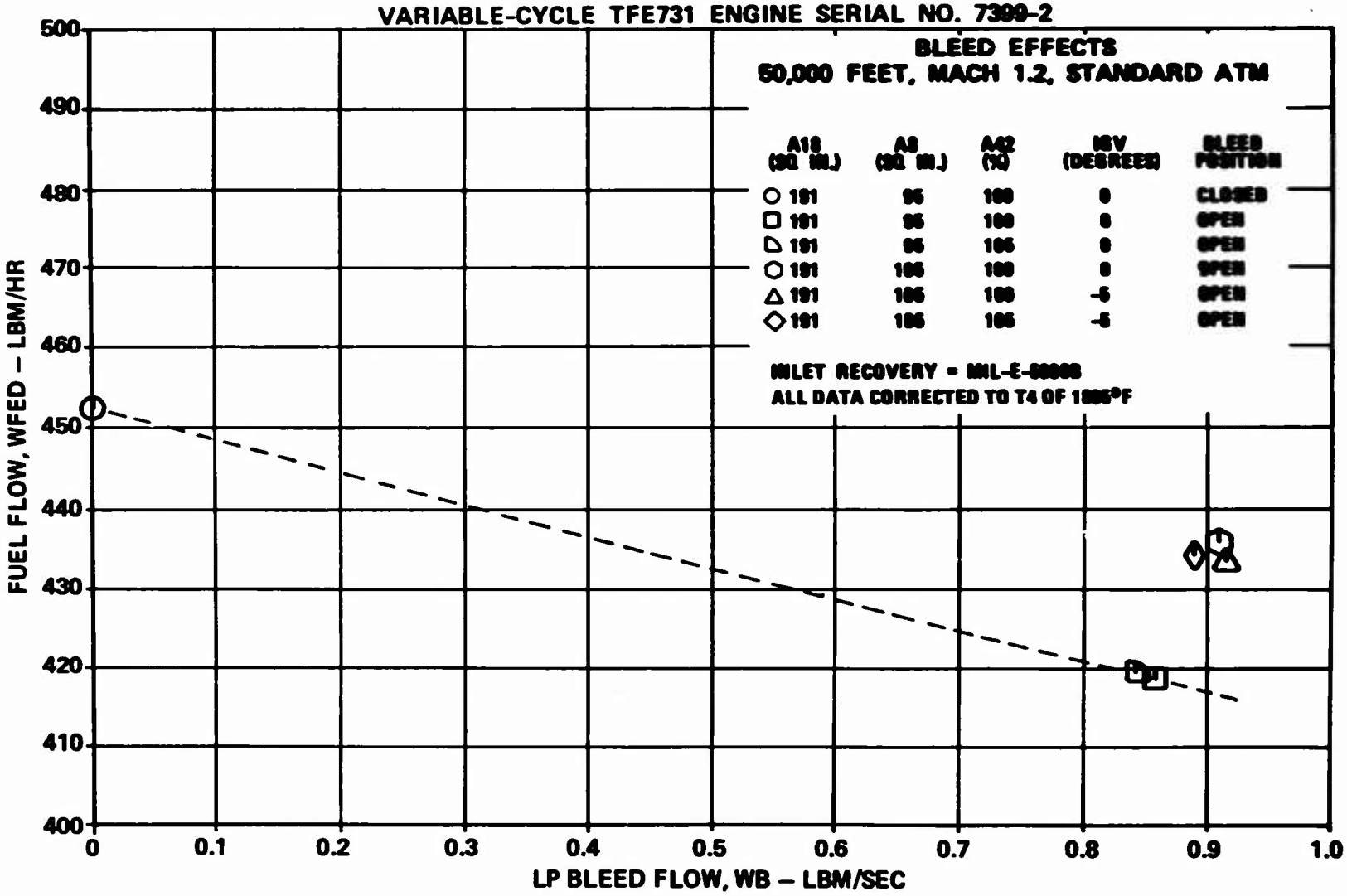

Figure 577. Bleed Effects at Mach 1.2, 50,000 Feet, Fuel Flow Versus LP Bleed Flow.

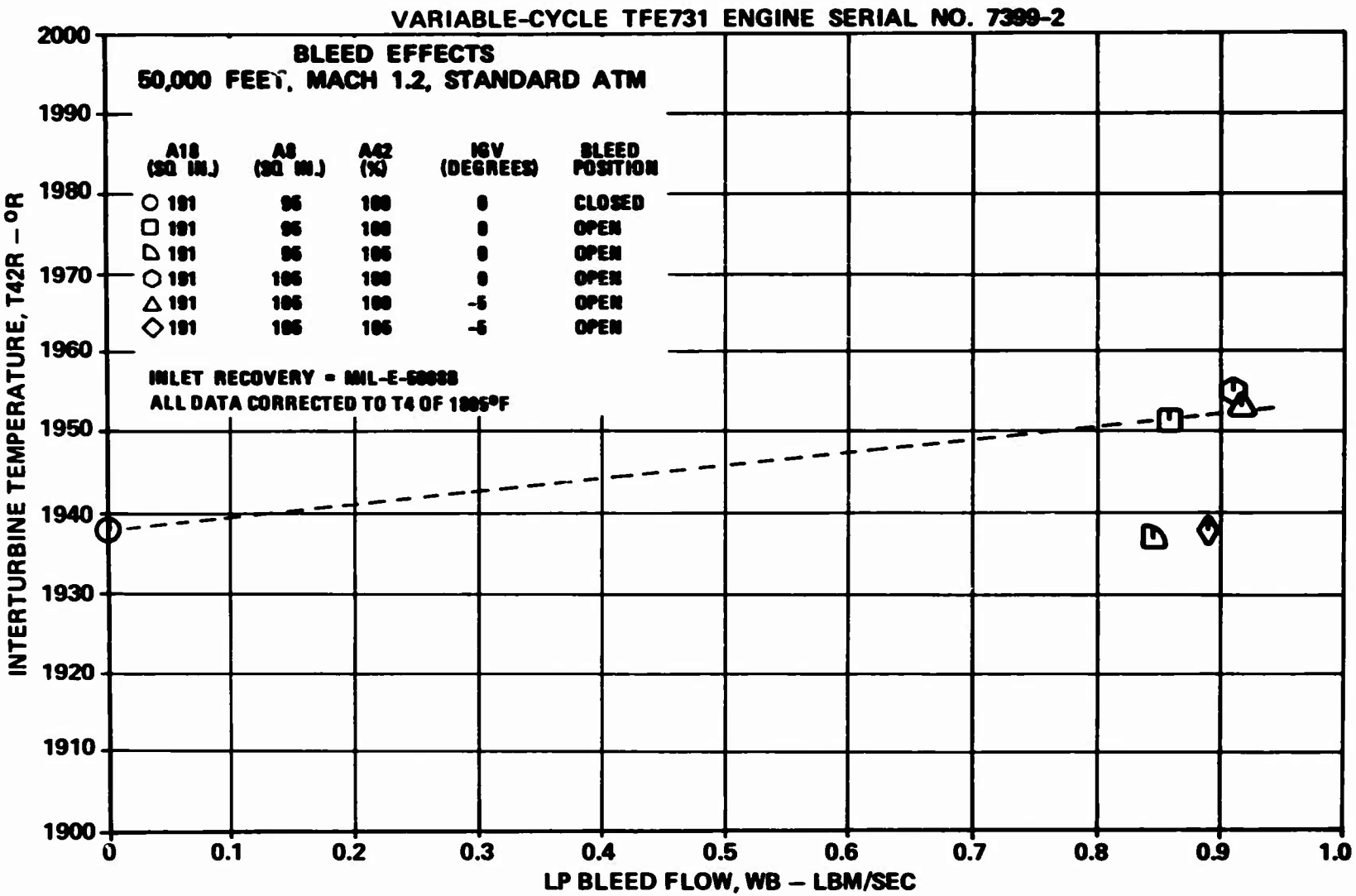

Figure 578. Bleed Effects at Mach 1.2, 50,000 Feet, Interturbine Temperature Versus LP Bleed Flow.

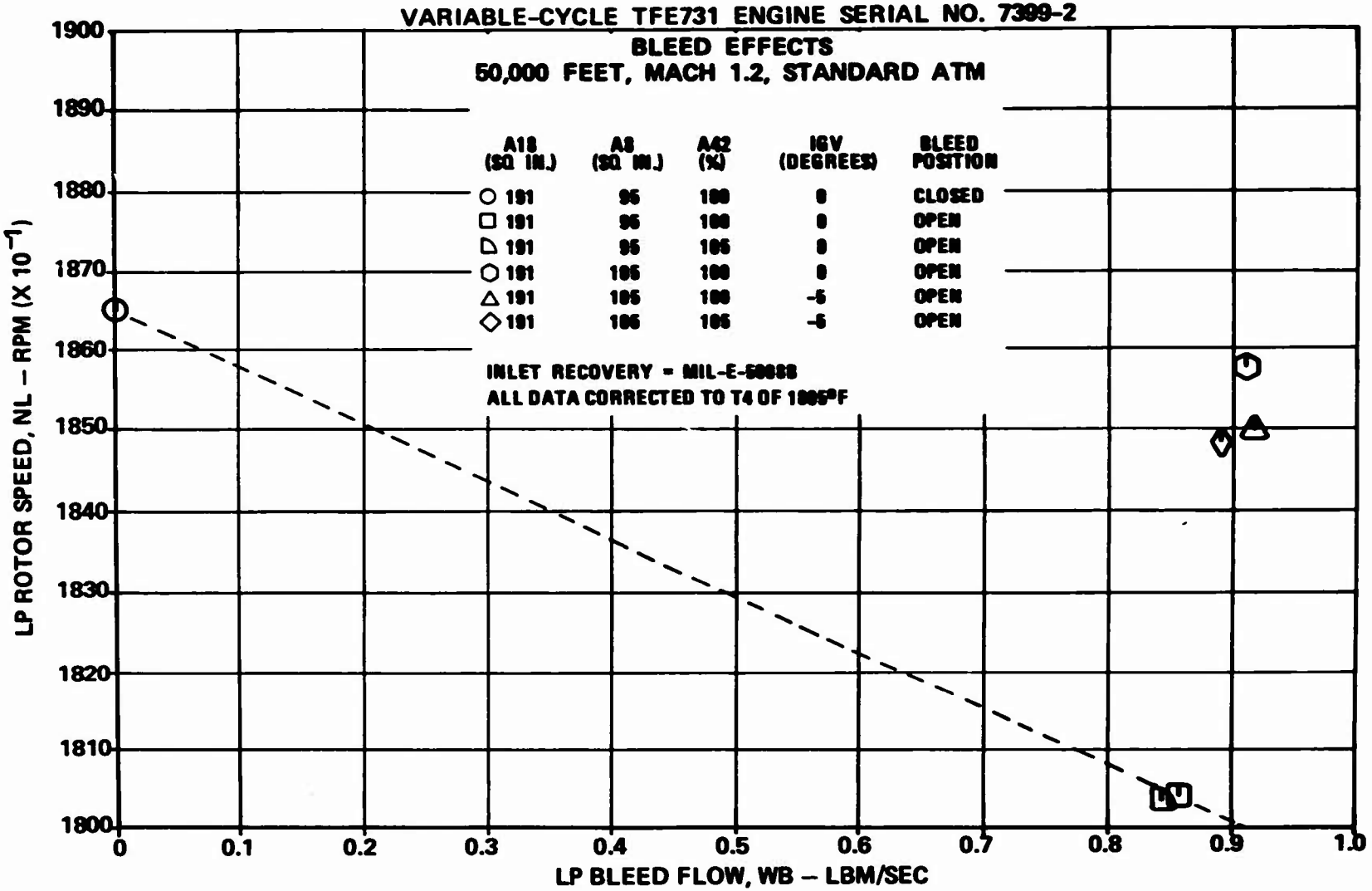

Figure 579. Bleed Effects at Mach 1.2, 50,000 Feet, LP Rotor Speed Versus LP Bleed Flow.

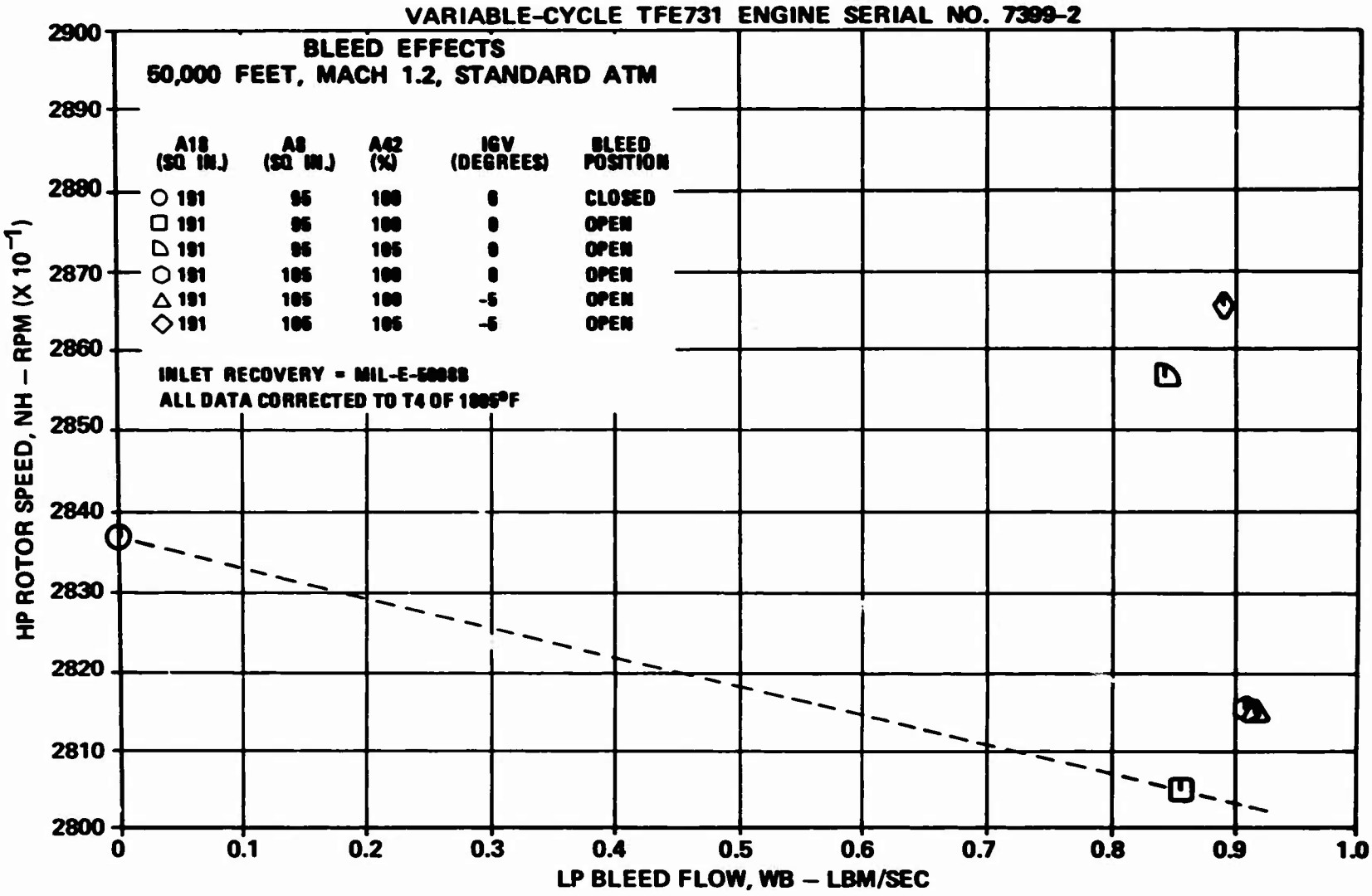

Figure 580. Bleed Effects at Mach 1.2, 50,000 Feet, HP Rotor Speed Versus LP Bleed Flow.

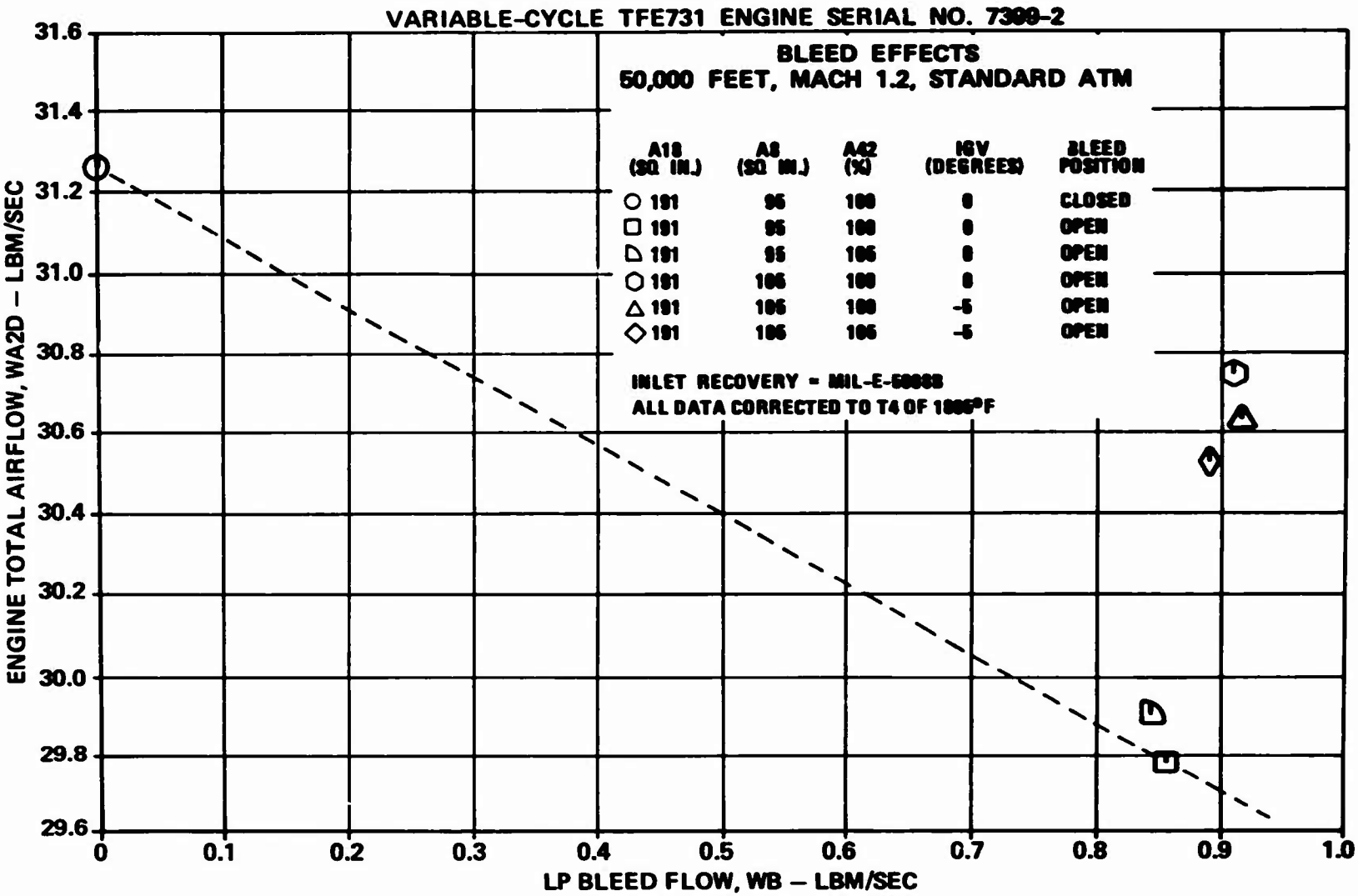

Figure 581. Bleed Effects at Mach 1.2, 50,000 Feet, Engine Total Airflow Versus LP Bleed Flow.

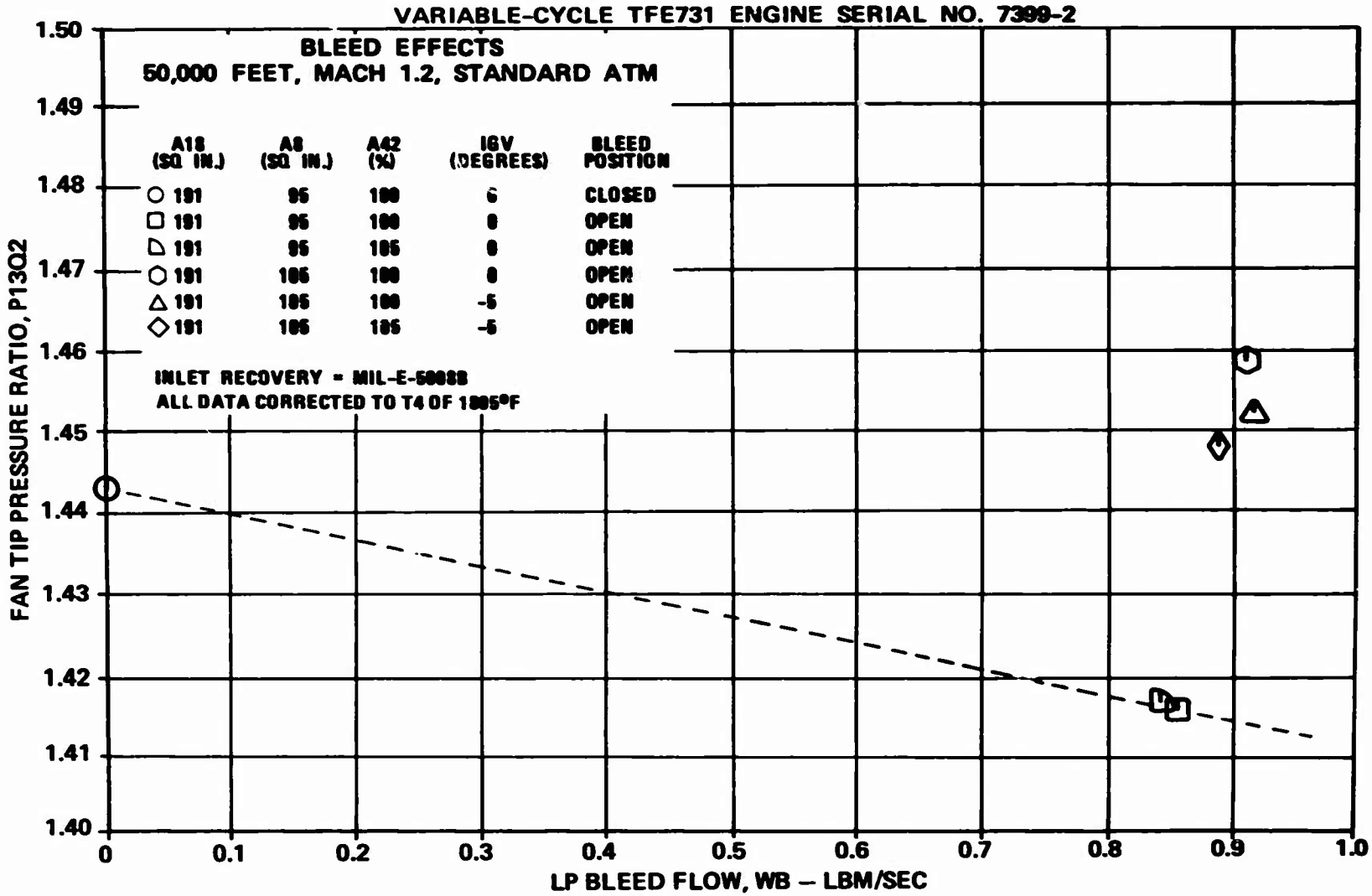

Figure 582. Bleed Effects at Mach 1.2, 50,000 Feet, Fan Tip Pressure Ratio Versus LP Bleed Flow.

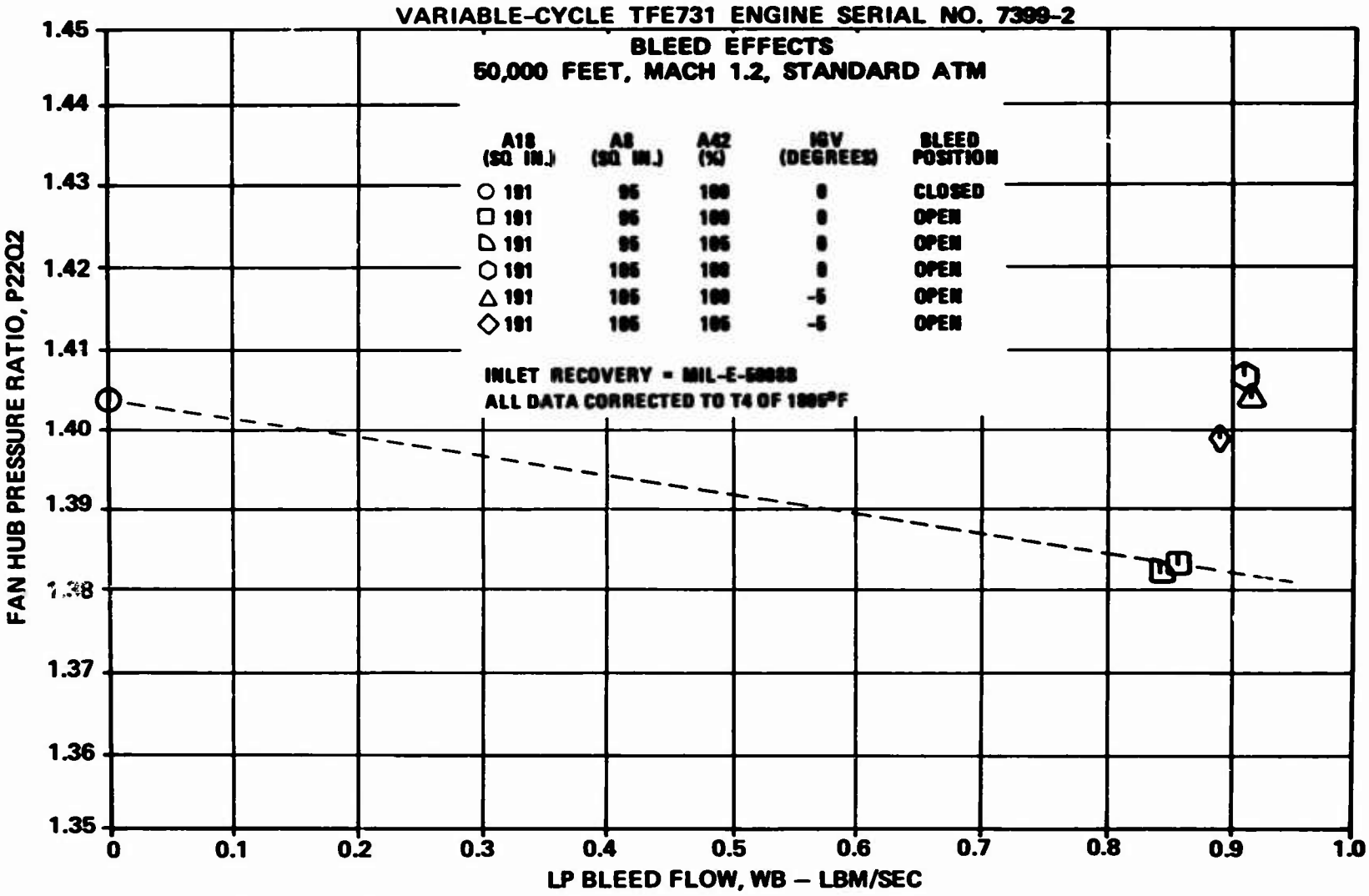

Figure 583. Bleed Effects at Mach 1.2, 50,000 Feet, Fan Hub Pressure Ratio Versus LP Bleed Flow.

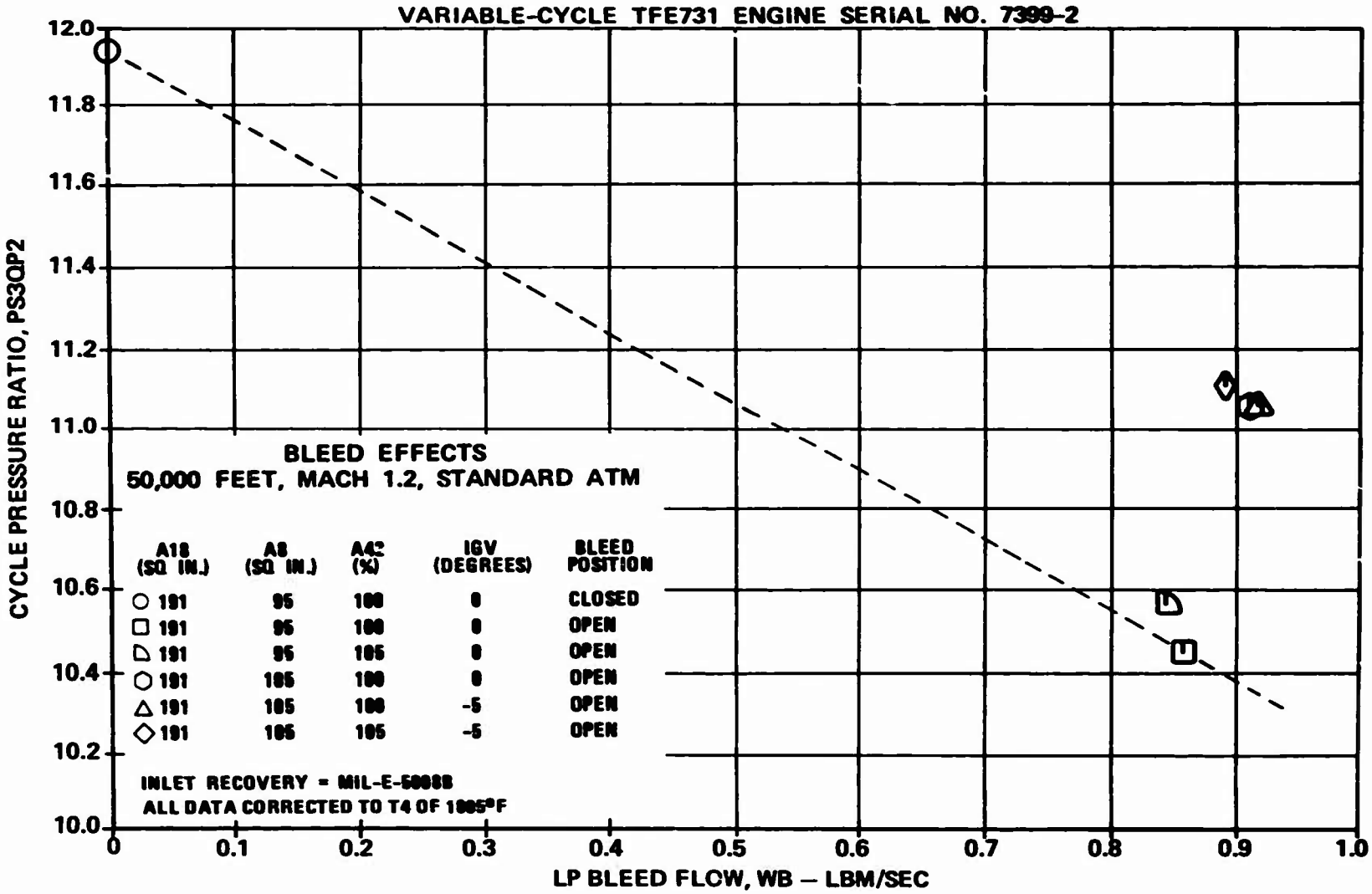

Figure 584. Bleed Effects at Mach 1.2, 50,000 Feet, Cycle Pressure Ratio Versus LP Bleed Flow.

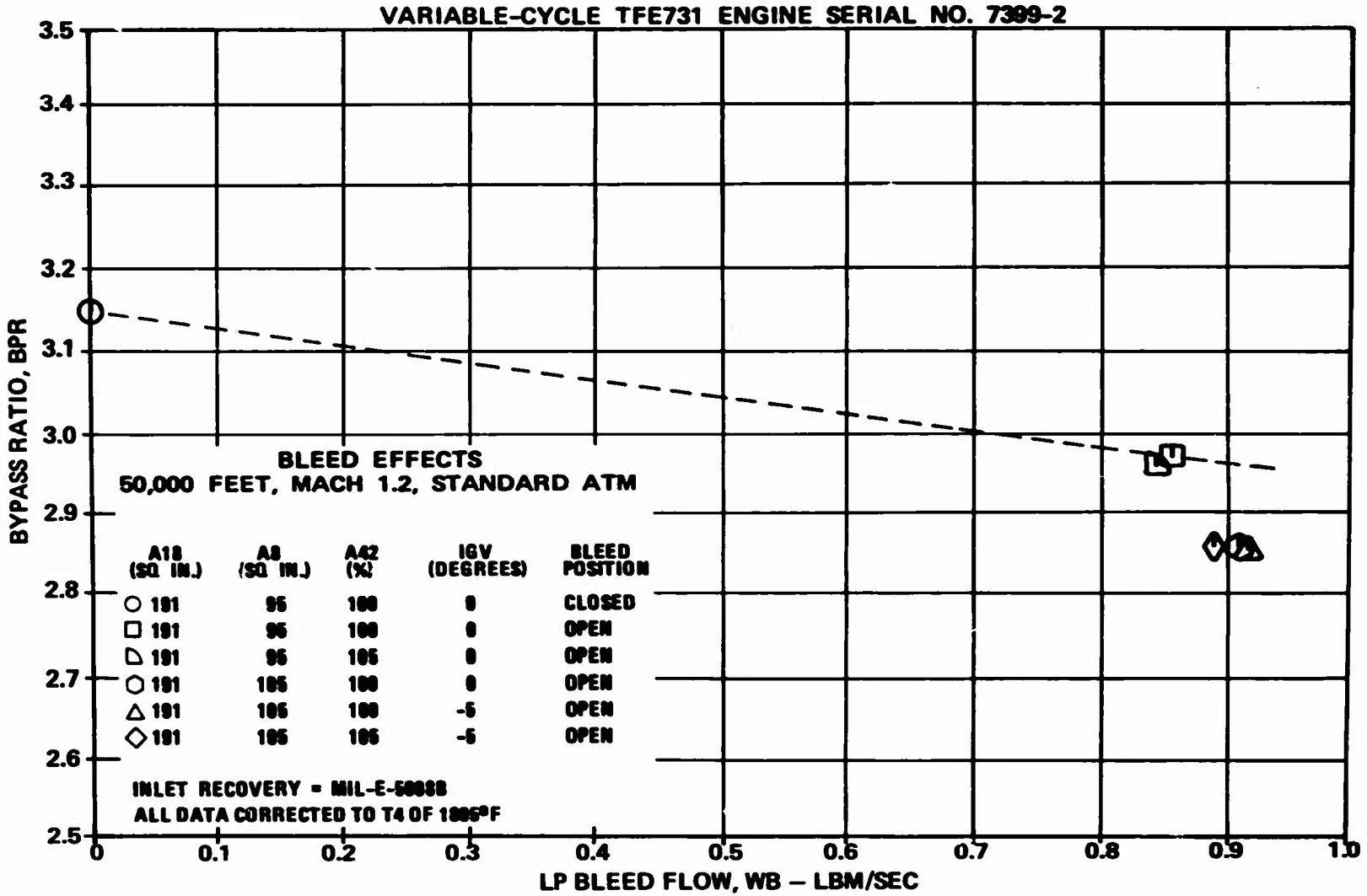

Figure 585. Bleed Effects at Mach 1.2, 50,000 Feet, Bypass Ratio Versus LP Bleed Flow.

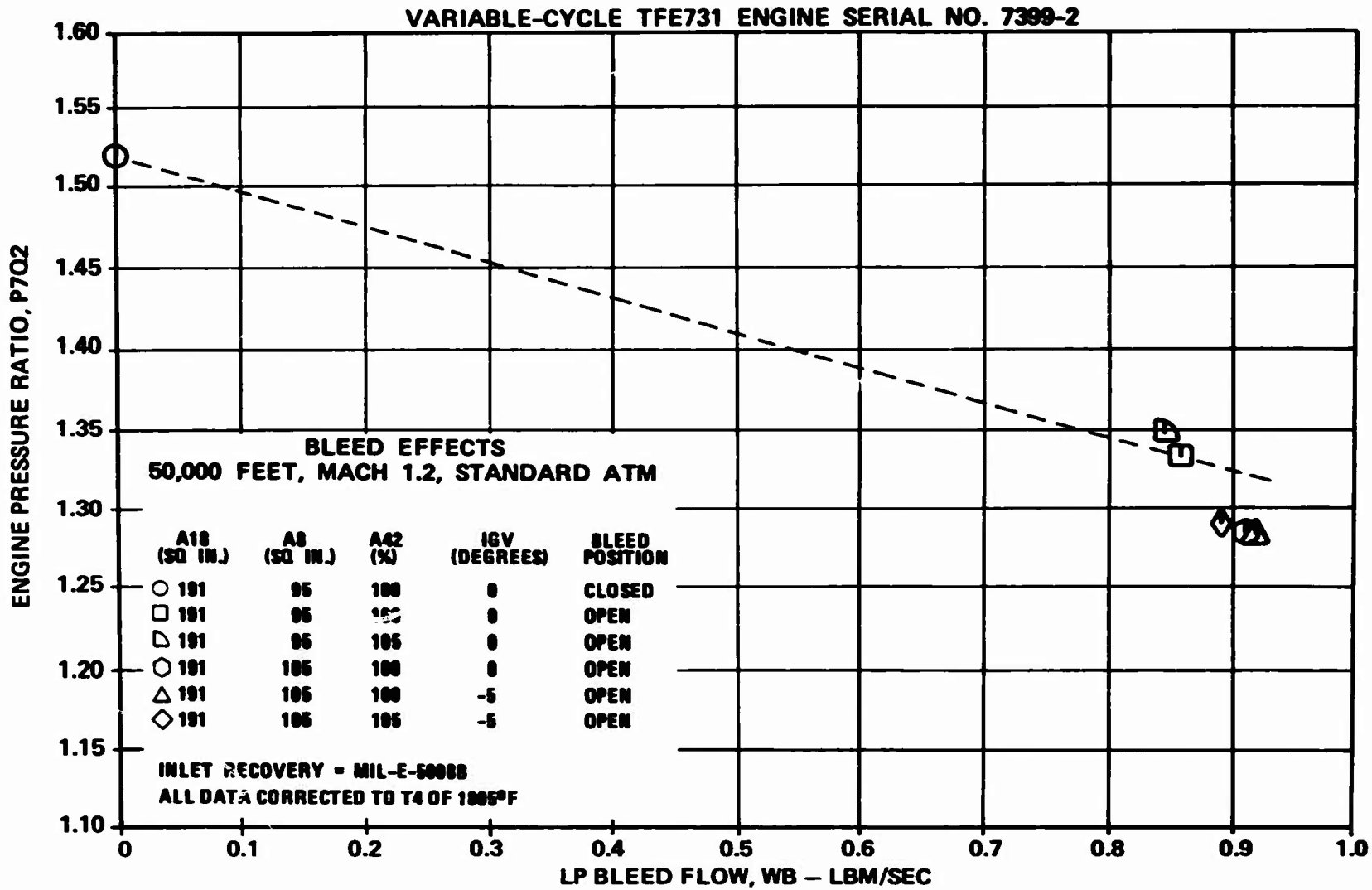

Figure 586. Bleed Effects at Mach 1.2, 50,000 Feet, Engine Pressure Ratio Versus LP Bleed Flow.

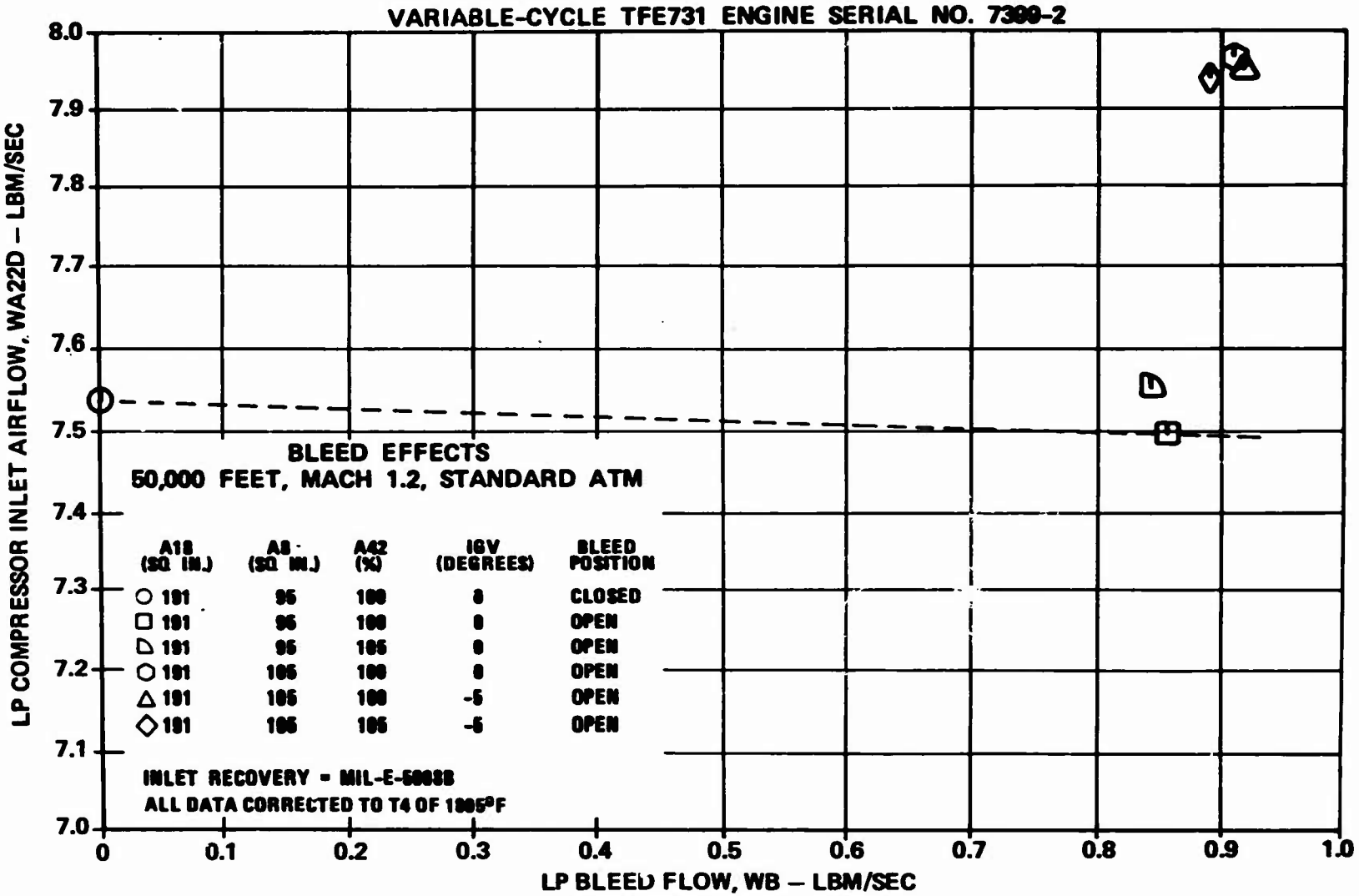

Figure 587. Bleed Effects at Mach 1.2, 50,000 Feet, LP Compressor Inlet Airflow Versus LP Bleed Flow.

TABLE 72. BLEED EFFECTS, 50,000 FEET, MACH 1.2, STANDARD ATM, AT AN HP TURBINE INLET TEMPERATURE OF 1805°F.

A18 (sq in.)	A8 (sq in.)	A42 (%)	LPC (degrees)	Net Thrust (lbf)	LPC Bleed Rate (lbm/sec)
191	95	100	0	428	0
191	95	100	0	370	0.8575
191	95	105	0	375	0.8575
191	105	100	0	397	0.8575
191	105	100	-5	394	0.8575
191	105	105	-5	393	0.8575

4.4.f 20,000 Feet, Mach 0.6

The results of the bleed testing at 20,000 feet, Mach 0.6, standard atmosphere, are presented in Figures 588 through 601. The parameters presented in these curves are listed in Table 73. All parameters have been corrected to a turbine inlet temperature of 1805°F.

The results of the bleed testing at 20,000 feet, Mach 0.6 show the same general trends as those determined at the other test conditions. During the 20,000 feet, Mach 0.6 testing, the maximum net thrust increase over that of the base bleed point was 66 pounds (5.5 percent), which represents a recovery of 28 percent of the thrust loss due to the LP bleed.

In order to determine if additional performance gains could be realized by increasing the primary exhaust-nozzle area beyond 105 square inches, an area of 110 square inches was tested. The increased primary exhaust-nozzle area resulted in further improved engine performance; however, the rate of gain from 105 to 110 square inches was less than that shown for the change from 95 to 105 square inches. In increasing the area from 95 square inches to 105 square inches, the net thrust was increased by 33 pounds. The rate of change was 3.3 pounds per square inch of area increase. Enlarging the primary exhaust-nozzle area from 105 to 110 square inches resulted in a net thrust increase of 11 pounds. This rate of change was 2.2 pounds per square inch increase in area.

A summary of the 20,000-feet, Mach 0.6 bleed testing is presented in Table 74.

TABLE 73. BLEED EFFECTS, 20,000 FEET, MACH 0.6, STANDARD ATM

Figure No.	Parameters Presented
588	Turbine inlet temperature versus LP bleed flow
589	Thrust specific fuel consumption versus LP bleed flow
590	Net thrust versus LP bleed flow
591	Fuel flow versus LP bleed flow
592	Interturbine temperature versus LP bleed flow
593	LP rotor speed versus LP bleed flow
594	HP rotor speed versus LP bleed flow
595	Engine total airflow versus LP bleed flow
596	Fan tip pressure ratio versus LP bleed flow
597	Fan hub pressure ratio versus LP bleed flow
598	Cycle pressure ratio versus LP bleed flow
599	Bypass ratio versus LP bleed flow
600	Engine pressure ratio versus LP bleed flow
601	LP compressor inlet airflow versus LP bleed flow

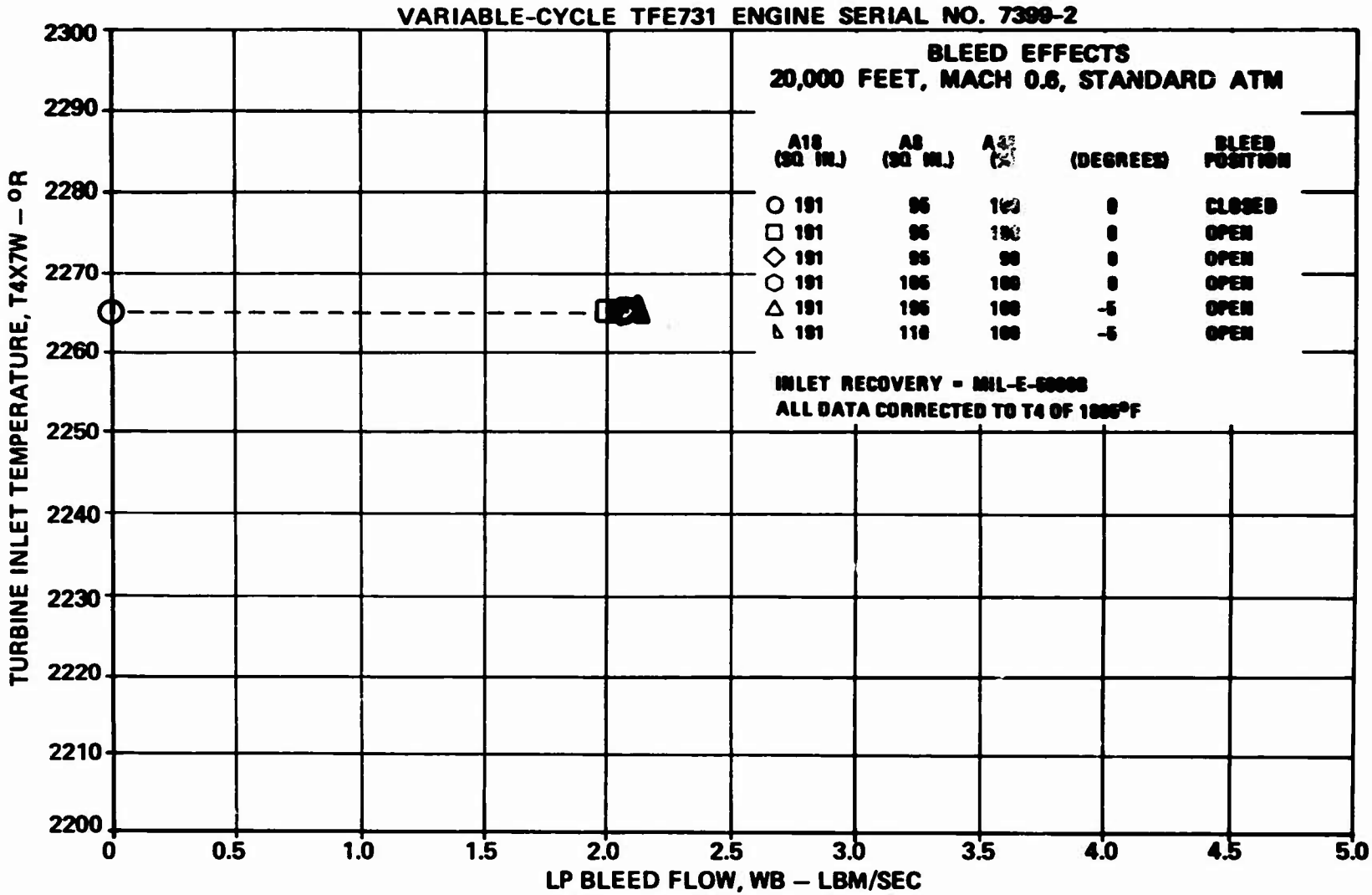

Figure 588. Bleed Effects at Mach 0.6, 20,000 Feet, Turbine Inlet Temperature Versus LP Bleed Flow.

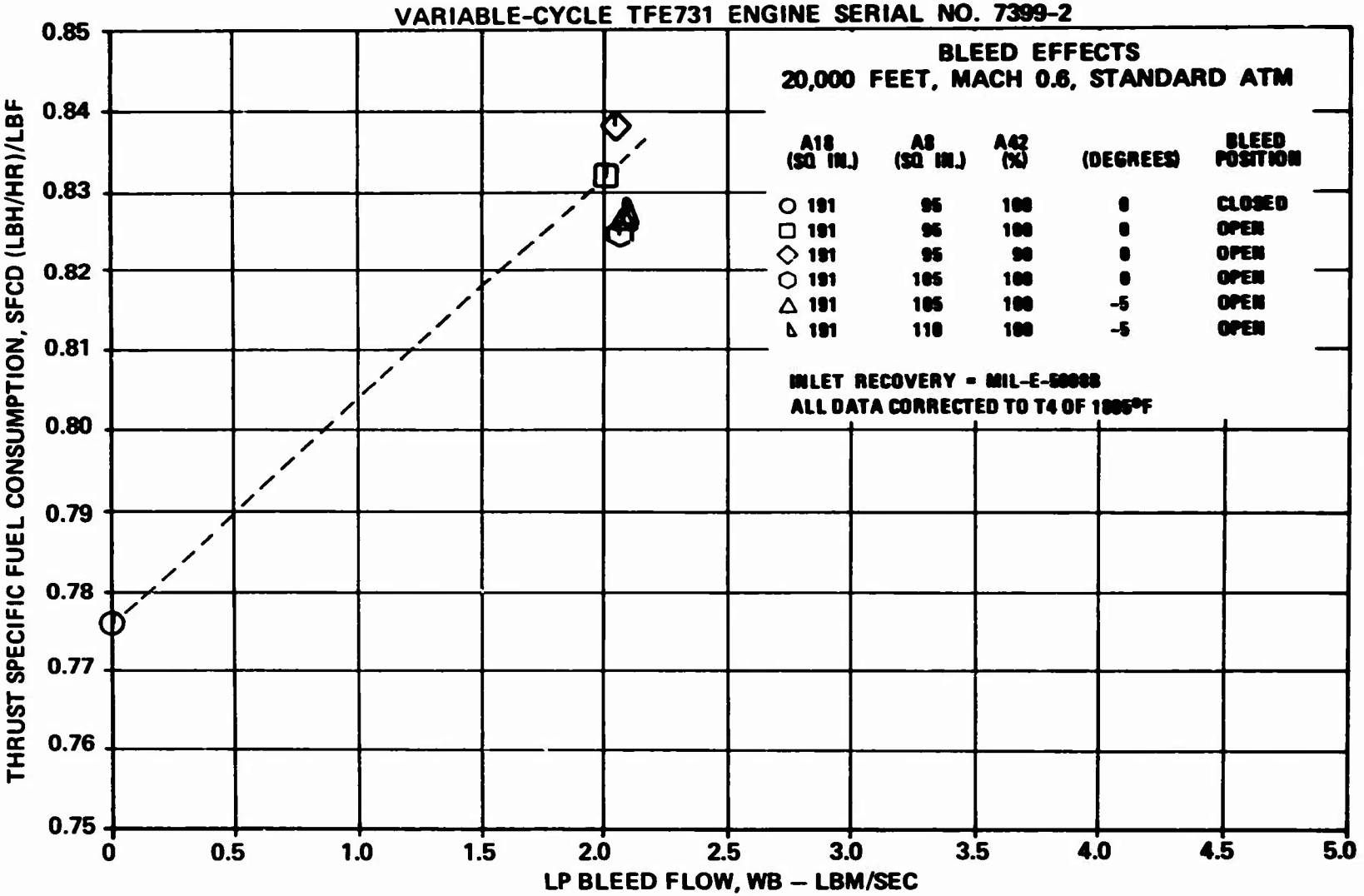

Figure 589. Bleed Effects at Mach 0.6, 20,000 Feet, Thrust Specific Fuel Consumption Versus LP Bleed Flow.

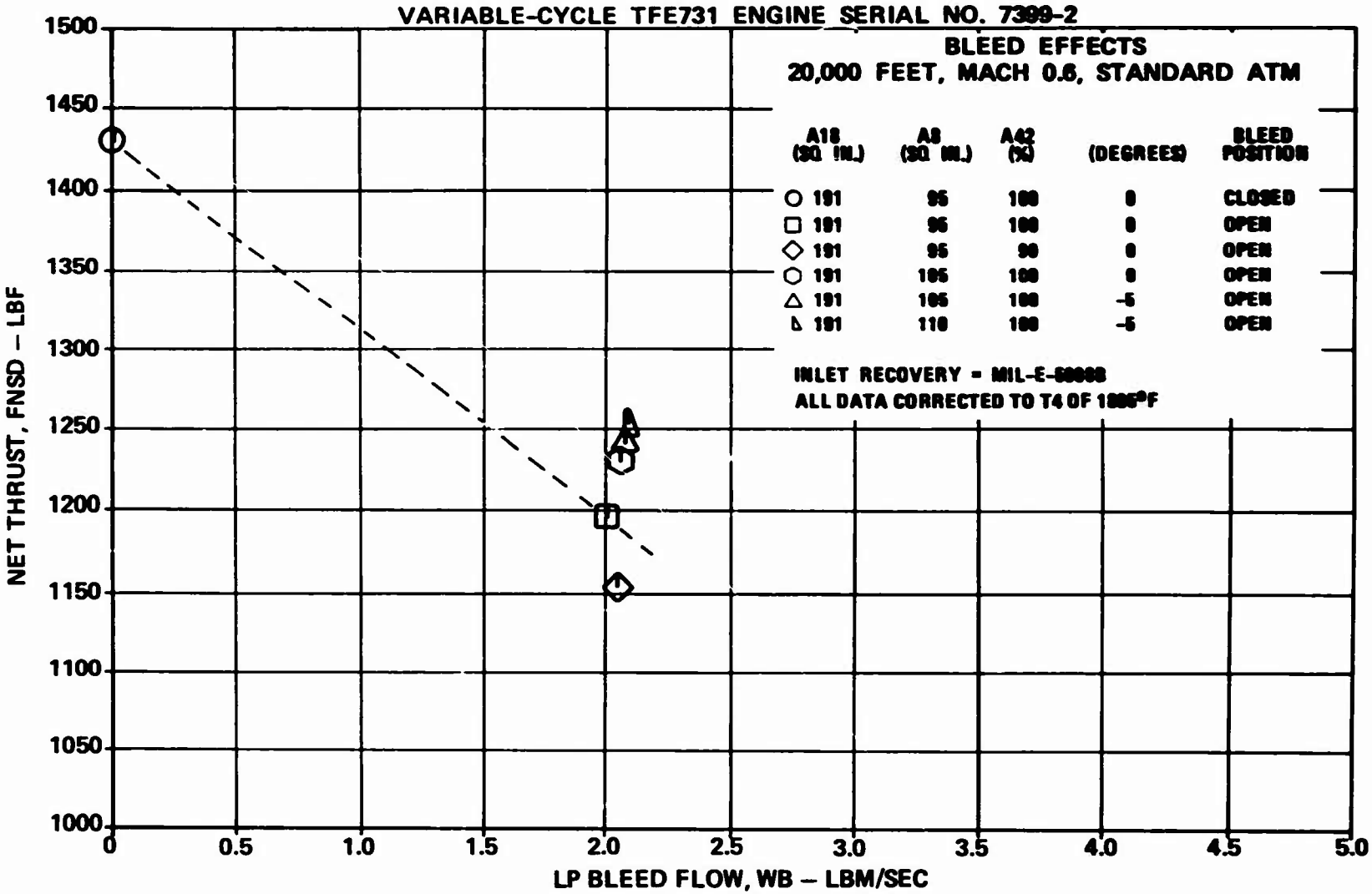

Figure 590. Bleed Effects at Mach 0.6, 20,000 Feet, Net Thrust Versus LP Bleed Flow.

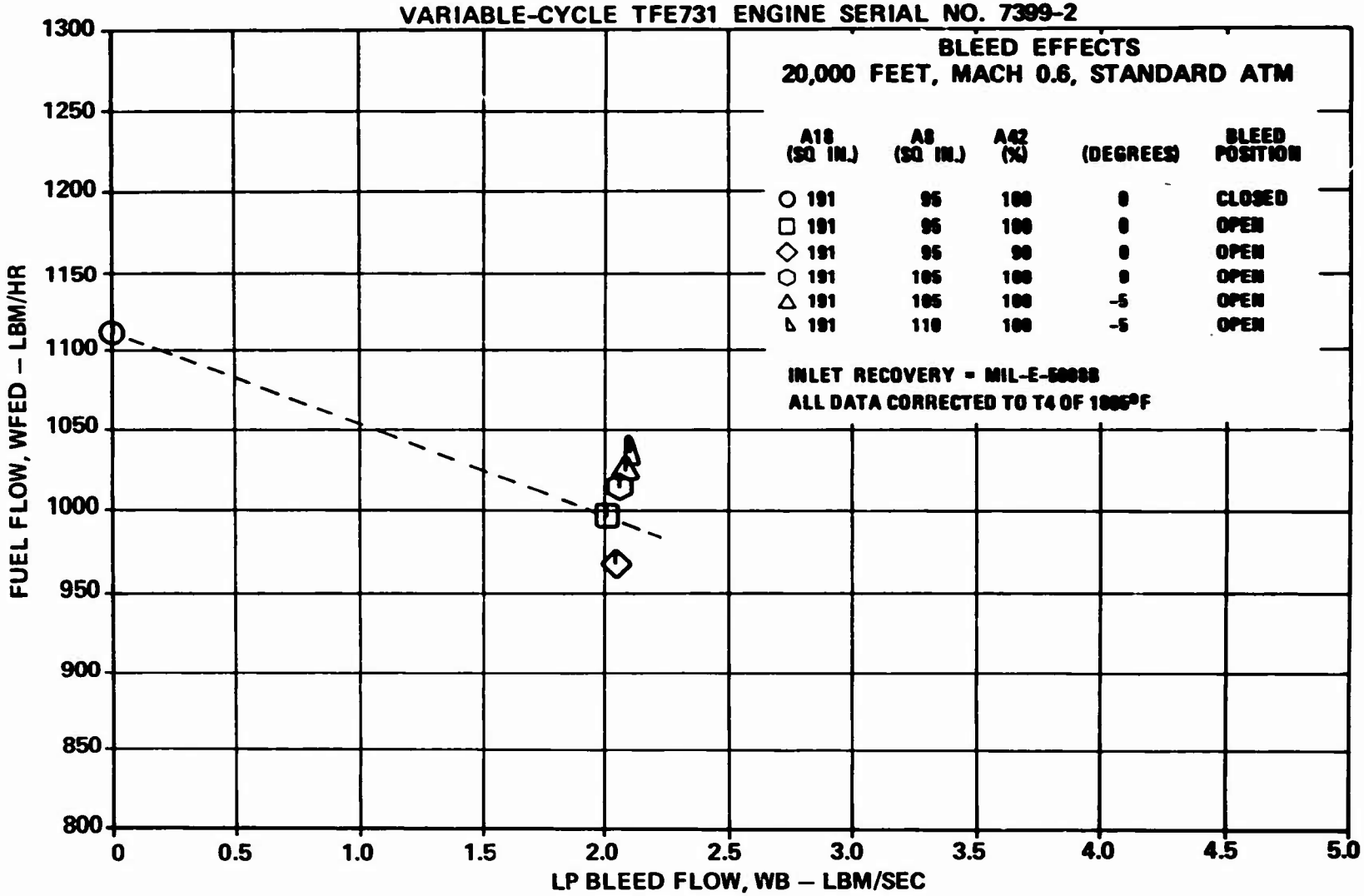

Figure 591. Bleed Effects at Mach 0.6, 20,000 Feet, Fuel Flow Versus LP Bleed Flow.

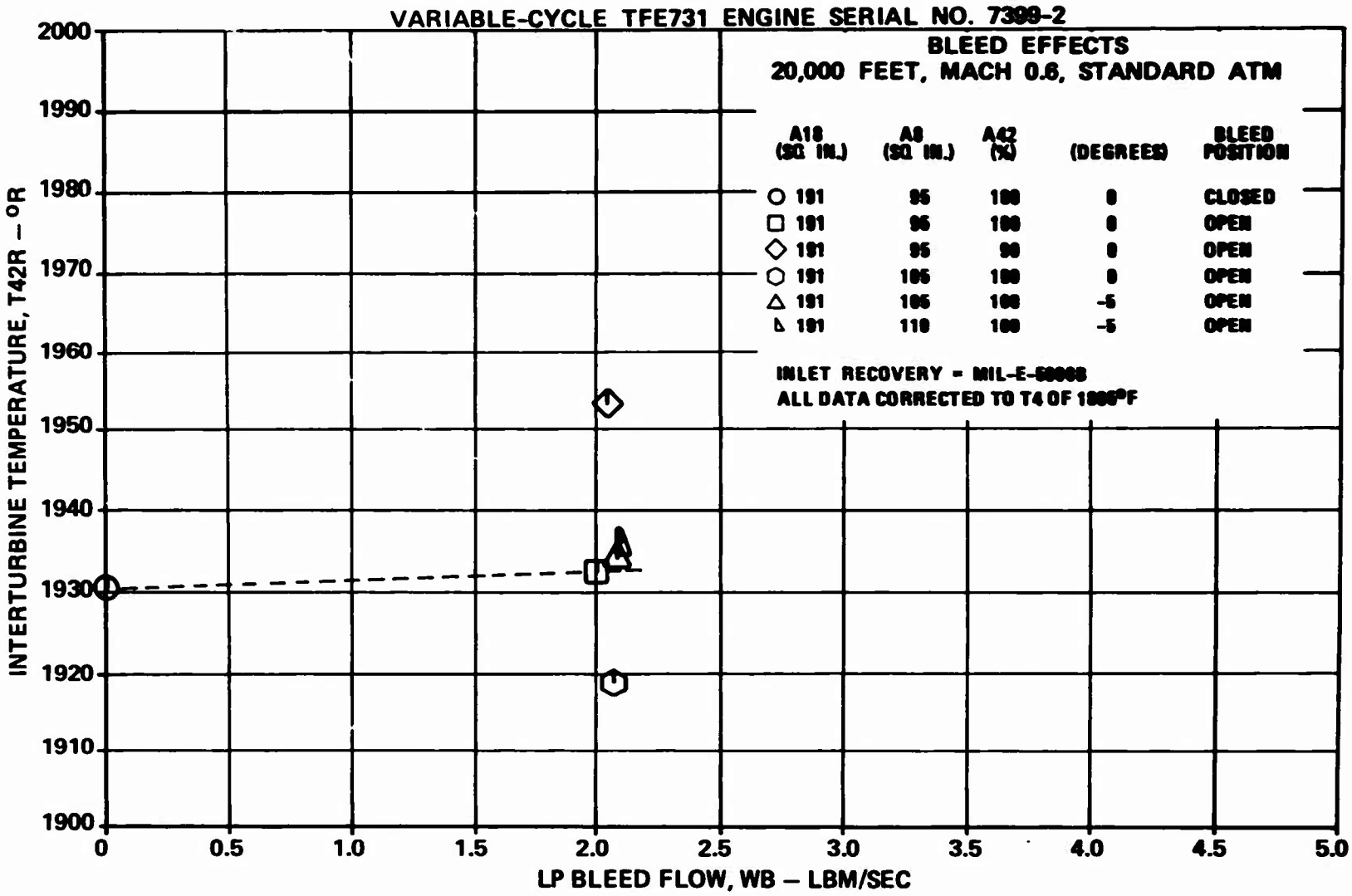

Figure 592. Bleed Effects at Mach 0.6, 20,000 Feet, Interturbine Temperature Versus LP Bleed Flow.

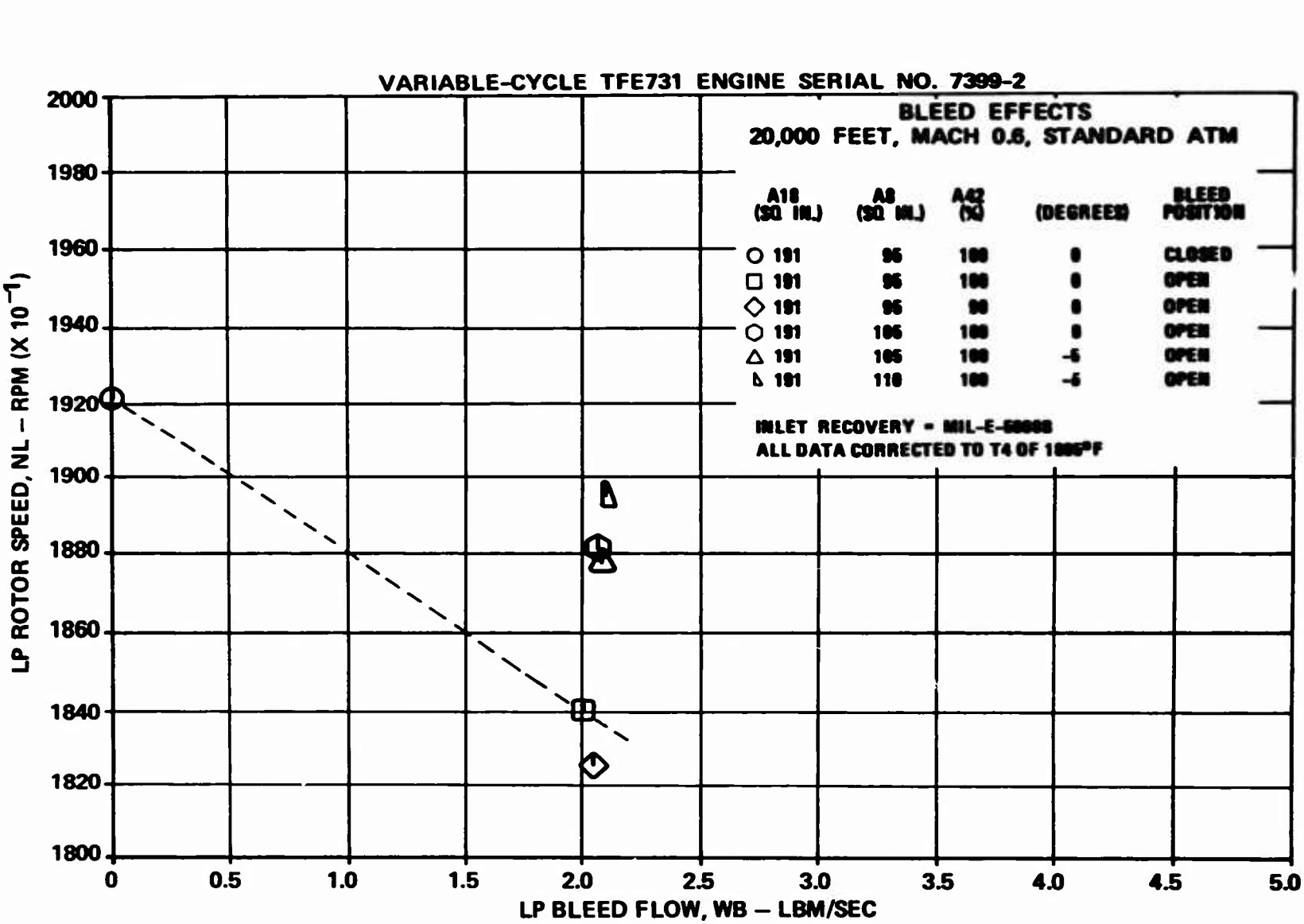

Figure 593. Bleed Effects at Mach 0.6, 20,000 Feet, LP Rotor Speed Versus LP Bleed Flow.

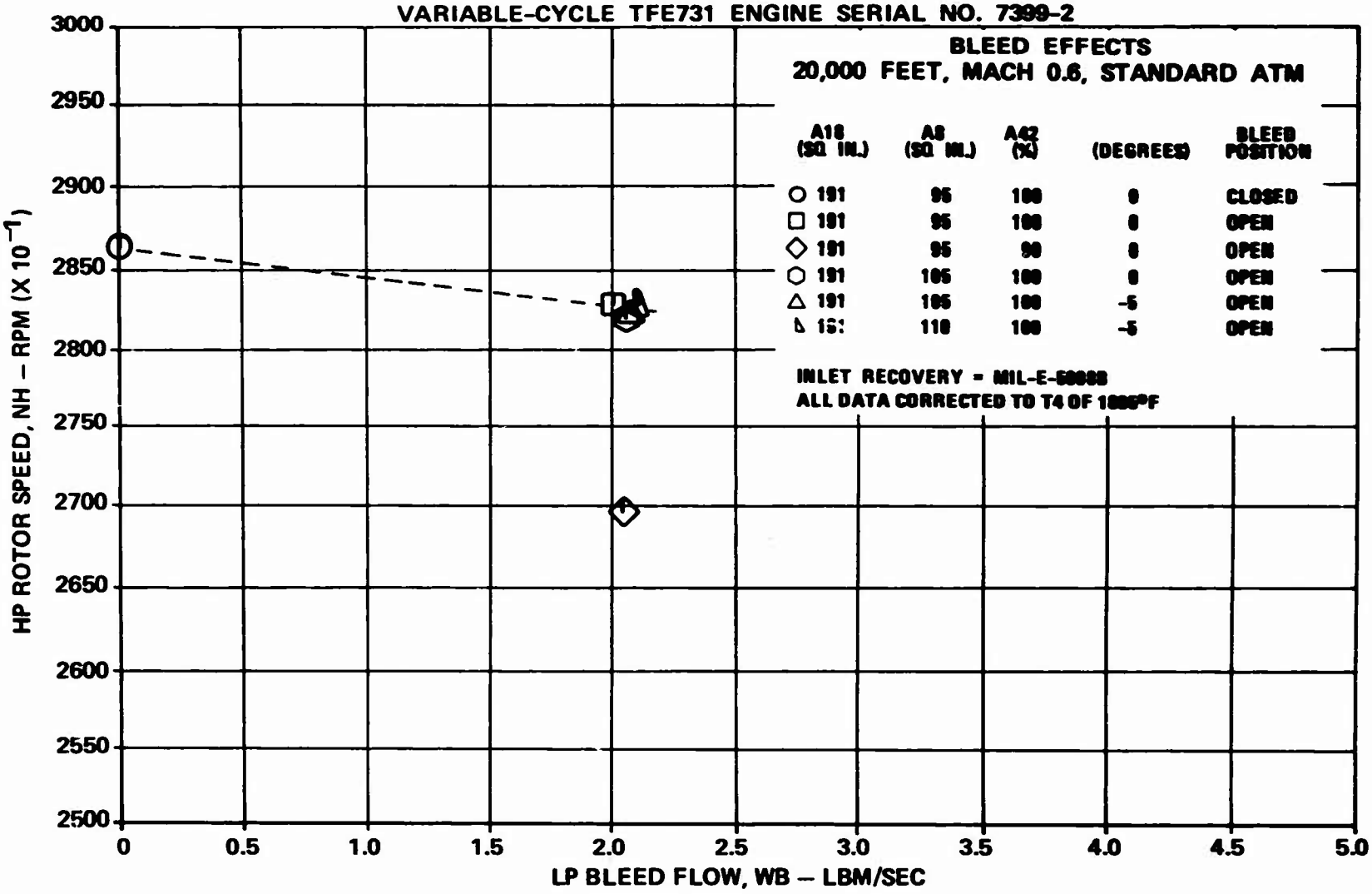

Figure 594. Bleed Effects at Mach 0.6, 20,000 Feet, HP Rotor Speed Versus LP Bleed Flow.

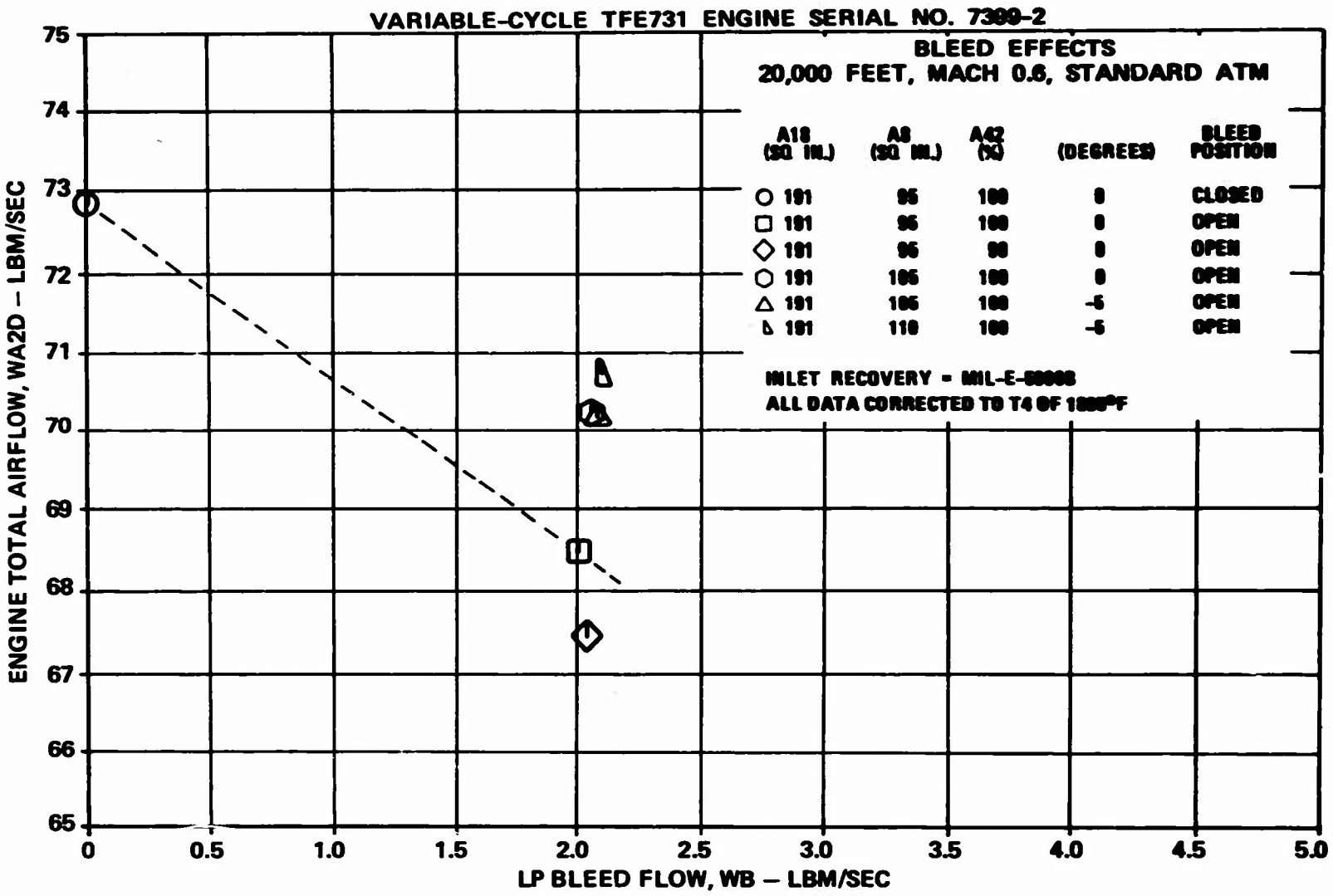

Figure 595. Bleed Effects at Mach 0.6, 20,000 Feet, Engine Total Airflow Versus LP Bleed Flow.

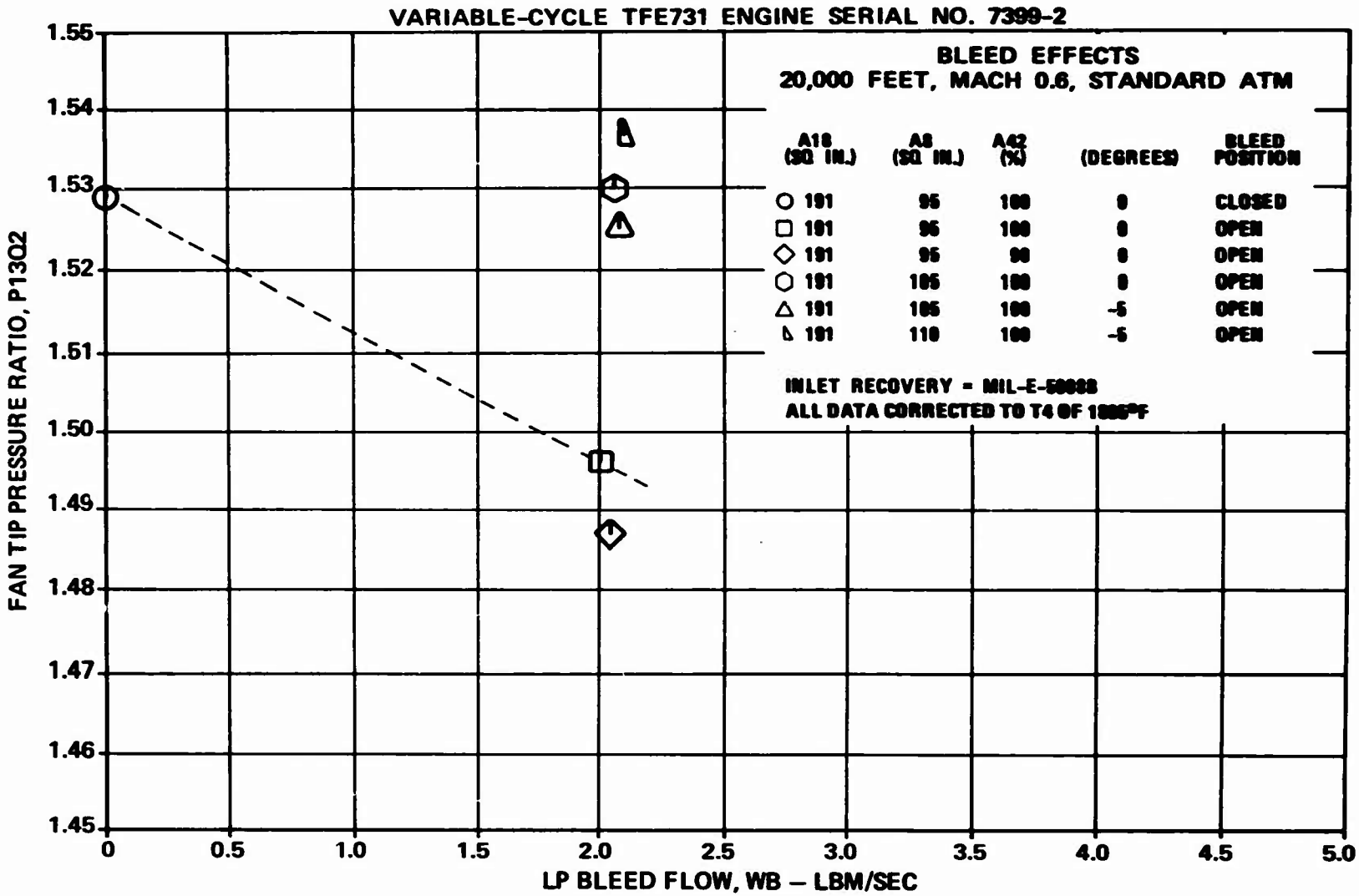

Figure 596. Bleed Effects at Mach 0.6, 20,000 Feet, Fan Tip Pressure Ratio Versus LP Bleed Flow.

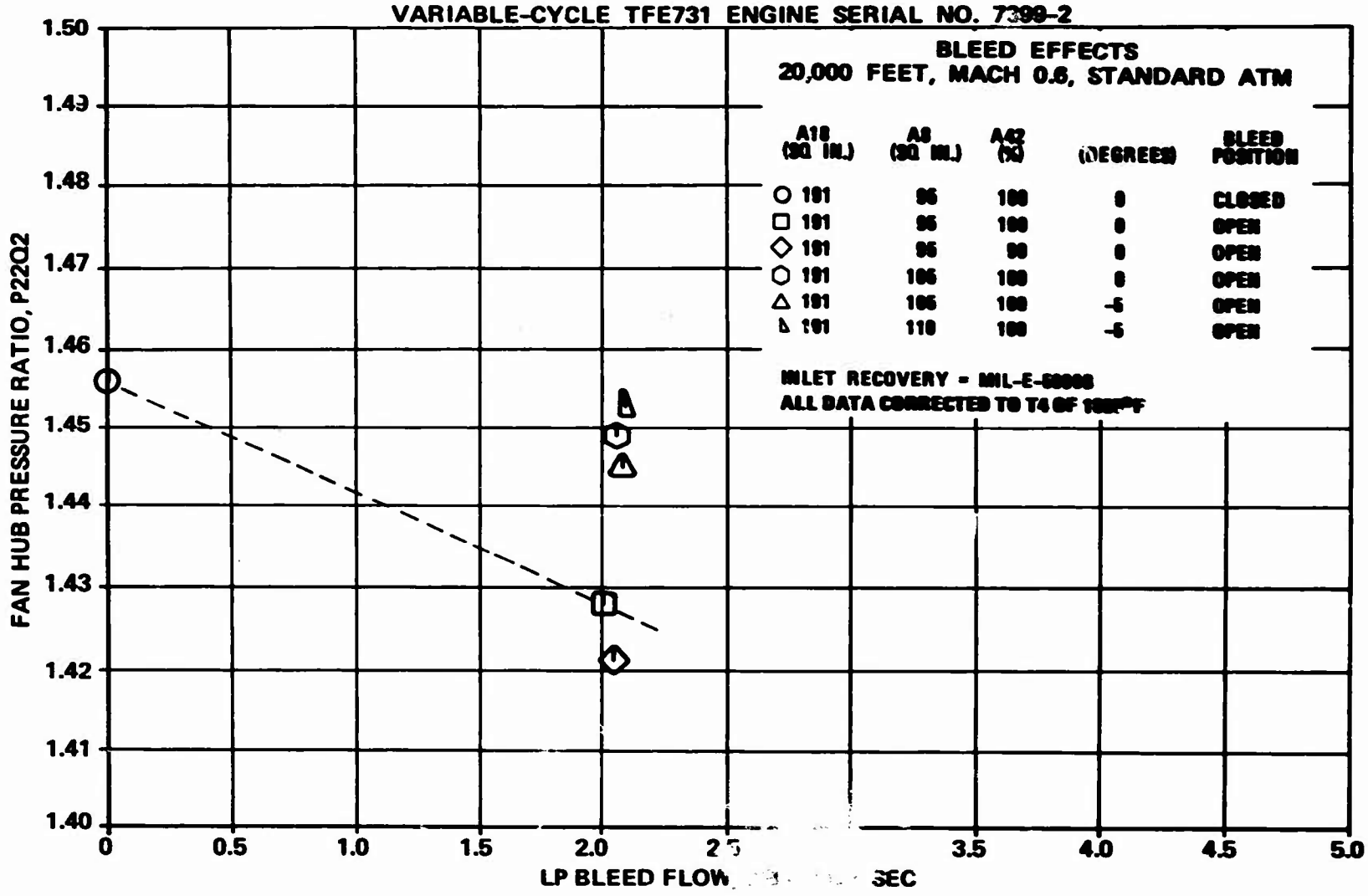

Figure 597. Bleed Effects at Mach 0.6, 20,000 Feet, Fan Hub Pressure Ratio Versus LP Bleed Flow.

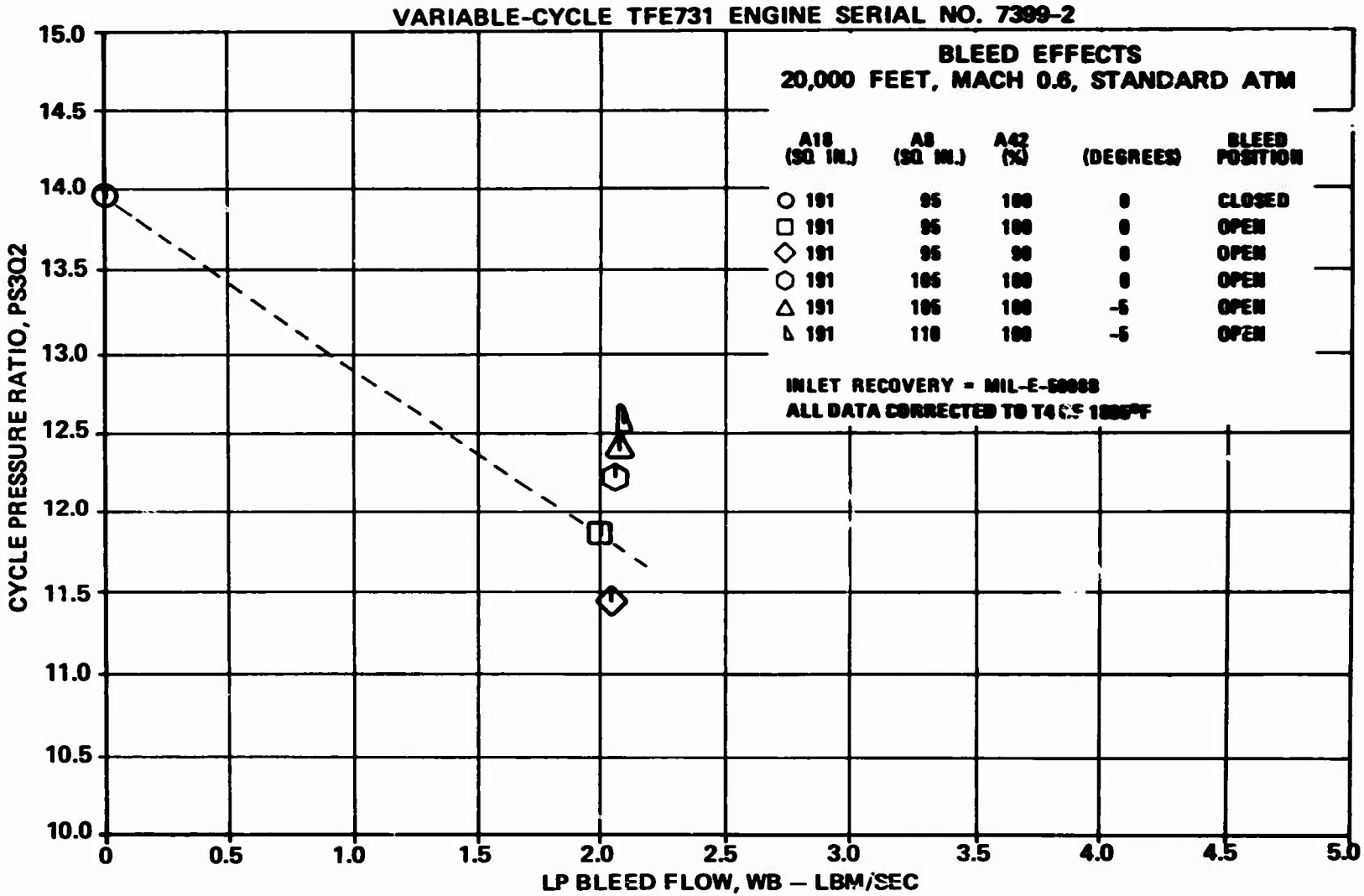

Figure 598. Bleed Effects at Mach 0.6, 20,000 Feet, Cycle Pressure Ratio Versus LP Bleed Flow.

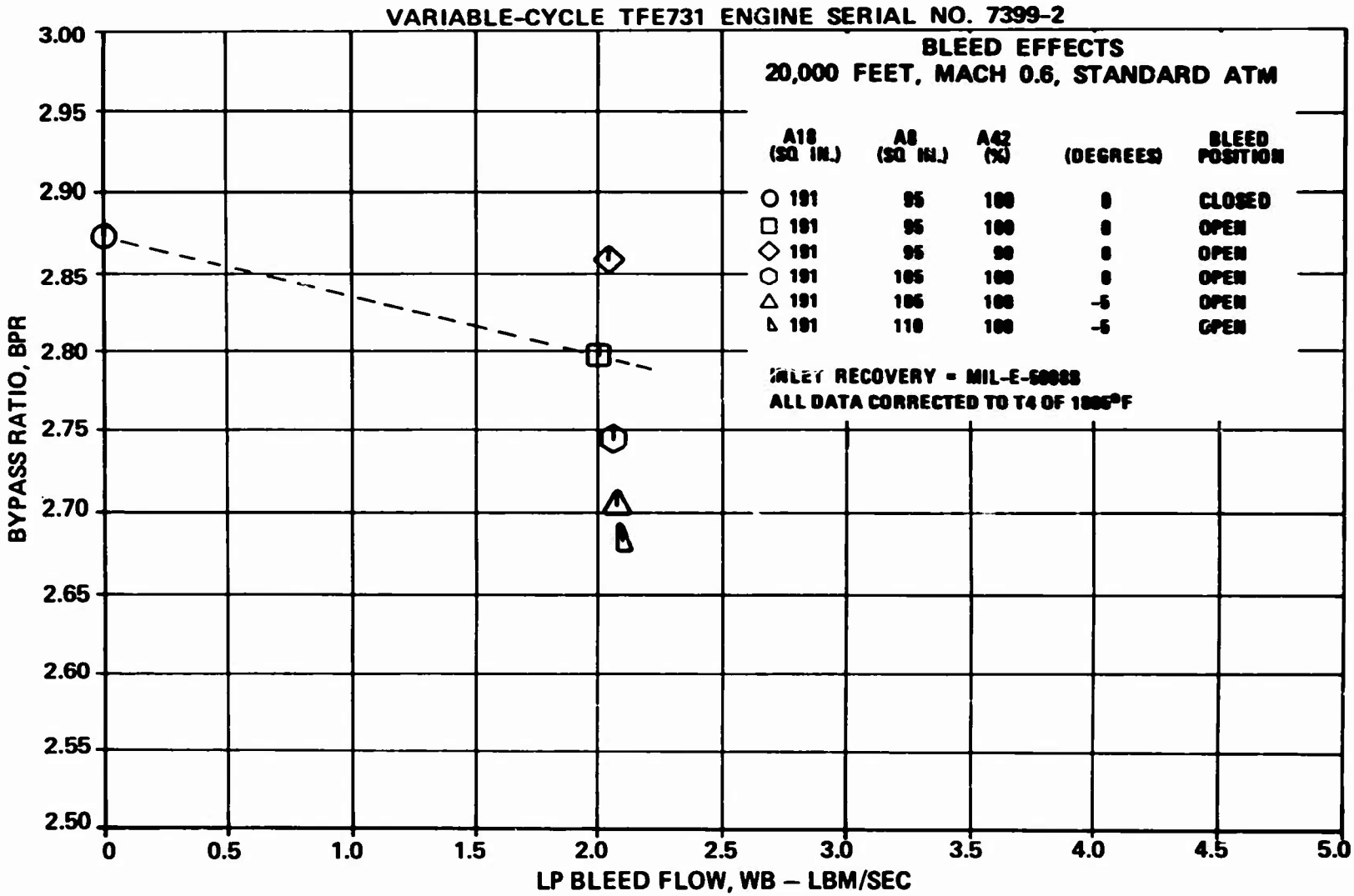

Figure 599. Bleed Effects at Mach 0.6, 20,000 Feet, Bypass Ratio Versus LP Bleed Flow.

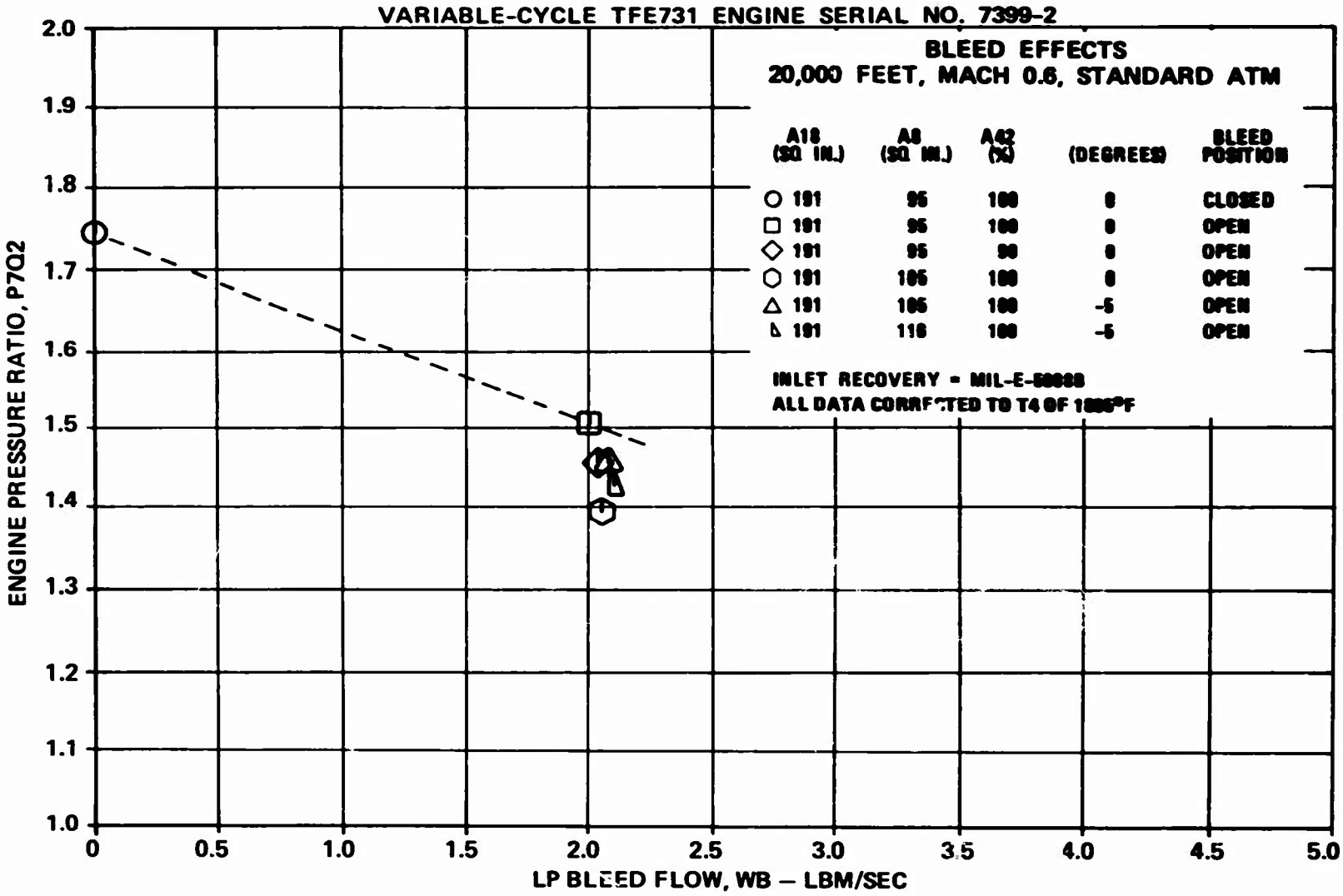

Figure 600. Bleed Effects at Mach 0.6, 20,000 Feet, Engine Pressure Ratio Versus LP Bleed Flow.

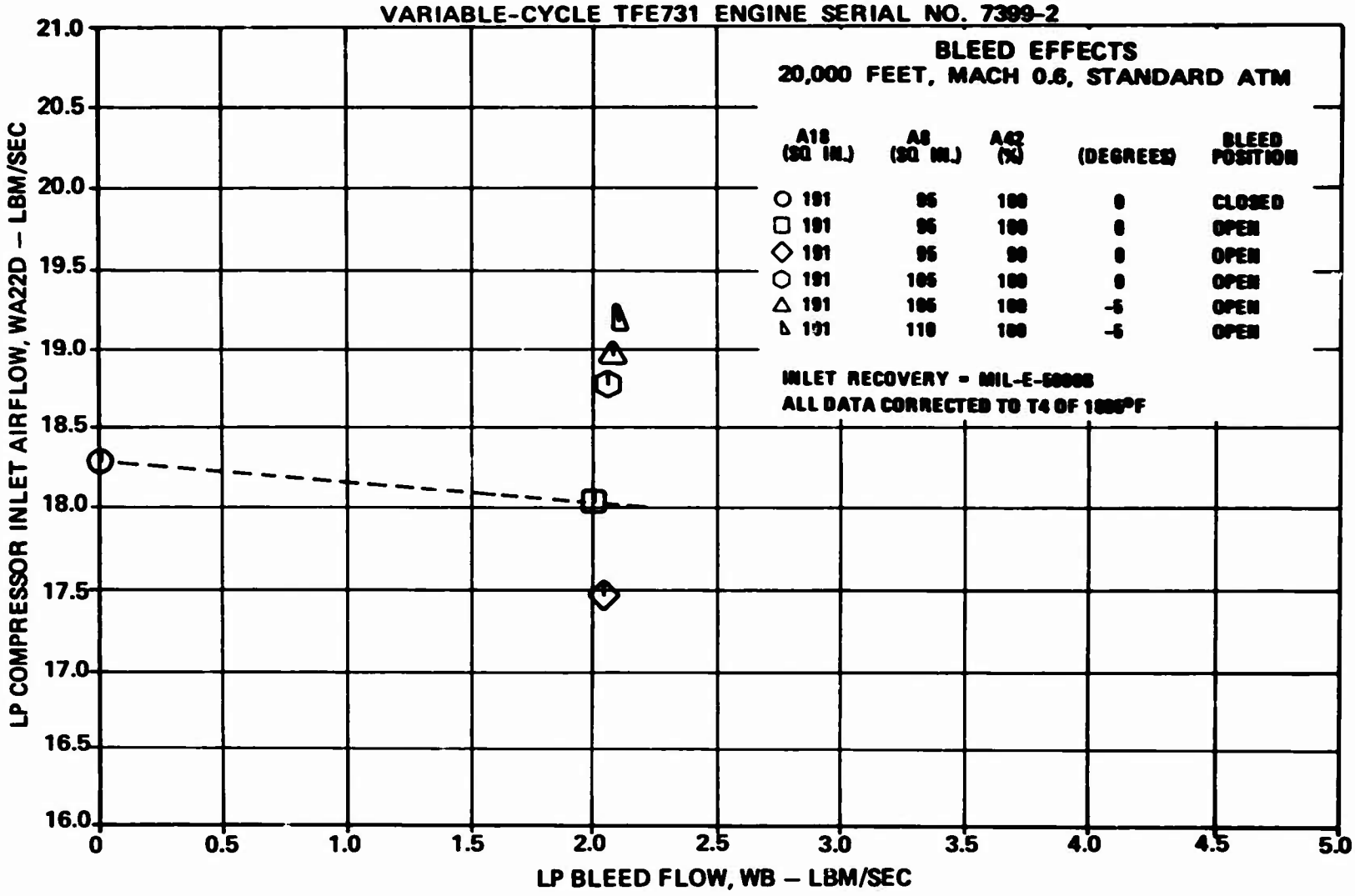

Figure 601. Bleed Effects at Mach 0.6, 20,000 Feet, LP Compressor Inlet Airflow Versus LP Bleed Flow.

TABLE 74. BLEED EFFECTS, 20,000 FEET, MACH 0.6, STANDARD ATM, AT AN HP TURBINE INLET TEMPERATURE OF 1805°F.

A18 (sq in.)	A8 (sq in.)	A42 (%)	LPC (degrees)	Net Thrust (lbf)	LPC Bleed Rate (lbm/sec)
191	95	100	0	1430	0
191	95	100	0	1198	2.002
191	95	90	0	1160	2.002
191	105	100	0	1238	2.002
191	105	100	-5	1250	2.002
191	110	100	-5	1264	2.002

4.4.8.5 Overall Results of Bleed Effects Testing

The bleed effects tests confirmed that variable-geometry modulation can be used to regain part of the performance loss due to bleed extraction. The overall results of these tests, summarized in Table 75, show that 28 to 47 percent of the net thrust loss due to bleed-air extraction was recovered by the use of variable-geometry modulation.

The LP turbine nozzle area was used to rematch the LP compressor to a more efficient operating point; however, losses in LP turbine efficiency associated with reduced LP turbine nozzle area counteracted the compressor gains. Possibly, this result could be changed by a turbine optimized for performance under maximum bleed-air extraction conditions.

Primary exhaust-nozzle area modulation was used to increase the LP rotor speed, which produced gains in net thrust. A negative preswirl setting of the LP compressor inlet guide vanes was used for minor gains by increasing the LP compressor airflow at a given rotor speed. However, no significant gains are available from this element of variable geometry because decreased LP compressor efficiency offsets the effect of increased LP compressor airflow.

TABLE 75. OVERALL RESULTS OF BLEED EFFECTS TESTING AT STANDARD ATM WHILE MAINTAINING HP TURBINE INLET TEMPERATURE AT 1805°F

Altitude (feet)	Flight Mach no.	A42 (percent)	LPC IGV Angle (degrees)	A8 (sq in.)	A18 (sq in.)	Net Thrust Loss (percent) ①	Net Thrust Gain (percent) ②	Net Thrust Loss Recovered (percent) ③
40,000	0.8	100	-5	105	191	15.9	6.1	32
50,000	0.8	90	-5	105	191	14.7	7.2	42
50,000	1.2	100	0	105	191	13.6	7.3	47
20,000	0.6	100	-5	110	191	16.2	5.5	28

① Percent of net thrust lost due to initial bleed-air extraction.

② Percent of net thrust gain due to variable-geometry modulation relative to the base-line bleed point.

③ Percent of net thrust loss recovered by variable-geometry modulation.

4.4.9 Low-Speed Airflow

4.4.9.1 Objective

Low-speed-airflow tests were conducted at 50,000 feet, Mach 0.5, standard atmosphere to accumulate test data, particularly airflow data, to correlate with the data accrued at higher flight Mach numbers at 50,000 feet and to use for future updates of the engine analytical model.

4.4.9.2 Results

The test results are presented in Figures 602 through 617. The parameters presented in these curves are listed in Table 76.

TABLE 76. LOW-SPEED AIRFLOW, 50,000 FEET, MACH 0.5, STANDARD ATM

Figure No.	Parameters Presented
602	Thrust specific fuel consumption versus net thrust
603	Interturbine temperature versus net thrust
604	Net thrust versus LP rotor speed
605	Fuel flow versus LP rotor speed
606	Interturbine temperature versus LP rotor speed
607	HP rotor speed versus LP rotor speed
608	Engine total airflow versus LP rotor speed
609	Fan tip pressure ratio versus LP rotor speed
610	Fan hub pressure ratio versus LP rotor speed
611	Cycle pressure ratio versus LP rotor speed
612	Bypass ratio versus LP rotor speed
613	Engine pressure ratio versus LP rotor speed
614	Combined nozzle thrust coefficient versus LP rotor speed
615	Primary nozzle flow coefficient versus LP rotor speed
616	Fan nozzle flow coefficient versus LP rotor speed
617	Turbine inlet temperature versus interturbine temperature

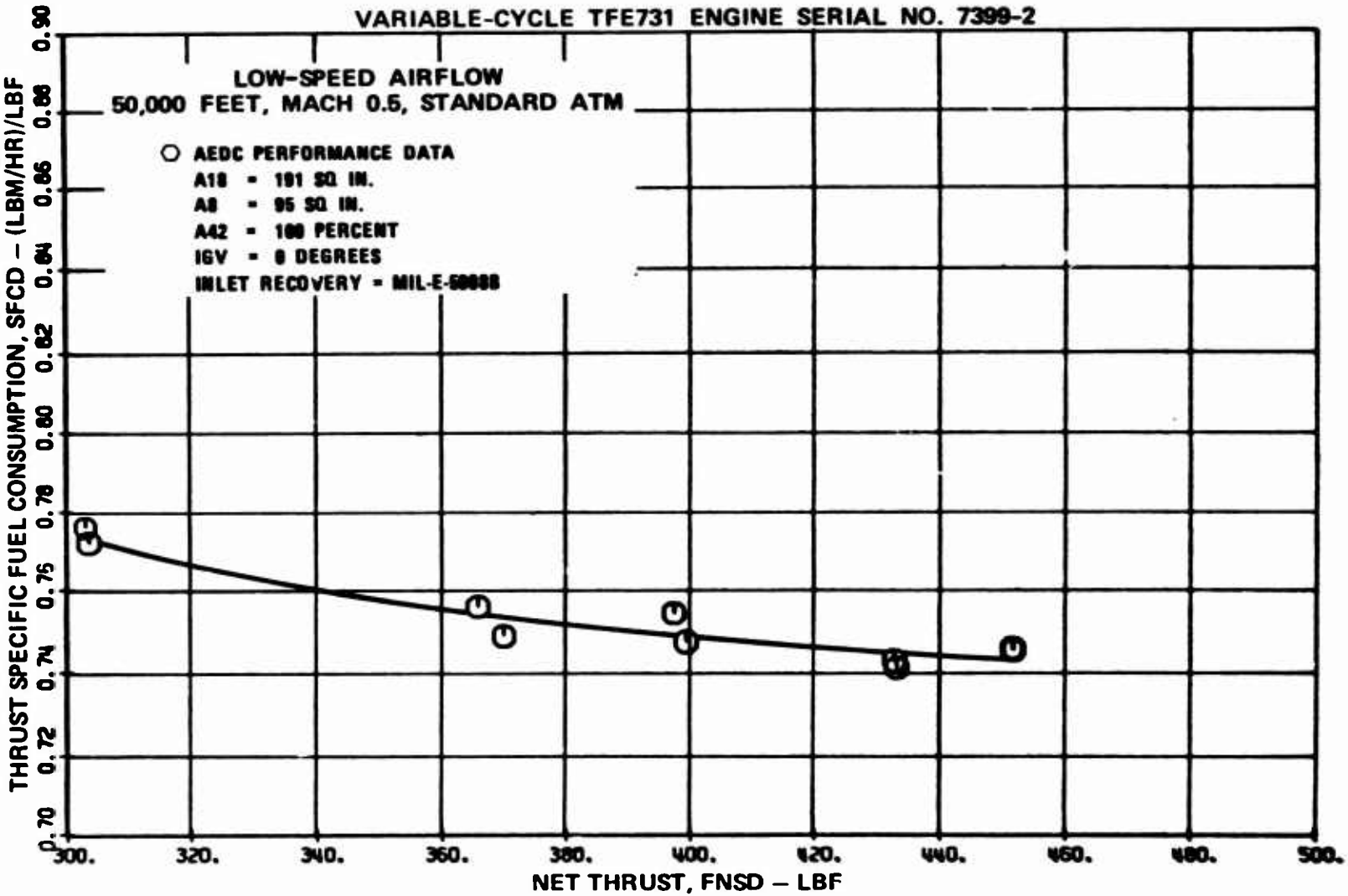

Figure 602. Low-Speed Airflow at Mach 0.5, 50,000 Feet, Thrust Specific Fuel Consumption Versus Net Thrust.

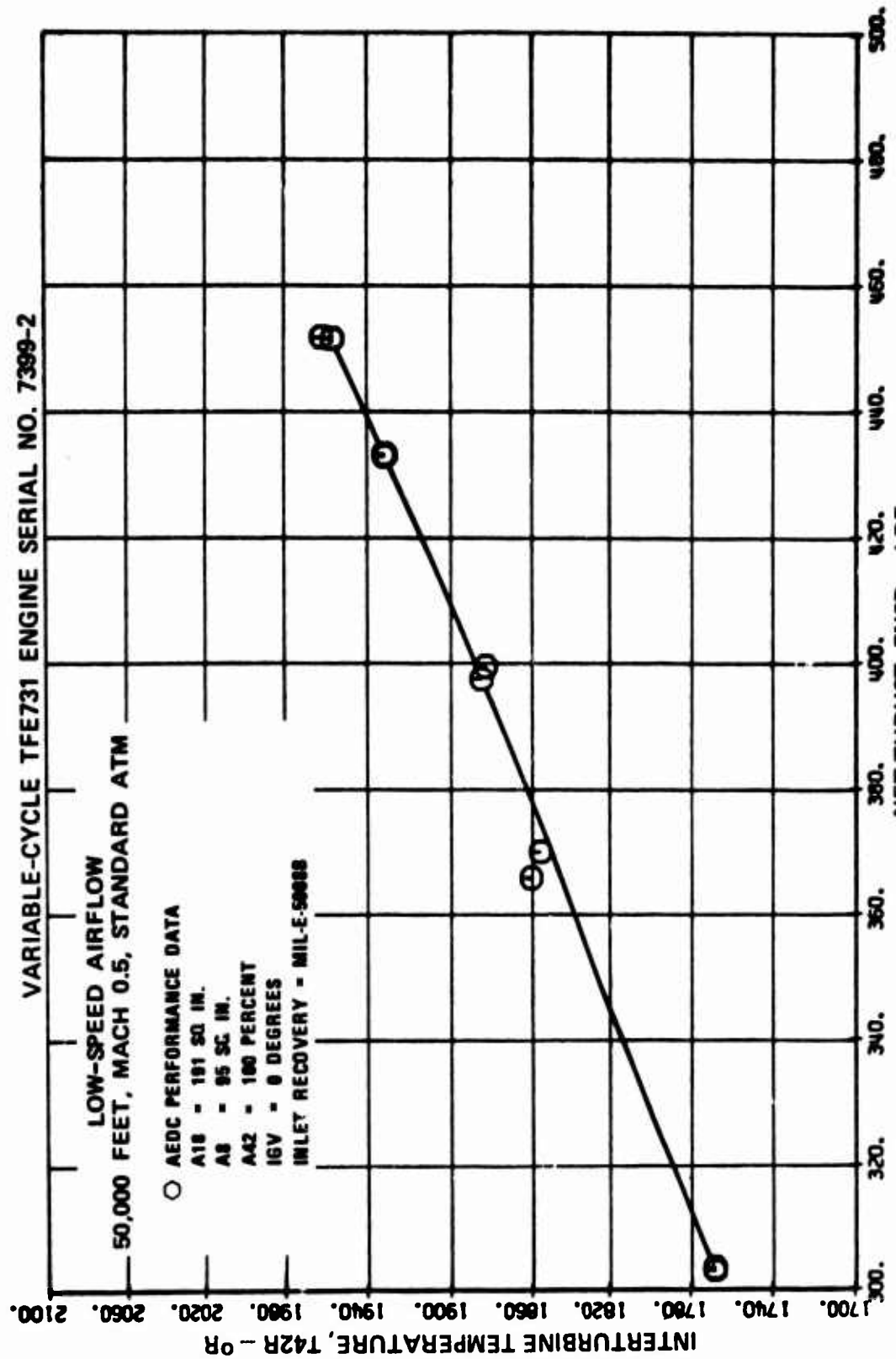

Figure 603. Low-Speed Airflow at Mach 0.5, 50,000 Feet, Interturbine Temperature Versus Net Thrust.

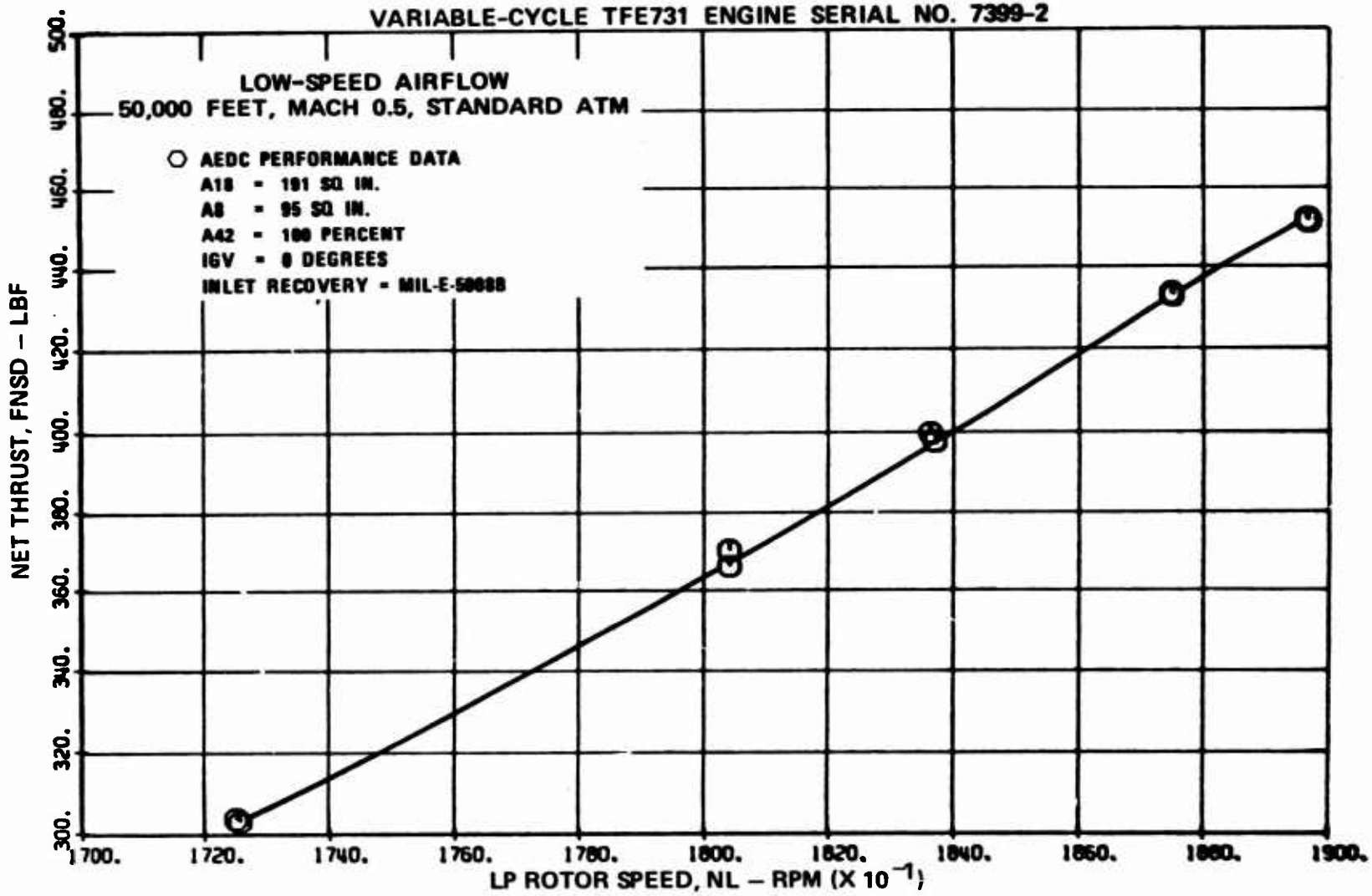

Figure 604. Low-Speed Airflow at Mach 0.5, 50,000 Feet, Net Thrust Versus LP Rotor Speed.

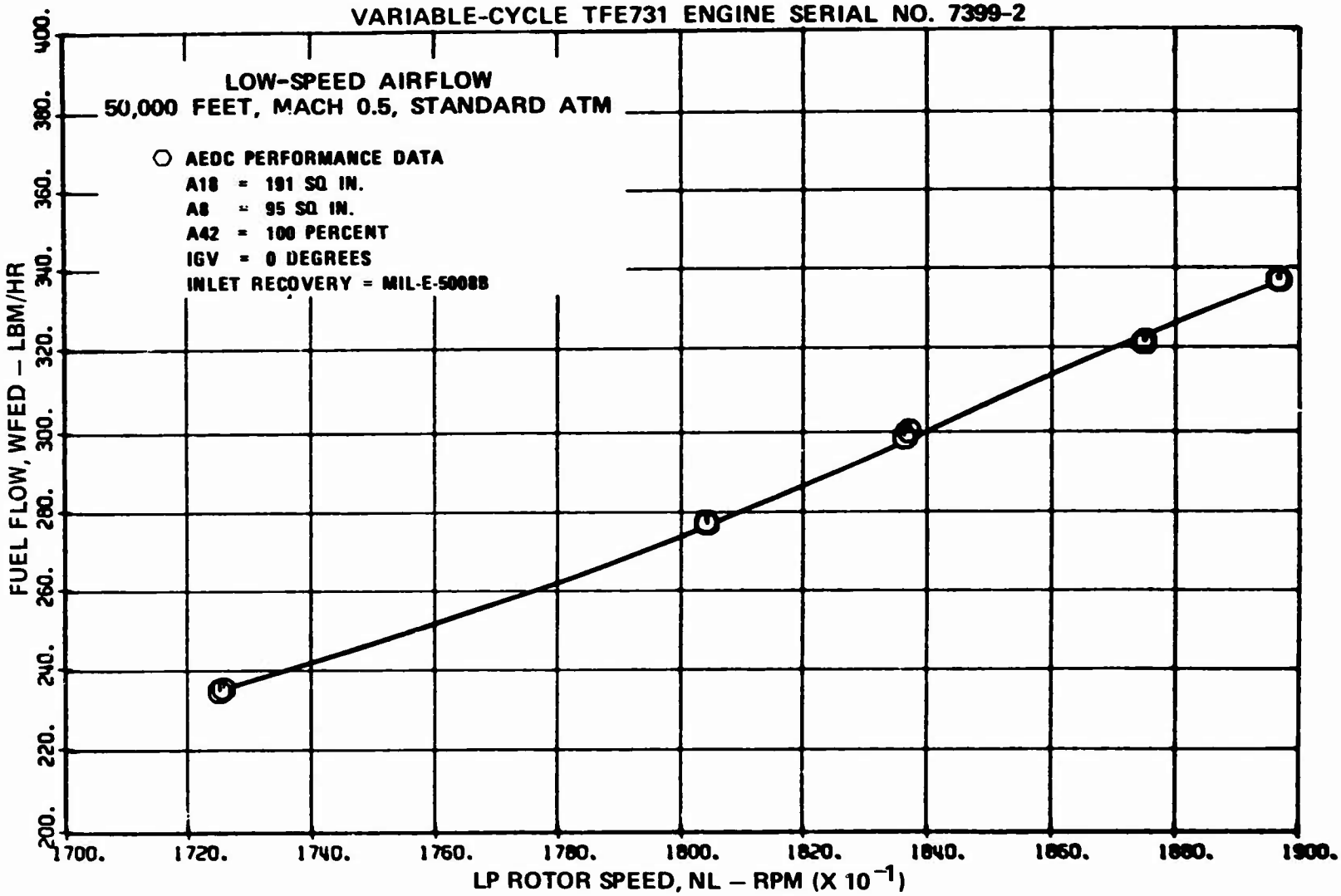

Figure 605. Low-Speed Airflow at Mach 0.5, 50,000 Feet, Fuel Flow Versus LP Rotor Speed.

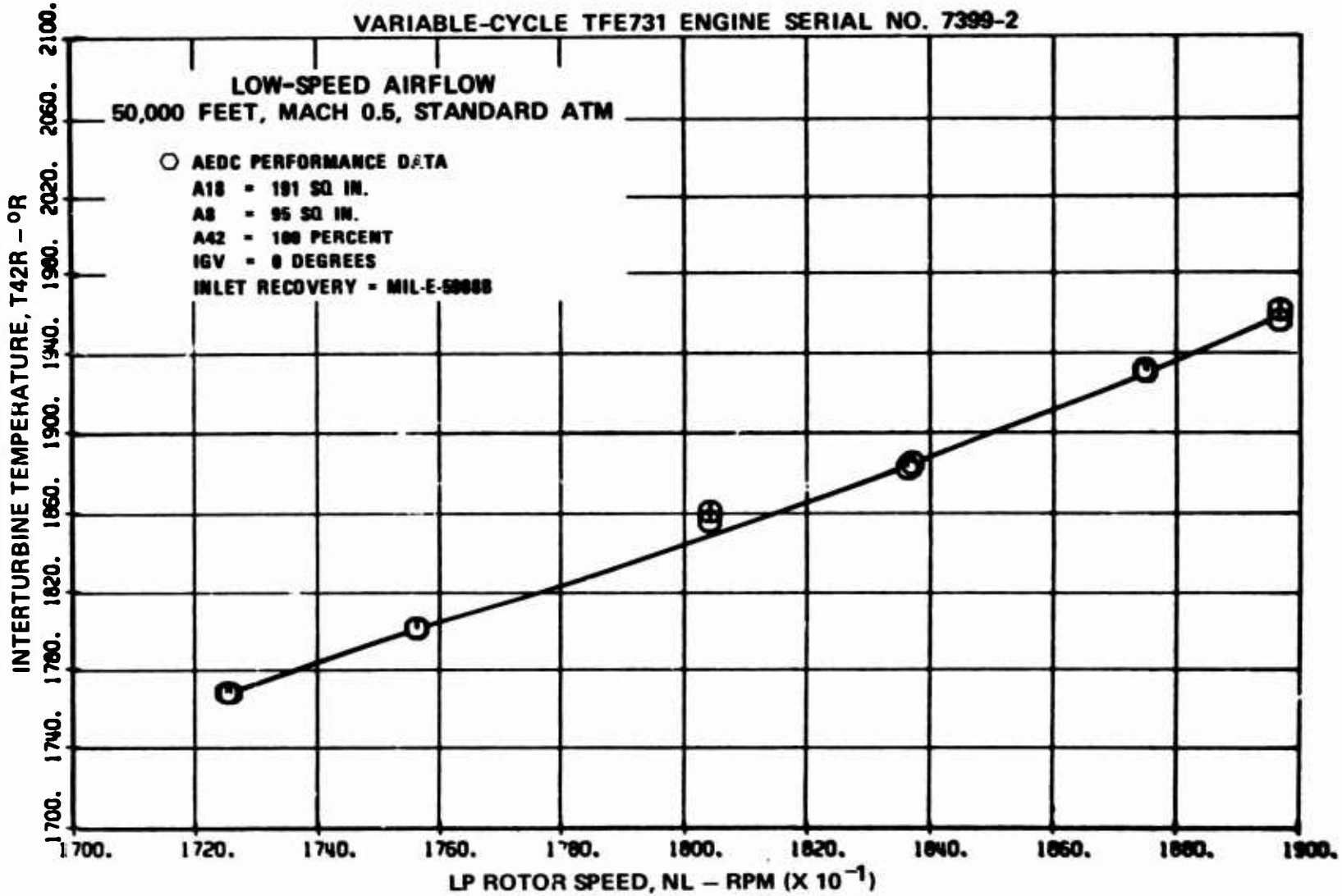

Figure 606. Low-Speed Airflow at Mach 0.5, 50,000 Feet, Interturbine Temperature Versus LP Rotor Speed.

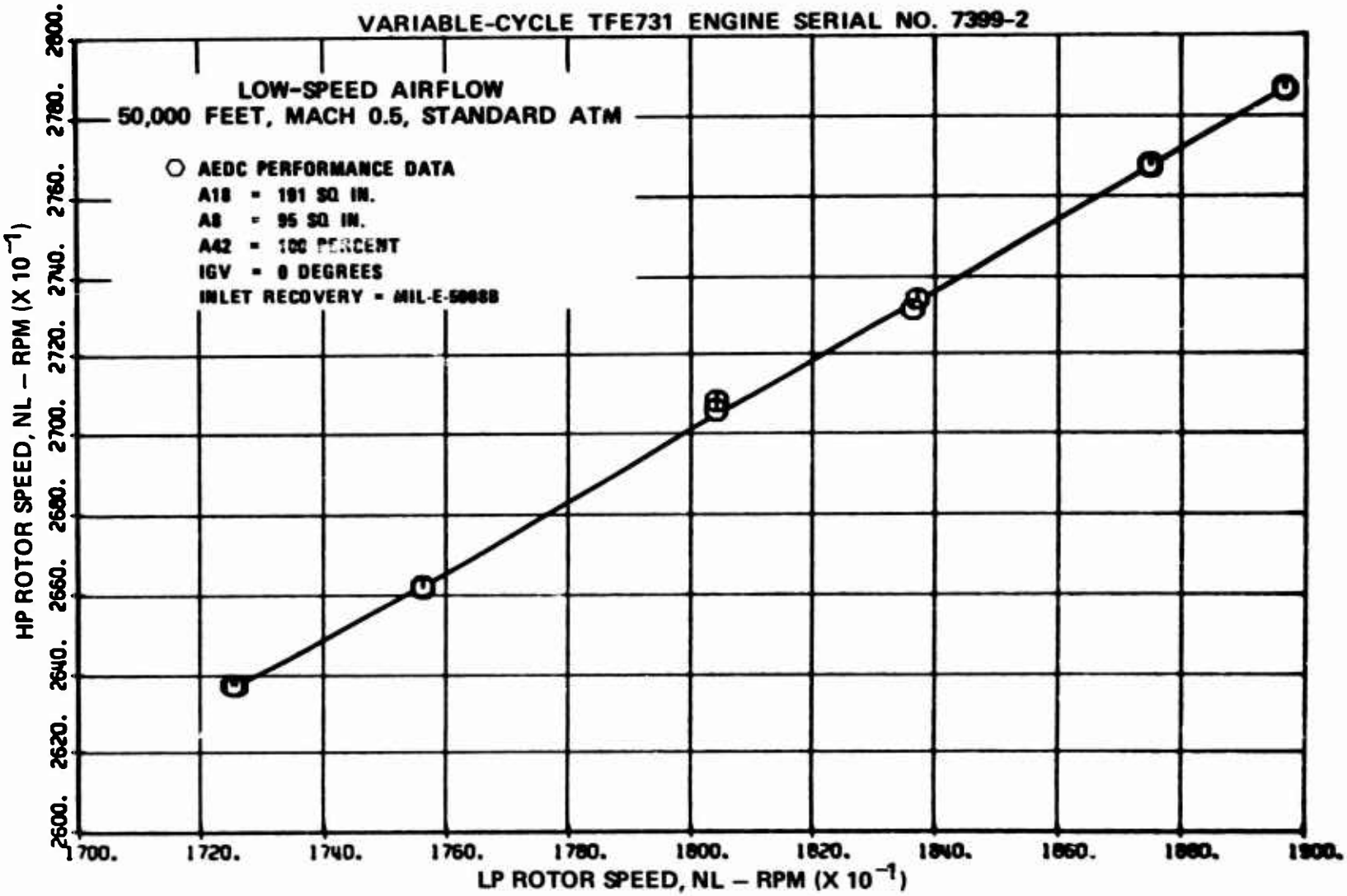

Figure 607. Low-Speed Airflow at Mach 0.5, 50,000 Feet, HP Rotor Speed Versus LP Rotor Speed.

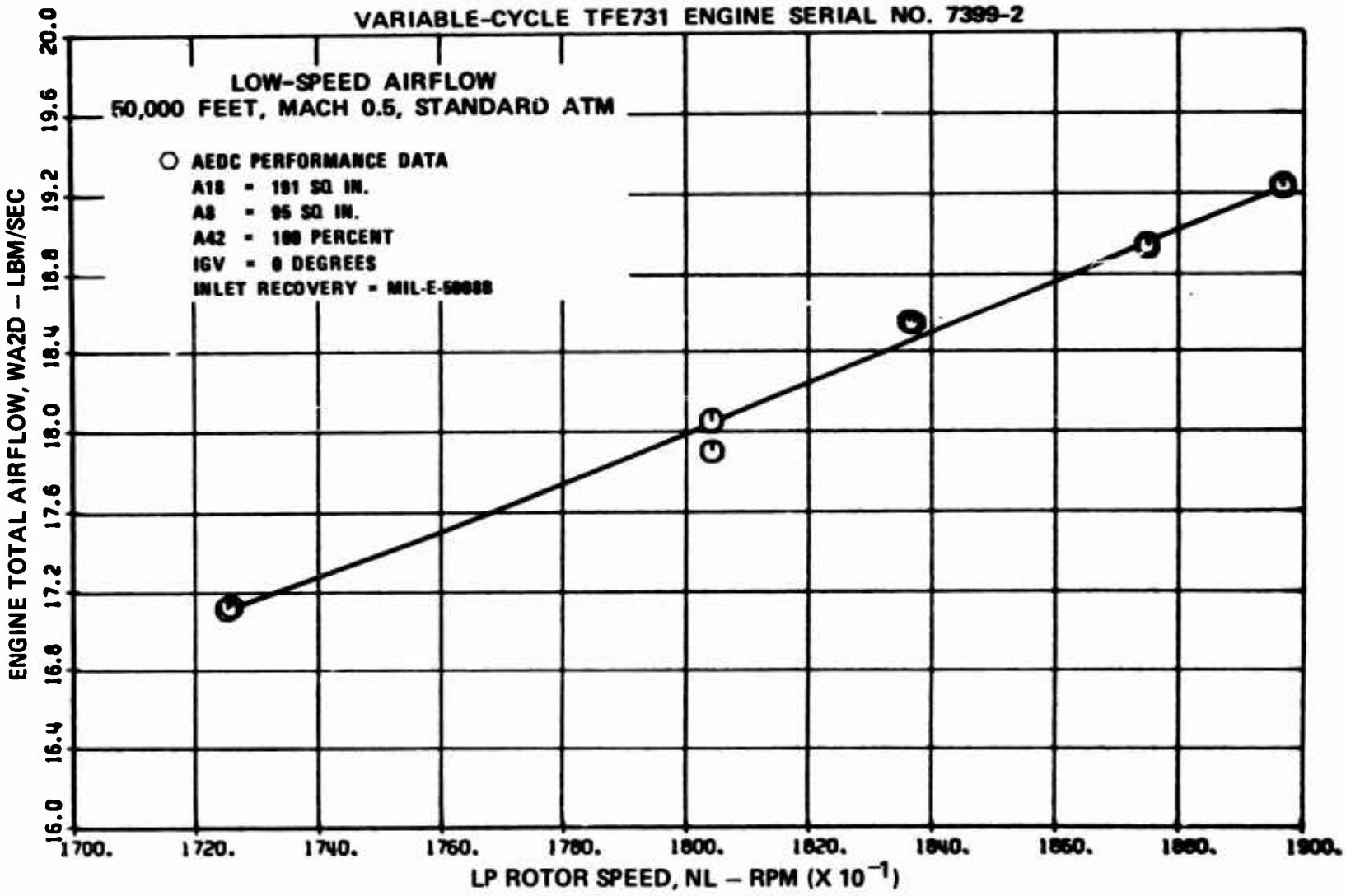

Figure 608. Low-Speed Airflow at Mach 0.5, 50,000 Feet, Engine Total Airflow Versus LP Rotor Speed.

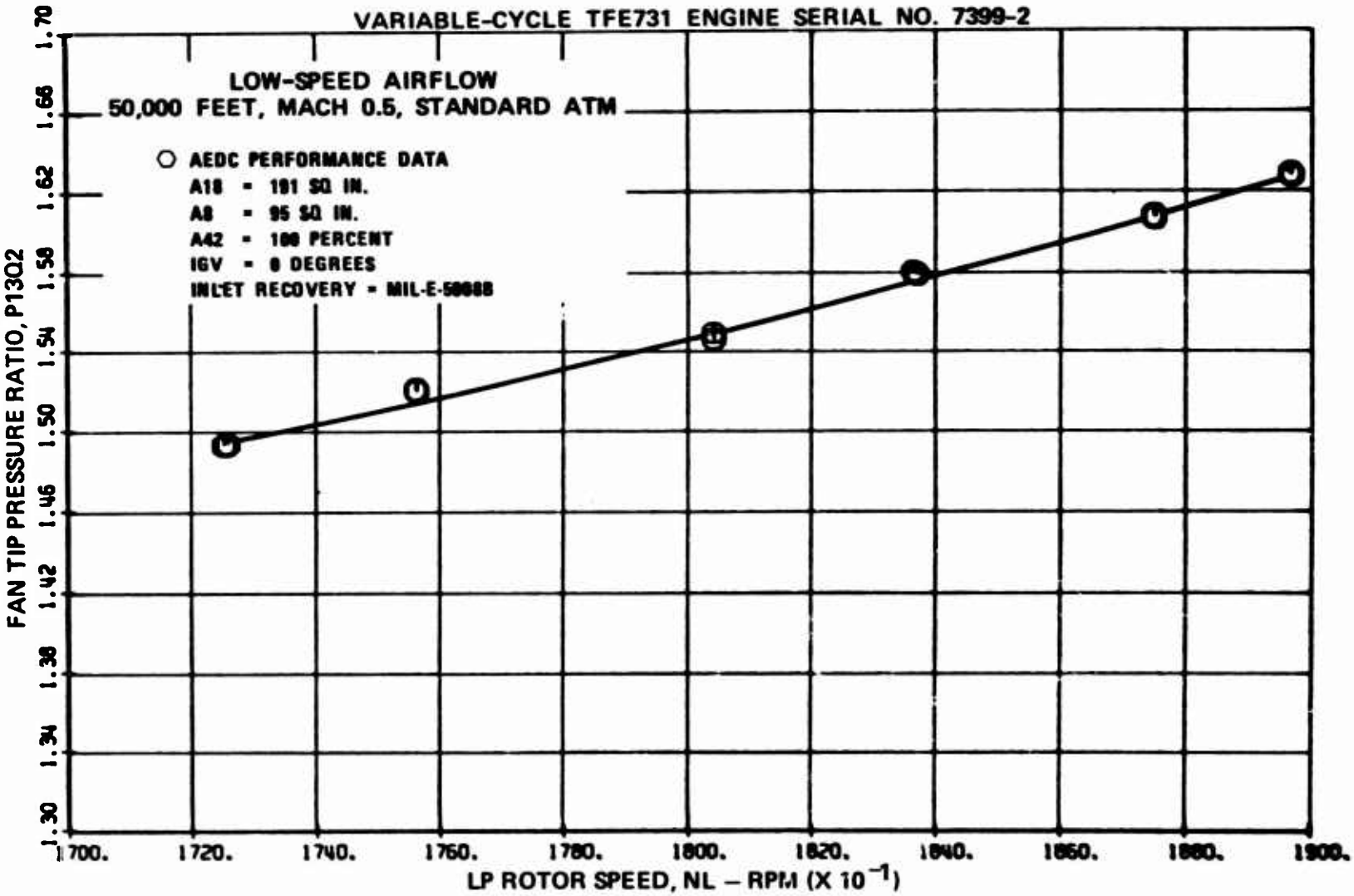

Figure 609. Low-Speed Airflow at Mach 0.5, 50,000 Feet, Fan Tip Pressure Ratio Versus LP Rotor Speed.

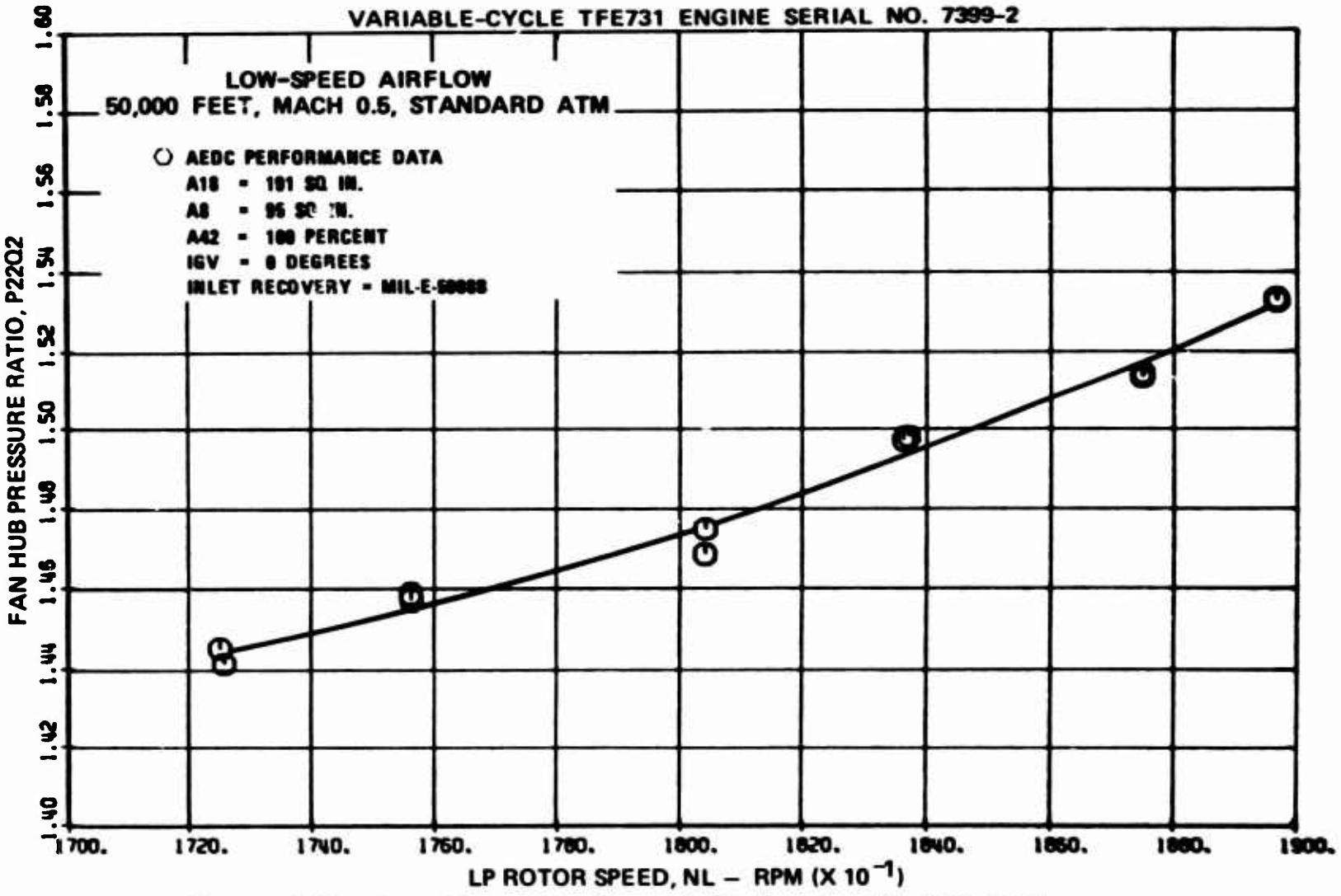

Figure 610. Low-Speed Airflow at Mach 0.5, 50,000 Feet, Fan Hub Pressure Ratio Versus LP Rotor Speed.

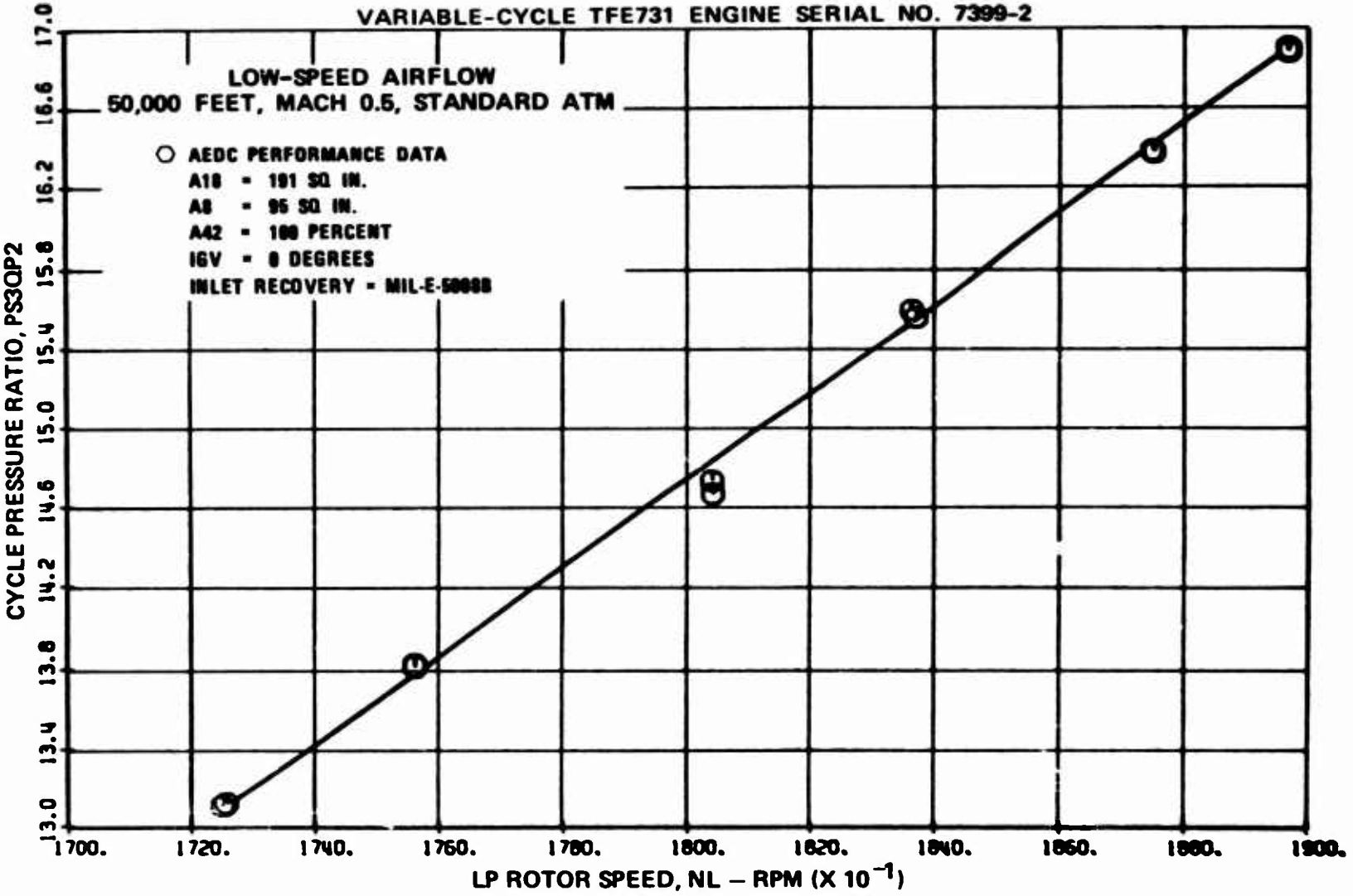

Figure 611. Low-Speed Airflow at Mach 0.5, 50,000 Feet, Cycle Pressure Ratio Versus LP Rotor Speed.

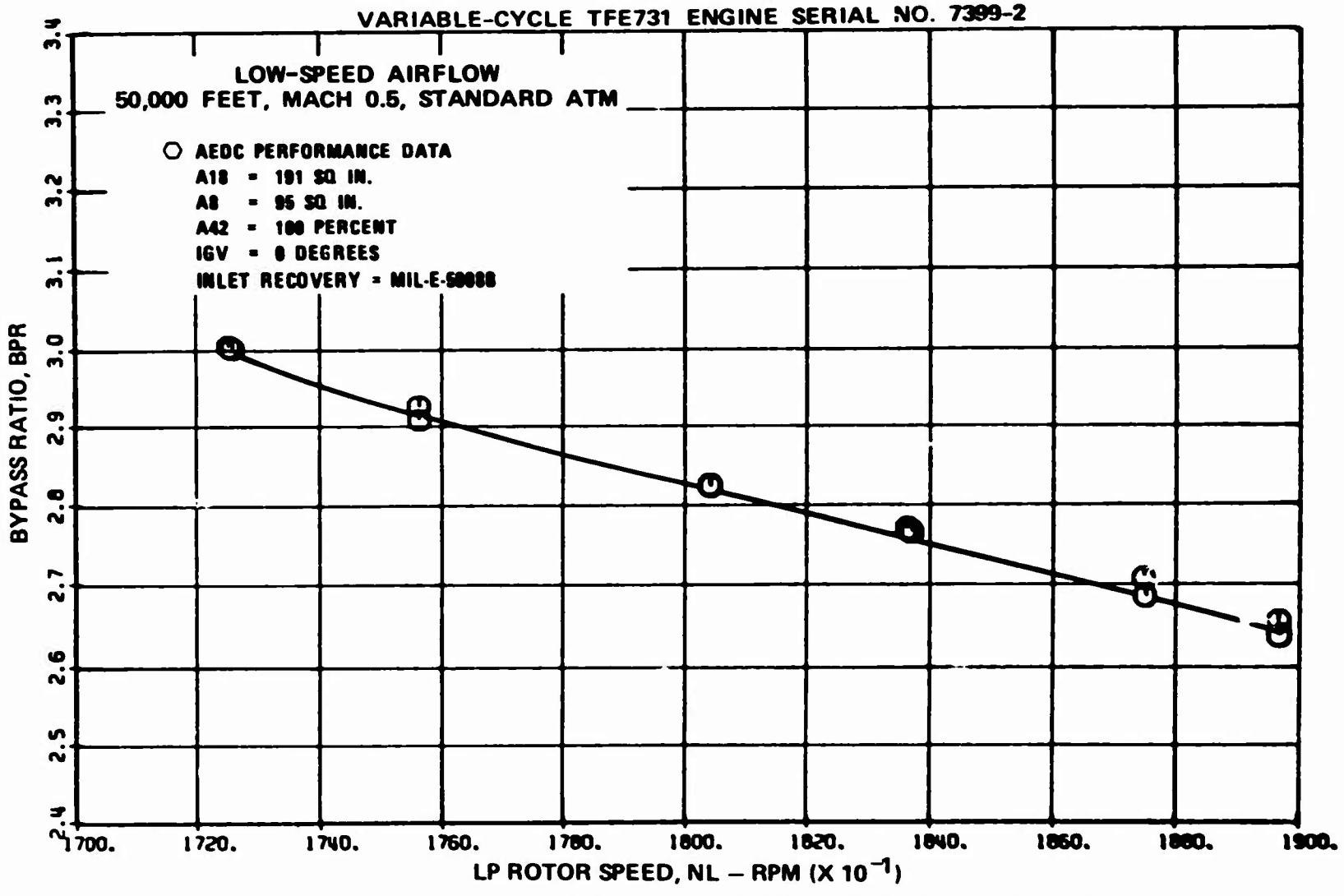

Figure 612. Low-Speed Airflow at Mach 0.5, 50,000 Feet, Bypass Ratio Versus LP Rotor Speed.

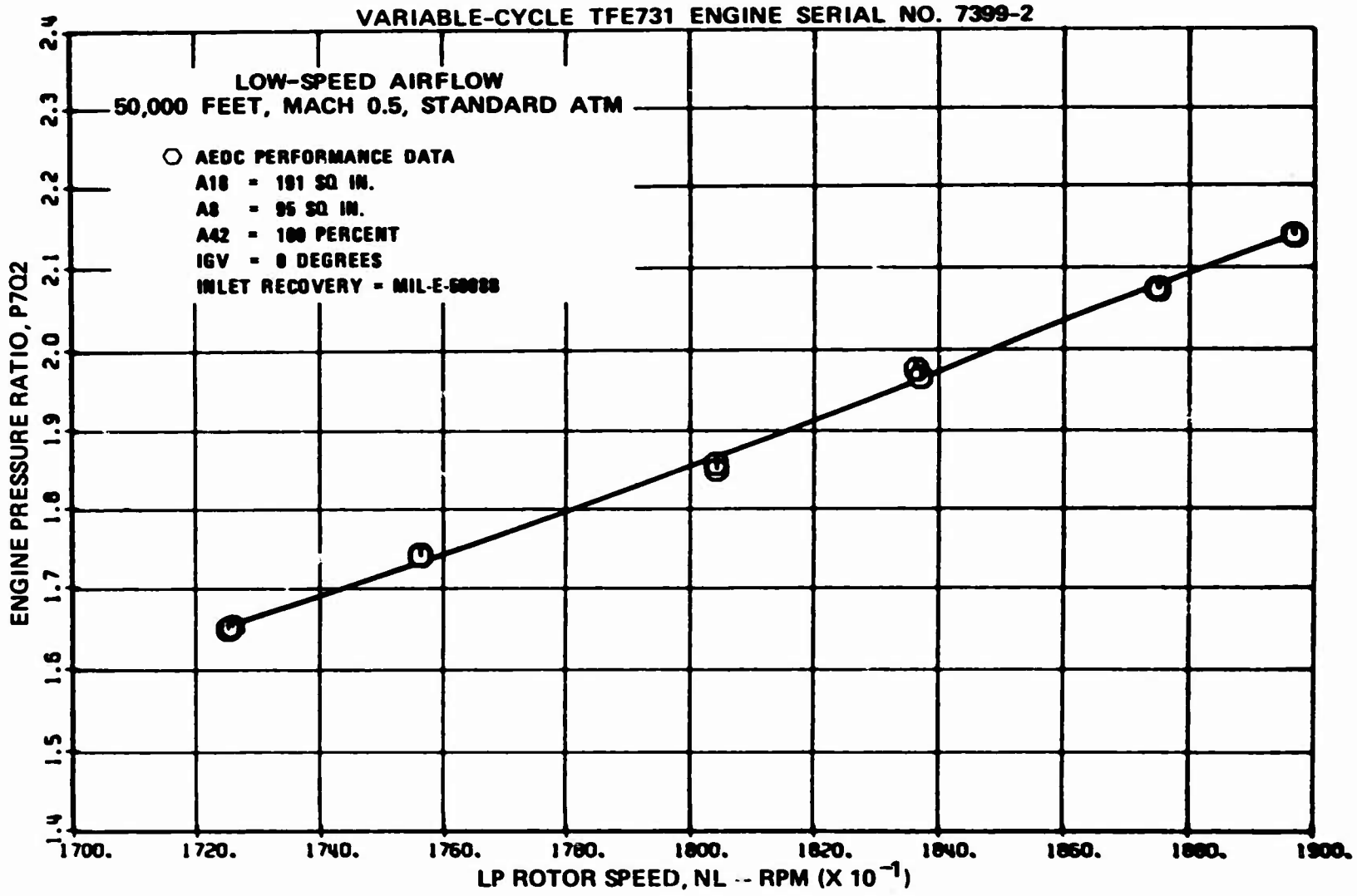

Figure 613. Low-Speed Airflow at Mach 0.5, 50,000 Feet, Engine Pressure Ratio Versus LP Rotor Speed.

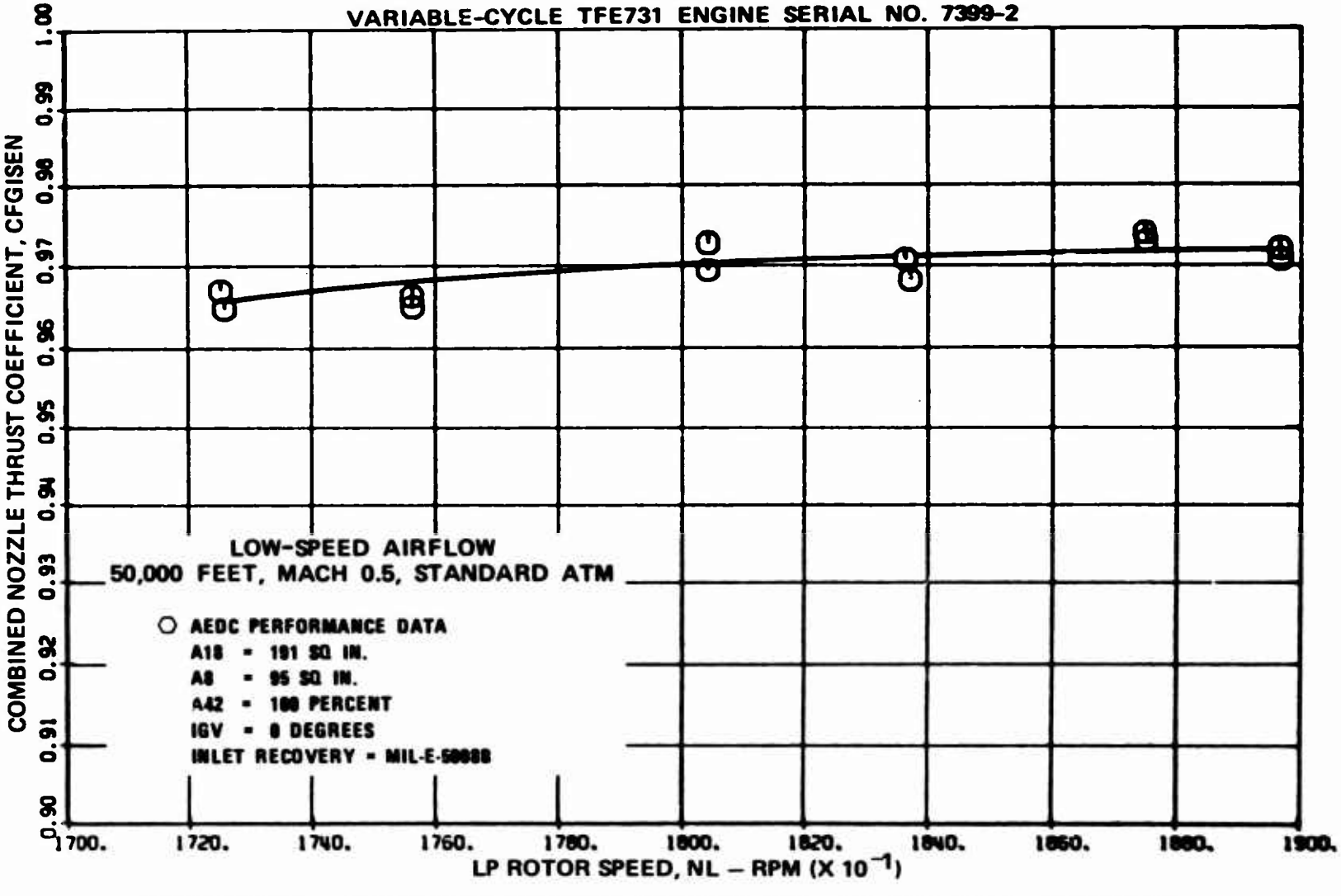

Figure 614. Low-Speed Airflow at Mach 0.5, 50,000 Feet, Combined Nozzle Thrust Coefficient Versus LP Rotor Speed.

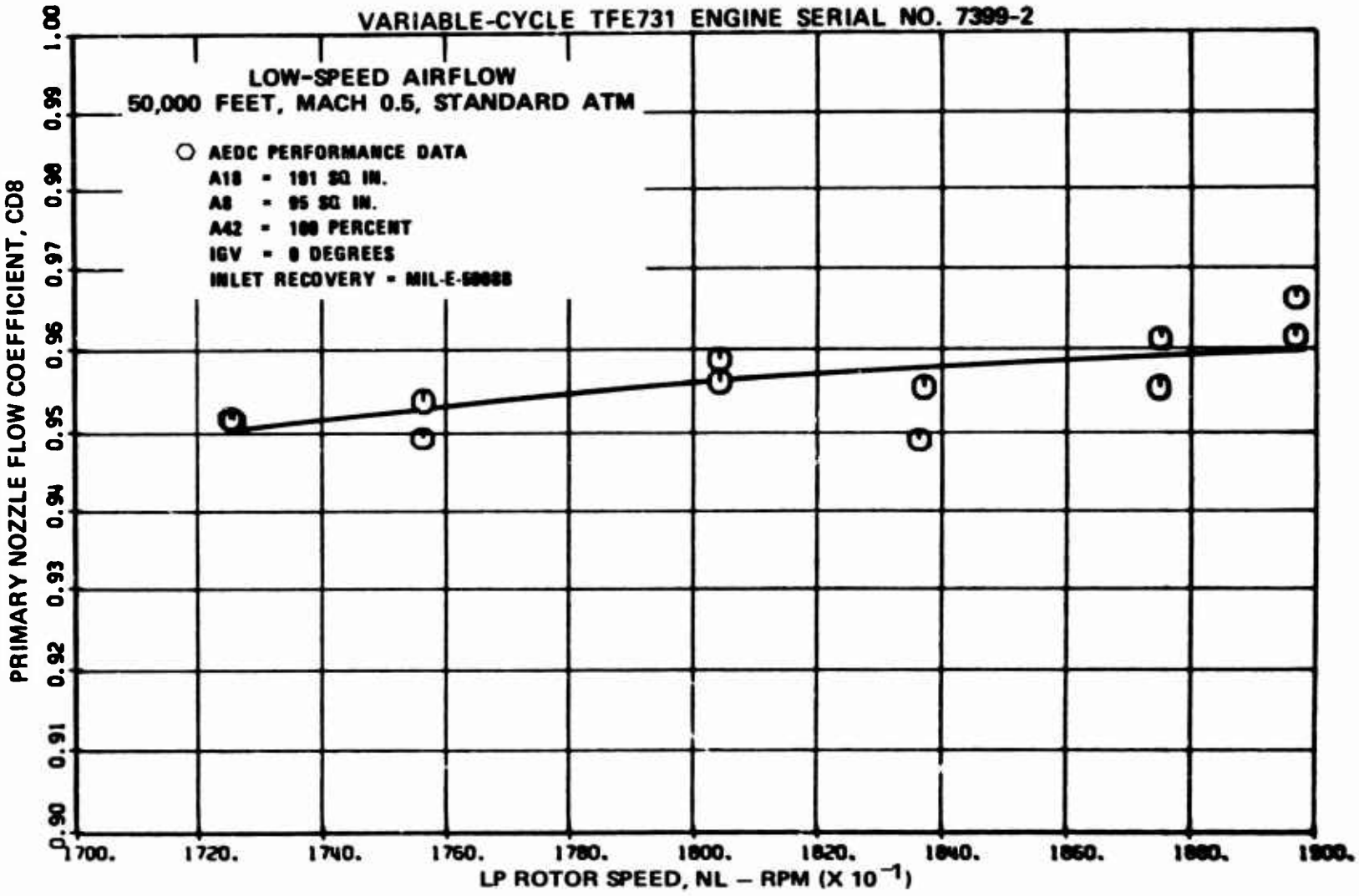

Figure 615. Low-Speed Airflow at Mach 0.5, 50,000 Feet, Primary Nozzle Flow Coefficient Versus LP Rotor Speed.

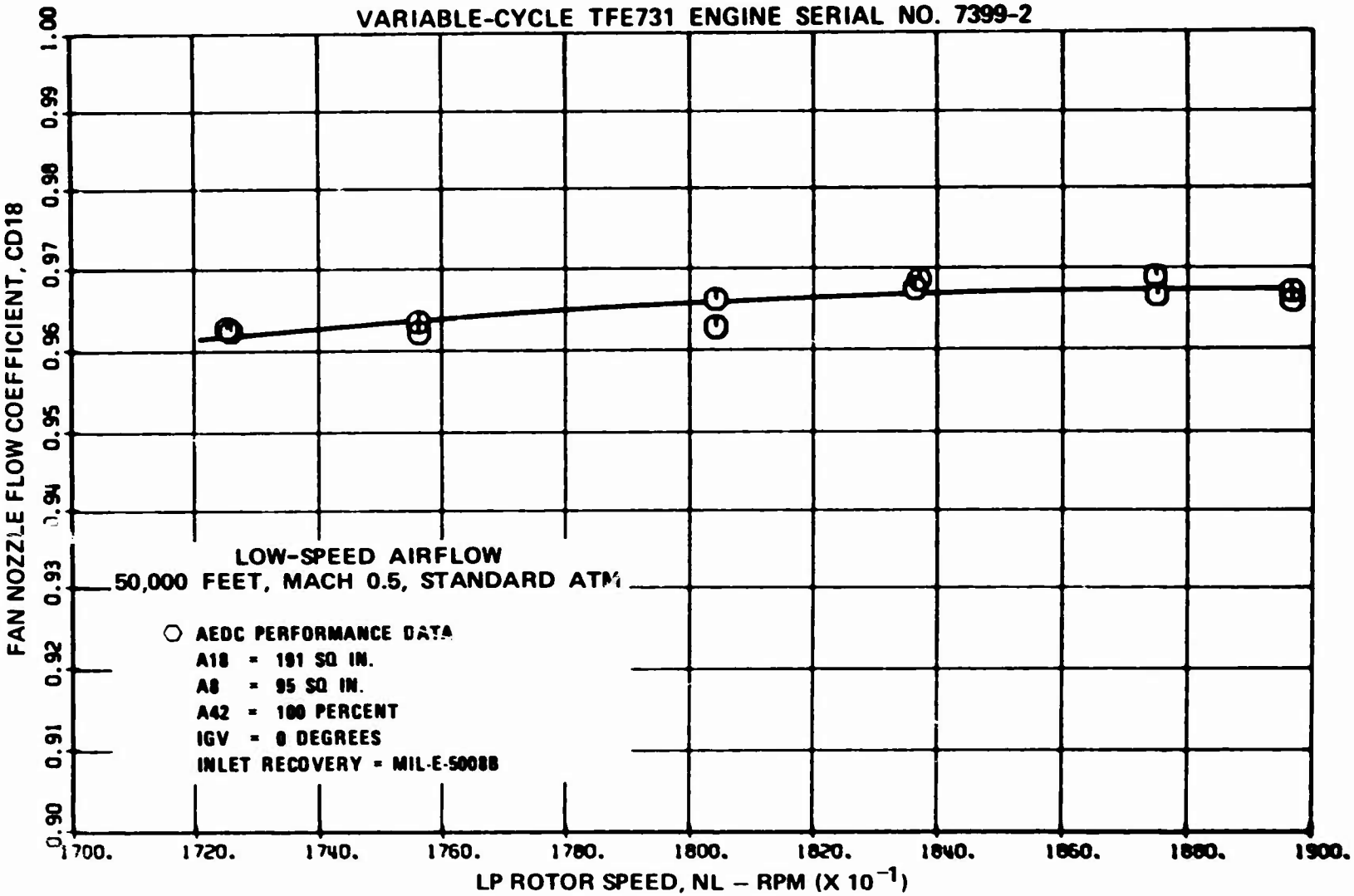

Figure 616. Low-Speed Airflow at Mach 0.5, 50,000 Feet, Fan Nozzle Flow Coefficient Versus LP Rotor Speed.

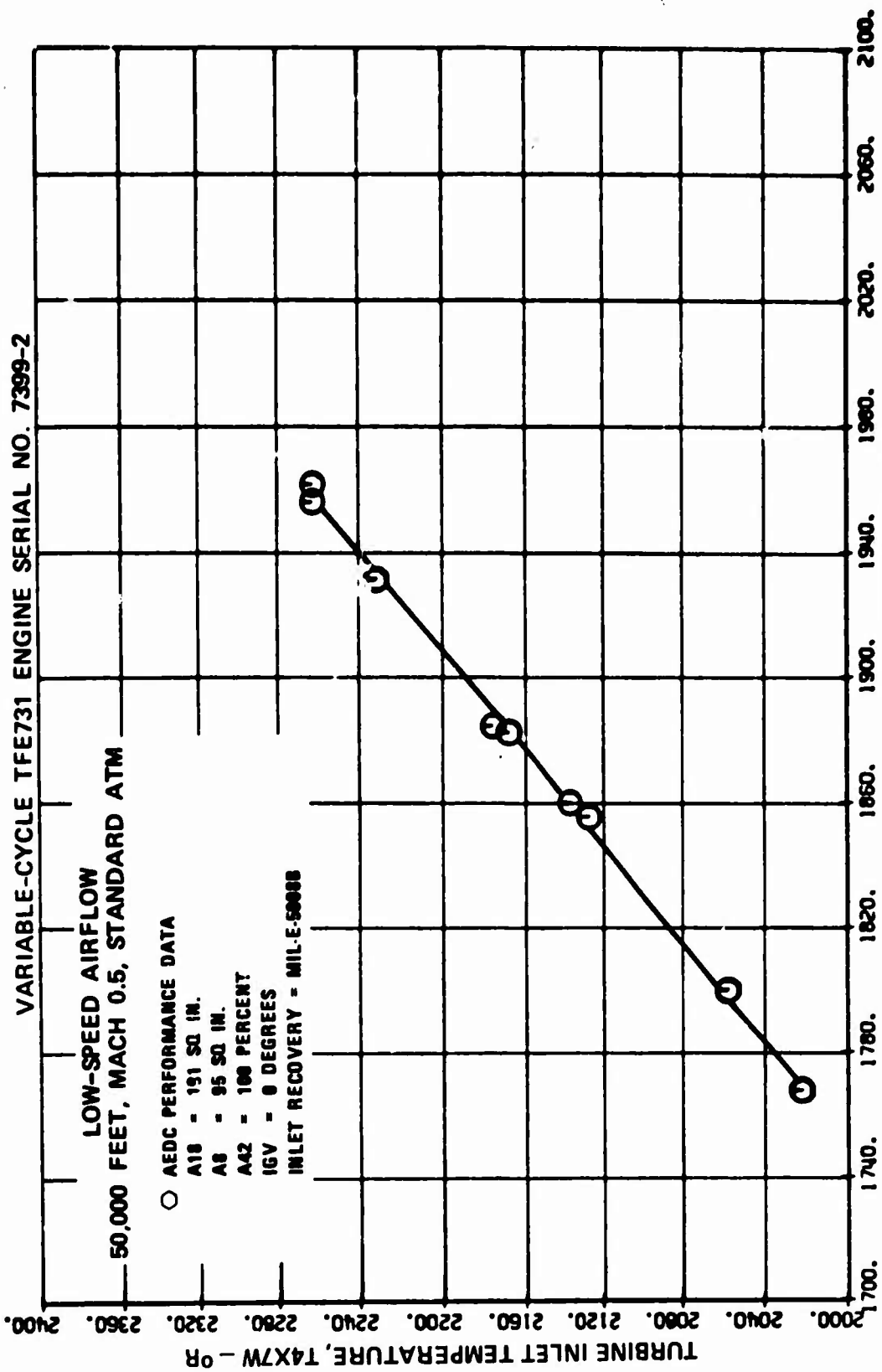

Figure 617. Low-Speed Airflow at Mach 0.5, 50,000 Feet, Turbine Inlet Temperature Versus Interturbine Temperature.

4.4.10 High Altitude

4.4.10.1 Objective

The original objective of this test series was to accumulate test data at 65,000 feet, Mach 0.6, standard atmosphere, with nominal geometry settings for use in updating the engine analytical model. However, this objective was expanded to include testing at 65,000 feet at Mach 0.5 and at 70,000 and 75,000 feet to accumulate data for a potential USAF application of the TFE731 Engine.

4.4.10.2 65,000 Feet, Mach 0.6

The results of the testing at 65,000 feet, Mach 0.6, standard atmosphere are presented in Figures 618 through 633. The parameters presented in these curves are listed in Table 77. The engine was tested with nominal geometry settings except for the LP turbine nozzle area. The LP turbine nozzle area was increased to 105 percent of nominal area to increase the LP surge margin because previous testing had indicated inadequate surge margin at low power settings at this operating condition with the nominal LP turbine nozzle area.

4.4.10.3 Special High-Altitude Test

The objective of the special high-altitude test was to determine the maximum altitude capability of a fixed-cycle TFE731 Engine in the 65,000- to 75,000-foot region, and to measure the engine performance at these altitudes. The test plan was to operate the engine at Mach 0.5 at 65,000, 70,000, and 75,000 feet, standard atmosphere, at interturbine temperatures of 1300, 1400, and 1500°F, with an LP turbine nozzle area as close to nominal as possible. The test was conducted with a fan exhaust-nozzle area of 195 square inches and a primary exhaust-nozzle area of 105 square inches.

TABLE 77. HIGH-ALTITUDE FIXED-GEOMETRY 65,000 FEET, MACH 0.6, STANDARD ATM

Figure No.	Parameters Presented
618	Thrust specific fuel consumption versus net thrust
619	Interturbine temperature versus net thrust
620	Net thrust versus LP rotor speed
621	Fuel flow versus LP rotor speed
622	Interturbine temperature versus LP rotor speed
623	HP rotor speed versus LP rotor speed
624	Engine total airflow versus LP rotor speed
625	Fan tip pressure ratio versus LP rotor speed
626	Fan hub pressure ratio versus LP rotor speed
627	Cycle pressure ratio versus LP rotor speed
628	Bypass ratio versus LP rotor speed
629	Engine pressure ratio versus LP rotor speed
630	Combined nozzle thrust coefficient versus LP rotor speed
631	Primary nozzle flow coefficient versus LP rotor speed
632	Fan nozzle flow coefficient versus LP rotor speed
633	Turbine inlet temperature versus interturbine temperature

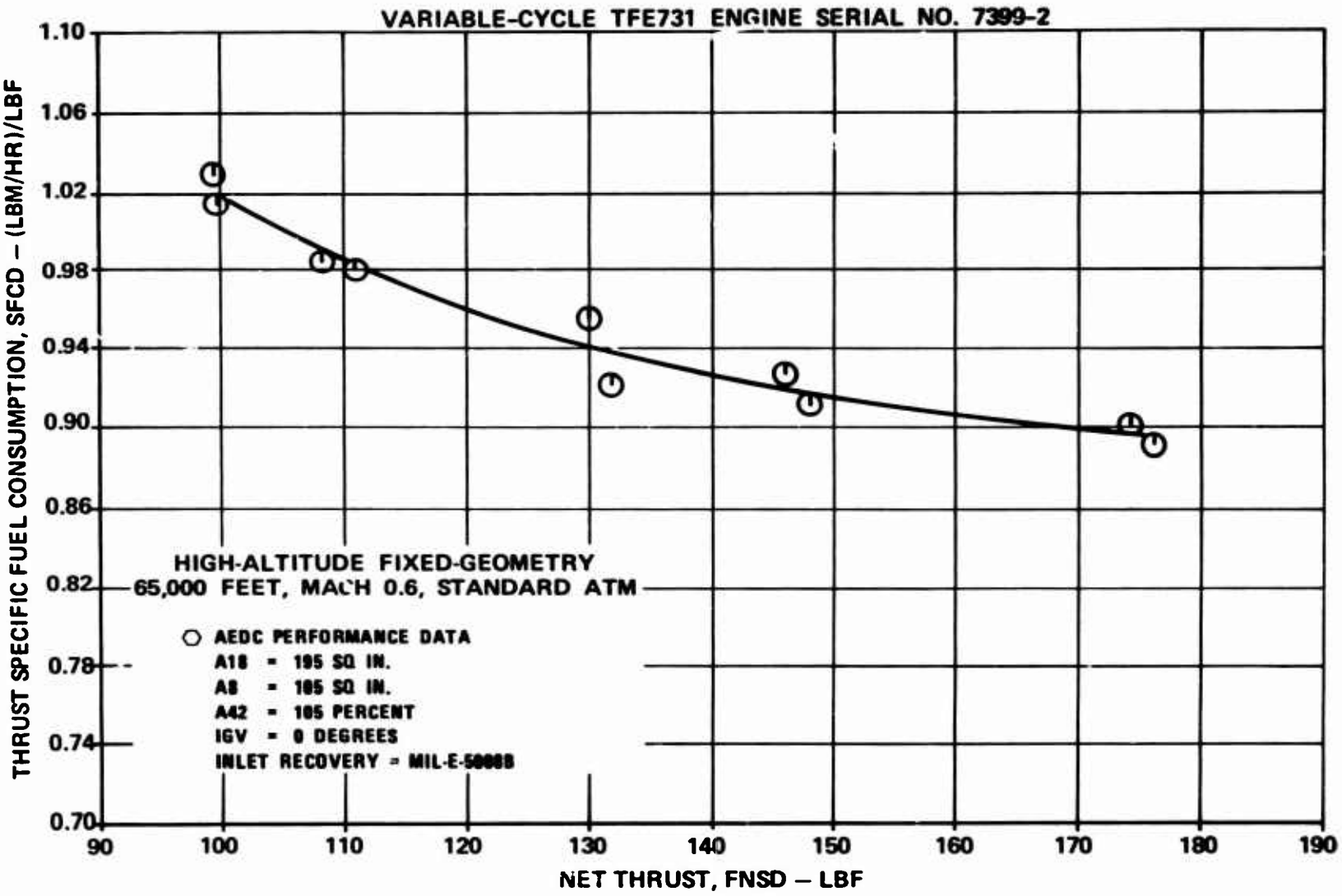

Figure 618. High-Altitude Fixed-Geometry at Mach 0.6, 65,000 Feet, Thrust Specific Fuel Consumption Versus Net Thrust.

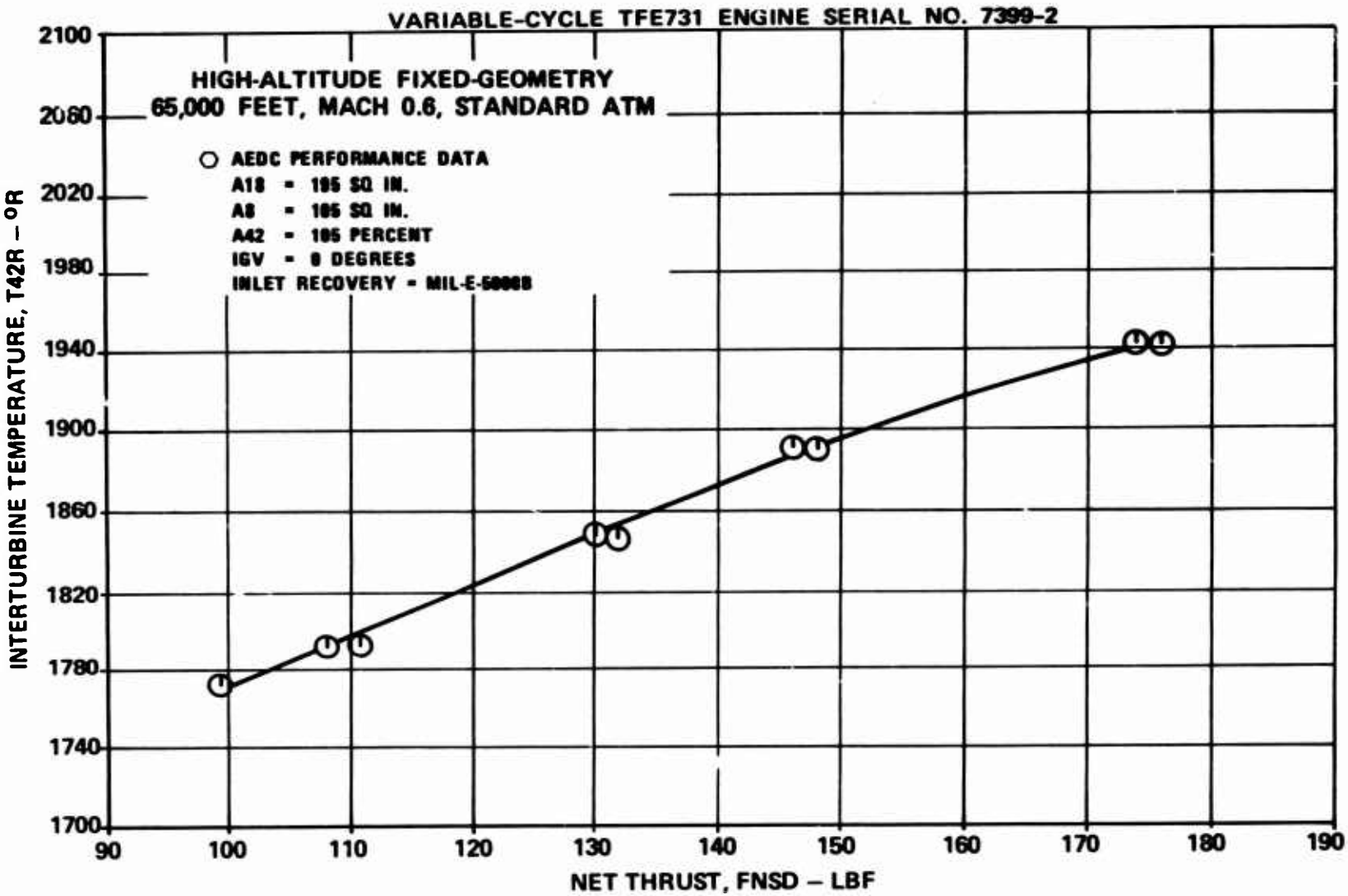

Figure 619. High-Altitude Fixed-Geometry at Mach 0.6, 65,000 Feet, Interturbine Temperature Versus Net Thrust.

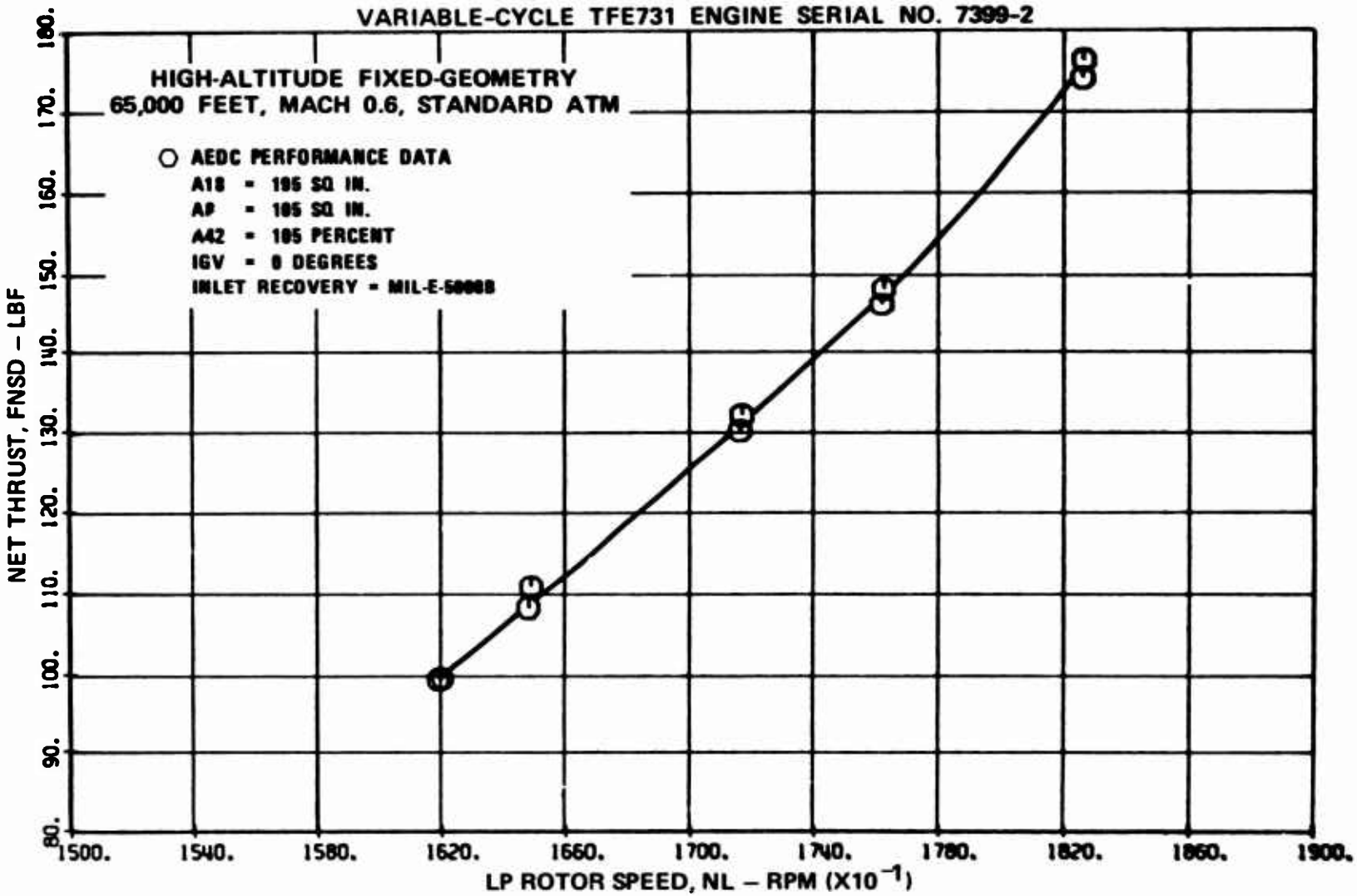

Figure 620. High-Altitude Fixed-Geometry at Mach 0.6, 65,000 Feet, Net Thrust Versus LP Rotor Speed.

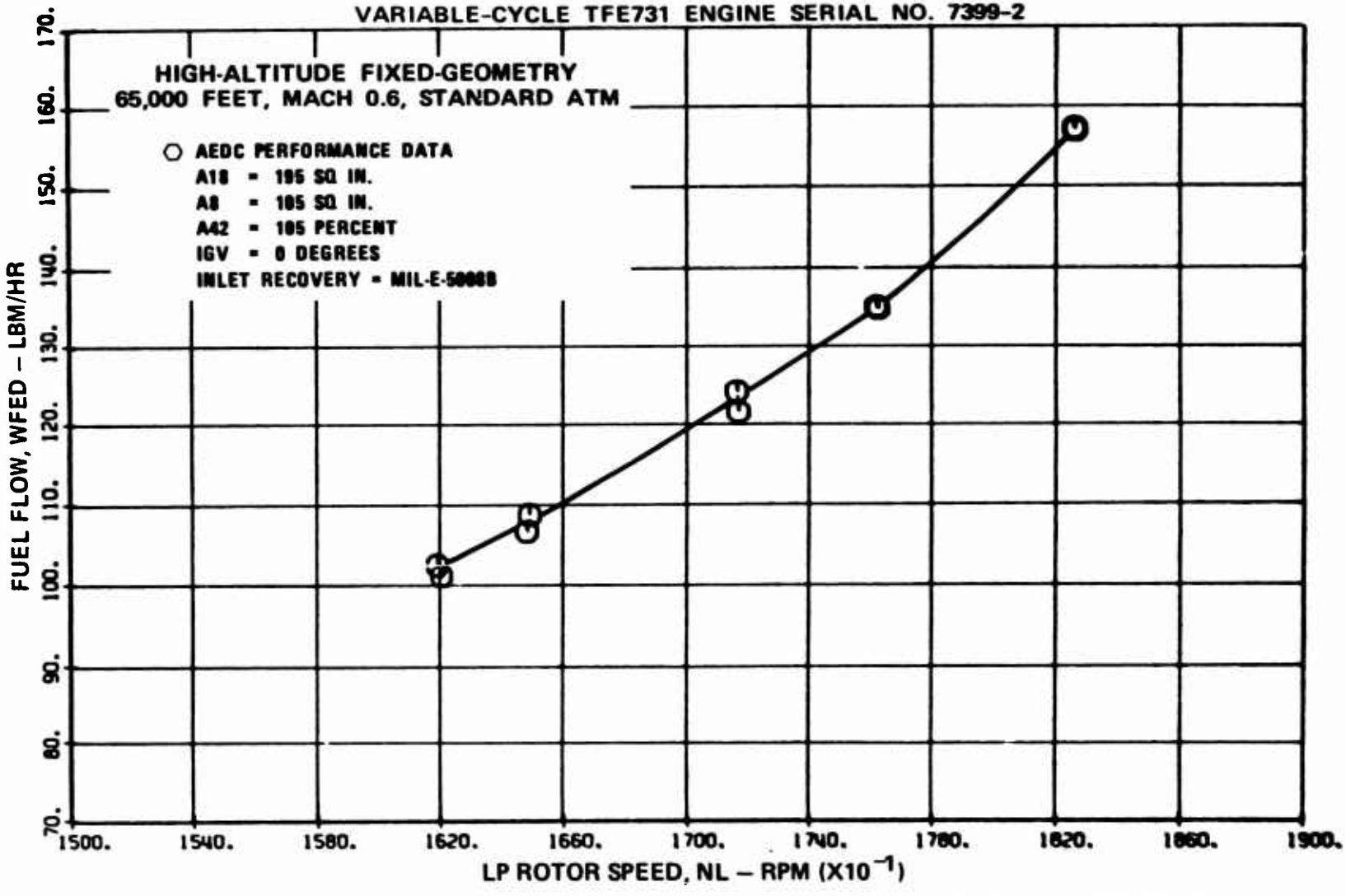

Figure 621. High-Altitude Fixed Geometry at Mach 0.6, 65,000 Feet, Fuel Flow Versus LP Rotor Speed.

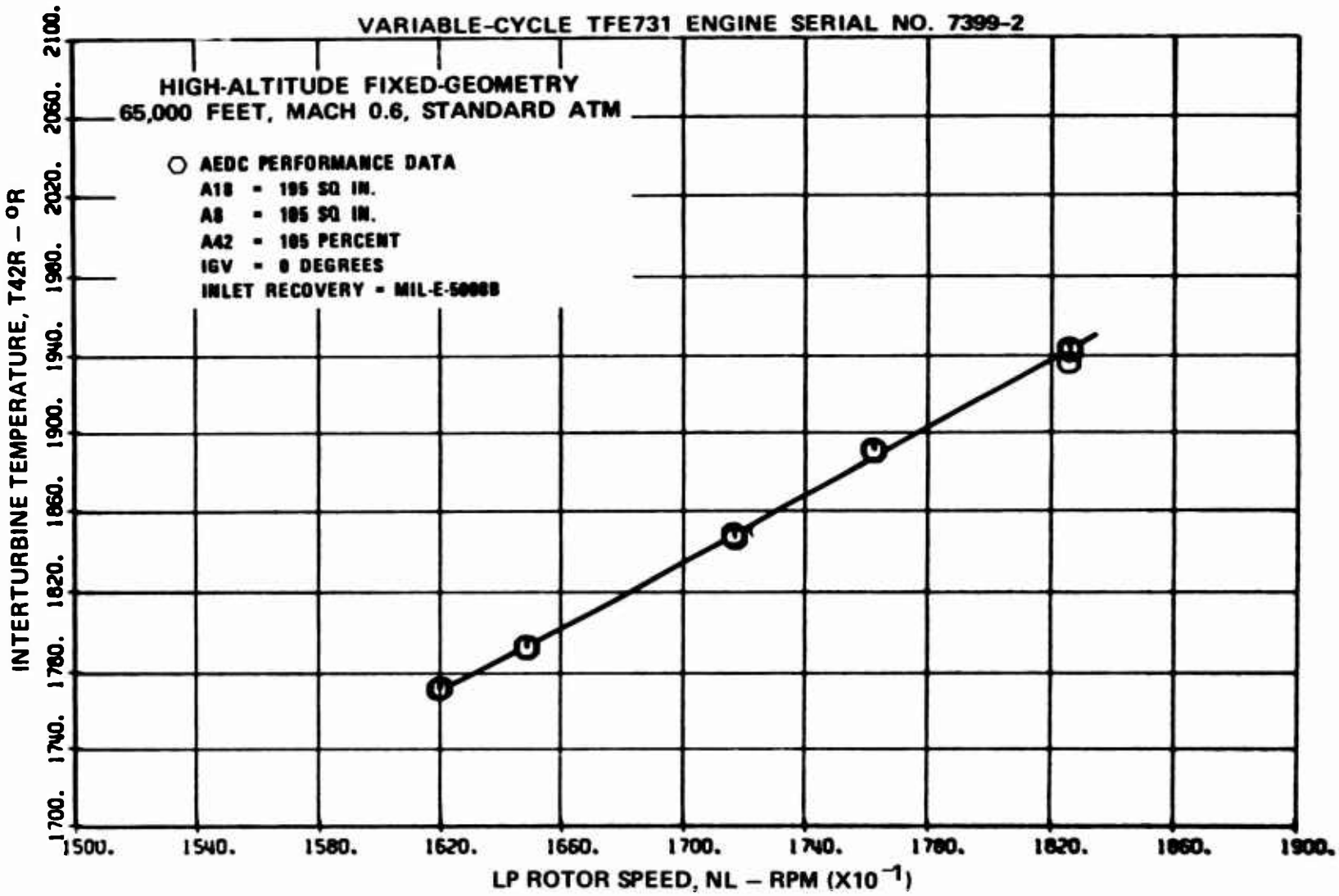

Figure 622. High-Altitude Fixed-Geometry at Mach 0.6, 65,000 Feet, Interturbine Temperature Versus LP Rotor Speed.

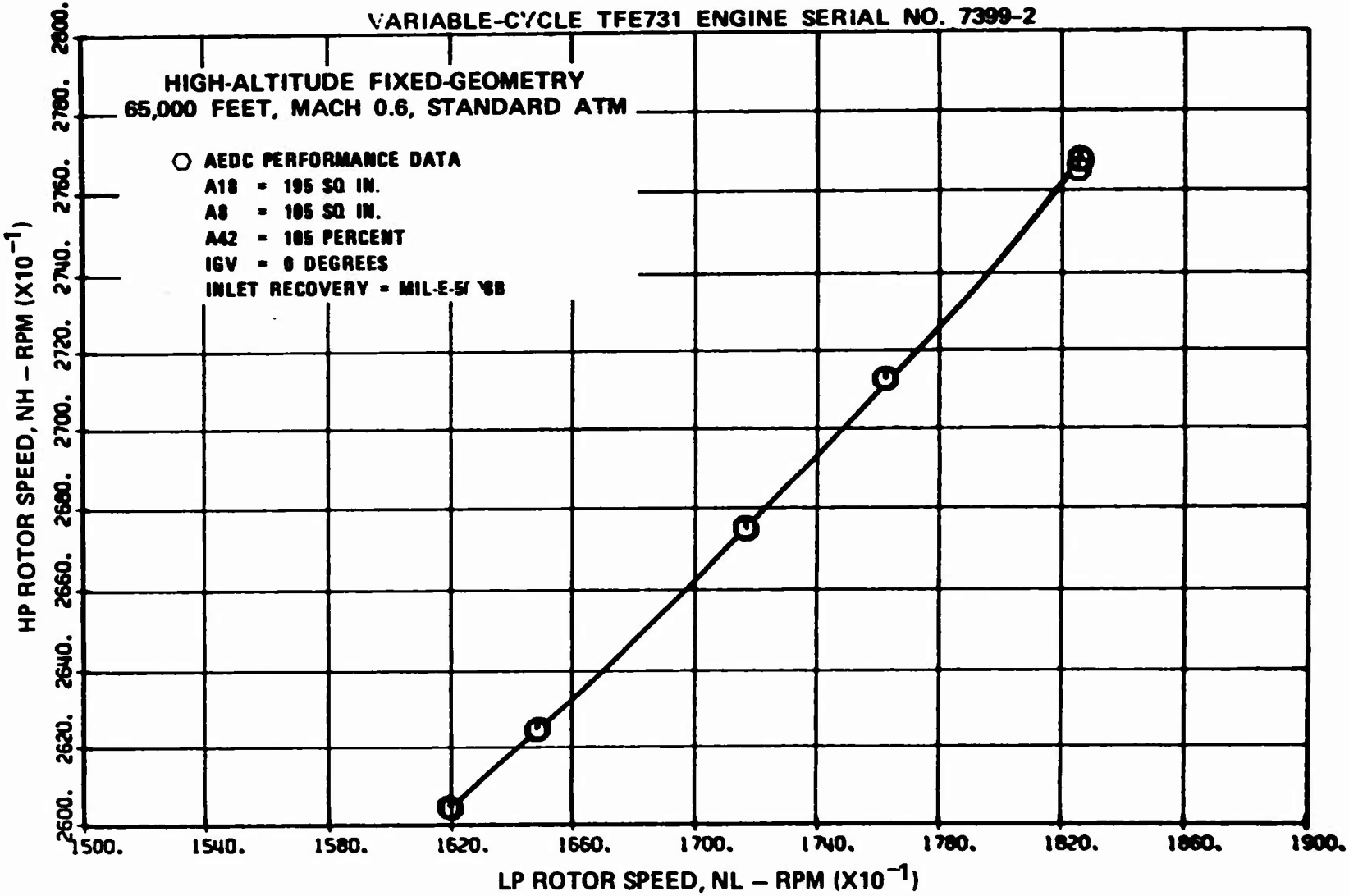

Figure 623. High-Altitude Fixed-Geometry at Mach 0.6, 65,000 Feet, HP Rotor Speed Versus LP Rotor Speed.

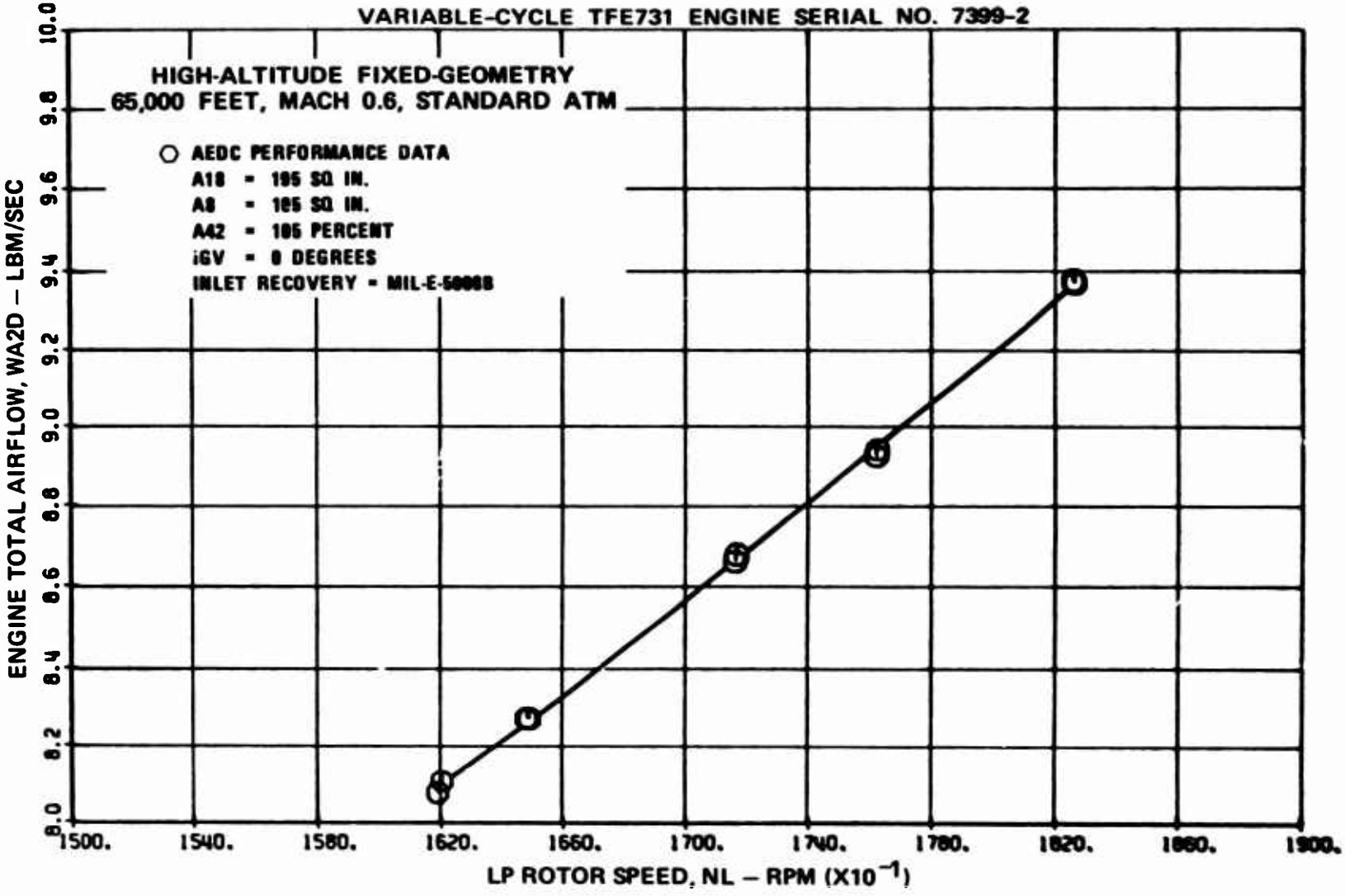

Figure 624. High-Altitude Fixed-Geometry at Mach 0.6, 65,000 Feet, Engine Total Airflow Versus LP Rotor Speed.

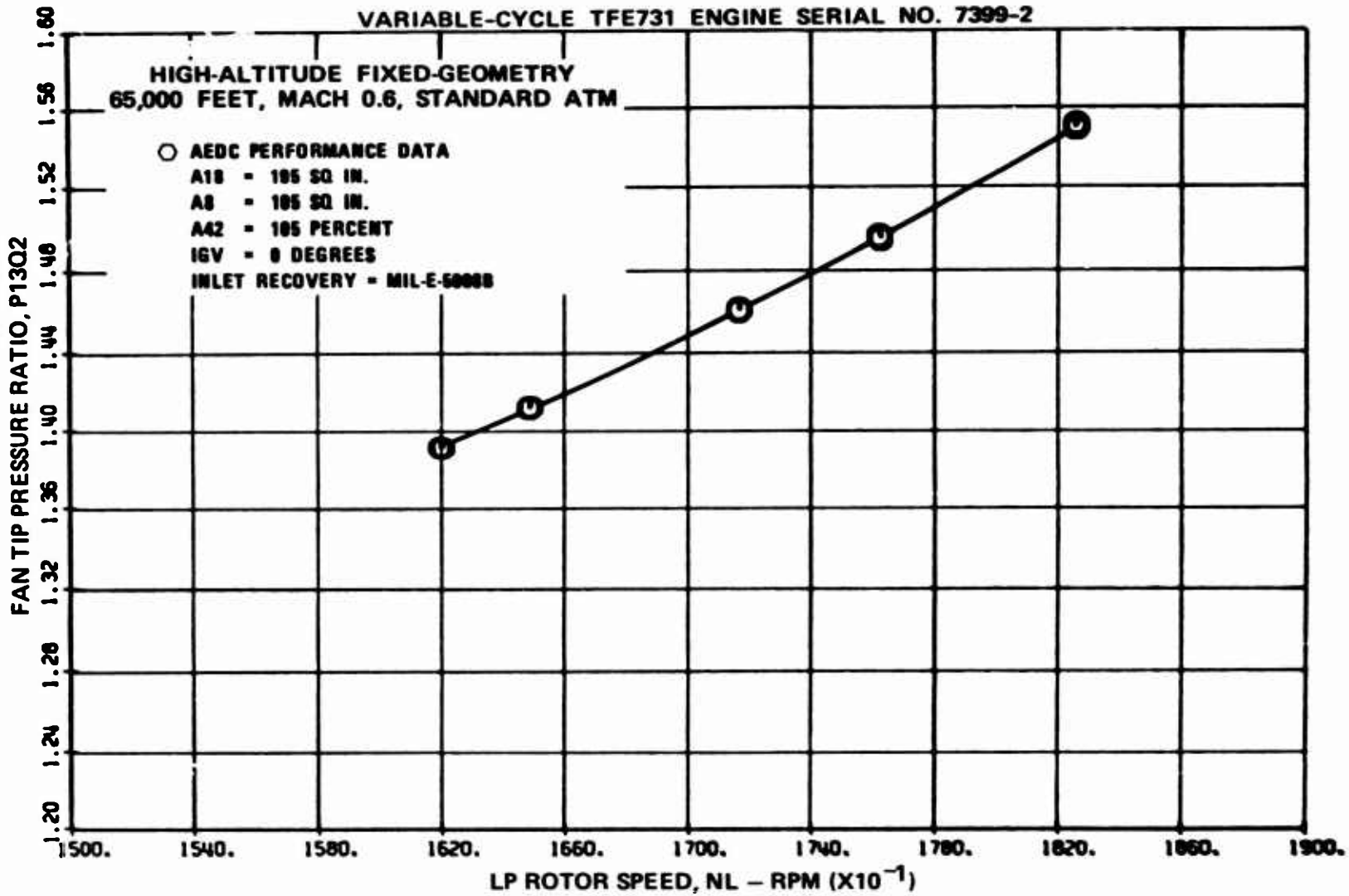

Figure 625. High-Altitude Fixed-Geometry at Mach 0.6, 65,000 Feet, Fan Tip Pressure Ratio Versus LP Rotor Speed.

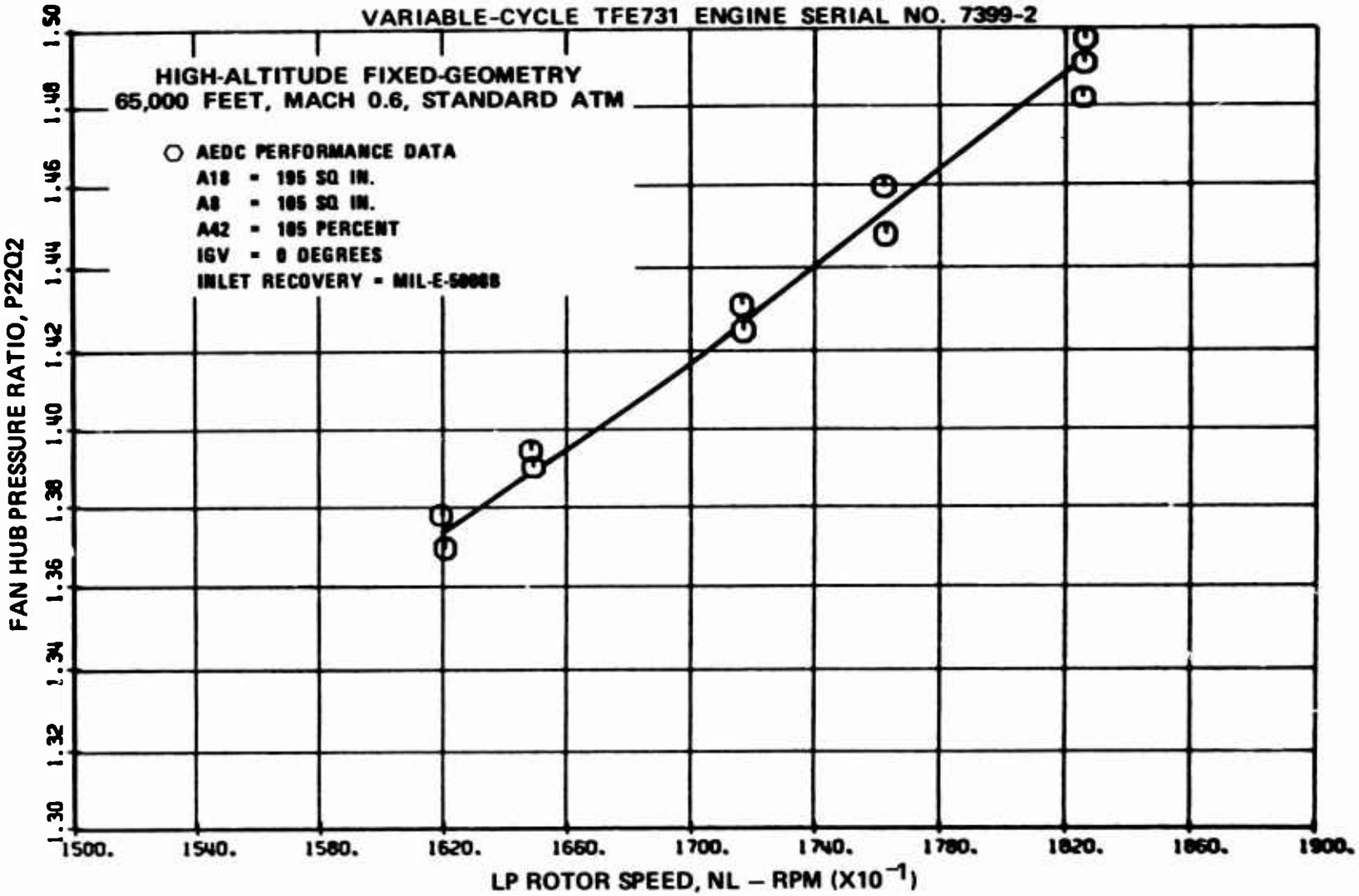

Figure 626. High-Altitude Fixed-Geometry at Mach 0.6, 65,000 Feet, Fan Hub Pressure Ratio Versus LP Rotor Speed.

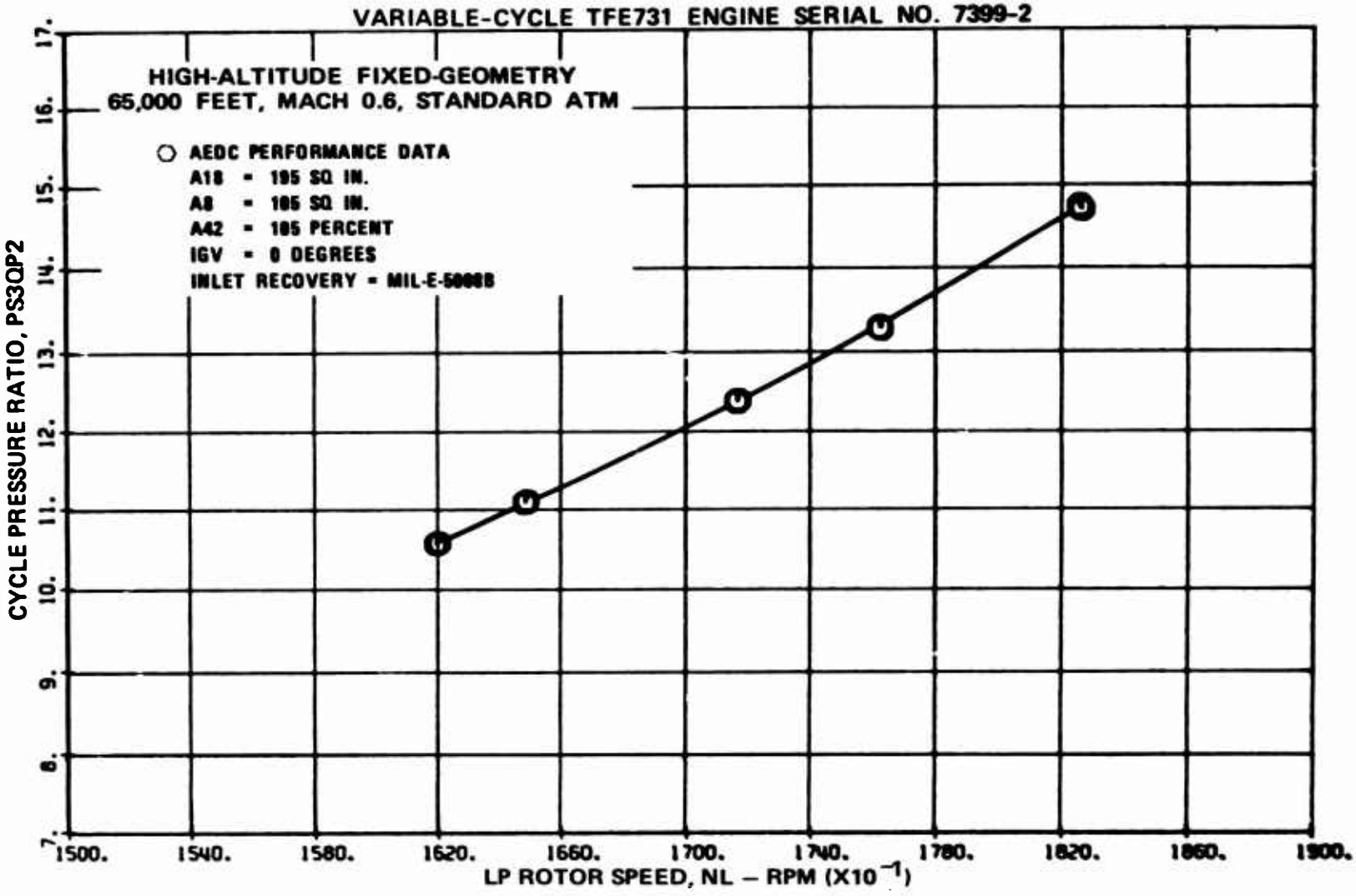

Figure 627. High-Altitude Fixed-Geometry at Mach 0.6, 65,000 Feet, Cycle Pressure Ratio Versus LP Rotor Speed.

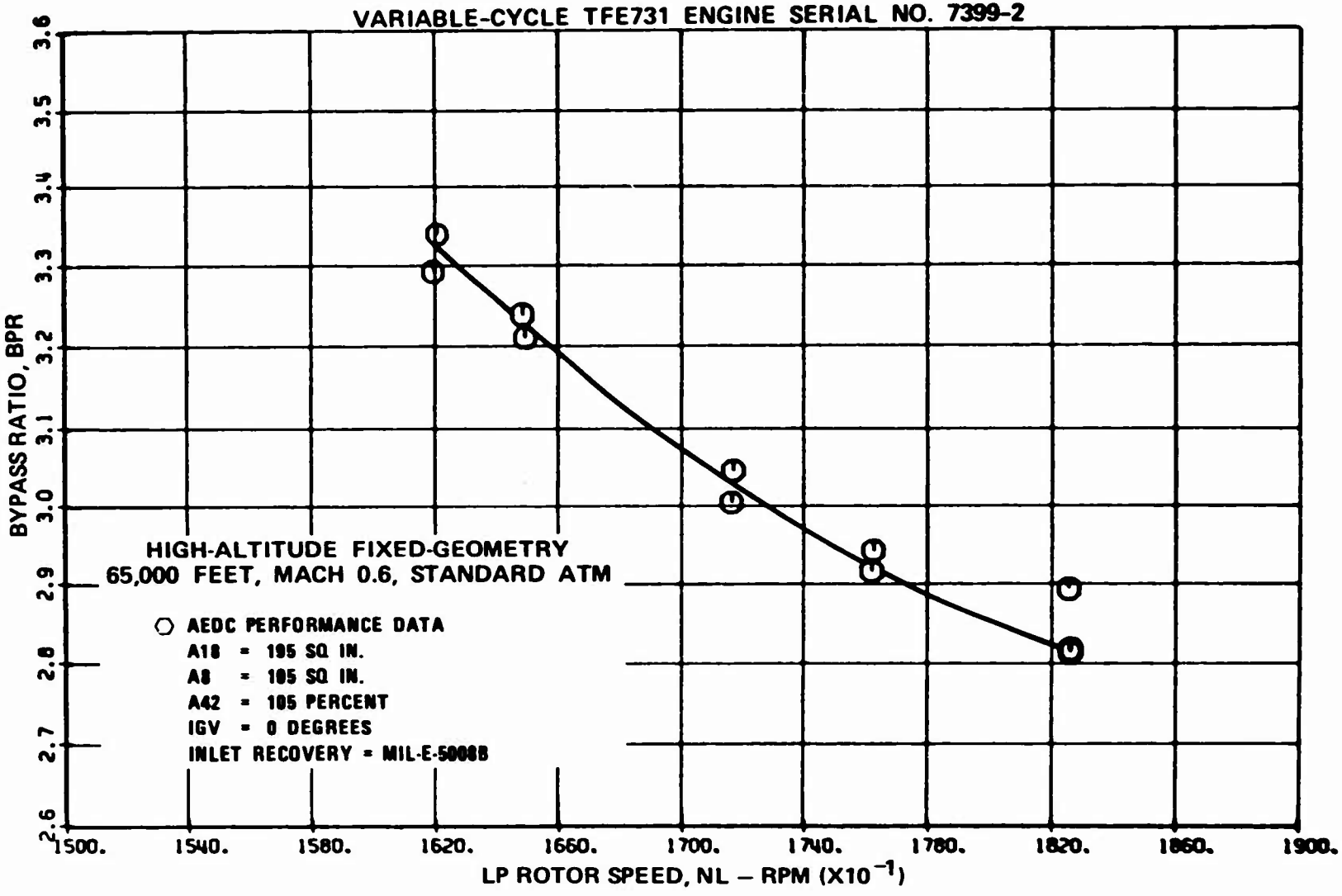

Figure 628. High-Altitude, Fixed-Geometry at Mach 0.6, 65,000 Feet, Bypass Ratio Versus LP Rotor Speed.

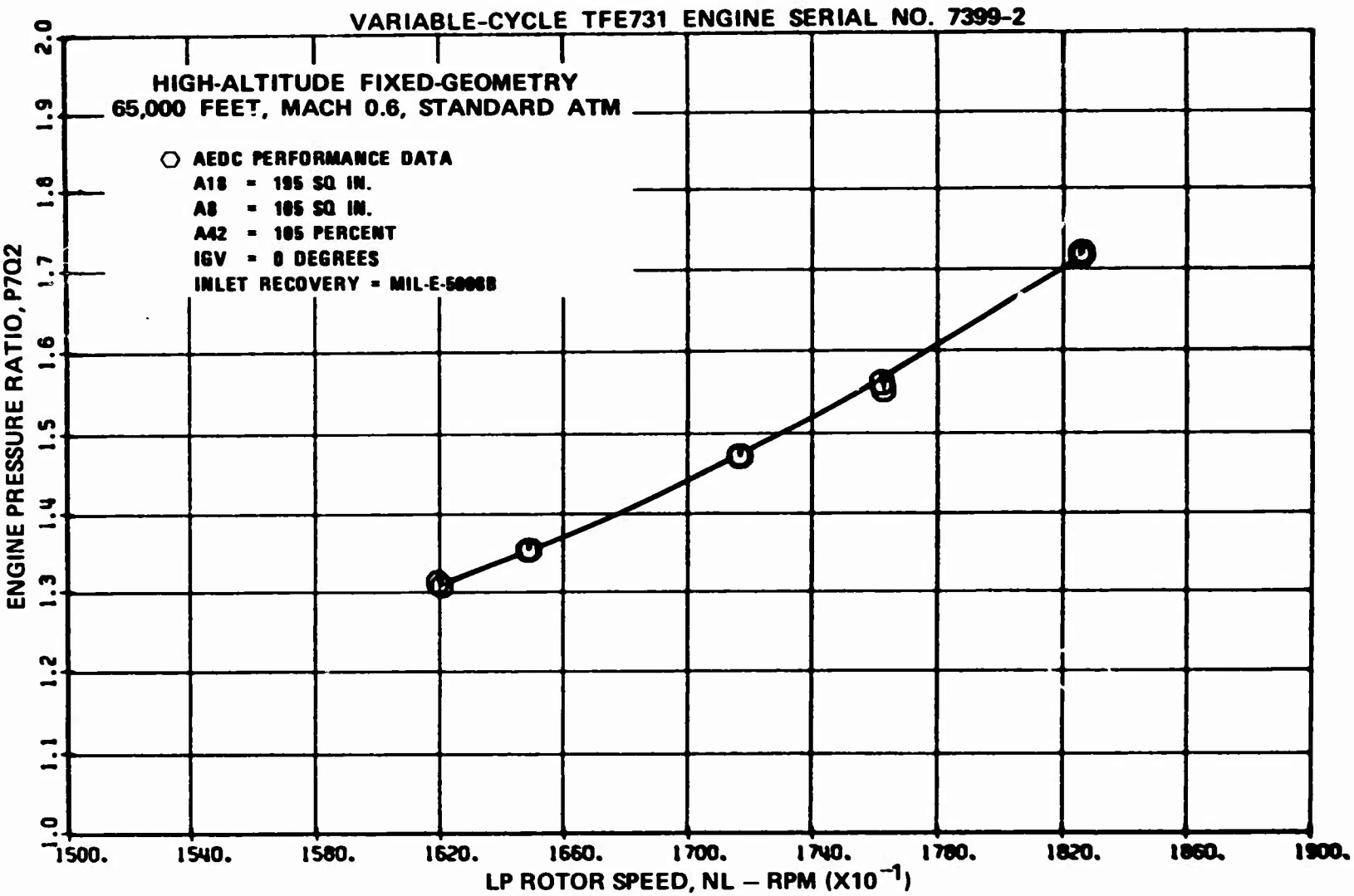

Figure 629. High-Altitude Fixed-Geometry at Mach 0.6, 65,000 Feet, Engine Pressure Ratio Versus LP Rotor Speed.

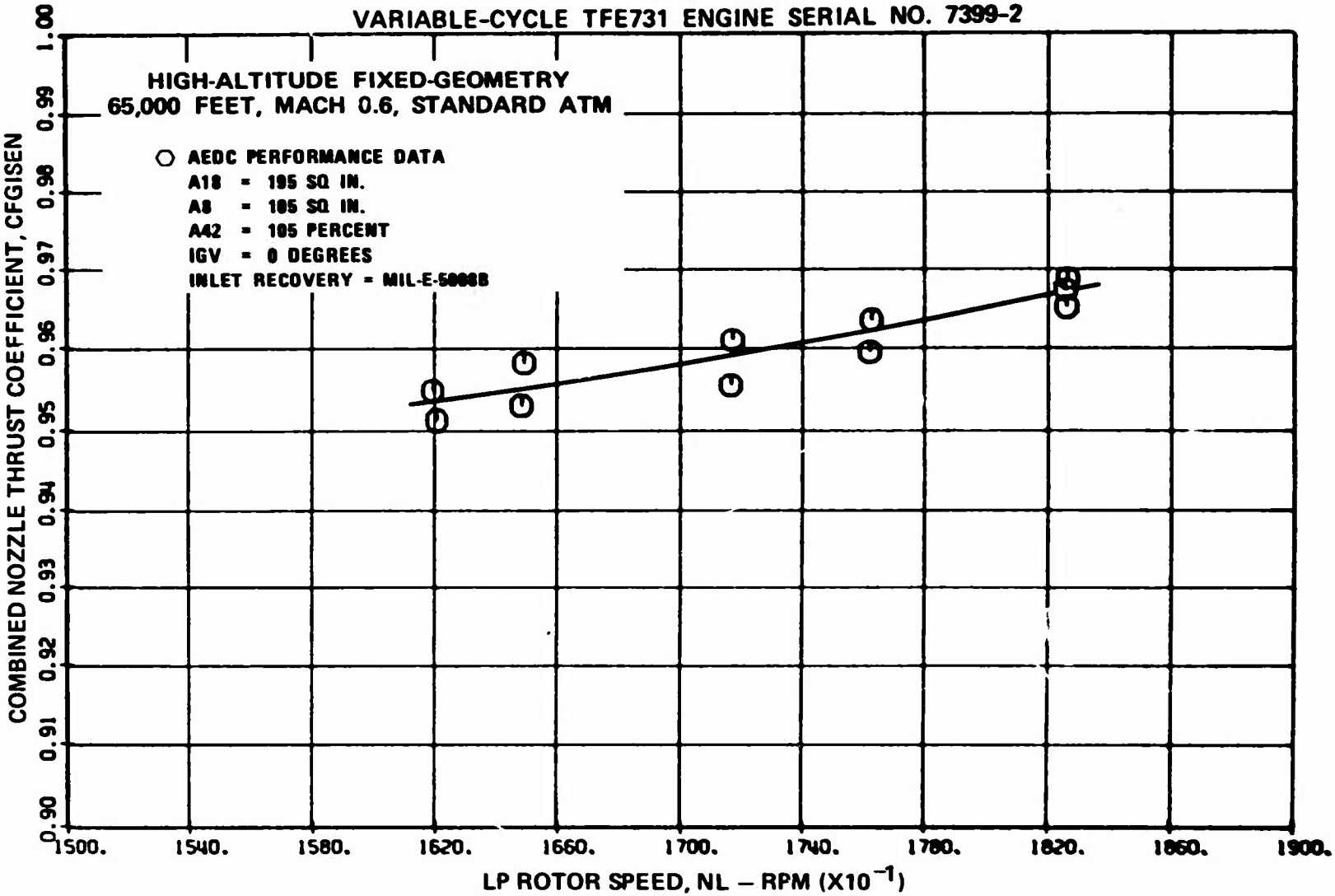

Figure 630. High-Altitude Fixed-Geometry at Mach 0.6, 65,000 Feet, Combined Nozzle Thrust Coefficient Versus LP Rotor Speed.

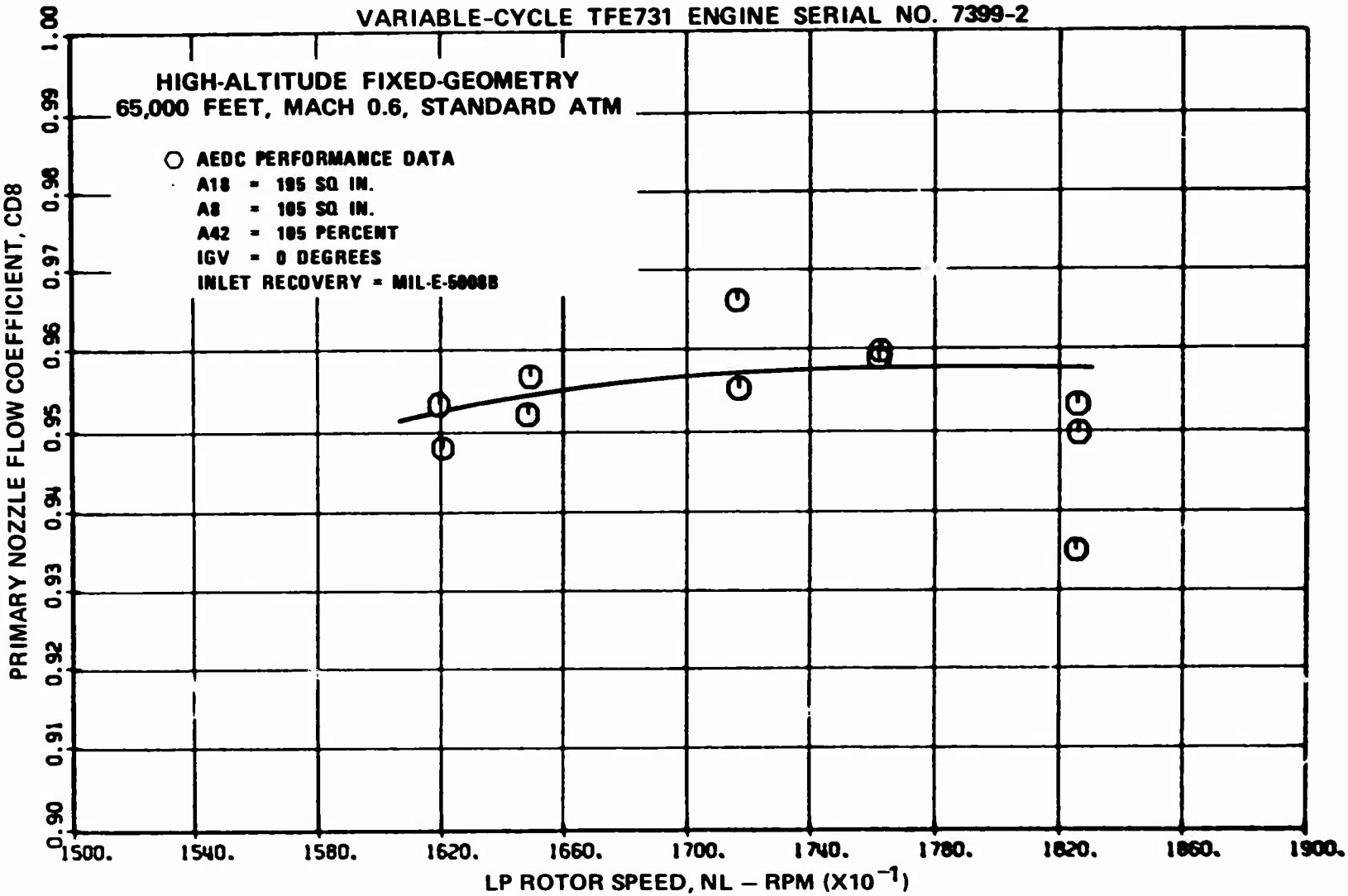

Figure 631. High-Altitude Fixed-Geometry at Mach 0.6, 65,000 Feet, Primary Nozzle Flow Coefficient Versus LP Rotor Speed.

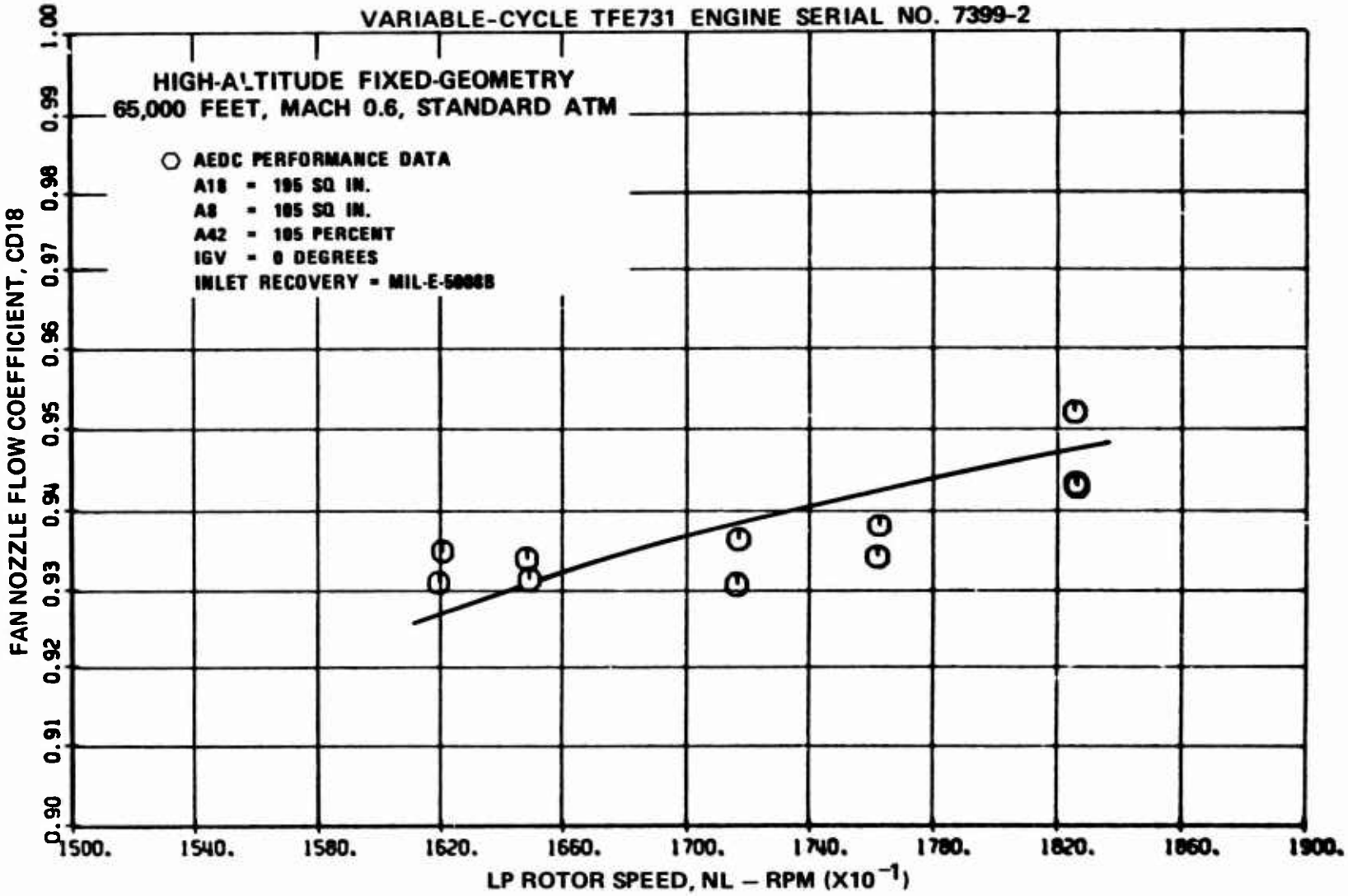

Figure 632. High-Altitude Fixed-Geometry at Mach 0.6, 65,000 Feet, Fan Nozzle Flow Coefficient Versus LP Rotor Speed.

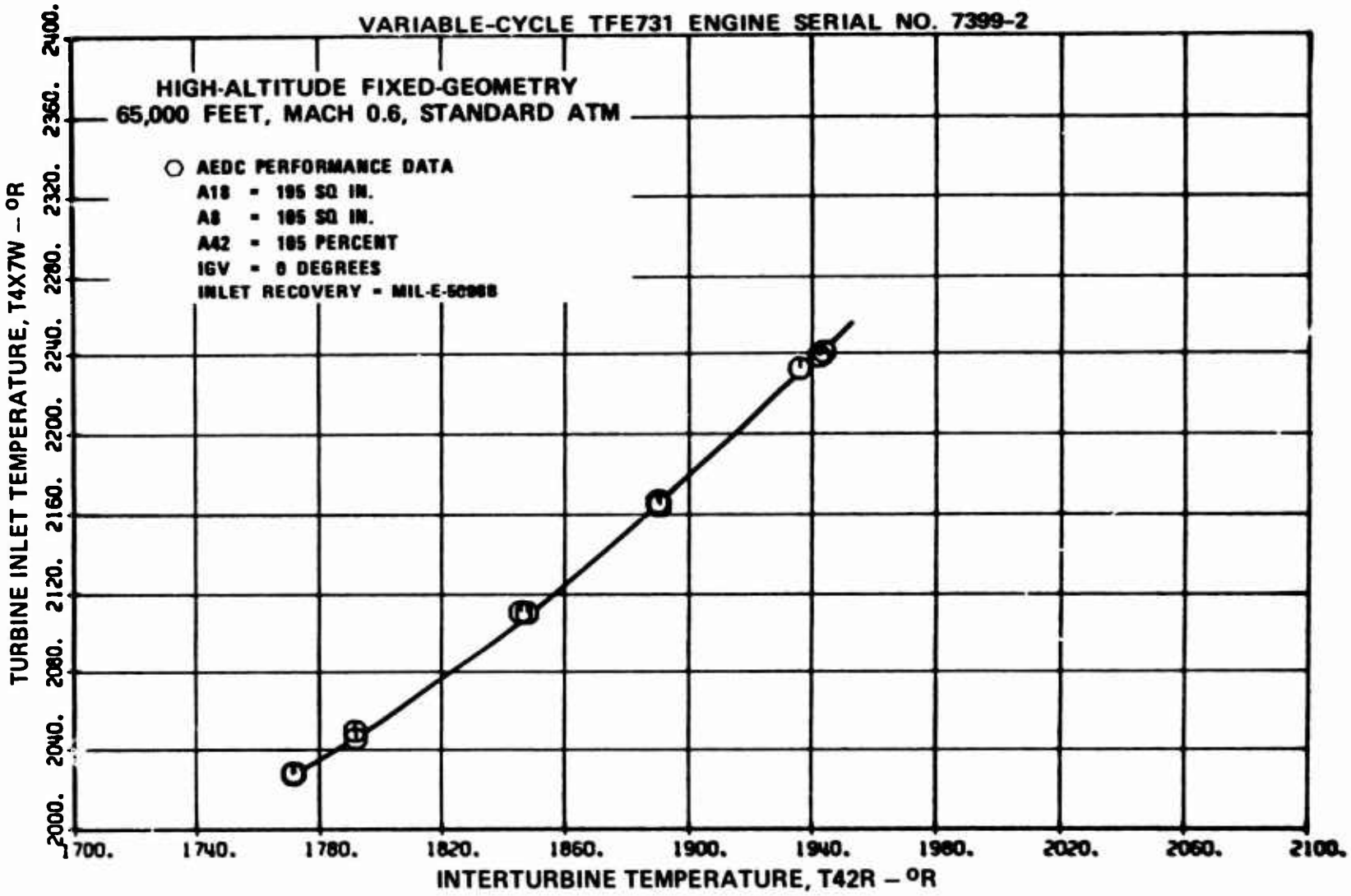

Figure 633. High-Altitude Fixed-Geometry at Mach 0.6, 65,000 Feet, Turbine Inlet Temperature Versus Interturbine Temperature.

The engine was successfully tested at Mach 0.5, 65,000 feet at all three desired interturbine temperature levels, with an LP turbine nozzle area of 105 percent. One LP compressor surge was experienced during a deceleration from an interturbine temperature of approximately 1400°F to a temperature of 1300°F, causing the operator to shut down the engine. After restarting the engine and re-establishing cell conditions, surge-free operation was maintained at 1300°F.

While attempting to set conditions for 70,000 feet, Mach 0.5, with the interturbine temperature set at approximately 1400°F and the LP turbine nozzle area set at 105 percent, another LP compressor surge was experienced. The LP compressor surge bleed valve was opened and the engine recovered. After several unsuccessful attempts to operate surge-free at Mach 0.5, 70,000 feet, with 110 percent LP turbine nozzle area, the flight Mach number was increased to 0.6. Successful operation was experienced at this condition at interturbine temperatures of approximately 1500 and 1400°F, but the LP compressor surged during the deceleration to 1300°F. The surge bleed valve was opened and the engine again recovered.

The LP turbine nozzle area was increased to 115 percent and the operating condition was set at 75,000 feet, Mach 0.7. With the surge bleed valve closed, an LP compressor surge was experienced at this condition and the operator shut down the engine. After restarting the engine and resetting cell conditions, the engine was subsequently operated successfully at Mach 0.83 at 75,000 feet at an interturbine temperature of approximately 1500°F. Attempts to obtain surge-free operation at 1400°F were unsuccessful.

Selected performance parameters from the surge-free operating points demonstrated during the special high-altitude test are presented in Table 78. Tested operating points from this special test and the originally scheduled test at 65,000 feet,

TABLE 78. HIGH-ALTITUDE TEST DATA CORRECTED TO DESIRED ALTITUDE AMBIENT PRESSURE

Altitude (feet)	Flight Mach No.	T_{amb} Tested/ Standard (^{o}R)	A42 (%)	T42 (^{o}F)	NL (rpm)	NH (rpm)	FNSD (lbf)	SFCD $\frac{lbm/hr}{lbf}$
65,000	0.52	386.4/390.0	104.6	1305	16,144	25,938	95.6	1.058
65,000	0.52	389.8/390.0	104.6	1405	17,212	26,851	126.7	0.9951
65,000	0.50	389.1/390.0	104.6	1506	18,417	27,835	174.3	0.9112
70,000	0.60	393.3/392.6	110.2	1503	17,834	27,950	114.1	1.064
70,000	0.60	393.6/392.6	110.2	1397	15,979	26,615	67.7	1.228
75,000	0.83	393.7/394.9	115.1	1503	16,953	27,413	63.1	1.362

A18 = 195 sq in.
A8 = 105 sq in.
IGV = 0 degrees

Mach 0.6 are superimposed on the analytical model LP compressor map presented in Figure 634. Extrapolation of the surge-free operating points at 70,000 and 75,000 feet indicates that the LP compressor should surge at the power settings where it was experienced.

A review of the parameters presented in Table 78 and Figure 634 indicated that the LP compressor surge margin is reduced by the drastic decrease in both LP and HP rotor speeds with increased altitude. Therefore, the surge margin at high altitudes can be improved by the use of increased LP turbine nozzle area to increase the HP rotor speed. Variable IGV's could also be used to increase the LP compressor surge margin, but with a resulting decrease in primary stream airflow.

The test results suggest an application for a variable-cycle engine. The application would require maximum potential performance at both low and high altitudes, with surge-free operation at both. The variable LP turbine nozzle area could be set close to the nominal value at sea level to maintain HP rotor speed within limits and could be opened at high altitudes to increase HP rotor speed to improve the engine performance and LP compressor surge margin. Variable LP compressor geometry might also be employed in conjunction with variable LP turbine nozzle area modulation for extremely high altitudes.

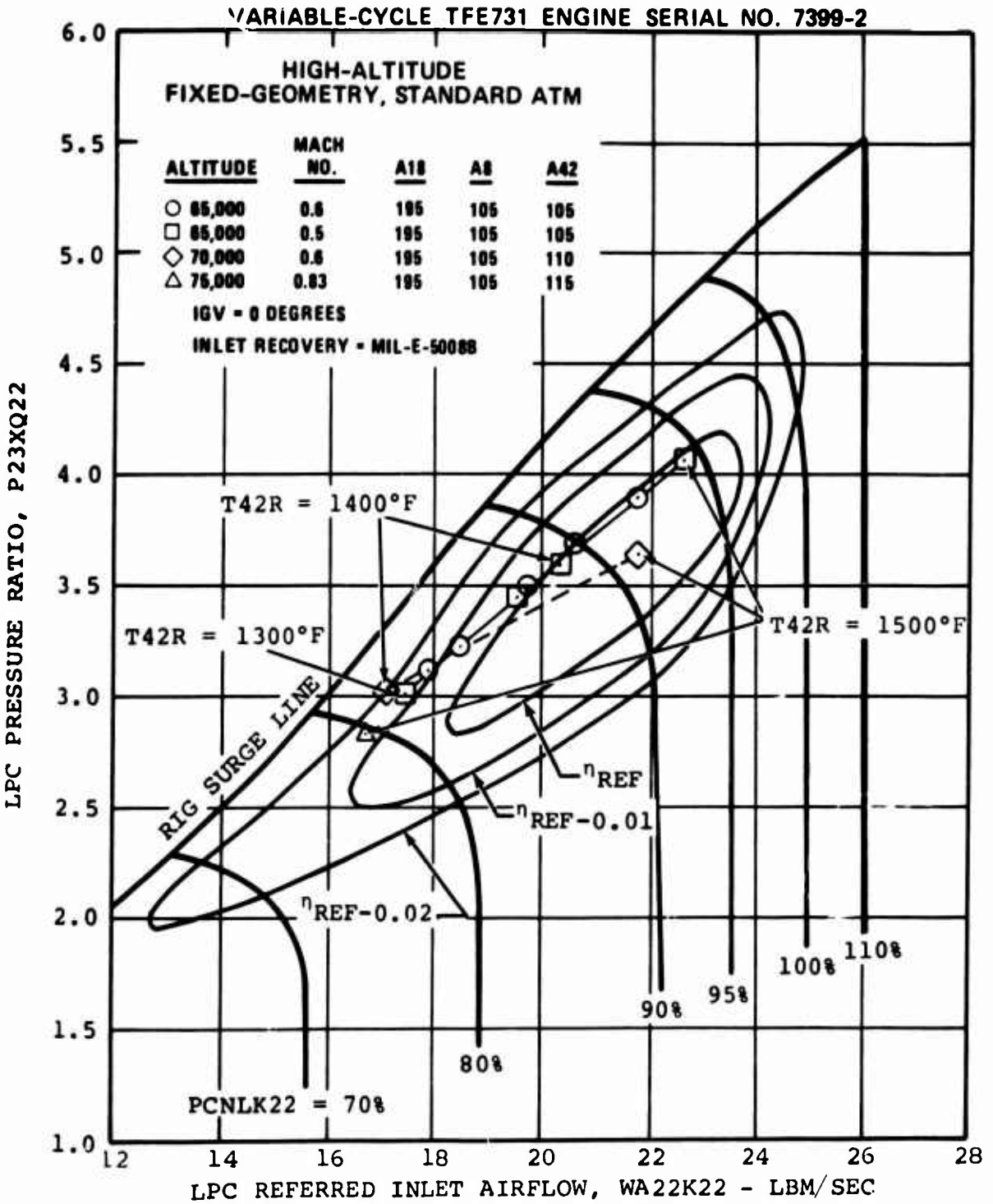

Figure 634. High-Altitude-Tested Surge-Free Operating Points Superimposed on LP Compressor Map Showing Decrease in Surge Margin with Increase in Altitude.

4.4.11 Surge Margin Check

4.4.11.1 Purpose

The surge margin check was conducted to confirm the surge lines previously established from the results of the LP compressor rig tests. Since several test series of this program involved an evaluation of the effect of variable-geometry components on LP compressor surge margin, it was considered necessary to confirm that the surge lines of the LP compressor operating in the engine environment were in agreement with those measured on the rig.

4.4.11.2 Method

The test involved a surge check at two referred speeds at zero degrees IGV and first-stage stator angles and at one referred speed at 30 degrees IGV and 10 degrees first-stage stator angles. The test was conducted at Mach 1.6 at 50,000 feet, standard atmosphere.

The technique used to establish accurate surge points was to start with an LP turbine nozzle area that would maintain the LP compressor operating point well away from surge and then, while holding the LP rotor speed constant, to reduce the LP turbine nozzle area in small steps until a surge was detected. Steady-state data was recorded after stabilization following each step change in LP turbine nozzle area. After a surge was detected, the LP compressor surge bleed valve was opened to move the operating point out of surge. The LP turbine nozzle area was then increased by approximately 1 percent, the surge bleed valve was closed, and following stabilization, steady-state data was recorded at this condition.

The surge detection system consisted of a pressure probe and transducer installed at the exit of the HP compressor and at the exit of the fan stator, which were monitored on strip recorders. The following parameters were recorded: P13, PS3, P24, NL, NH, and T42. A diagram of this system and the surge bleed valve is shown in Figure 335 of Paragraph 4.2.

4.4.11.3 Results

The results of the surge margin testing are presented in Figures 635 through 638. The parameters presented in these figures are listed in Table 79.

TABLE 79. SURGE MARGIN CHECK, 50,000 FEET, MACH 1.6, STANDARD ATM

Figure No.	Parameters Presented
635	Referred LP Rotor Speed Versus LP Turbine Nozzle Area
636	LP Compressor Referred Inlet Airflow Versus LP Turbine Nozzle Area
637	LP Compressor Pressure Ratio Versus LP Turbine Nozzle Area
638	LP Compressor Pressure Ratio Versus Referred Inlet Airflow

The overall results of this testing are presented in Figure 638 in terms of LP compressor pressure ratio versus referred inlet airflow. This figure shows the rig surge lines for inlet guide vane (IGV) angles of zero and 30 degrees and referred speed lines of 70 percent for 30 degrees IGV angle and 70 and 80 percent for zero degrees IGV angle, superimposed on a plot of the test data.

The comparison of the AiResearch rig and AEDC engine surge points at the same referred speeds, presented in Table 80, indicates agreement of the two sets of data within a tolerance of plus or minus 2.5 percent. This is considered to be within the limits of engine-to-engine variation and repeatability and, therefore, represents good agreement.

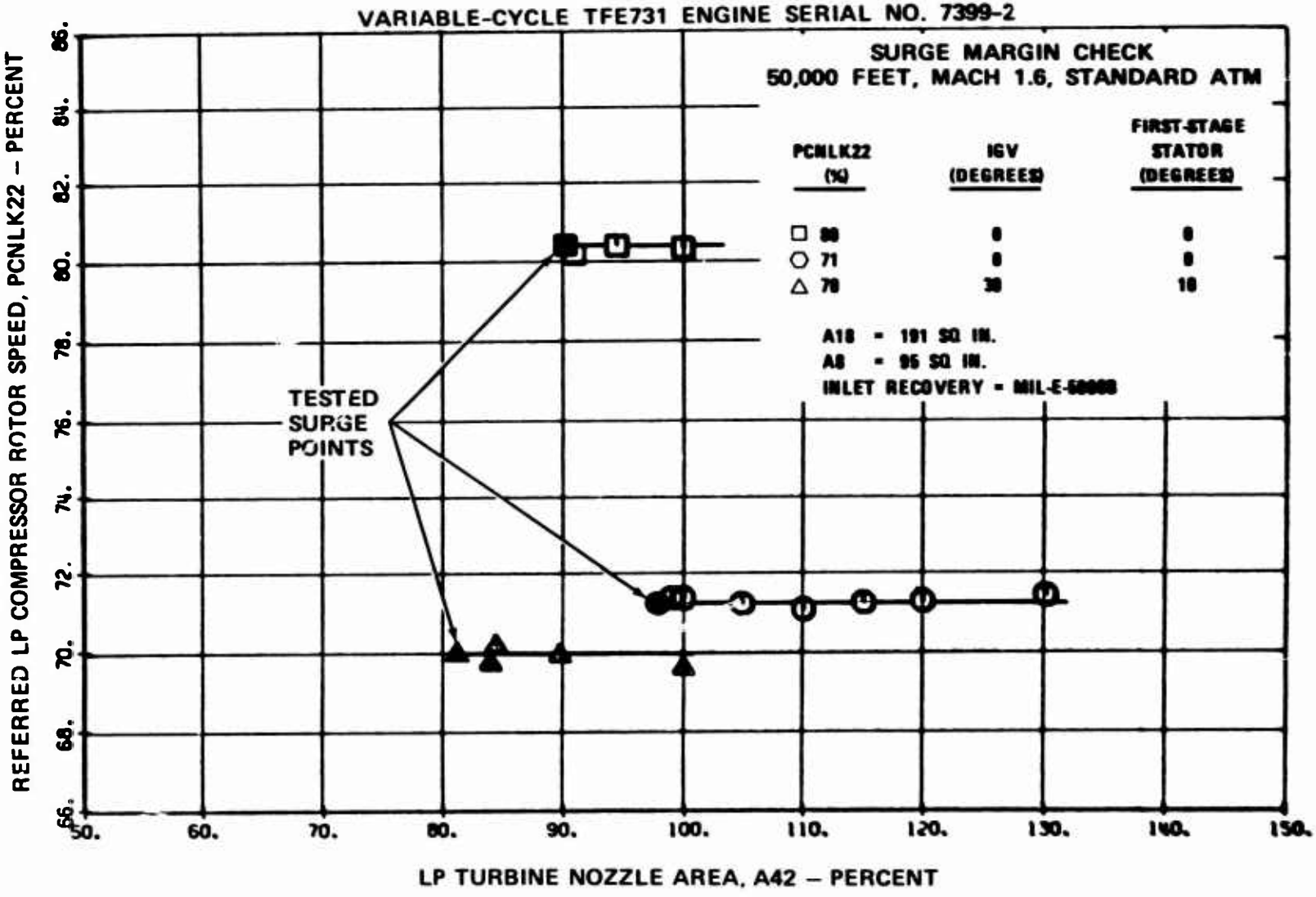

Figure 635. Surge Margin Check, Referred LP Compressor Rotor Speed Versus LP Turbine Nozzle Area.

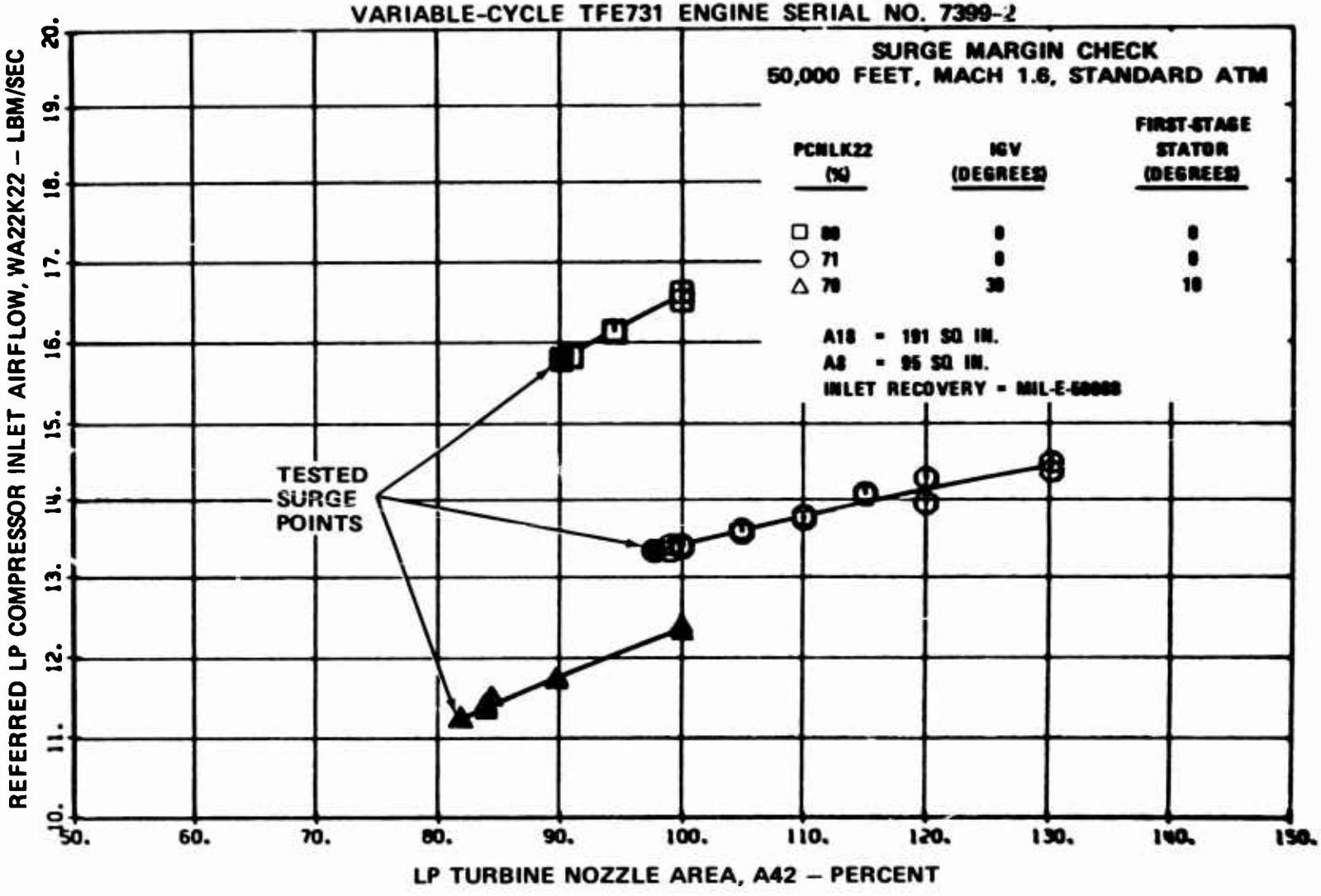

Figure 636. Surge Margin Check, Referred LP Compressor Inlet Airflow Versus LP Turbine Nozzle Area.

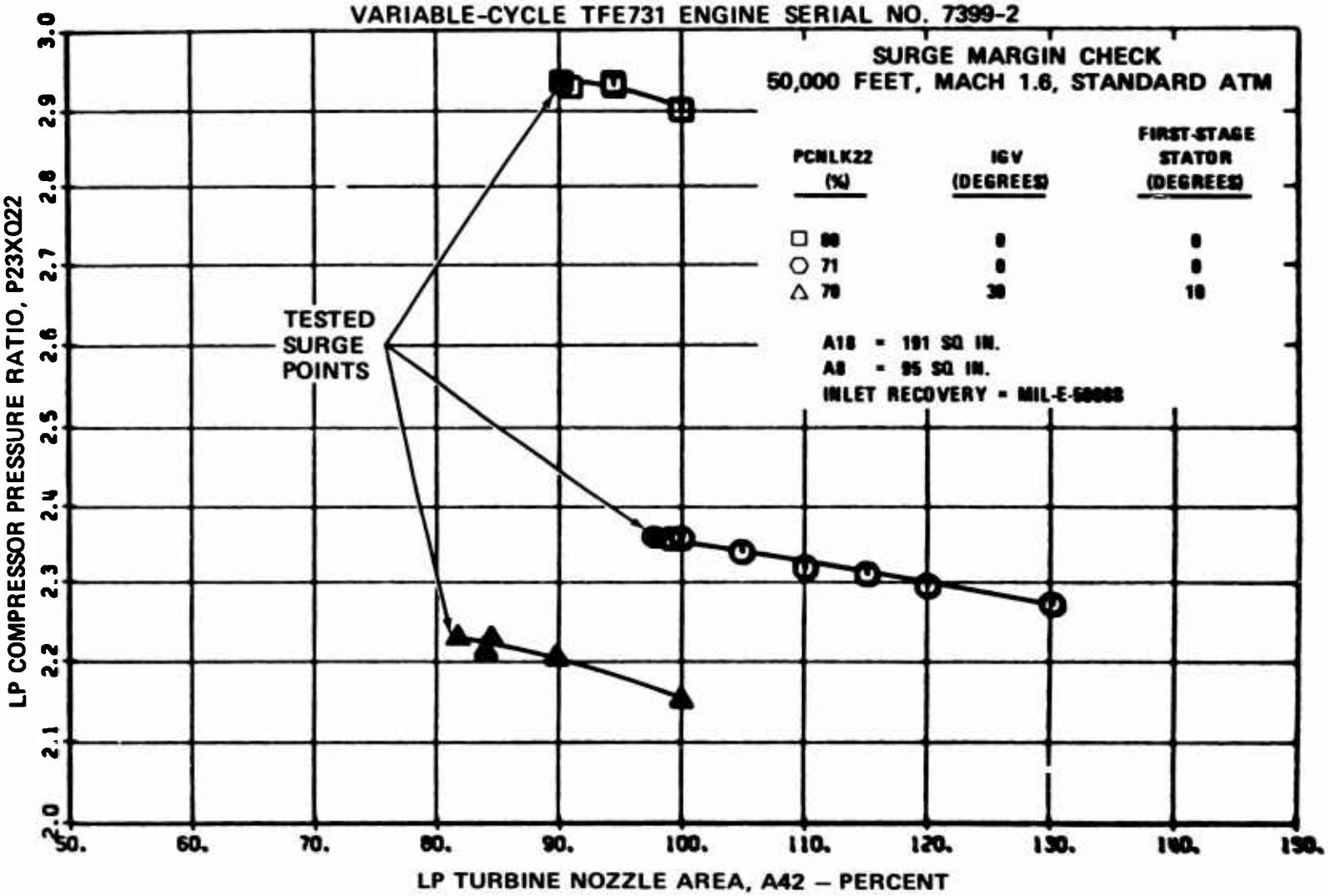

Figure 637. Surge Margin Check, LP Compressor Pressure Ratio Versus LP Turbine Nozzle Area.

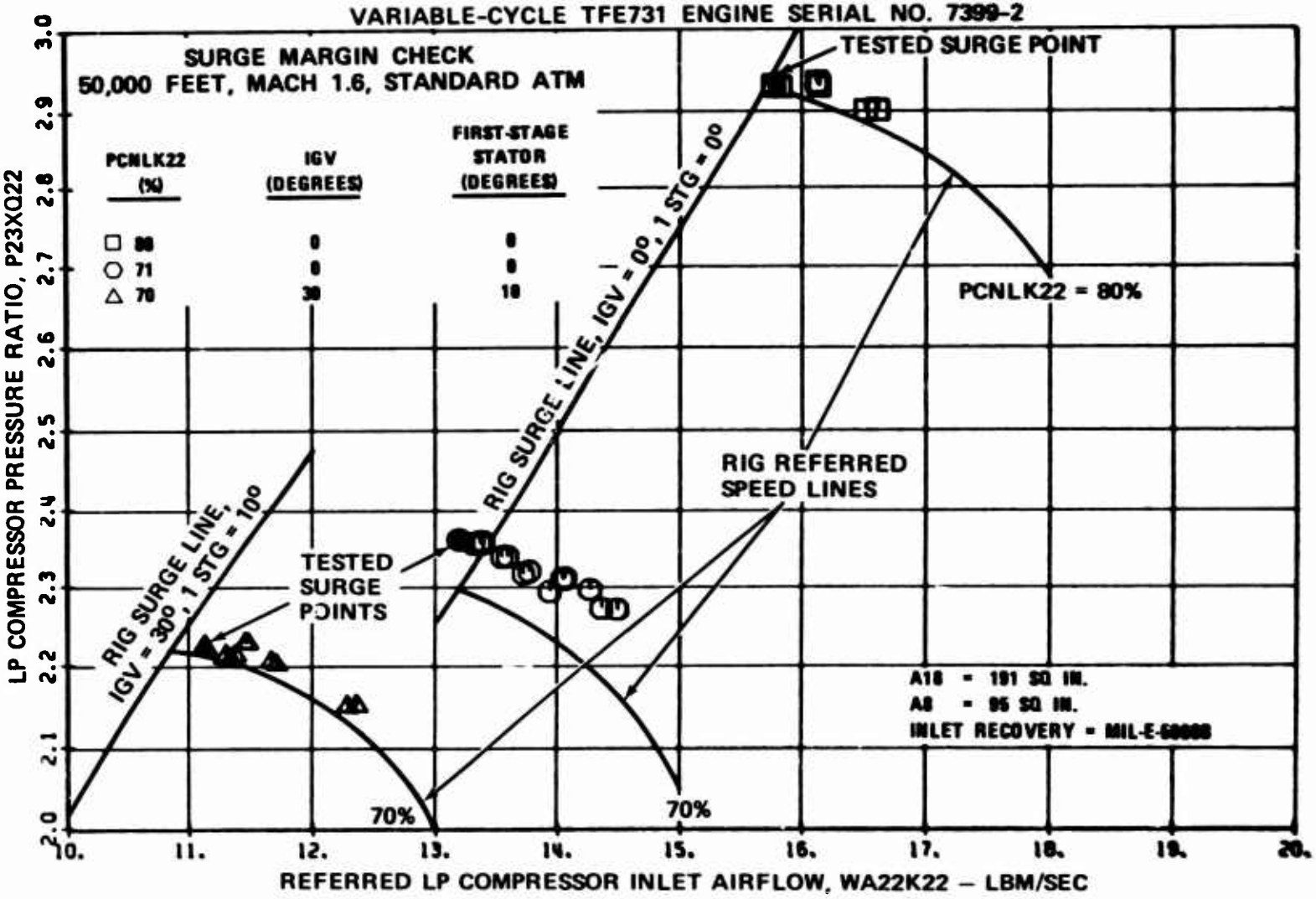

Figure 638. Surge Margin Check, LP Compressor Ratio Versus Referred LP Compressor Inlet Airflow.

TABLE 30. COMPARISON OF AIRESEARCH RIG AND AEDC LP COMPRESSOR SURGE DATA, 50,000 FEET, MACH 1.6, STANDARD ATM

IGV Angle (degrees)	1- Stg Stator Angle (degrees)	Referred Speed (percent)	Surge WA22K22/P23XQ22 (lbm/sec/ratio)		Percent difference
			AiResearch Rig	AEDC Engine	
30	10	70.0	10.88/2.23 = 4.879	11.15/2.23 = 5.000	-2.5
0	0	71.3	13.4/2.25 = 5.702	13.2/2.36 = 5.593	+1.9
0	0	80.4	15.8/2.96 = 5.338	15.8/2.93 = 5.392	-1.0

A18 = 191 sq in.
A8 = 95 sq in.

4.4.12 High-Mach-Number Capability

4.4.12.1 Purpose

The main purpose of the High-Mach-Number test series was to demonstrate the ability of variable compressor and turbine geometry to extend the TFE731 Engine operating envelope to Mach 2.2 at 50,000 feet, MIL-STD-210 cold atmosphere.

The LP compressor inlet guide vanes were set at 30 degrees and the first-stage stators were set at 10 degrees to obtain sufficient LP compressor surge margin so that the LP turbine nozzles could be modulated through the 90- to 110-percent area range. Two different combinations of fan and primary exhaust-nozzle areas were tested in order to accumulate exhaust-nozzle performance data at high nozzle pressure ratios.

The measurement of overall engine performance at this operating condition was not an important objective because Mach 2.2 represents an unrealistic condition for an unaugmented turbofan engine.

4.4.12.2 Results

The results of the 50,000 feet, Mach 2.2, MIL-STD-210 cold atmosphere testing are presented in Figures 639 through 654. The parameters presented in these curves are listed in Table 81. The overall test results at the above flight condition at a constant calculated HP turbine inlet temperature of 1540°F are summarized in Table 82. This table presents LP rotor speed, HP rotor speed, net thrust, specific fuel consumption, and LP compressor surge margin.

TABLE 81. HIGH-MACH-NUMBER CAPABILITY, 50,000 FEET, MACH 2.2, MIL-STD-210 COLD ATM

Figure No.	Parameters Presented
639	Thrust specific fuel consumption versus net thrust
640	Turbine inlet temperature versus LP turbine nozzle area
641	Net thrust versus LP turbine nozzle area
642	Fuel flow versus LP turbine nozzle area
643	Interturbine temperature versus LP turbine nozzle area
644	LP rotor speed versus LP turbine nozzle area
645	HP rotor speed versus LP turbine nozzle area
646	Engine total airflow versus LP turbine nozzle area
647	Fan tip pressure ratio versus LP turbine nozzle area
648	Fan hub pressure ratio versus LP turbine nozzle area
649	Cycle pressure ratio versus LP turbine nozzle area
650	Bypass ratio versus LP turbine nozzle area
651	Engine pressure ratio versus LP turbine nozzle area
652	Combined nozzle thrust coefficient versus LP turbine nozzle area
653	Primary nozzle flow coefficient versus LP turbine nozzle area
654	Fan nozzle flow coefficient versus LP turbine nozzle area

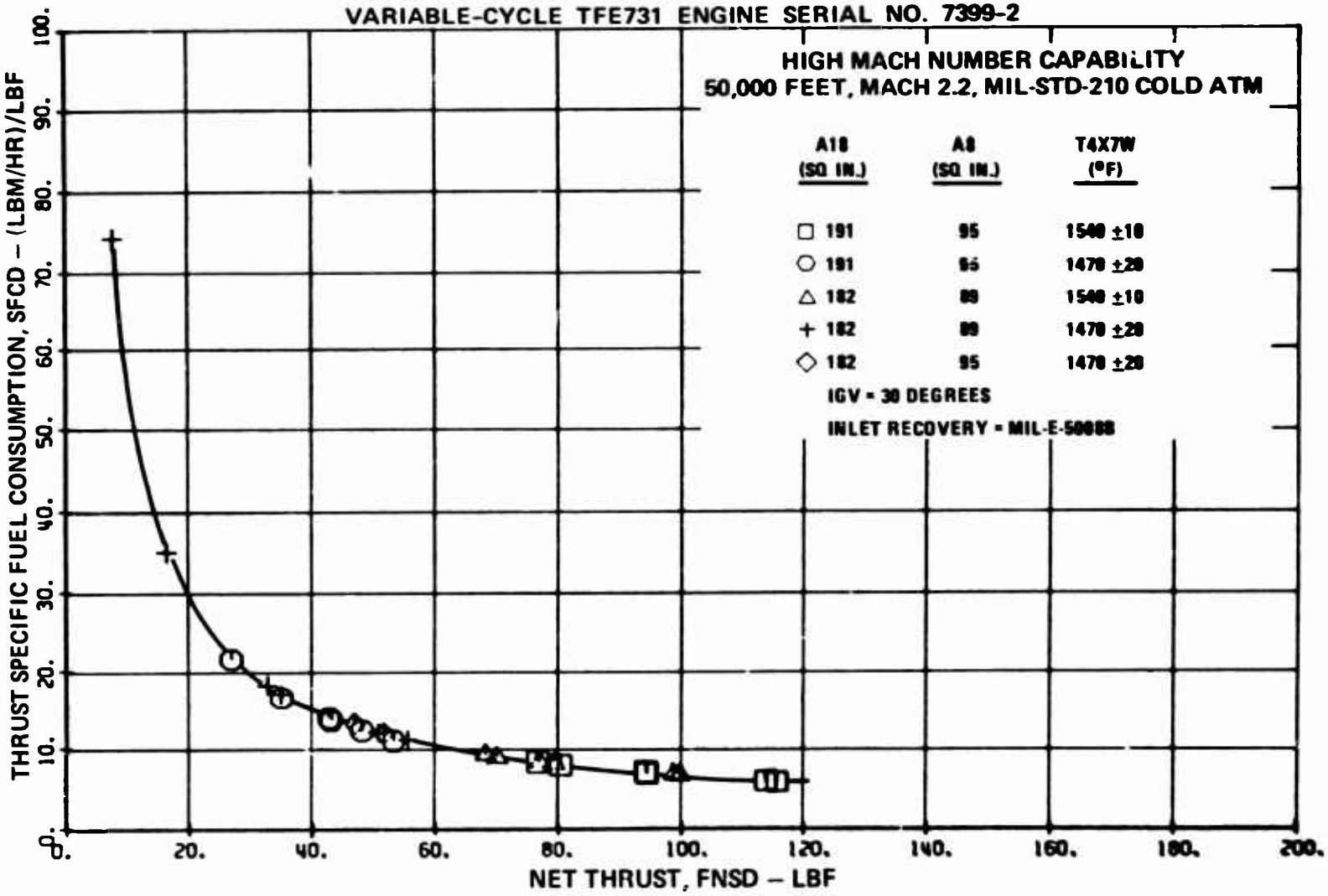

Figure 639. High-Mach-Number Capability, Mach 2.2, 50,000 Feet, Thrust Specific Fuel Consumption Versus Net Thrust.

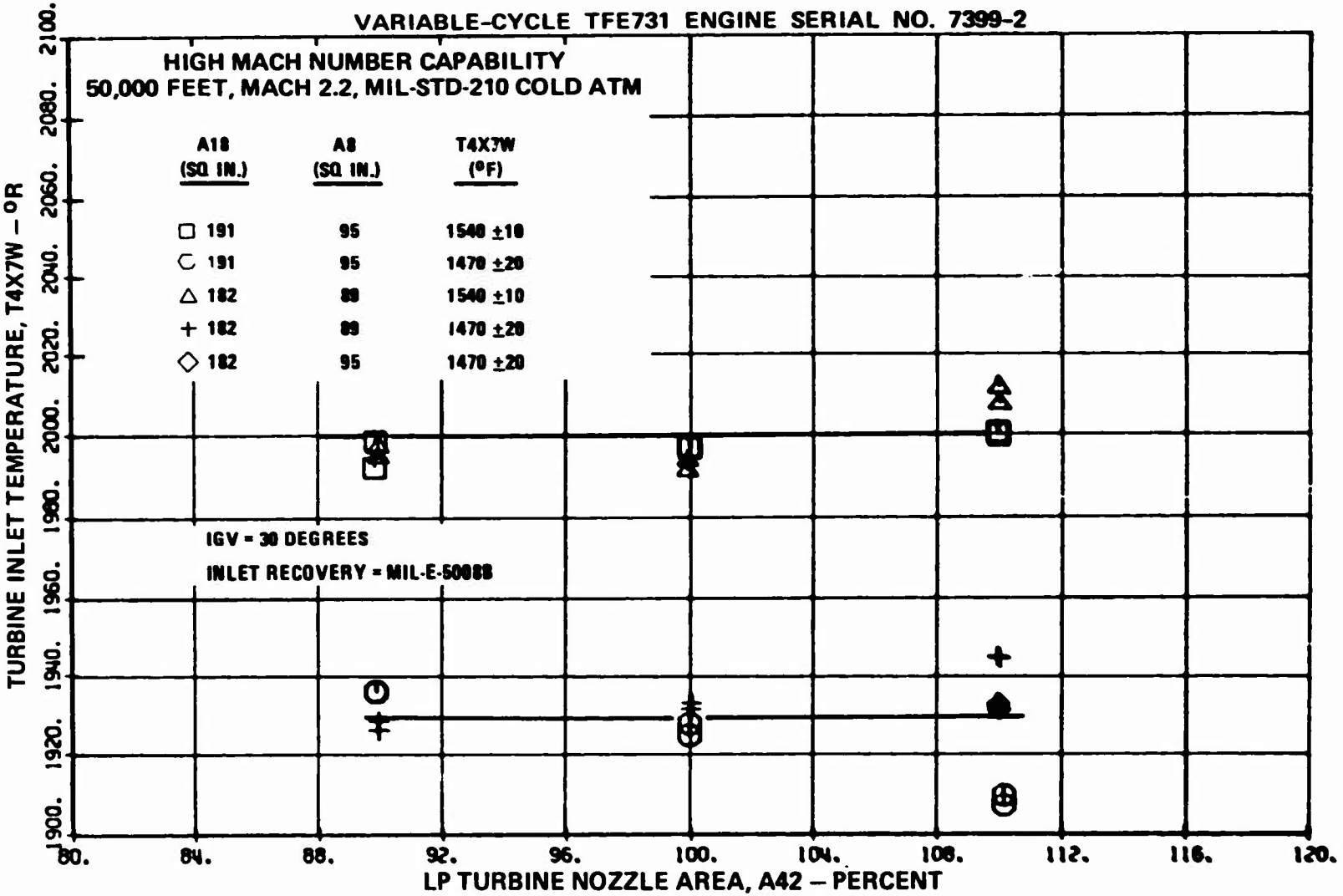

Figure 640. High-Mach-Number Capability, Mach 2.2, 50,000 Feet, Turbine Inlet Temperature Versus LP Turbine Nozzle Area.

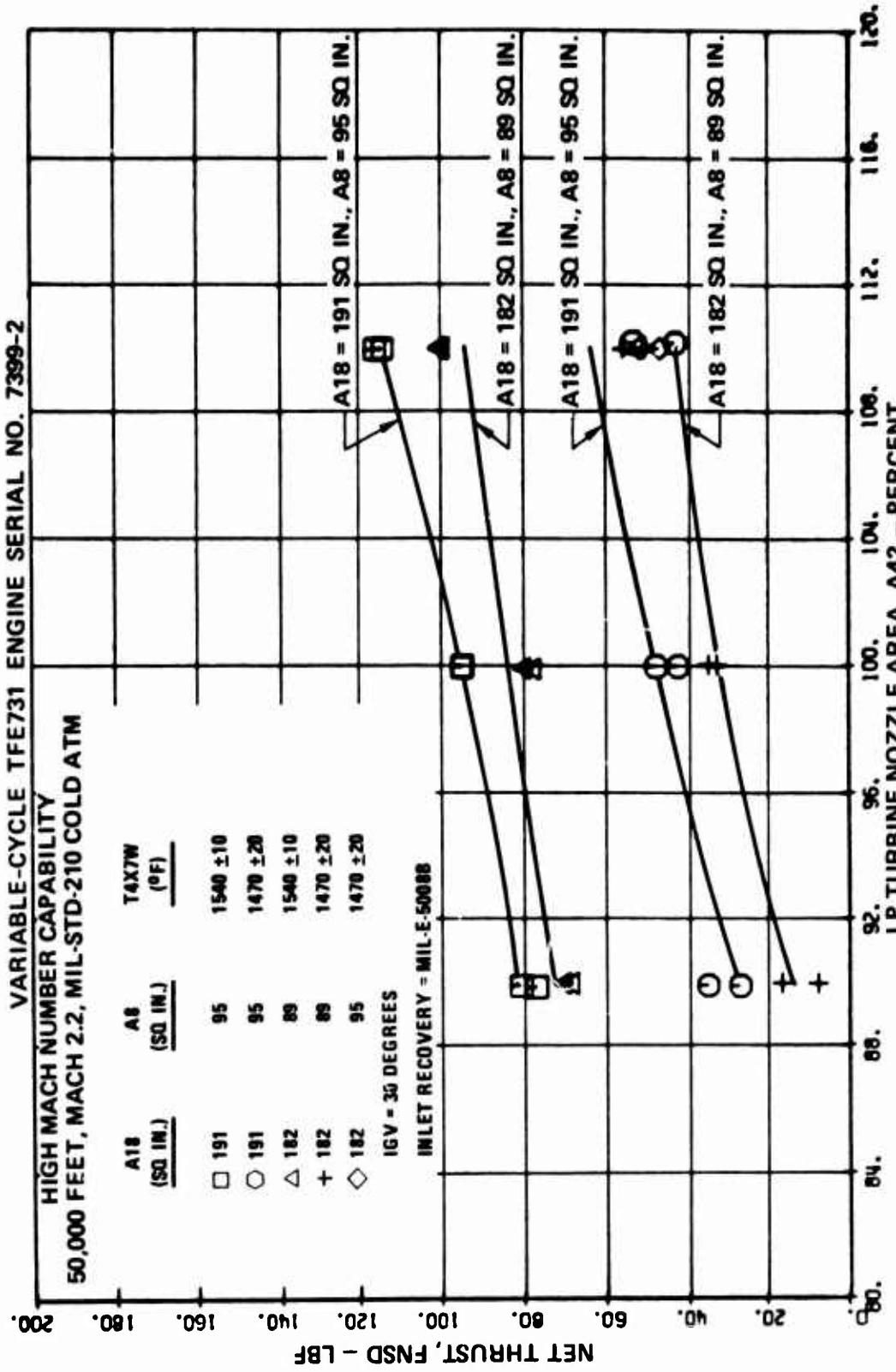

Figure 641. High-Mach-Number Capability, Mach 2.2, 50,000 Feet, Net Thrust Versus LP Turbine Nozzle Area.

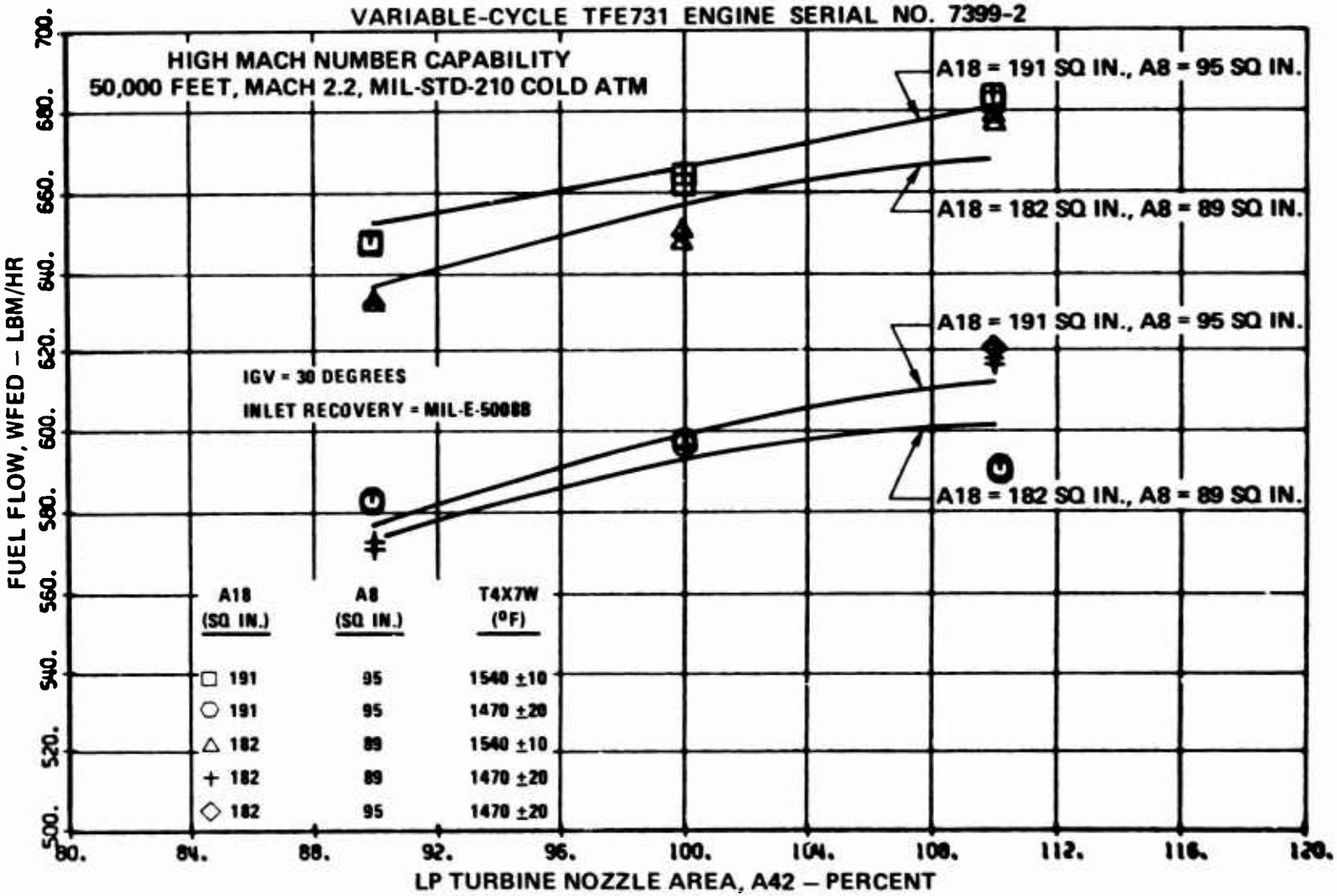

Figure 642. High-Mach-Number Capability, Mach 2.2, 50,000 Feet, Fuel Flow Versus LP Turbine Nozzle Area.

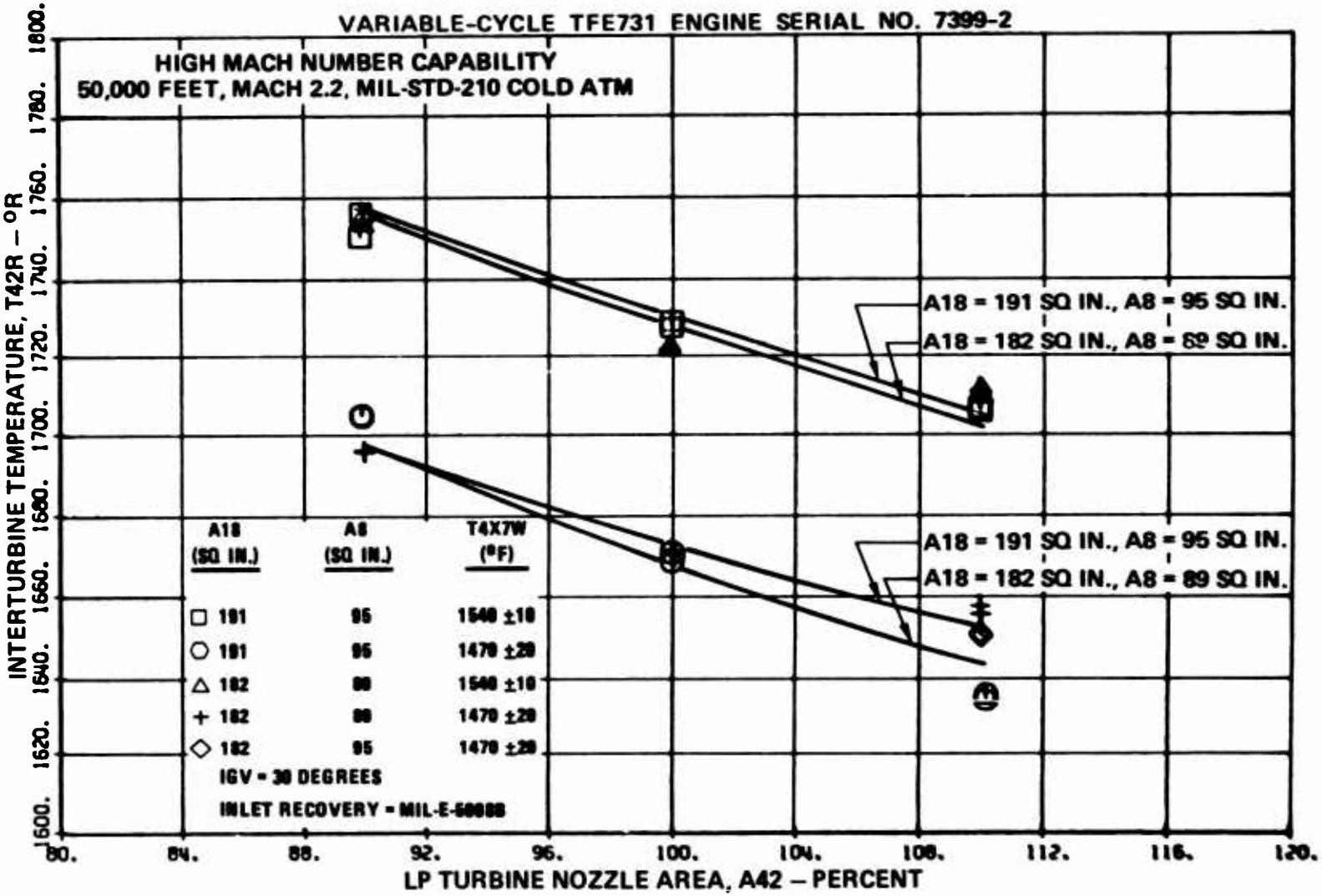

Figure 643. High-Mach-Number Capability, Mach 2.2, 50,000 Feet, Interturbine Temperature Versus LP Turbine Nozzle Area.

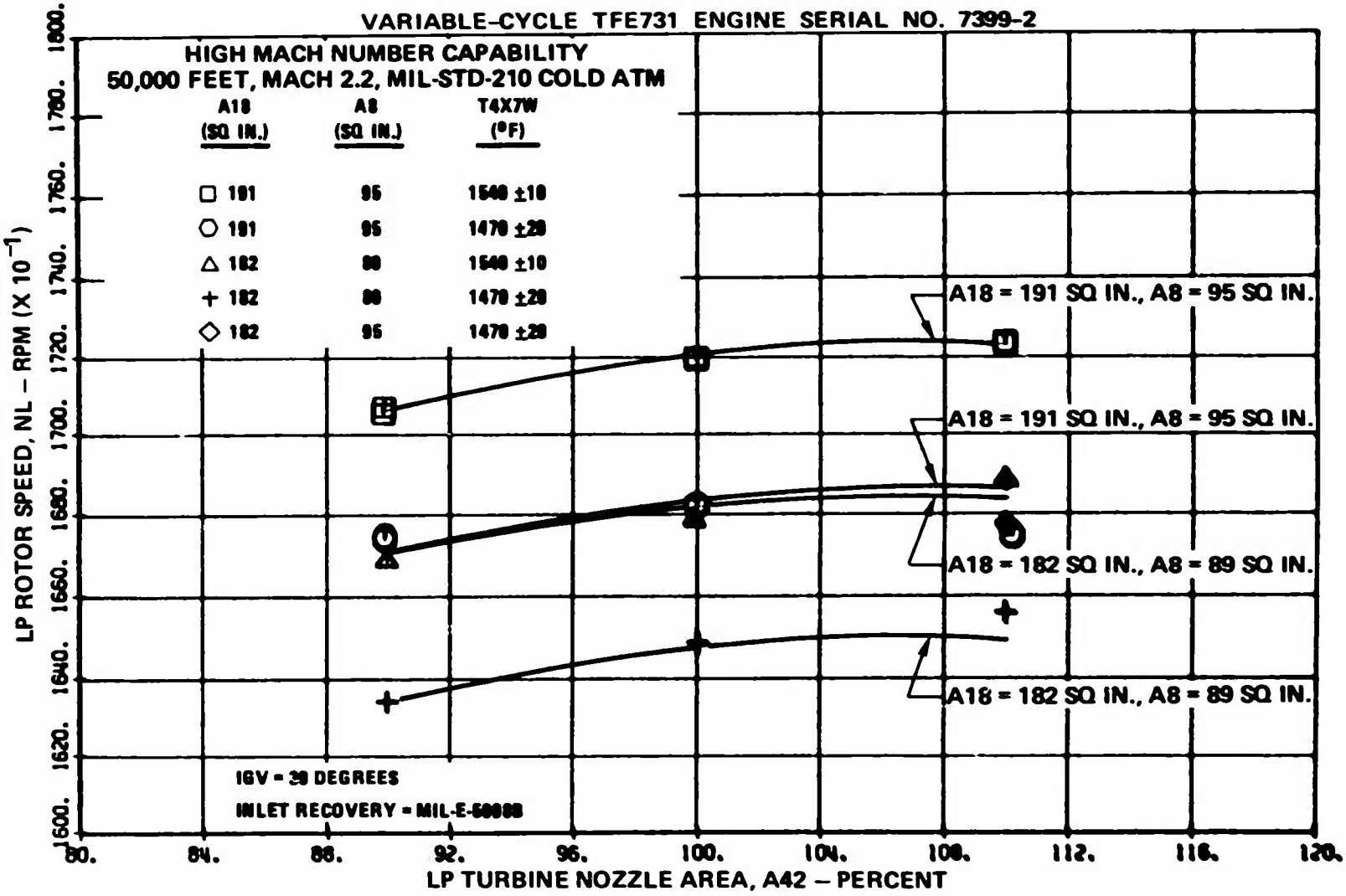

Figure 644. High-Mach-Number Capability, Mach 2.2, 50,000 Feet, LP Rotor Speed Versus LP Turbine Nozzle Area.

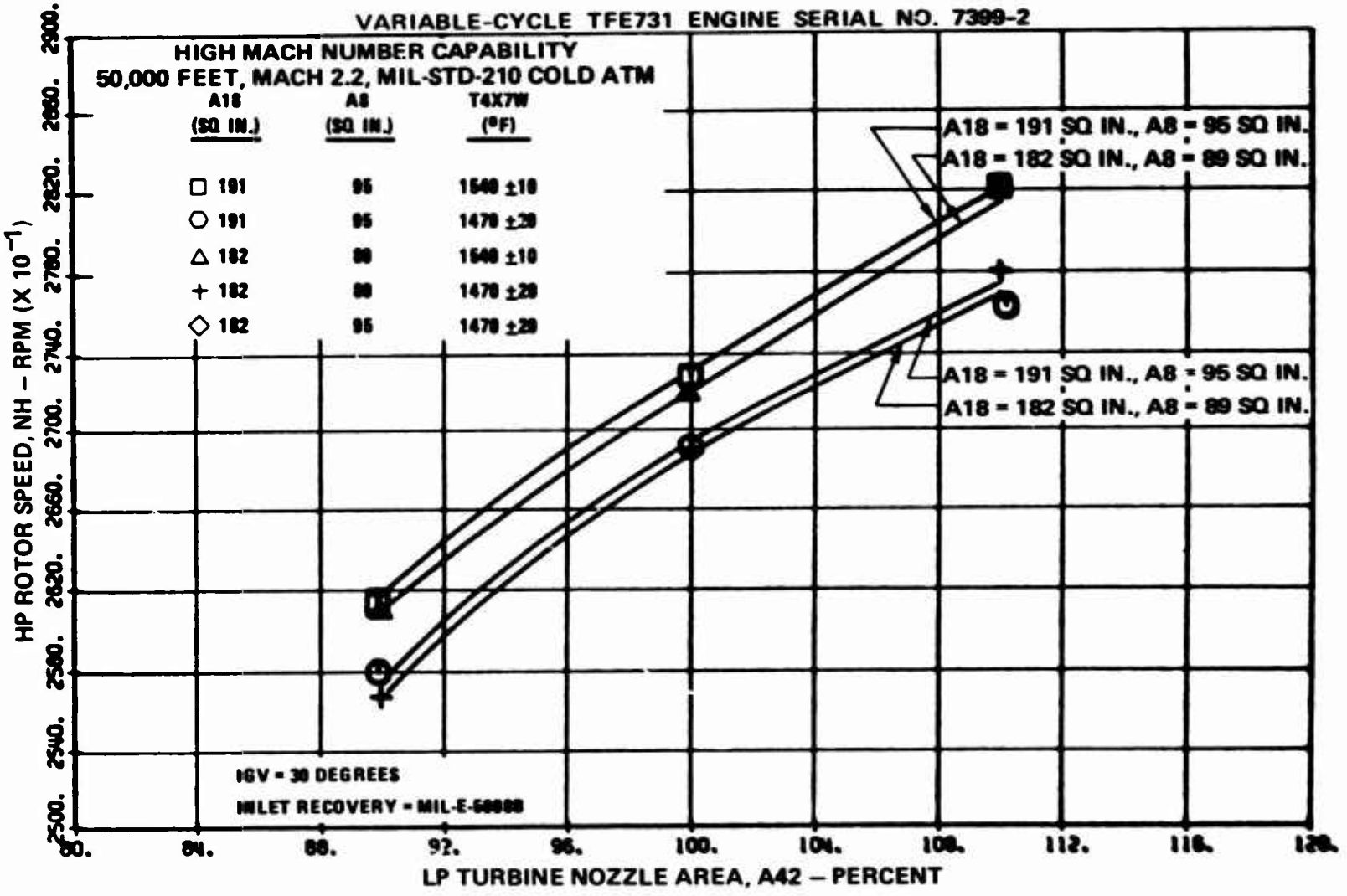

Figure 645. High-Mach-Number Capability, Mach 2.2, 50,000 Feet, HP Rotor Speed Versus LP Turbine Nozzle Area.

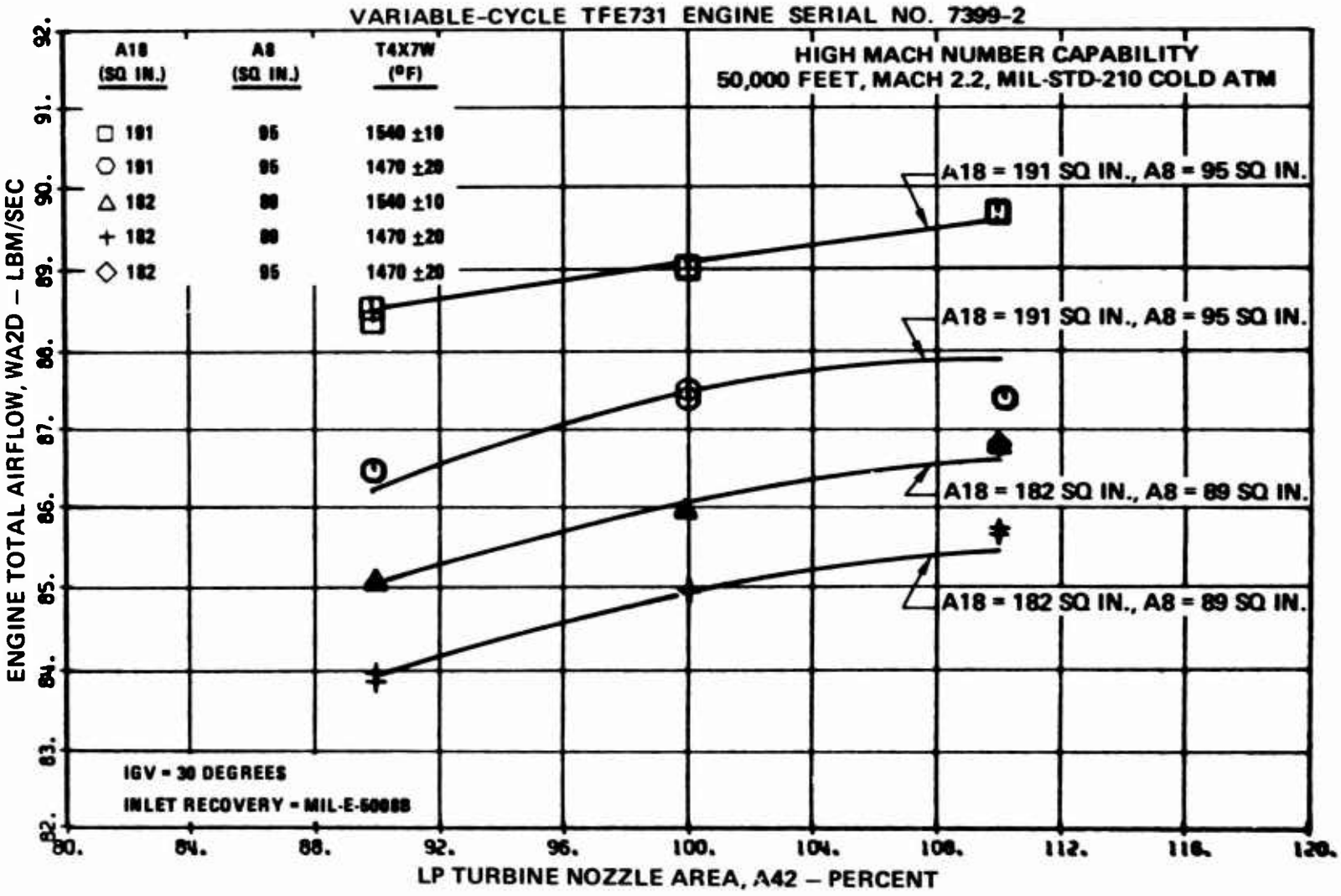

Figure 646. High-Mach-Number Capability, Mach 2.2, 50,000 Feet, Engine Total Airflow Versus LP Turbine Nozzle Area.

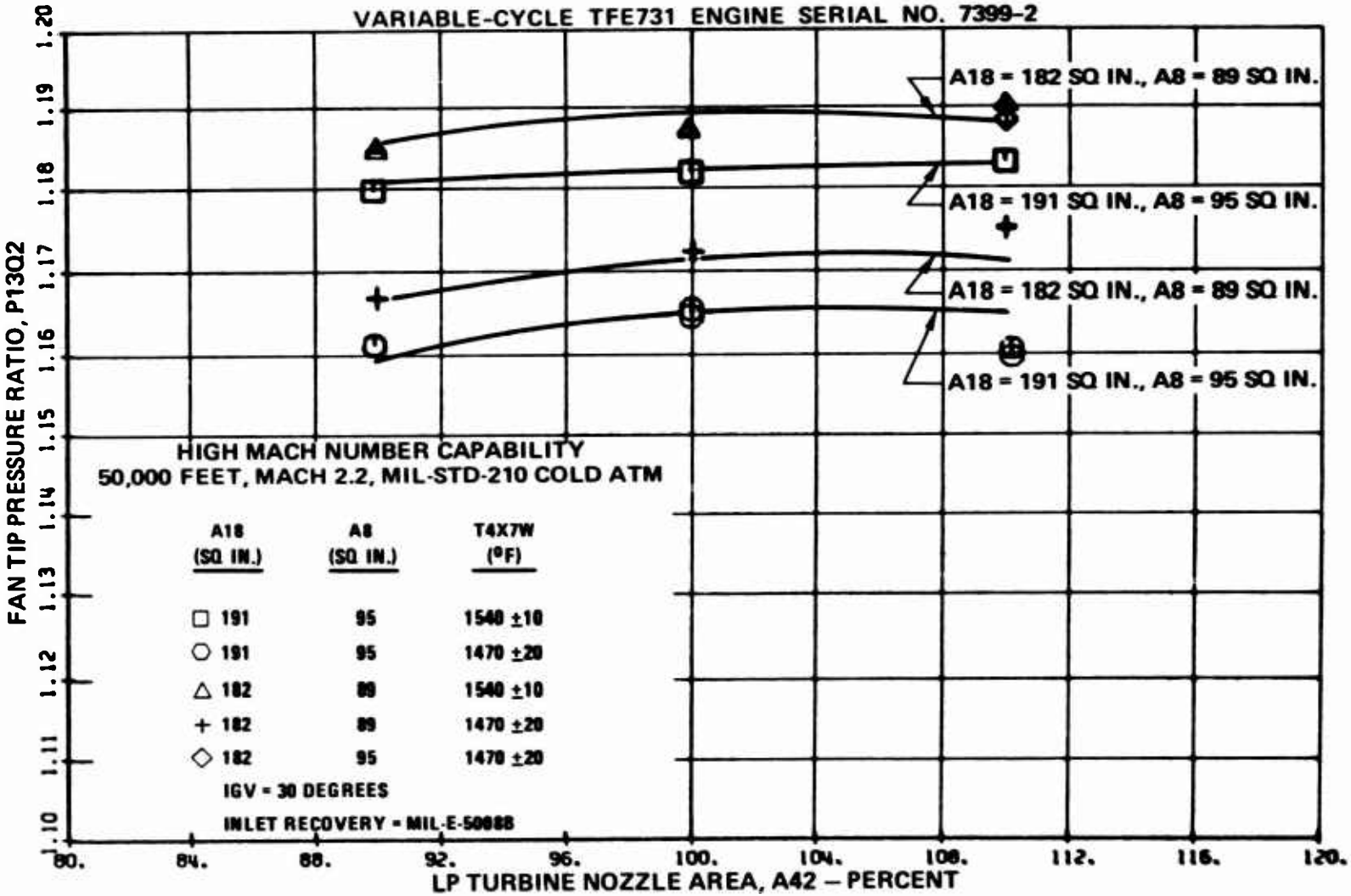

Figure 647. High-Mach-Number Capability, Mach 2.2, 50,000 Feet, Fan Tip Pressure Ratio Versus LP Turbine Nozzle Area.

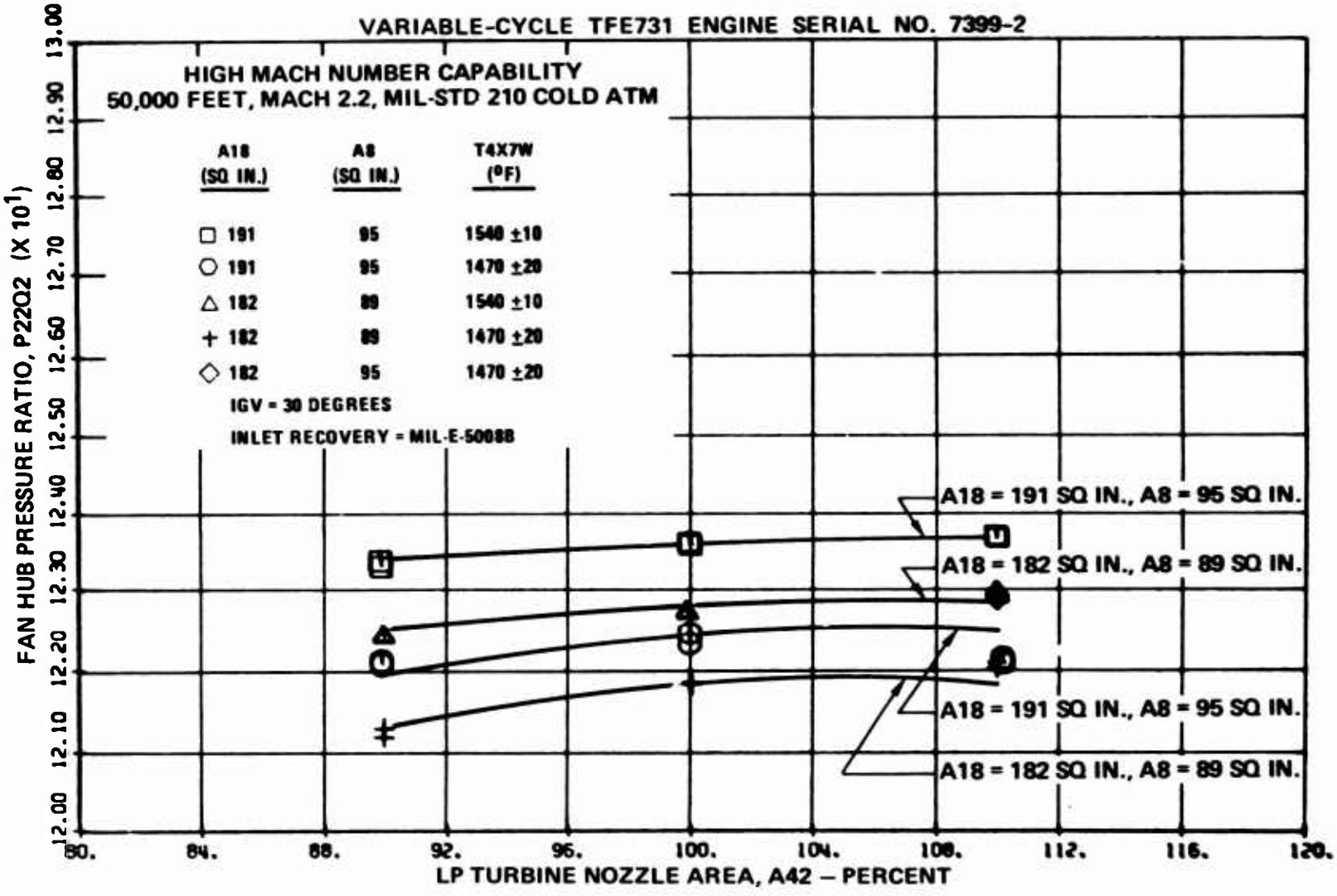

Figure 648. High-Mach-Number Capability, Mach 2.2, 50,000 Feet, Fan Hub Pressure Ratio Versus LP Turbine Nozzle Area.

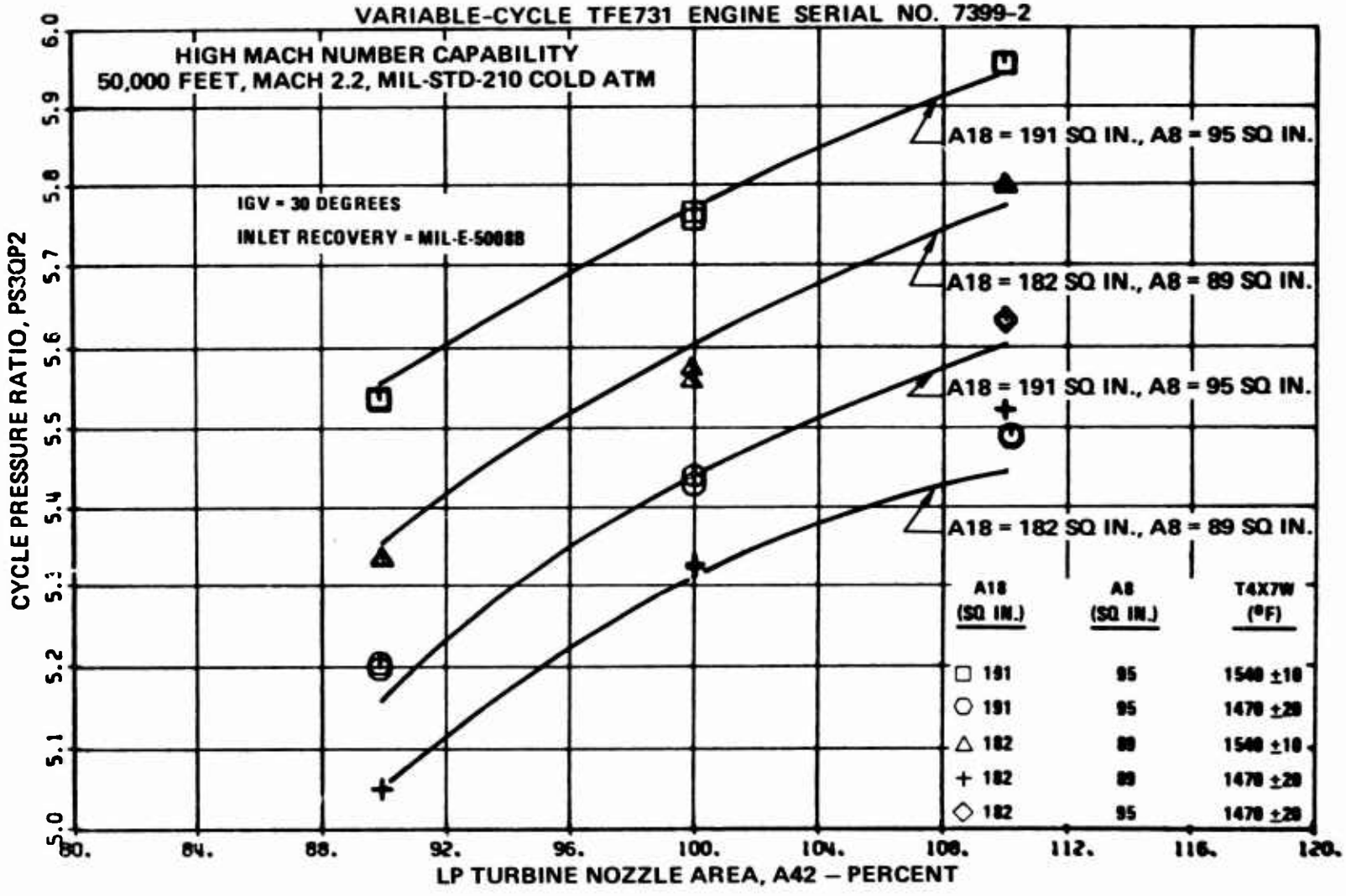

Figure 649. High-Mach-Number Capability, Mach 2.2, 50,000 Feet, Cycle Pressure Ratio Versus LP Turbine Nozzle Area.

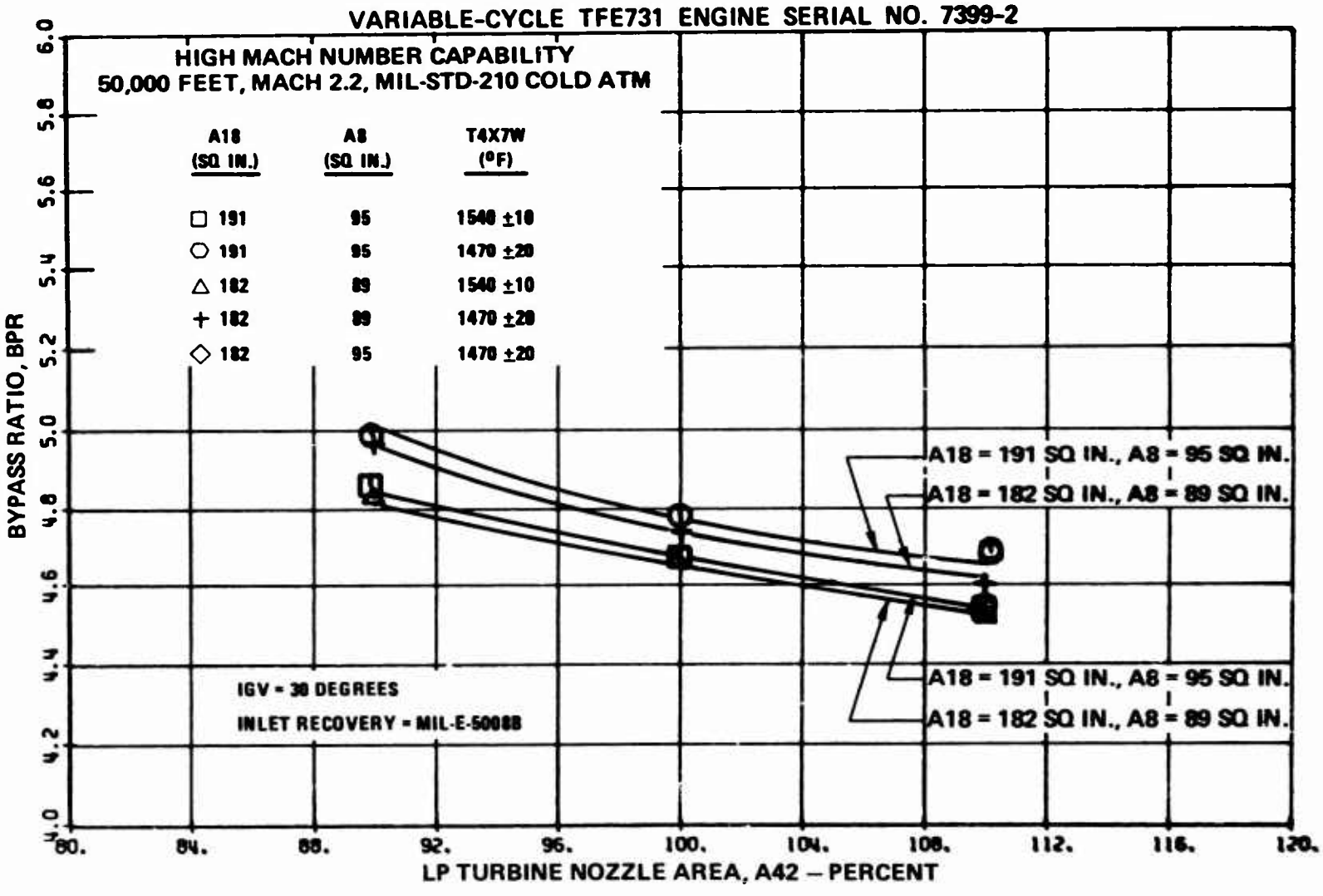

Figure 650. High-Mach-Number Capability, Mach 2.2, 50,000 Feet, Bypass Ratio Versus LP Turbine Nozzle Area.

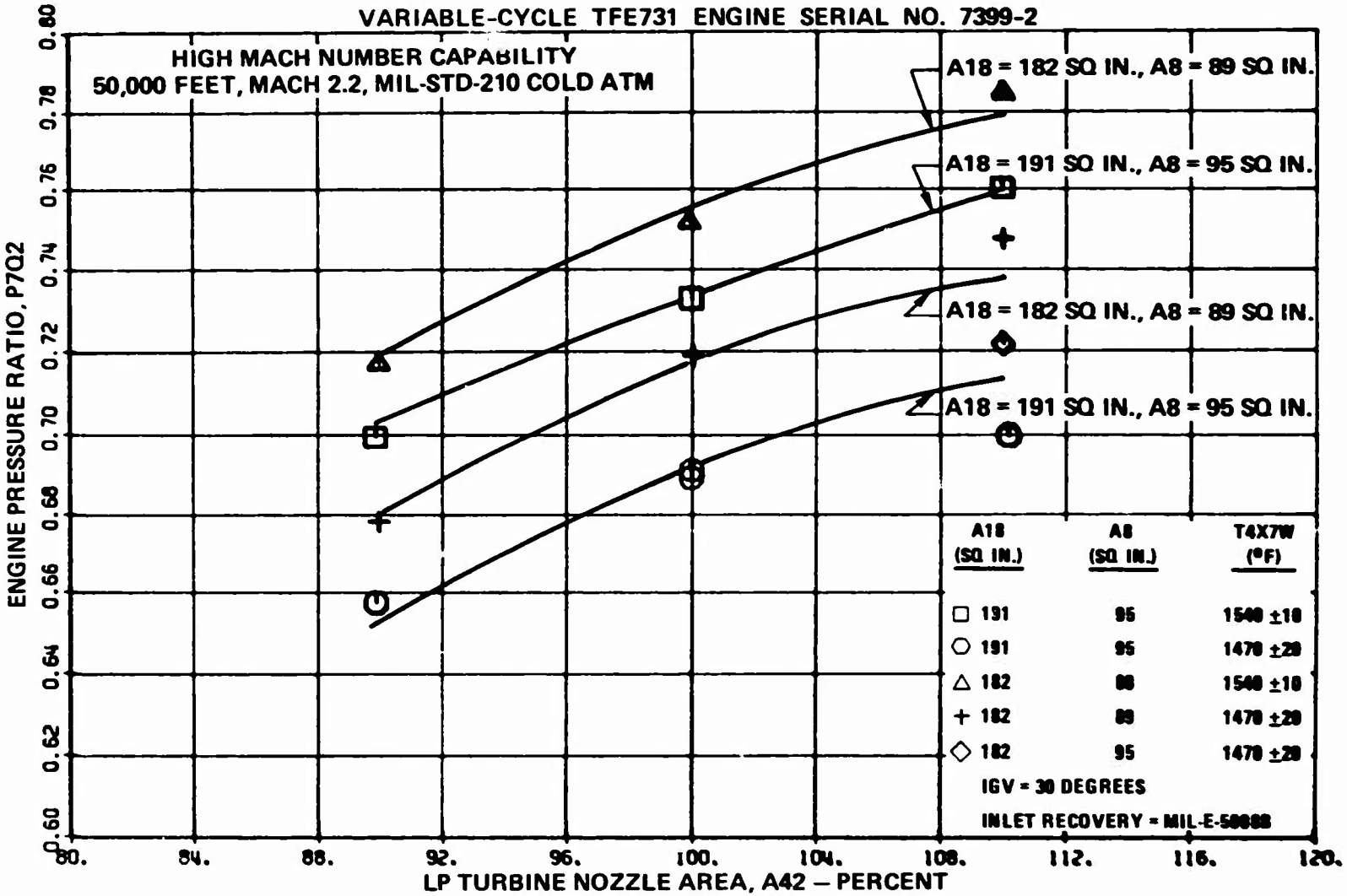

Figure 651. High-Mach-Number Capability, Mach 2.2, 50,000 Feet, Engine Pressure Ratio Versus LP Turbine Nozzle Area.

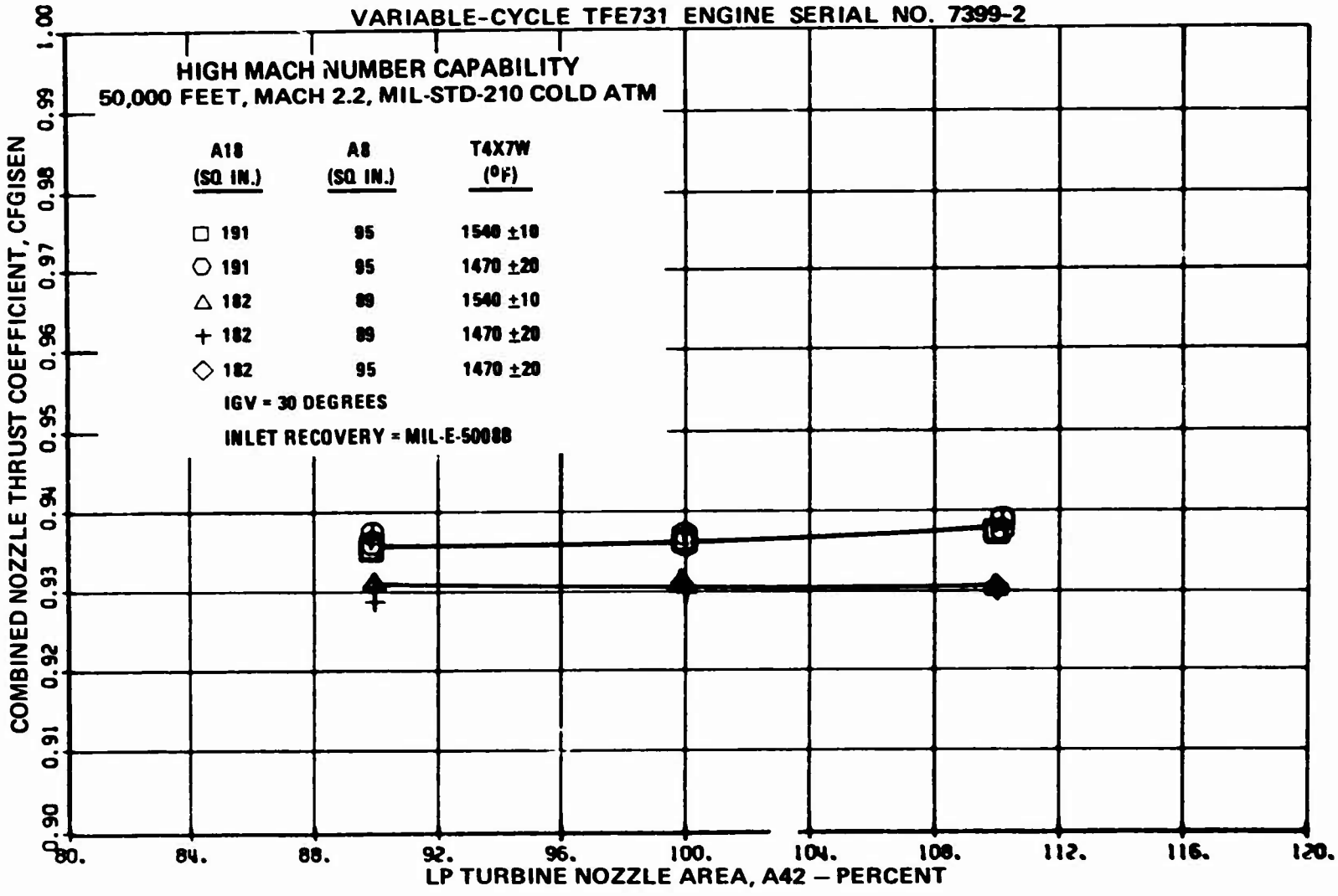

Figure 652. High-Mach-Number Capability, Mach 2.2, 50,000 Feet, Combined Nozzle Thrust Coefficient Versus LP Turbine Nozzle Area.

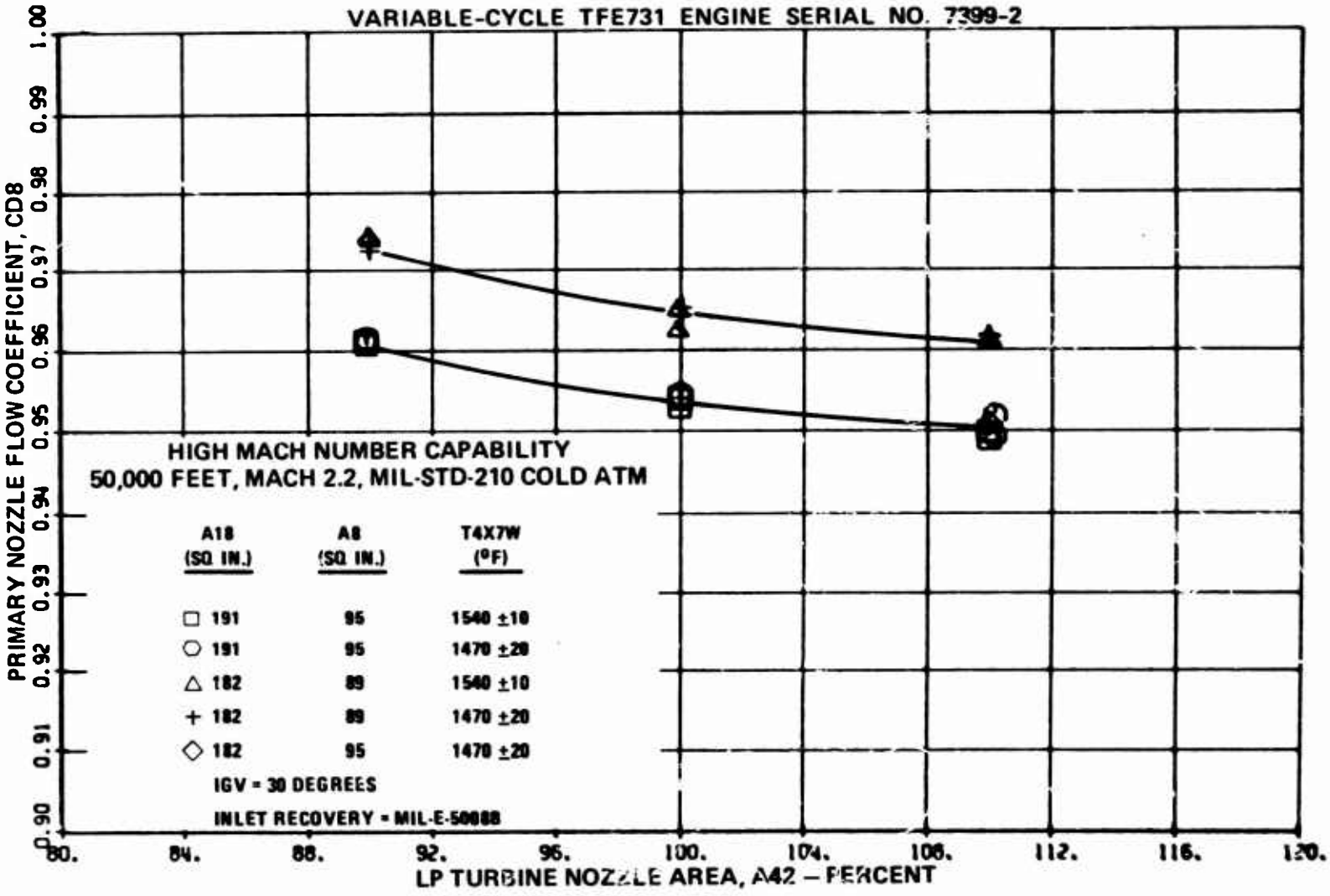

Figure 653. High-Mach-Number Capability, Mach 2.2, 50,000 Feet, Primary Nozzle Flow Coefficient Versus LP Turbine Nozzle Area.

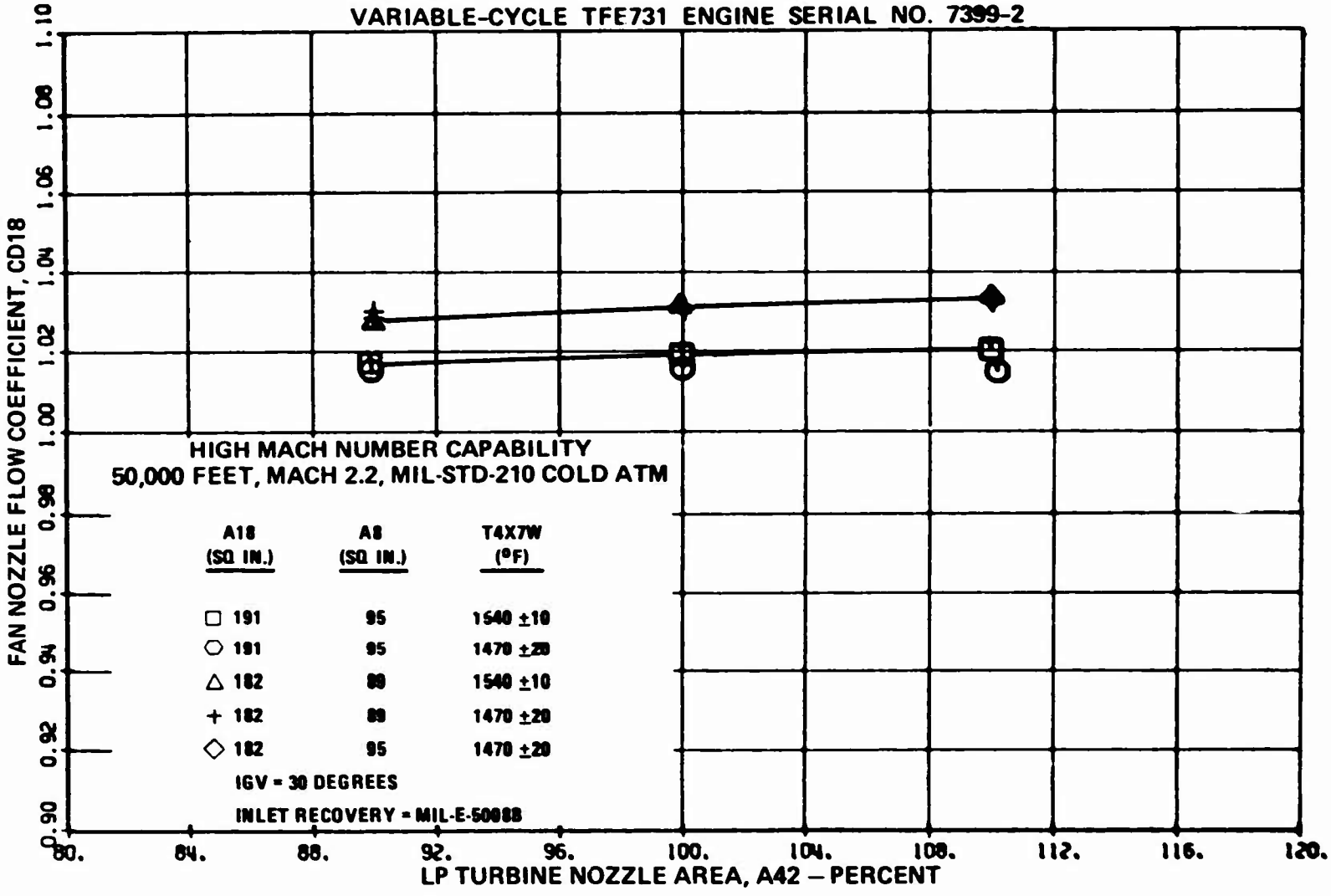

Figure 654. High-Mach-Number Capability, Mach 2.2, 50,000 Feet, Fan Nozzle Flow Coefficient Versus LP Turbine Nozzle Area.

TABLE 82. HIGH-MACH-NUMBER CAPABILITY, 50,000 FEET, MACH 2.2, MIL-STD-210, COLD ATM, WITH HP TURBINE INLET TEMPERATURE AT 1540 ±10°F.

A18 (sq in.)	A8 (sq in.)	A42 (percent)	LP Rotor Speed (rpm)	HP Rotor Speed (rpm)	Net Thrust (lbf)	SFC lbm/hr lbf	LPC Surge Margin (percent)
191	95	90	17,07[illegible]	26,160	83	7.867	14.2
191	95	100	17,210	27,300	97	6.866	21.0
191	95	110	17,230	28,200	114	5.970	27.3
182	89	90	16,700	26,100	73	8.712	15.2
182	89	100	16,820	27,200	84	7.821	21.4
182	89	110	16,840	28,150	93	7.183	28.2

Surge bleed valve closed
IGV = 30 degrees

The data in Table 82 shows that variable LP turbine nozzles are still effective in controlling LP compressor surge margin at this extreme flight condition. The sensitivity of the surge margin change with LP turbine nozzle area modulation was of the order of 0.62 to 0.68 percent change in surge margin for each percent change in LP turbine nozzle area. This compares to a sensitivity of 0.74 to 1.08 for flight Mach numbers from 0.8 to 1.6 at 50,000 feet, standard atmosphere.

The surge margin data shown in Paragraph 4.4.11 indicates that changing the inlet guide vanes from zero to 30 degrees increases the LP compressor surge margin by approximately 17.5 percent at a referred speed of 70 percent. This referred speed is representative of those tested at the Mach-2.2 condition. The test-derived surge margins presented in Table 82 confirm that the range of turbine nozzle area modulation would have been severely restricted if the 30-degree IGV setting had not been used. The data also indicated that the surge margin at 100 percent LP turbine nozzle area would also have been insufficient if use of IGV and first-stage stator settings of zero degrees had been attempted.

Although the variable-geometry changes at this test condition showed some significant effects, percentagewise, on net thrust and specific fuel consumption, these results are considered to be academic for an unaugmented turbofan engine at this condition. Therefore, the results are presented for the record but are not discussed further.

4.4.13 Sea-Level Static Post-Test Calibration

The objective of the sea-level post-test calibration was to determine the extent of engine performance deterioration that occurred during the altitude test.

The post-test calibration was conducted on June 18, 1974, at a simulated altitude of 5000 feet and an engine inlet temperature of 59°F. These are the conditions that were simulated during the pretest sea-level cell correlation. All the variable-geometry settings were set to the same values used in the pretest sea-level static, standard atmosphere calibration. The post-test calibration was conducted prior to the Mach-2.2 test and the high-altitude test. Comparisons of the pretest and post-test AEDC sea-level results are presented in Figures 655 through 669. The parameters presented in these curves are listed in Table 83.

A summary comparison of selected parameters is presented for a constant net thrust of 3300 pounds in Table 84. The data presented in Table 84 indicates that, at a constant net thrust of 3300 pounds, the SFC had increased by 1.2 percent and the inter-turbine temperature by 23°F. These two parameters and the others presented in Table 84 indicate that there was minimal performance deterioration during the test.

TABLE 83. SEA-LEVEL STATIC, STANDARD ATM POST-TEST CALIBRATION PERFORMANCE CURVES

Figure No.	Parameters Presented
655	Referred thrust specific fuel consumption versus referred net thrust
656	Referred interturbine temperature versus referred net thrust
657	Referred net thrust versus referred LP rotor speed
658	Referred fuel flow versus referred LP rotor speed
659	Referred interturbine temperature versus referred LP rotor speed
660	Referred HP rotor speed versus referred LP rotor speed
661	Referred engine total airflow versus referred LP rotor speed
662	Fan tip pressure ratio versus referred LP rotor speed
663	Fan hub pressure ratio versus referred LP rotor speed
664	Cycle pressure ratio versus referred LP rotor speed
665	Engine pressure ratio versus referred LP rotor speed
666	Bypass ratio versus referred LP rotor speed
667	Combined nozzle thrust coefficient versus referred LP rotor speed
668	Primary nozzle flow coefficient versus referred LP rotor speed
669	Fan nozzle flow coefficient versus referred LP rotor speed

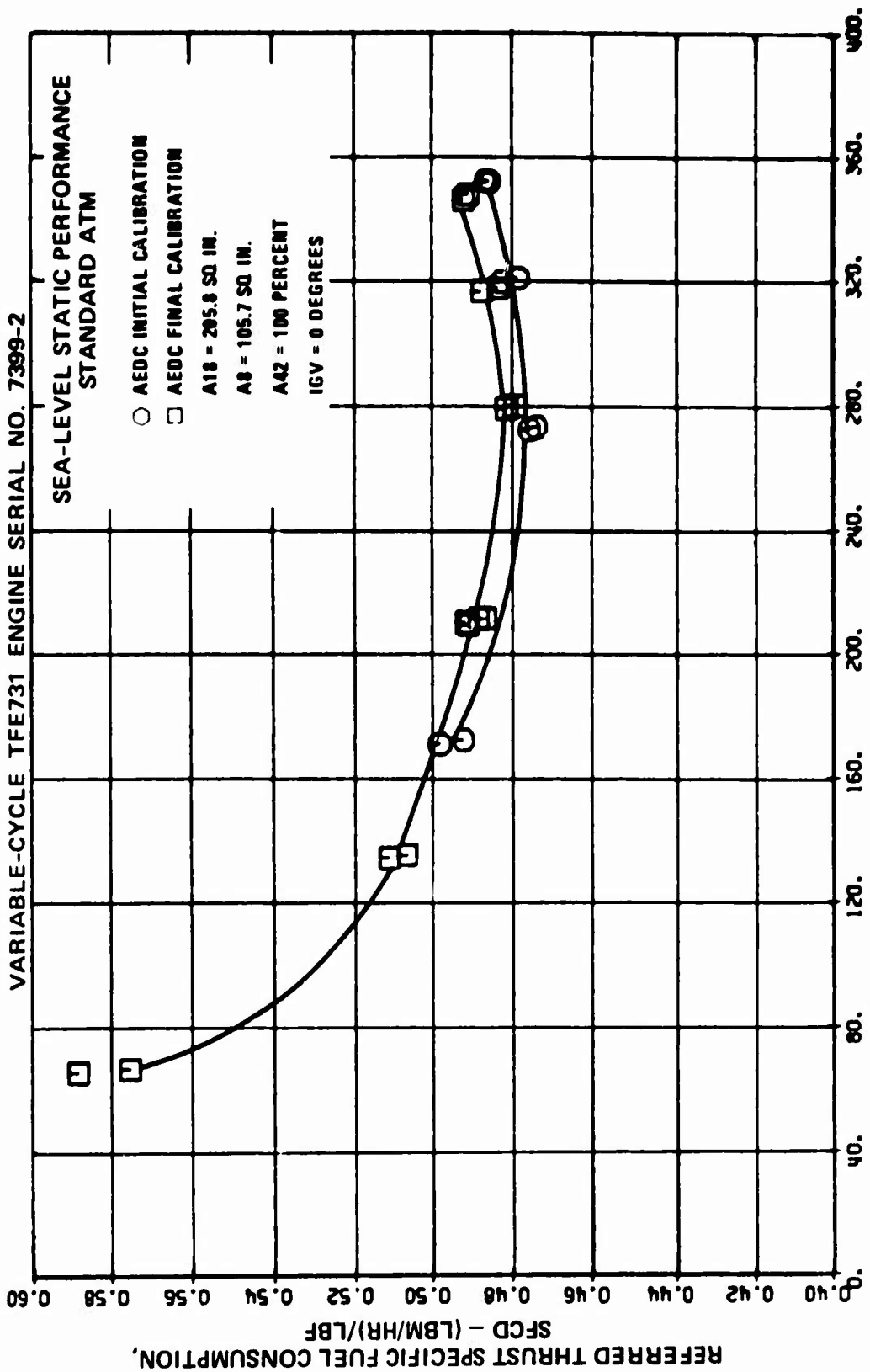

Figure 655. Sea-Level Static, Post-Test Calibration, Referred Thrust Specific Fuel Consumption Versus Referred Net Thrust.

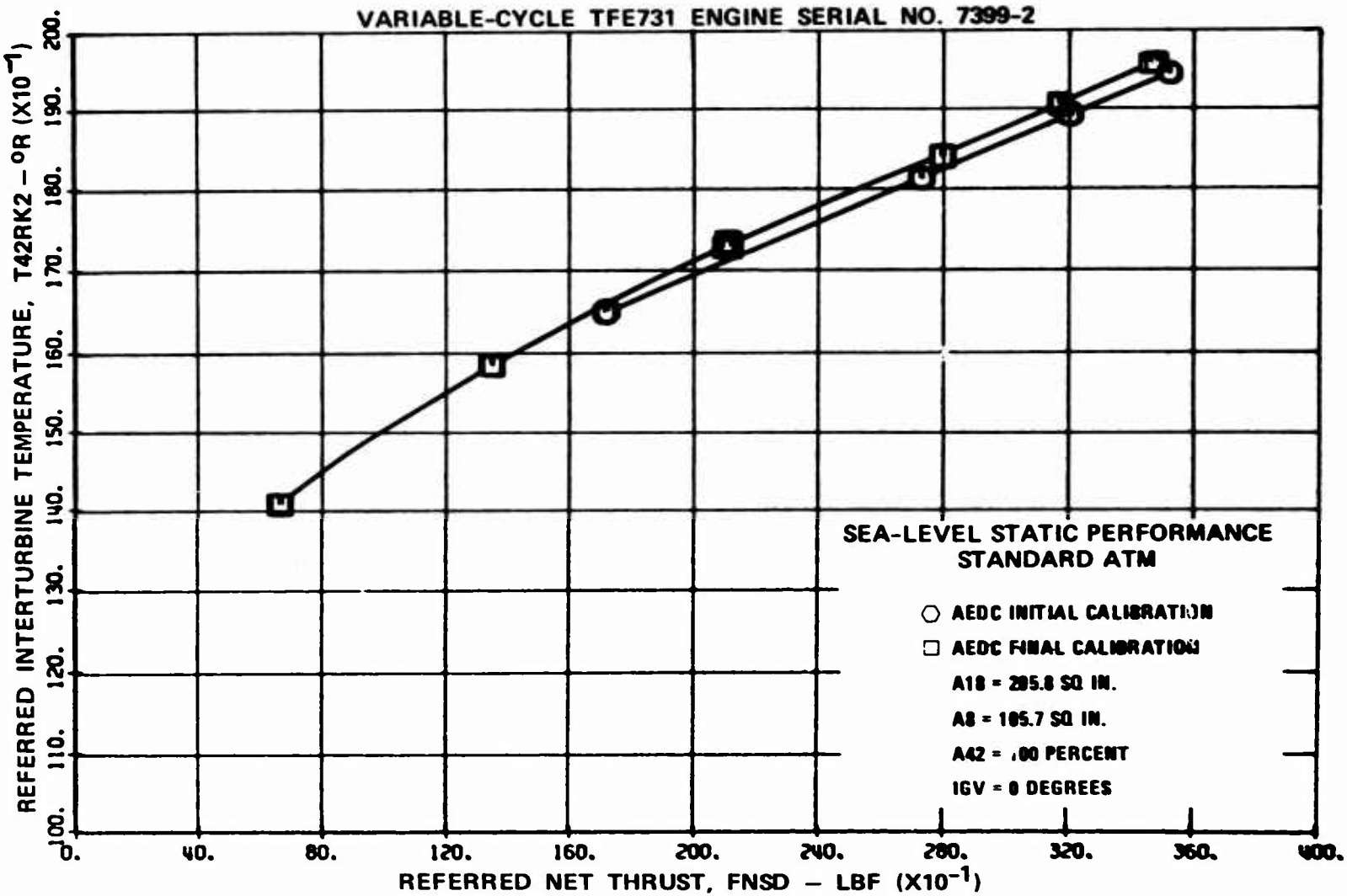

Figure 656. Sea-Level Static, Post-Test Calibration, Referred Interturbine Temperature Versus Referred Net Thrust.

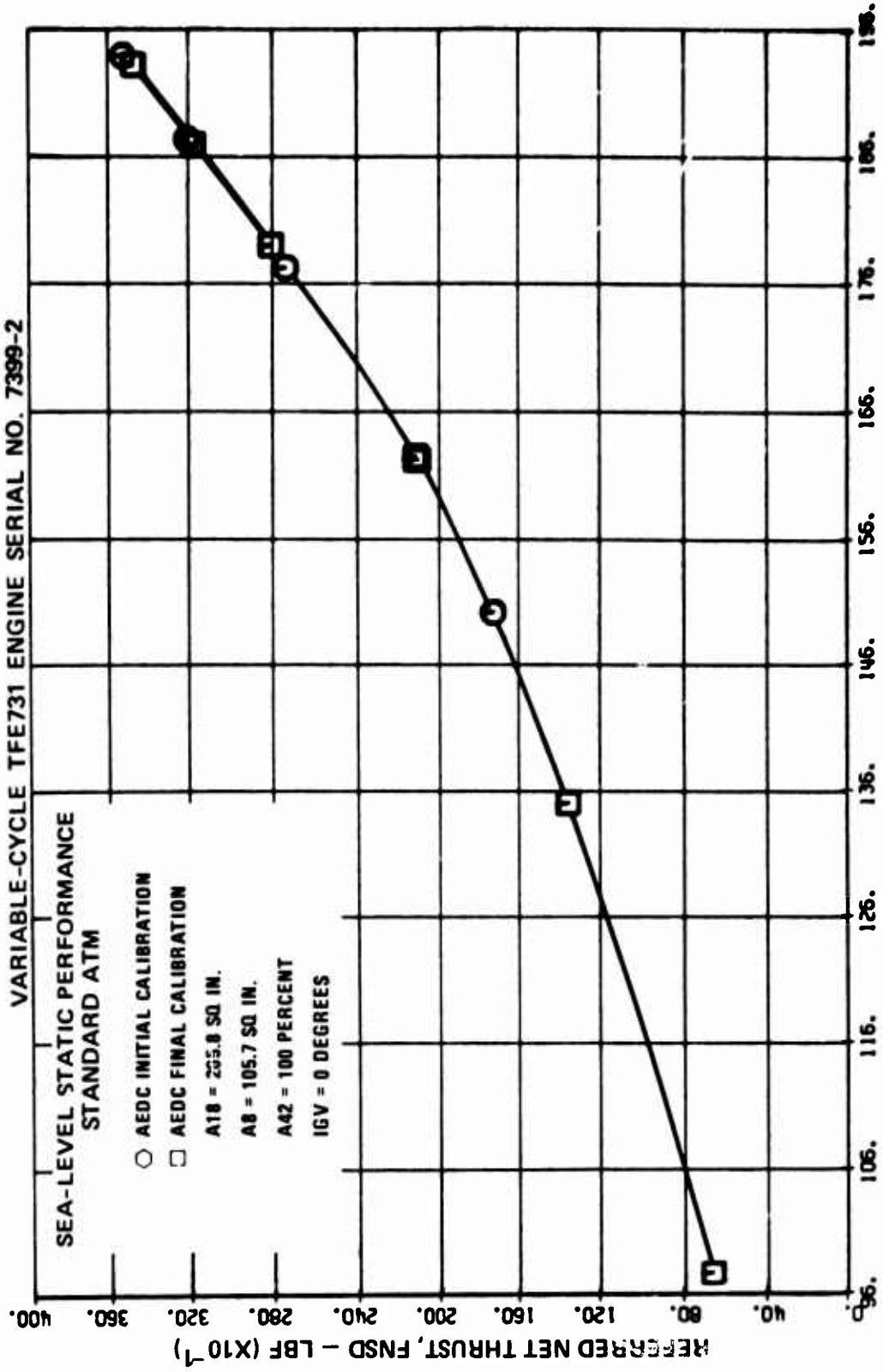

Figure 657. Sea-Level Static, Post-Test Calibration, Referred Net Thrust Versus Referred LP Rotor Speed.

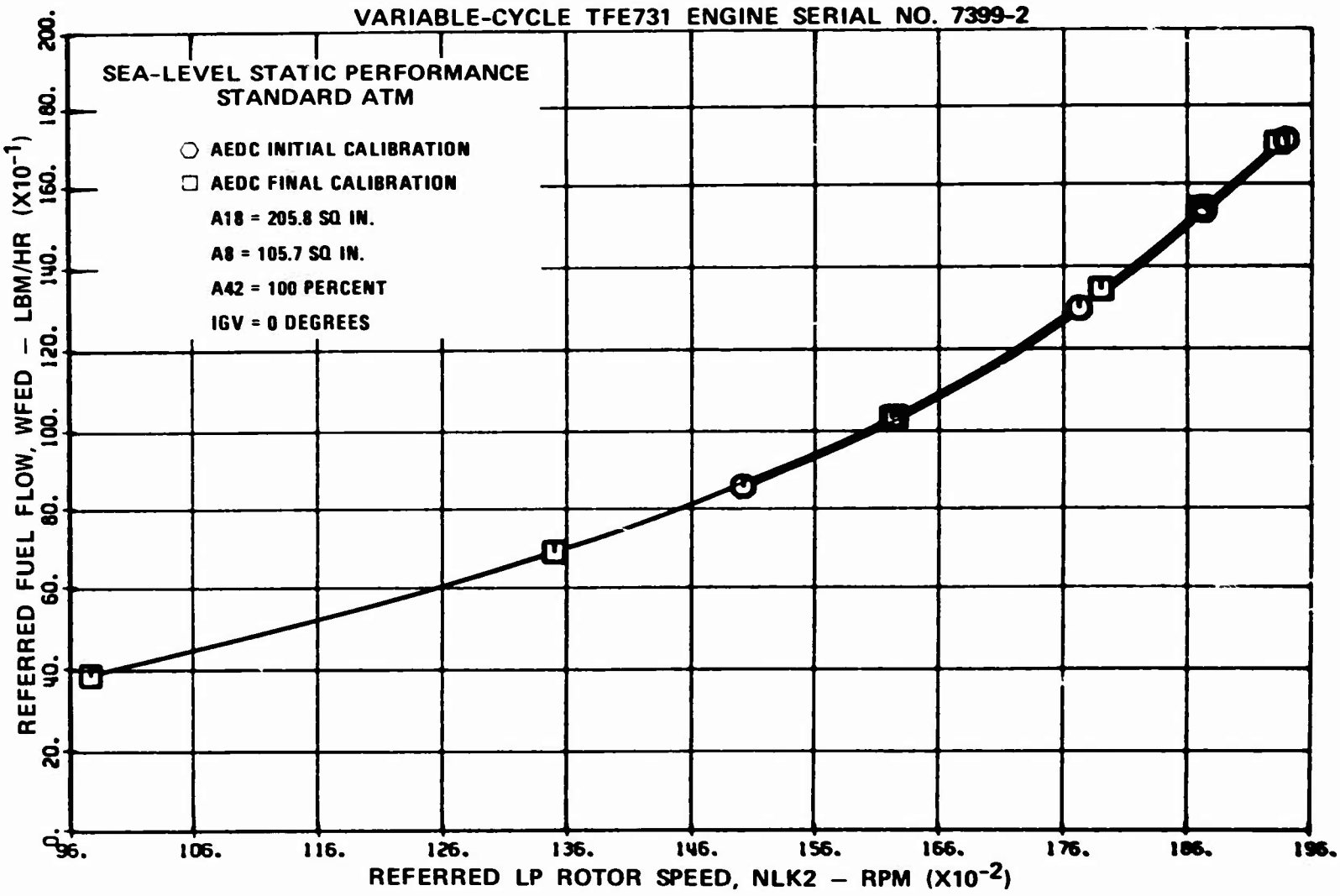

Figure 658. Sea-Level Static, Post-Test Calibration, Referred Fuel Flow Versus Referred LP Rotor Speed.

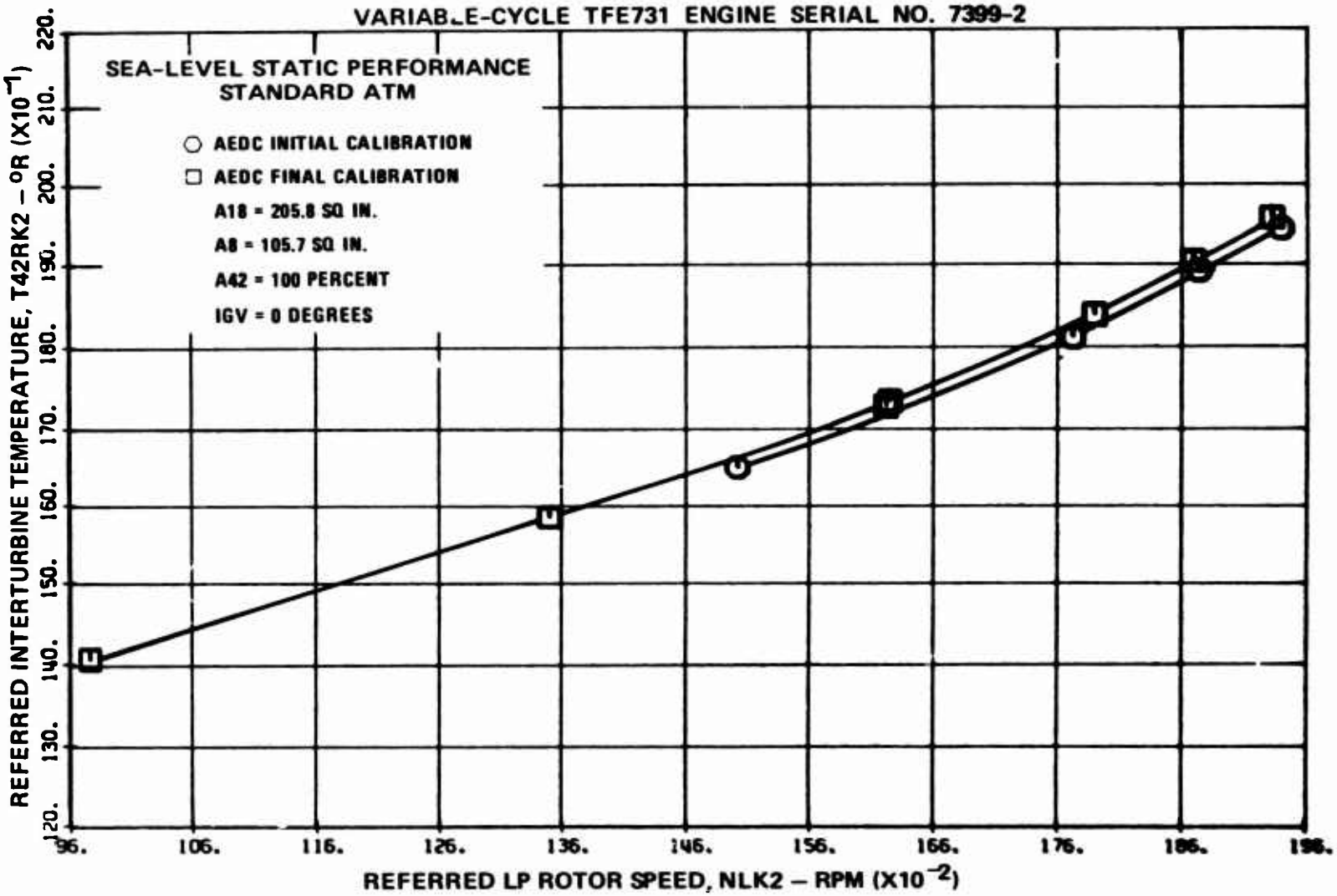

Figure 659. Sea-Level Static, Post-Test Calibration, Referred Interturbine Temperature Versus Referred LP Rotor Speed.

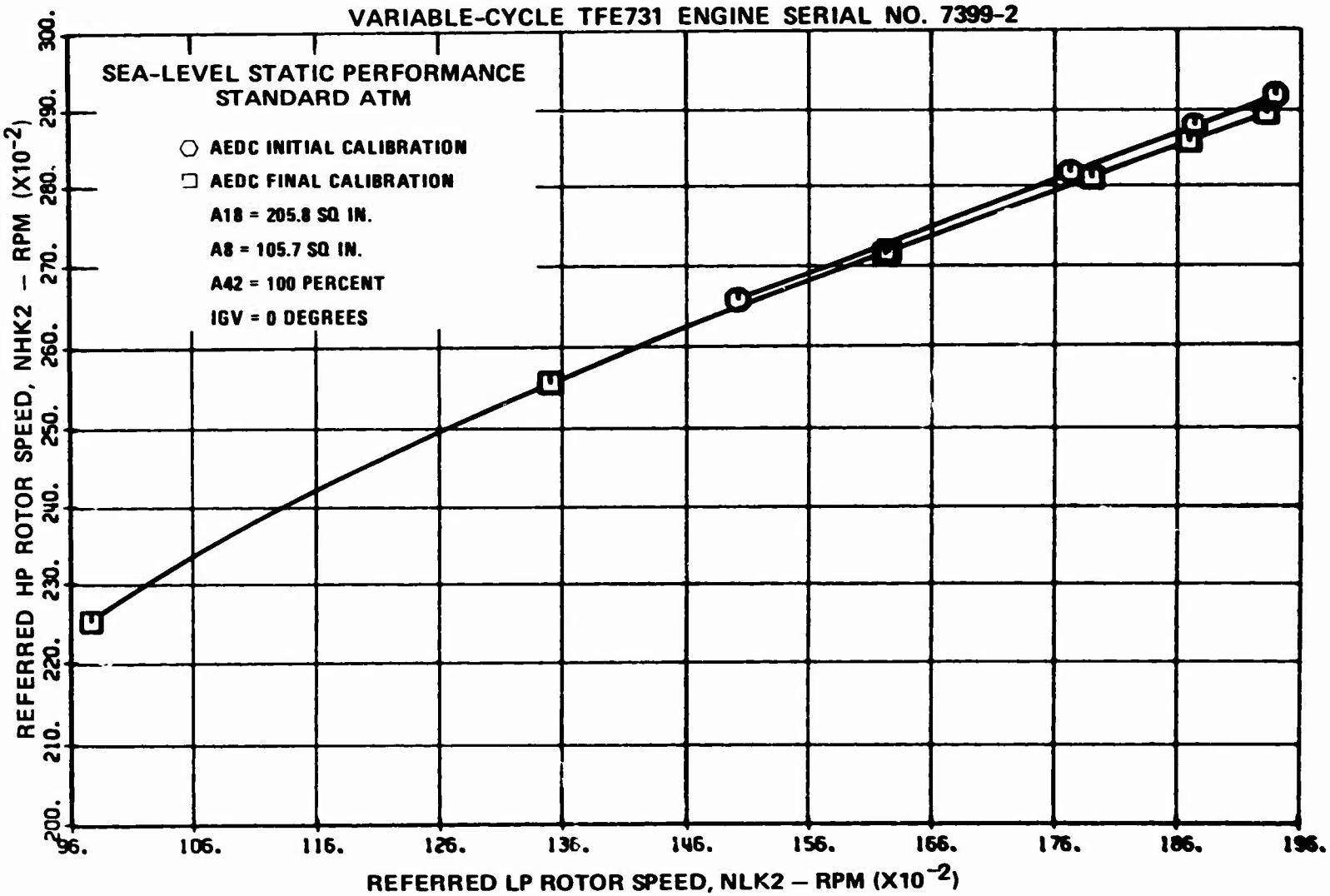

Figure 660. Sea-Level Static, Post-Test Calibration, Referred HP Rotor Speed Versus Referred LP Rotor Speed.

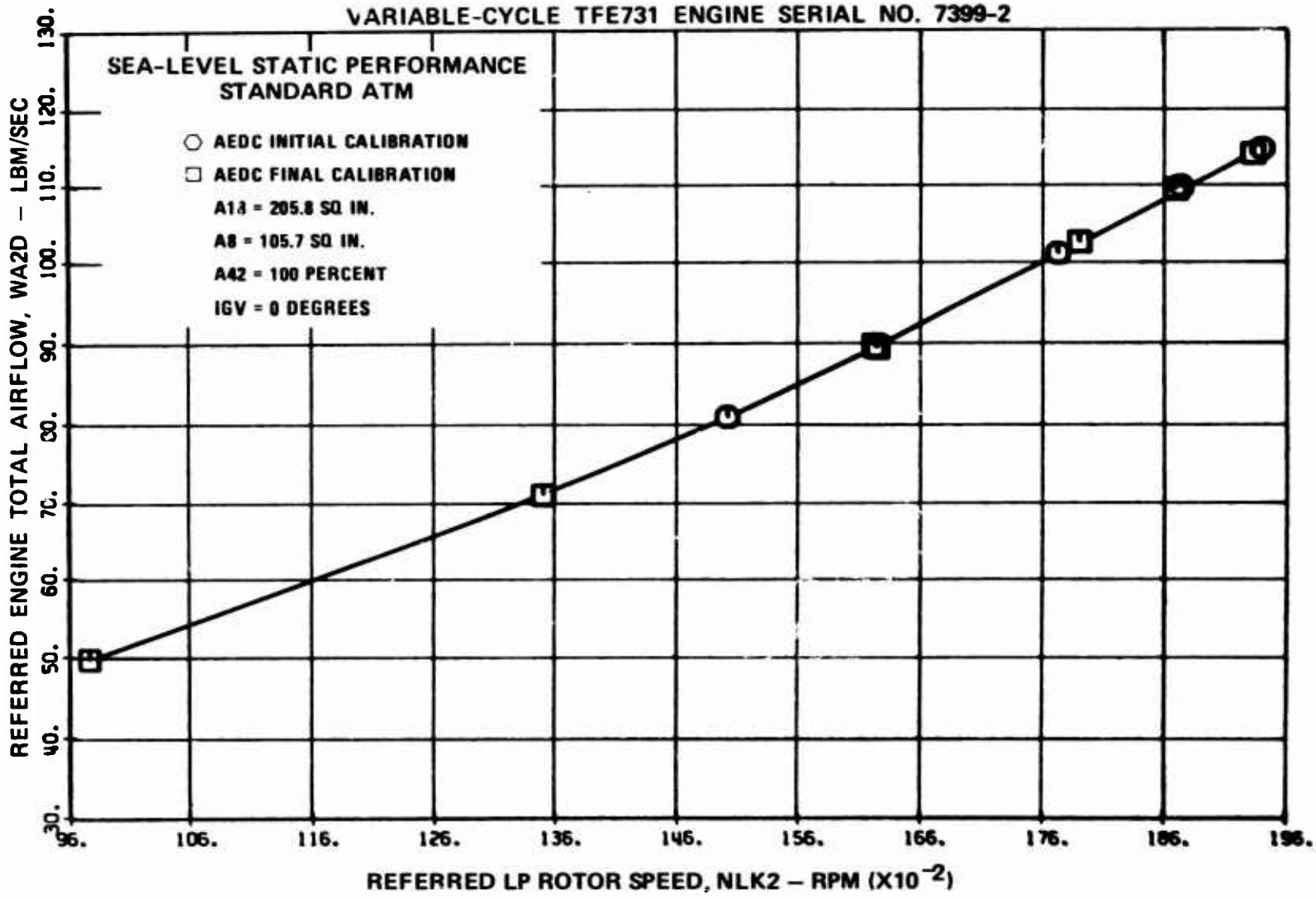

Figure 661. Sea-Level Static, Post-Test Calibration, Referred Engine Total Airflow Versus Referred LP Rotor Speed.

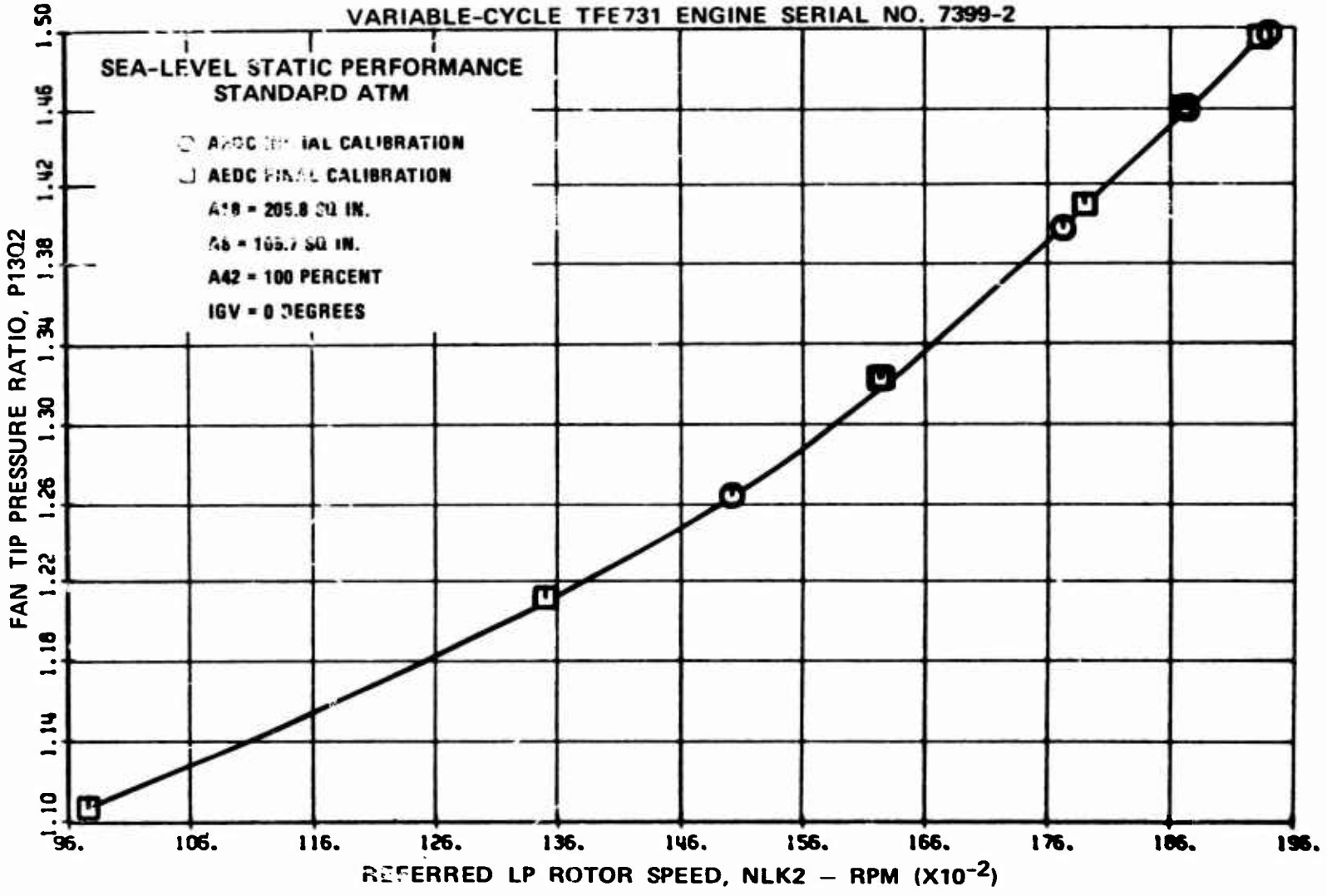

Figure 662. Sea-Level Static, Post-Test Calibration, Fan Tip Pressure Ratio Versus Referred LP Rotor Speed.

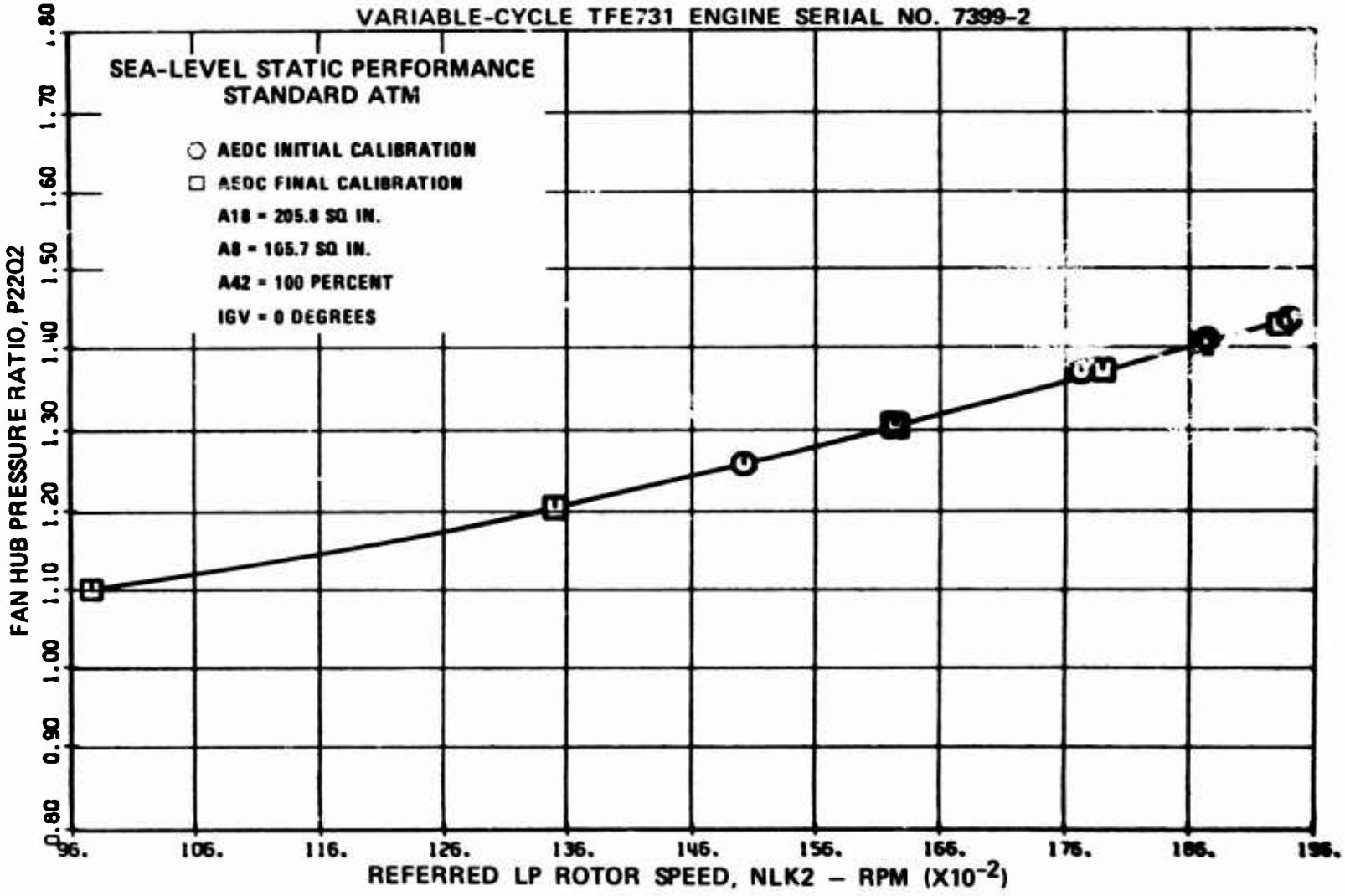

Figure 663. Sea-Level Static, Post-Test Calibration, Fan Hub Pressure Ratio Versus Referred LP Rotor Speed.

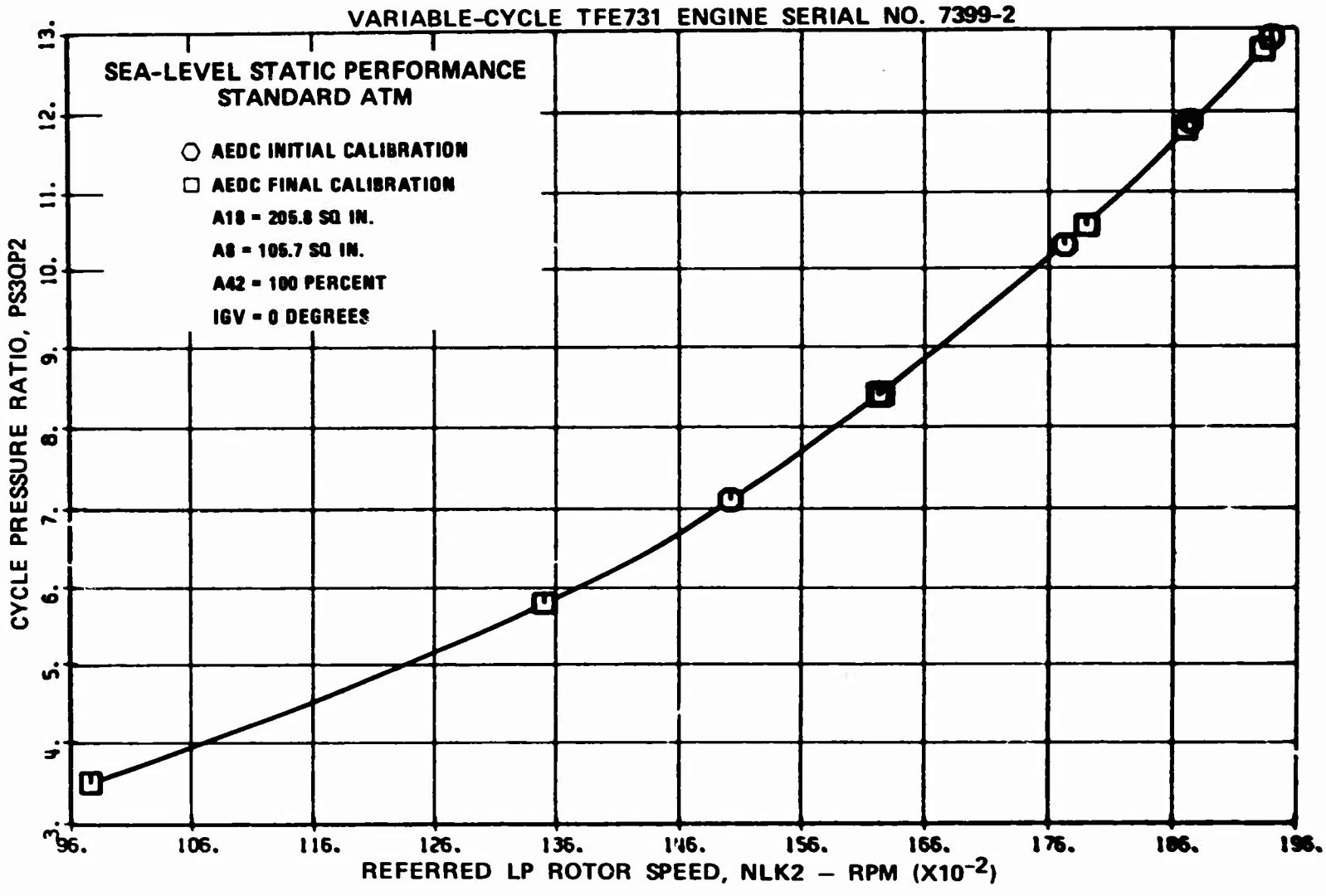

Figure 664. Sea-Level Static, Post-Test Calibration, Cycle Pressure Ratio Versus Referred LP Rotor Speed.

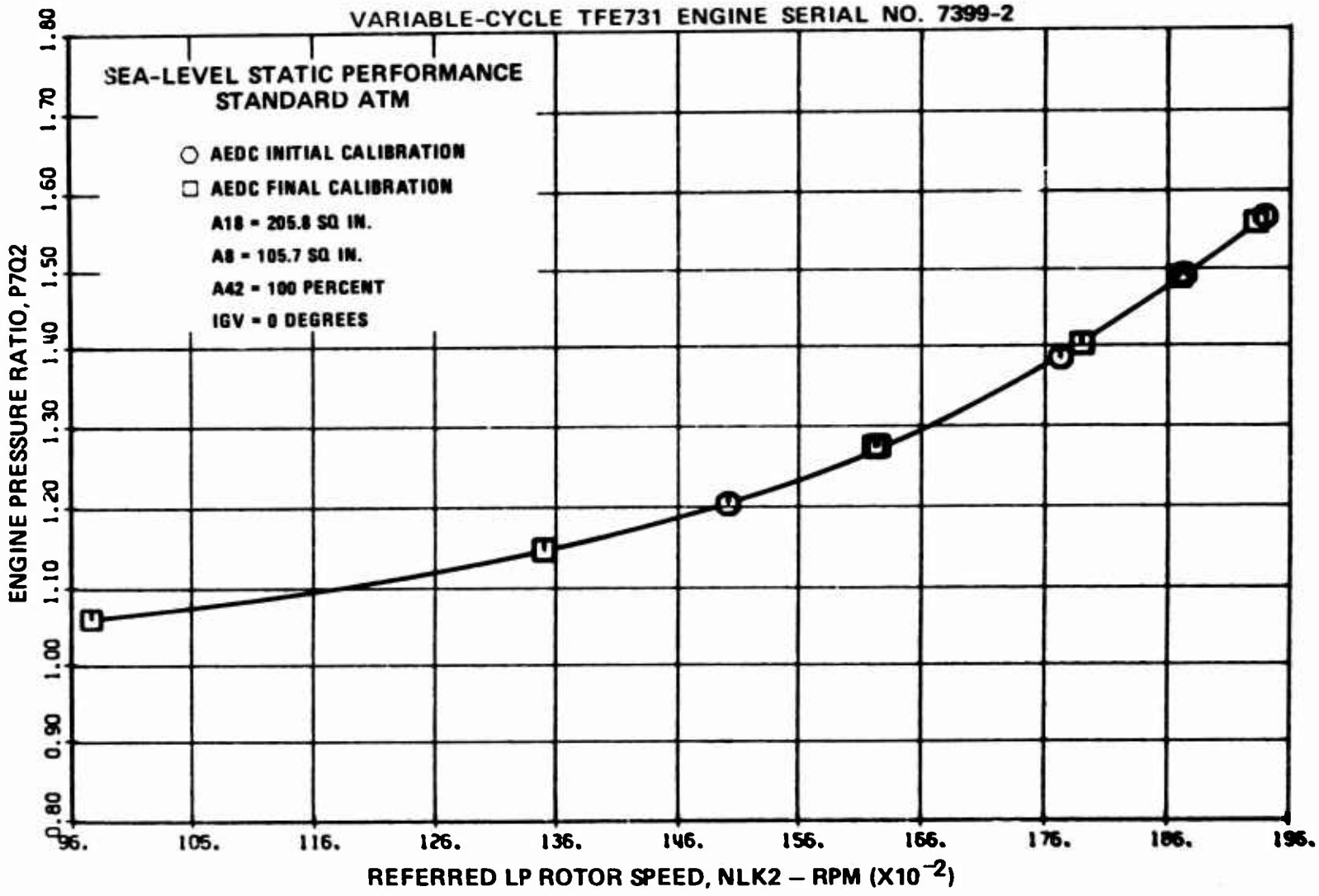

Figure 665. Sea-Level Static, Post-Test Calibration, Engine Pressure Ratio Versus Referred LP Rotor Speed.

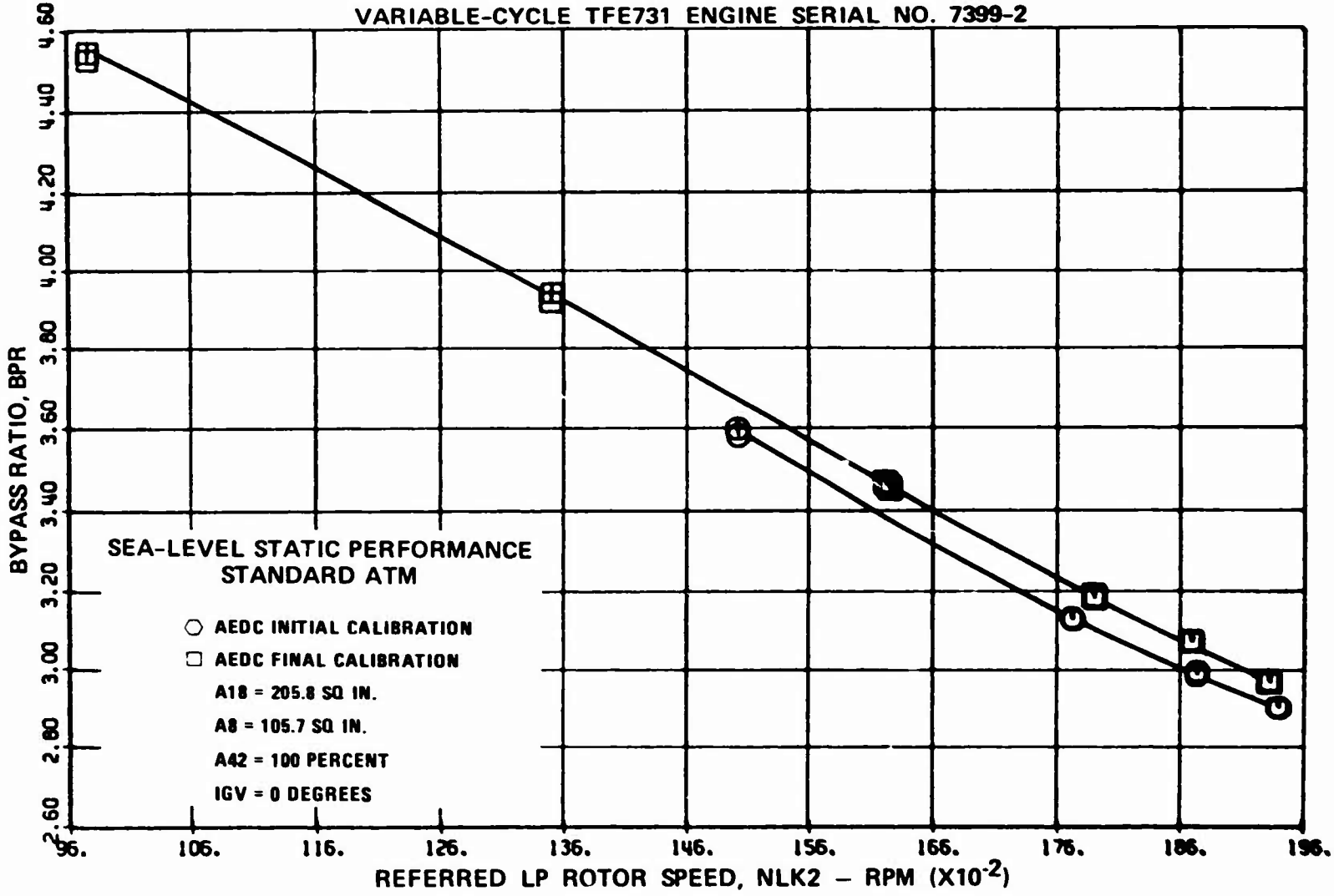

Figure 666. Sea-Level Static, Post-Test Calibration, Bypass Ratio Versus Referred LP Rotor Speed.

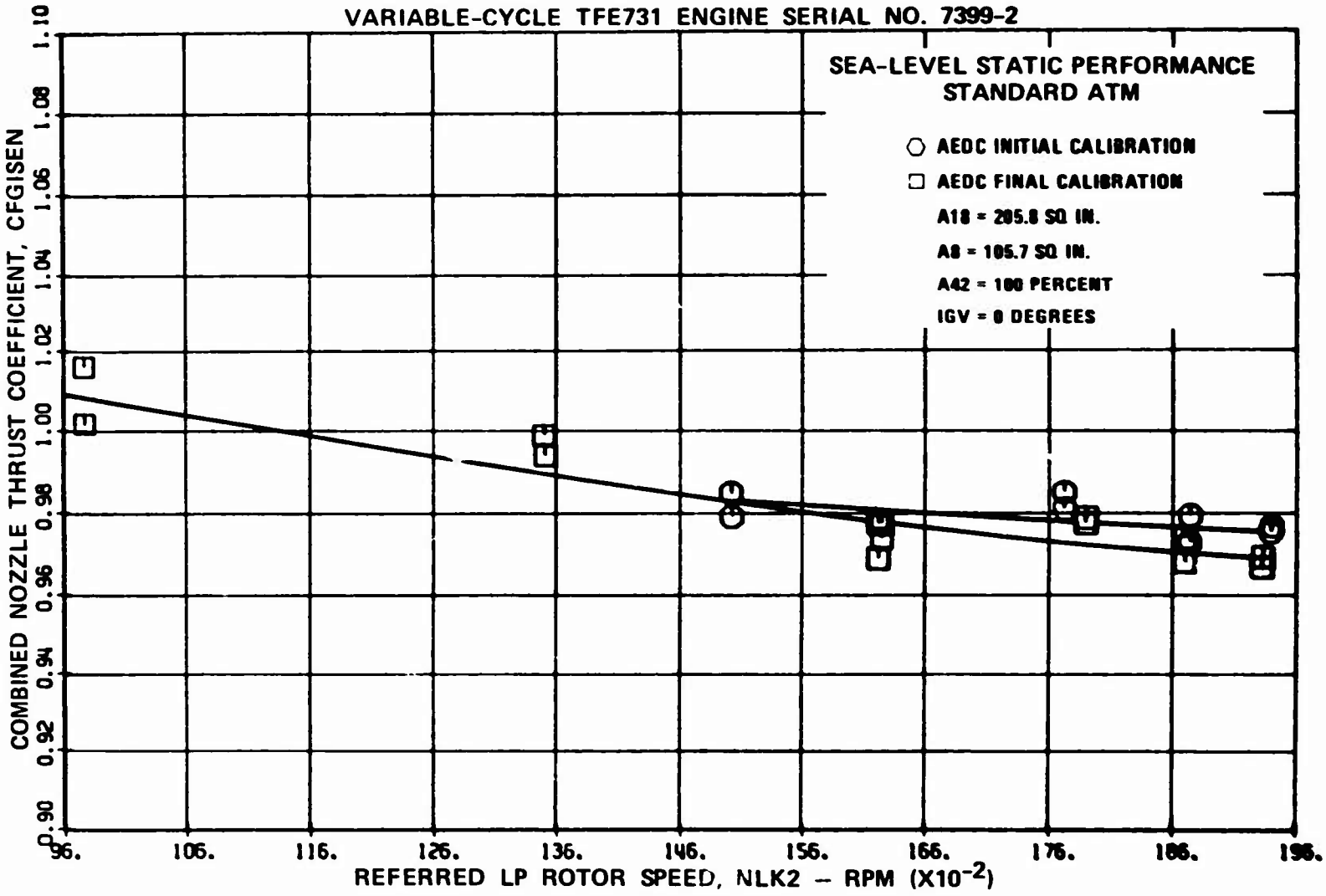

Figure 66. Sea-Level Static, Post-Test Calibration, Combined Nozzle Thrust Coefficient Versus Referred LP Rotor Speed.

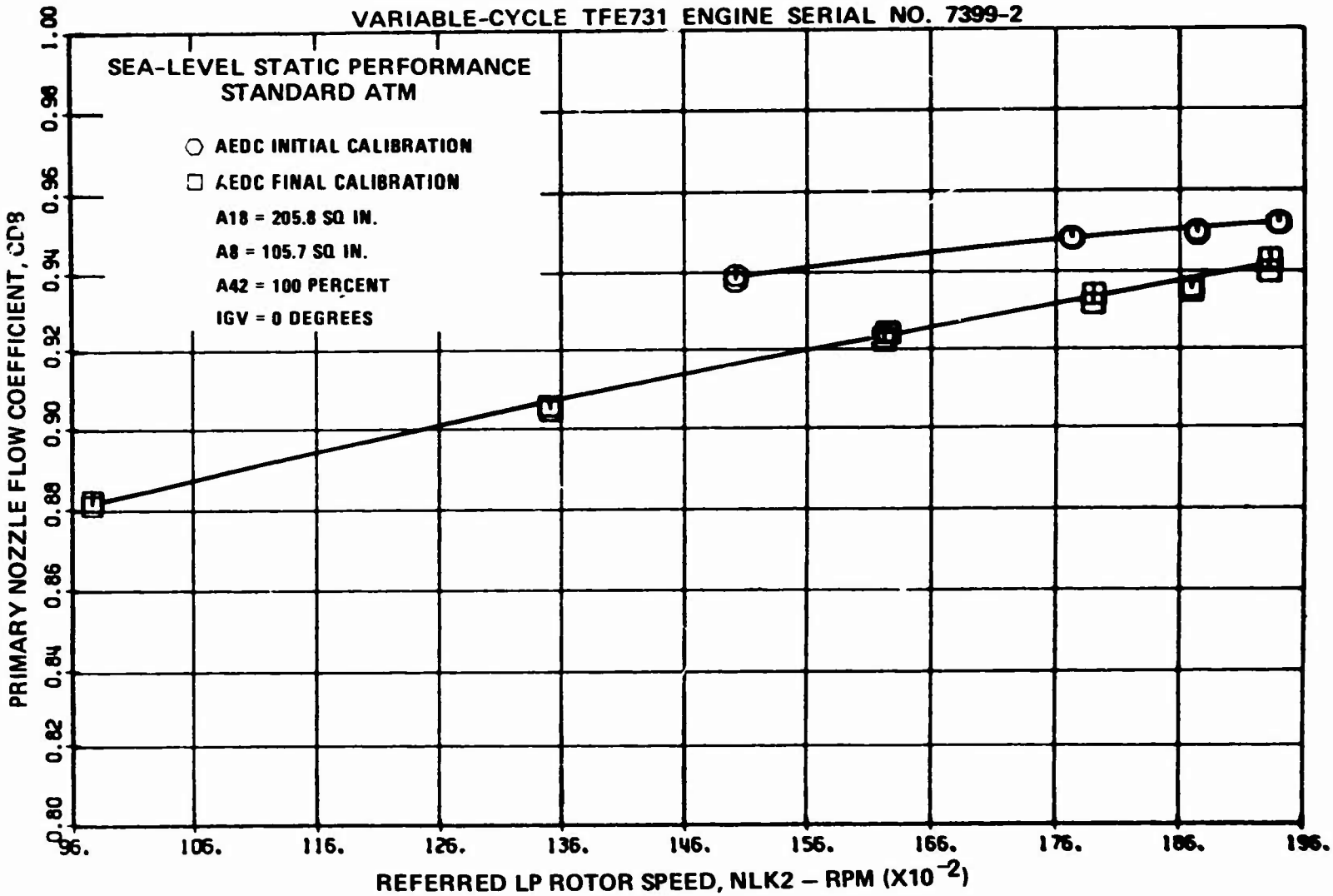

Figure 668. Sea-Level Static, Post-Test Calibration, Primary Nozzle Flow Coefficient Versus Referred LP Rotor Speed.

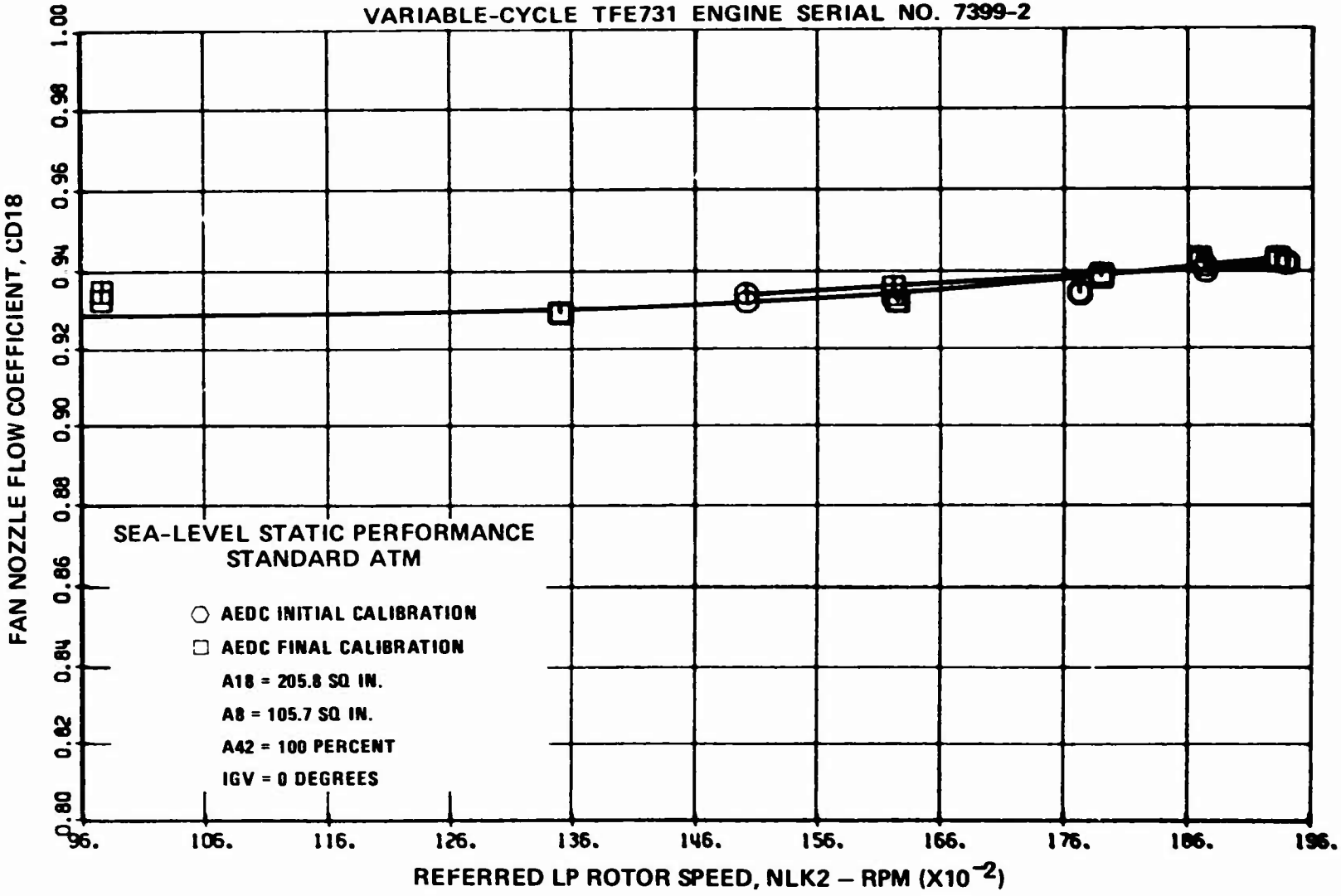

Figure 669. Sea-Level Static, Post-Test Calibration, Fan Nozzle Flow Coefficient Versus Referred LP Rotor Speed.

TABLE 84. COMPARISON OF PRE- AND POST-TEST CALIBRATION RESULTS AT AEDC FOR SEA-LEVEL STATIC, STANDARD ATM AT A NET THRUST OF 3300 LBF.

Facility	Referred SFC [(lbm/hr)/lbf]	Referred Fuel Flow (lbm/hr)	Referred Interturbine Temperature (°R/°F)	Referred LP Rotor Speed (rpm)	Referred HP Rotor Speed (rpm)	Overall Cycle Pressure Ratio	Referred Inlet Airflow (lbm/sec)	Fan Tip Pressure Ratio	Engine Pressure Ratio
AEDC (Pretest)	0.483	1593.9	1905/1445	18950	28950	12.20	110.9	1.471	1.515
AEDC (Post-test)	0.489	1613.7	1928/1468	19000	28750	12.25	111.4	1.475	1.517
Percent Change	+1.2	+1.2	+1.2	+0.3	-0.7	+0.4	+0.4	+0.3	+0.1

A18 = 205.8 sq in.

A8 = 105.7 sq in.

A42 = 100 percent

IGV = 0 degrees

4.4.14 Exhaust-Nozzle Performance Analysis

4.4.14.1 Purpose

A comparison of the measured performance of the TFE731 variable-cycle engine with nominal geometry settings and a fixed-cycle TFE731-2 engine, previously tested at NASA-LeRC, at the TFE731-2 design point of 40,000 feet, Mach 0.8, standard atmosphere is presented in 4.4.3. This comparison indicated lower performance for the variable-cycle engine due to lower thrust coefficients for the variable exhaust nozzles. Refer to 4.4.3 for the technical discussion leading to this conclusion.

The results of the performance analysis of the variable exhaust-nozzle component data accumulated during the AEDC altitude test are presented in the following paragraphs. This analysis is presented to explain the cause of the lower variable exhaust-nozzle system performance, as well as to define possible changes in design to improve the variable-nozzle performance.

4.4.14.2 Design Approach

The variable-area exhaust-nozzle system, described in 4.1.2, was designed for the AiResearch TFE731 variable-cycle turbofan engine to provide independent and continuously variable fan and primary exhaust-nozzle areas.

4.4.14.3 Predicted Exhaust-Nozzle Performance Characteristics

Since no test data was available for this variable exhaust-nozzle configuration, estimates were made for use in the variable-cycle engine analytical model. The general approach used in making these estimates was as follows.

The static performance of the variable-geometry exhaust nozzles was predicted with the use of existing nozzle data correlations, with the assumption that there are no interactions between the primary and the fan exhaust-nozzle flows. The throat thrust for both nozzles is not significantly influenced by the local environment. Hence, only the primary plug thrust and the fan plug thrust are sensitive to changes in the local flow field. The primary nozzle plug thrust is altered in the lower pressure ratio ranges, where its contribution to overall thrust is small. Hence, it was assumed that the primary nozzle performance is unchanged due to the presence of the bypass flow.

The predicted performance for the isolated primary nozzle is presented in Figure 670. The primary nozzle thrust coefficient is defined as:

$$CFG8 = \frac{FG8}{FG8I}$$

where: FG8 = actual primary exhaust nozzle gross thrust, lbf
FG8I = ideal primary exhaust nozzle gross thrust, lbf

This equation may be expanded into the following form, which is more useful for exhaust nozzle performance prediction and analysis:

$$CFG8 = \frac{CS8 \left[\frac{WG8}{g} V8E + (PS8E)\ A8E\right] - (PSO)\ A8E}{\frac{WG8}{g} V8ISEN}$$

where: CFG8 = primary exhaust-nozzle thrust coefficient, dimensionless

CS8 = primary nozzle vacuum thrust coefficient, dimensionless

WG8 = primary exhaust-nozzle flow rate, lbm/sec

g = gravitational constant, lbm-ft/lbf-sec^2

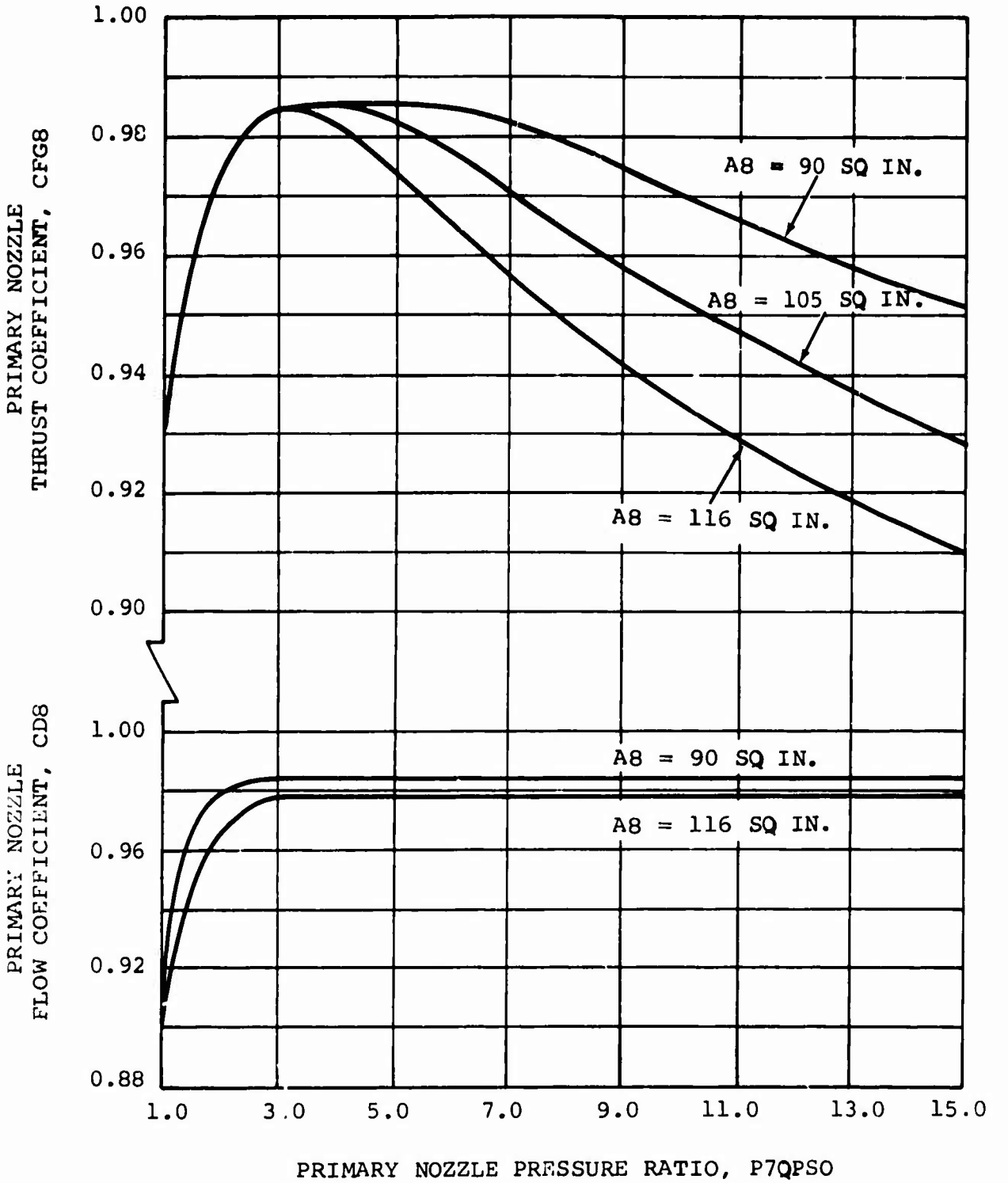

Figure 670. Predicted Performance for Variable Primary Exhaust Nozzle.

V8E = primary stream velocity at nozzle (plug) exit, ft/sec

PS8E = static pressure at nozzle (plug) exit, psia

A8E = projected flow area at nozzle (plug) exit, square inch

PSO = ambient pressure, psia

V8ISEN = isentropic velocity for full expansion of primary stream to ambient pressure, ft/sec

The primary nozzle vacuum thrust coefficient, CS8, which is defined as the ratio of actual-to-ideal momentum plus PA forces, is a function of the throat Reynolds number, the equivalent hydraulic diameter, the plug angle, θ, the design Prandtl-Meyer angle, and the plug truncation ratio. Refer to Figure 671 for clarification of nozzle plug angle, truncation ratio, and location of exit Station E for a typical truncated plug nozzle.

The predicted performance for the fan exhaust nozzle is presented in Figure 672. The fan nozzle thrust coefficient is defined as:

$$CFG18 = \frac{FG18}{FG18I}$$

where: FG18 = actual fan exhaust nozzle gross thrust, lbf
FG18I = ideal fan exhaust nozzle gross thrust, lbf

The following expanded form of this equation is a more convenient expression for exhaust-nozzle performance analysis:

$$CFG18 = \frac{CS18\left[\frac{(WA18)}{g}\,V18T + (PS18T)\,A18T\right] + \int_{18T}^{18E}(PS)\,dAs - (PSO)\,A18E}{\frac{(WA18)\,V18ISEN}{g}}$$

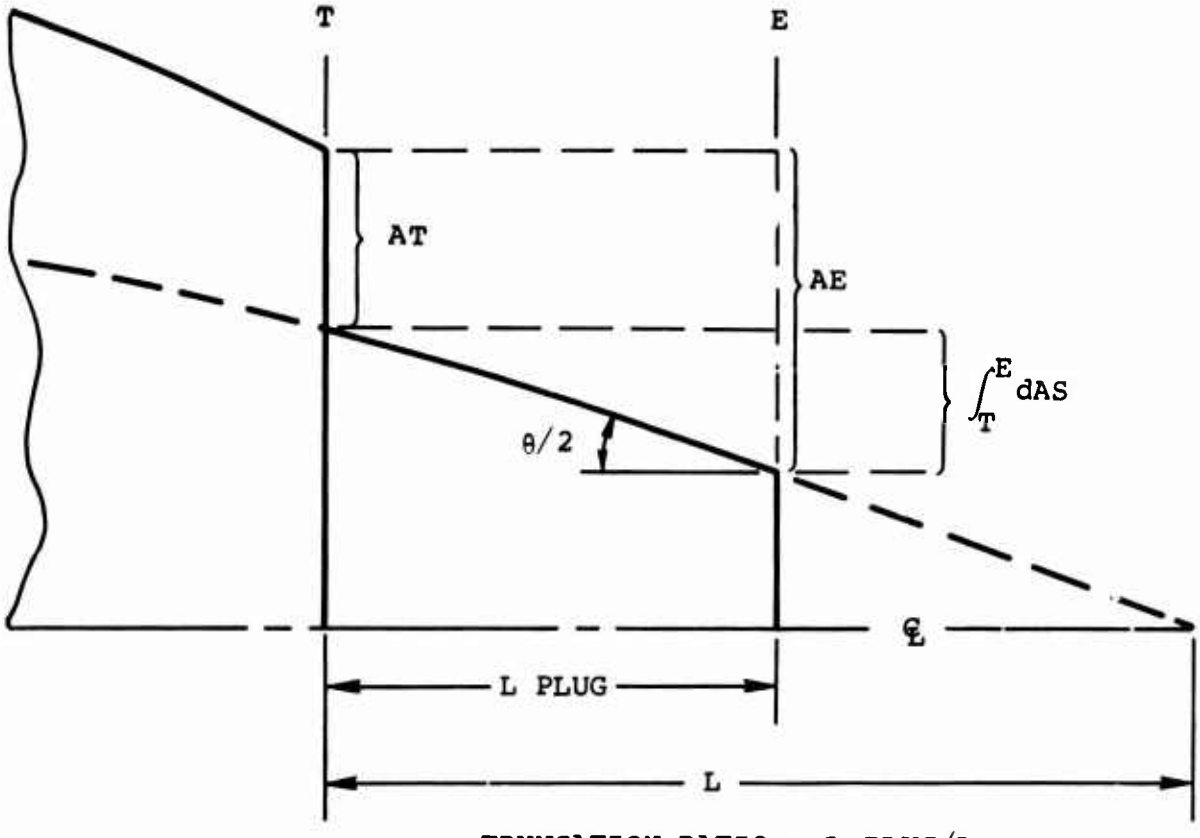

Figure 671. Identification of Typical Plug Nozzle Parameters.

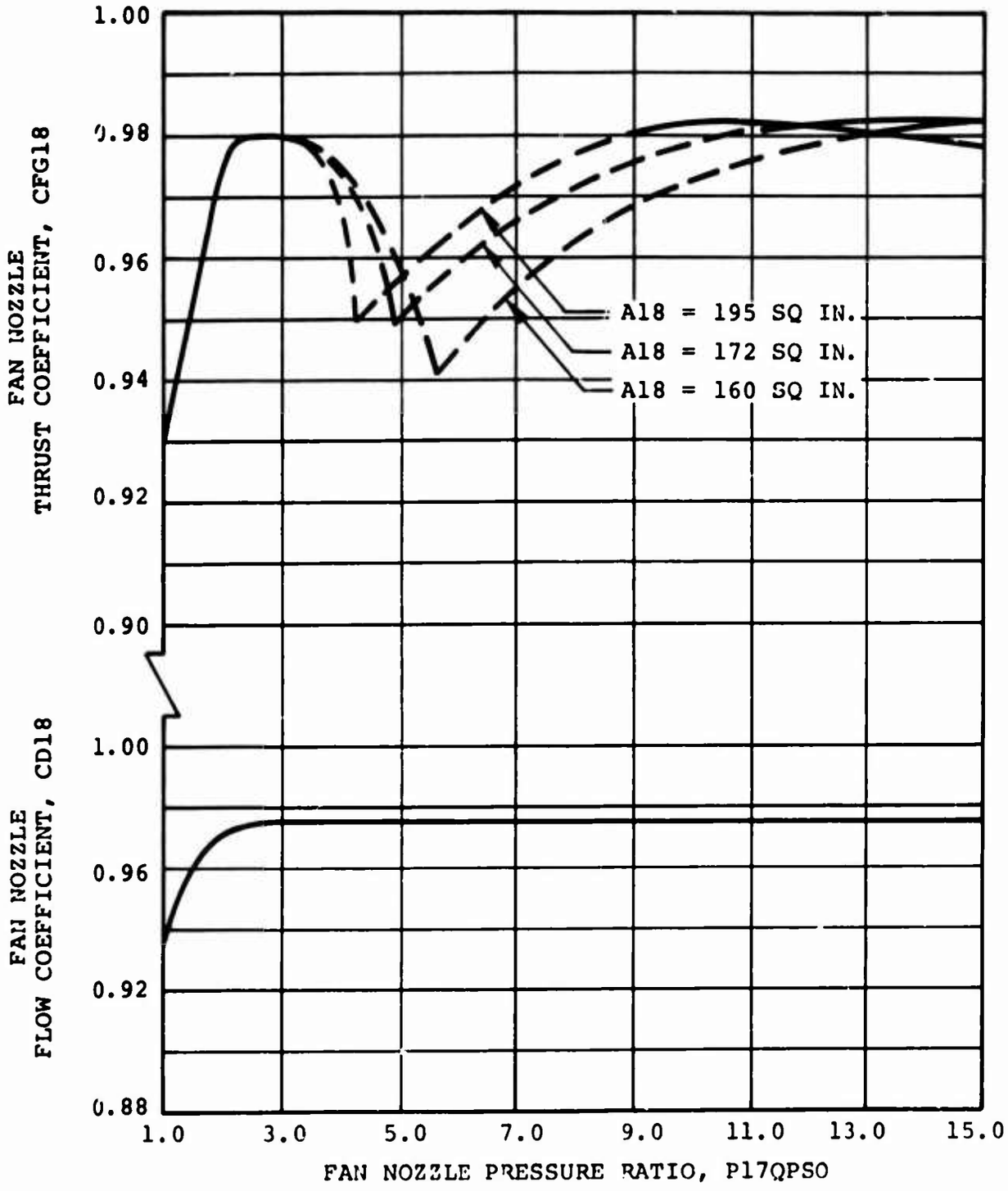

Figure 672. Predicted Performance for Fan Exhaust Nozzle.

where: CFG18 = fan nozzle thrust coefficient, dimensionless

CS18 = fan nozzle vacuum thrust coefficient, dimensionless

WA18 = fan nozzle flow rate, lbm/sec

V18T = fan nozzle flow velocity at nozzle throat, ft/sec

PS18T = static pressure at fan nozzle throat, psia

A18T = fan nozzle throat flow area, square inches

A18E = projected flow area at fan plug exit, square inches

V18ISEN = isentropic velocity for full expansion of fan nozzle stream to ambient pressure

dAs = differential change in fan plug projected surface area, square inches

The fan nozzle thrust can be partitioned into two convenient coefficients. The first of these is the fan nozzle throat thrust coefficient, which is defined as:

$$CFGT18 = \frac{CS18\left[\frac{WA18}{g}\,V18T + (PS18T)(A18T)\right] - (PSO)\,A18T}{\frac{(WA18)\,V18ISEN}{g}}$$

The second coefficient is the fan plug thrust coefficient, defined as:

$$CFPLUG = \frac{\int_{18T}^{18E} (PS - PSO)\,dAs}{\frac{(WA18)\,V18ISEN}{g}}$$

This partitioning is particularly convenient when considering interaction between the primary and the fan nozzle flow streams. CFGT18 is unaffected by the interaction; hence, CFPLUG can be determined for each data point and compared with the predicted values to pinpoint the deficiency in nozzle performance. The predicted throat and plug thrust coefficients are presented in Figure 673.

4.4.14.4 Comparison of Predicted and Measured Fan Plug Thrust Coefficients

The fan plug static pressures were measured for each data point throughout the AEDC program. Selected data points were used to compare the predicted plug thrust coefficients with the integrated values. The static pressure distribution for each selected point, shown in Figures 674 through 677, was numerically integrated with use of a second-order piecewise-curve-fit routine and then divided by the fan nozzle ideal thrust to generate the measured fan plug thrust coefficients. Comparison of these coefficients to the predicted values, presented in Figure 678, shows that the measured fan plug thrust is significantly below the predicted values.

The lower plug thrust is attributed to two effects. First, the fan plug has a gradually increasing included angle, which causes the fan flow to expand more on the plug outside surface than it would for a constant angle conical plug. This moves the recompression and/or shock system downstream and lowers the resultant integral pressure-area force. Secondly, the presence of a high-velocity core jet lowers the pressure downstream of the recompression system, which weakens it and moves it still farther aft. This problem could be alleviated by recontouring the plug and scheduling the throat angle as illustrated in Figure 679. Such a system should have improved performance throughout the entire operating range of the AEDC program.

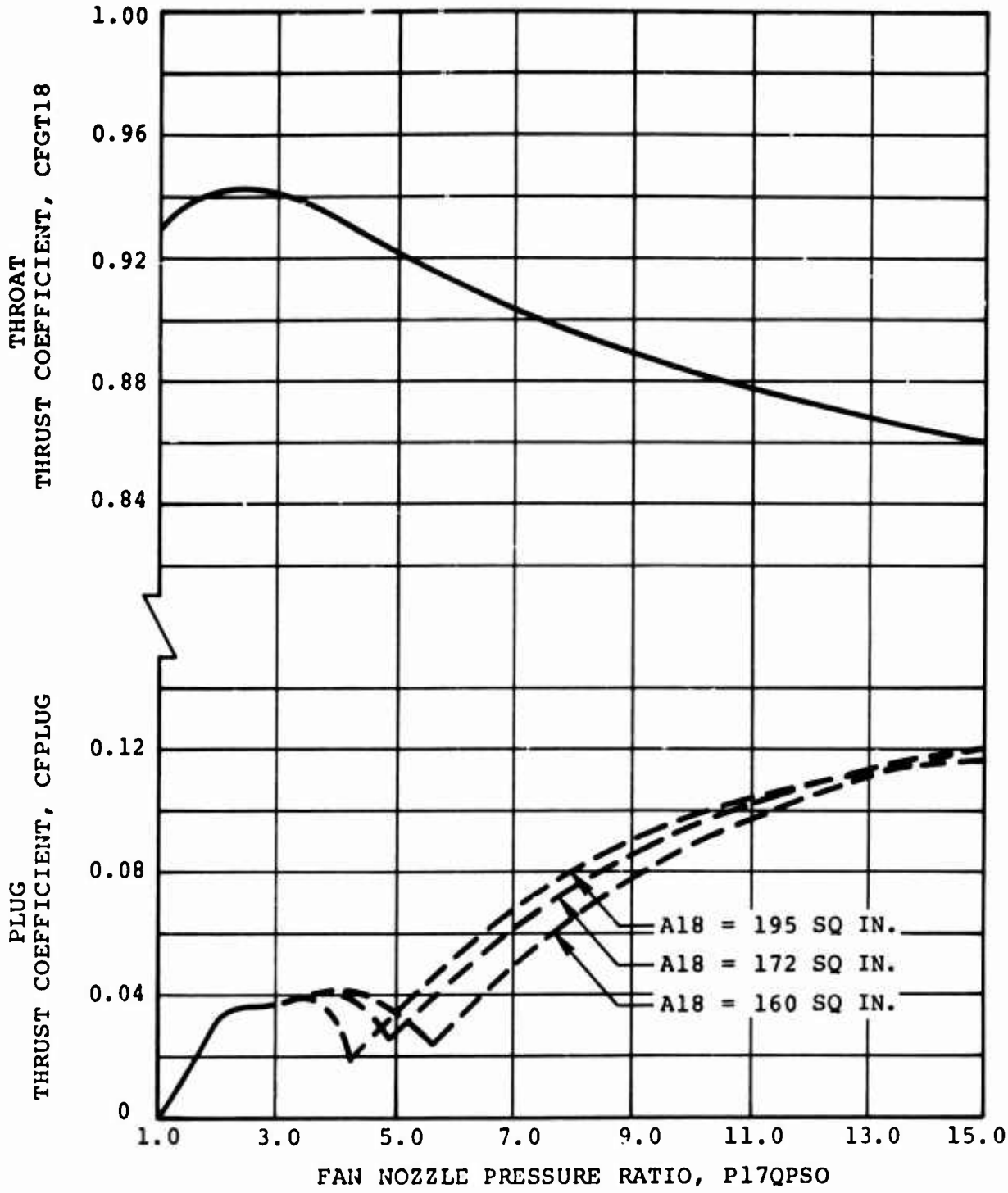

Figure 673. Predicted Performance for Variable Fan Exhaust Nozzle.

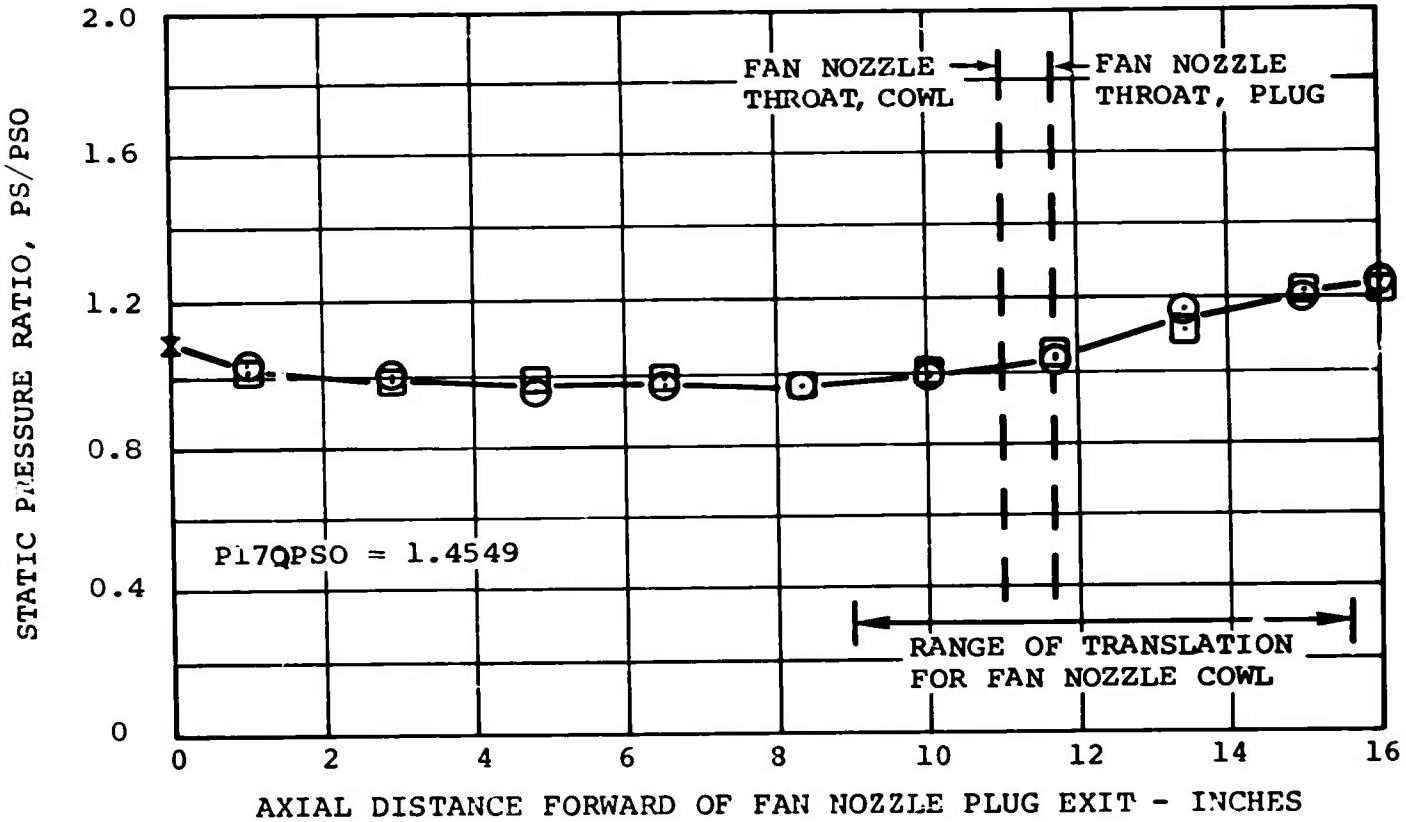

Figure 674. Measured Fan Nozzle Plug Static Pressure Distribution.

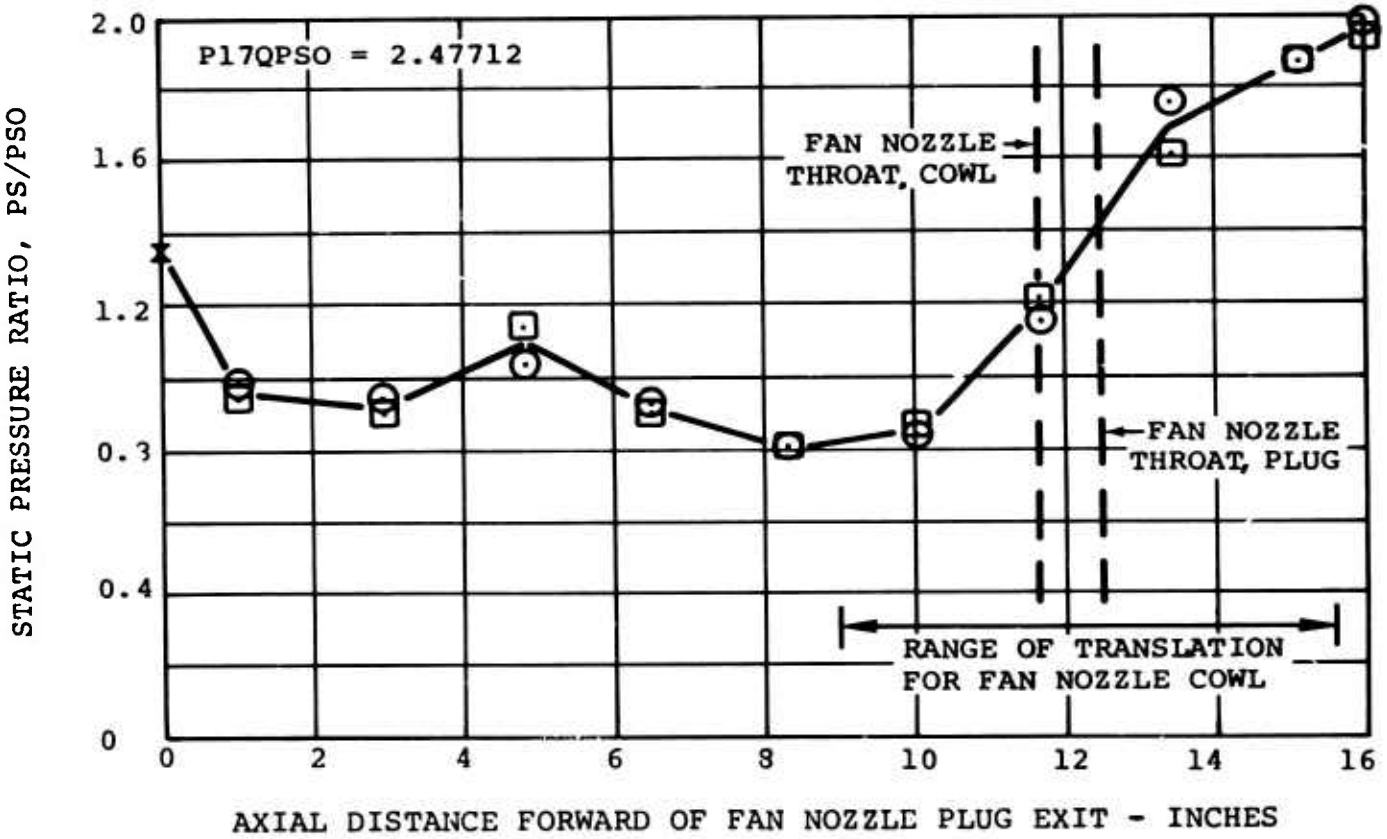

Figure 675. Measured Fan Nozzle Plug Static Pressure Distribution.

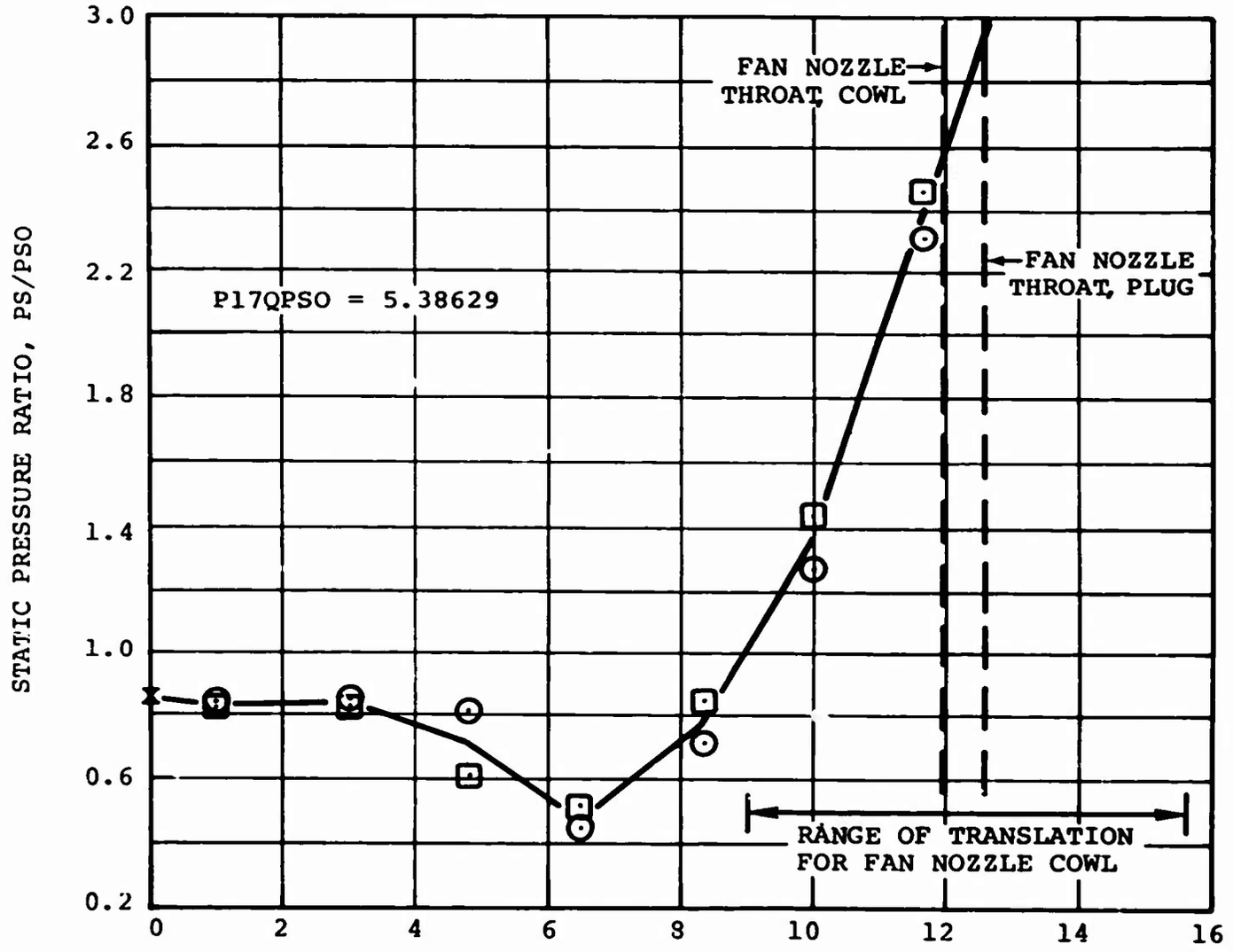

Figure 676. Measured Fan Plug Static Pressure Distribution.

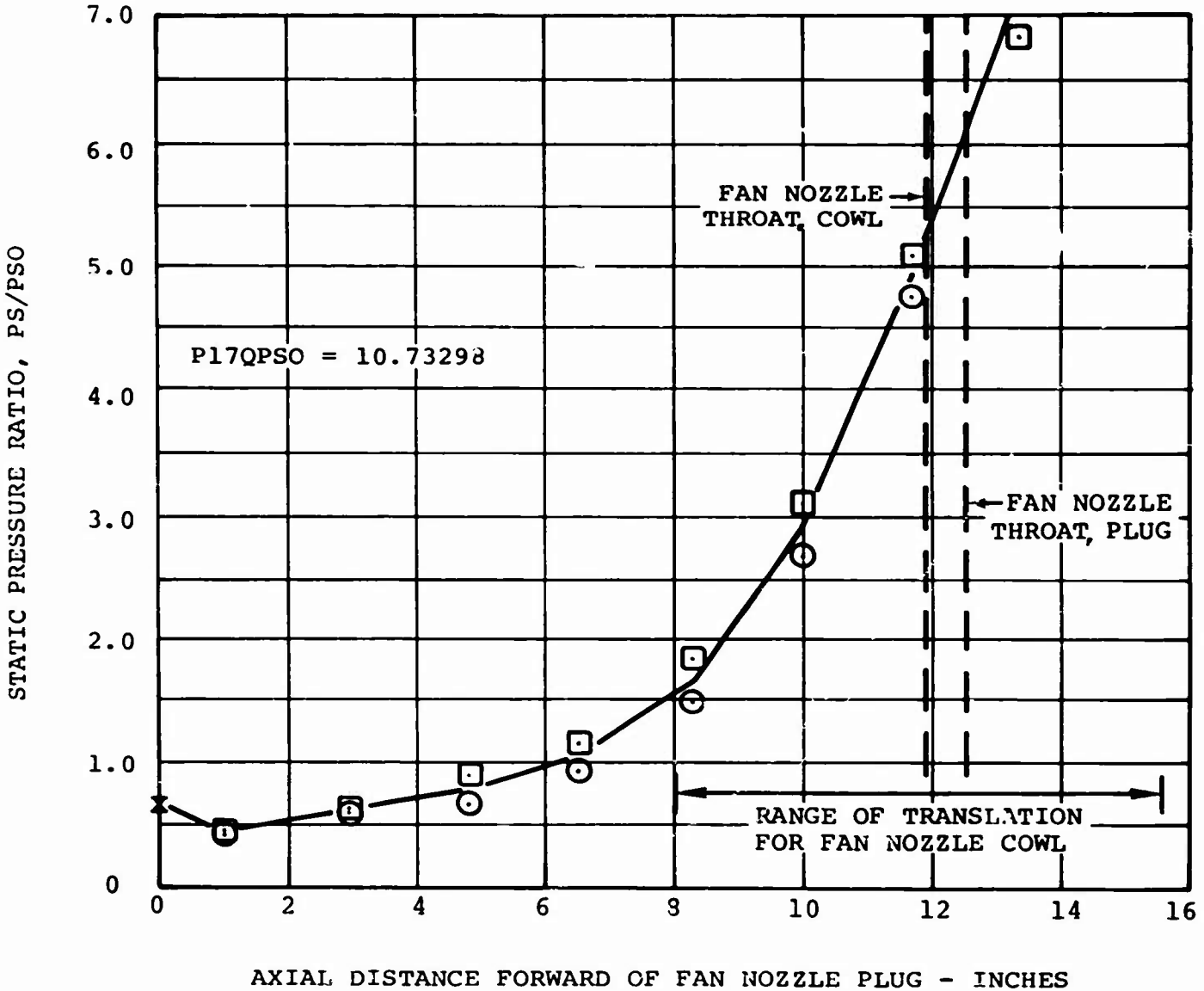

Figure 677. Measured Fan Plug Static Pressure Distribution.

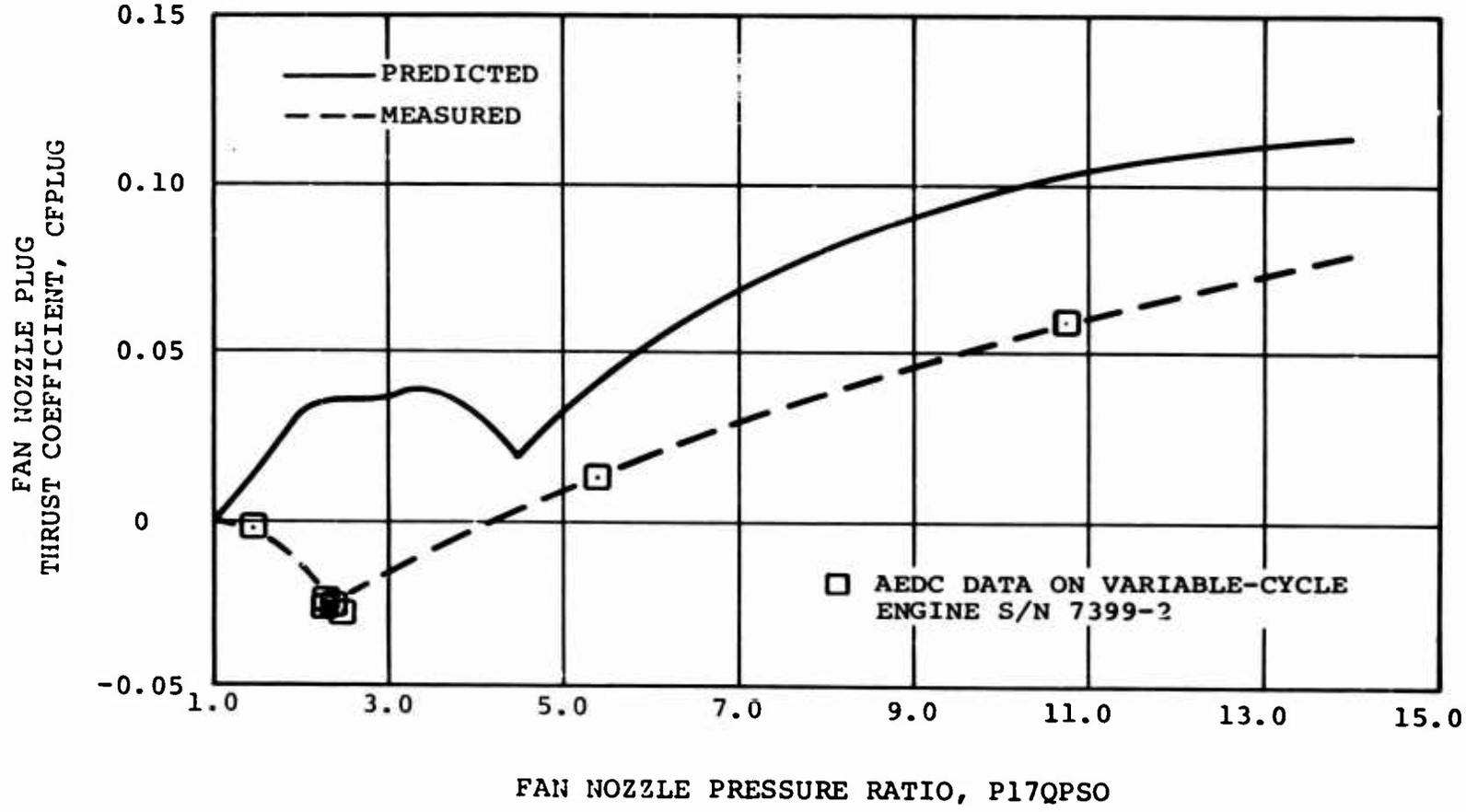

Figure 678. Comparison of Predicted and Measured Fan Nozzle Plug Thrust.

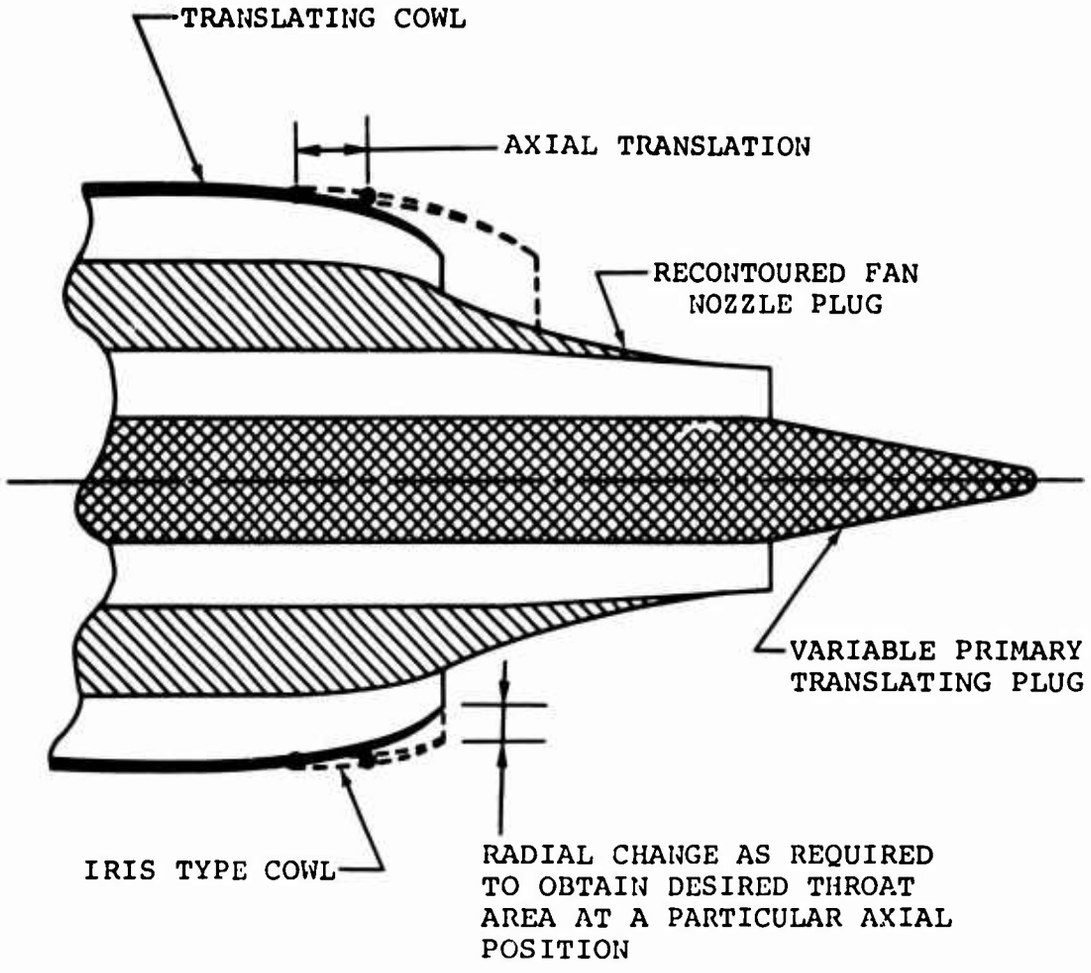

Figure 679. Nozzle Configuration for Improving Variable-Fan Nozzle Performance.

4.4.14.5 Comparison of Combined Variable-Nozzle Thrust Coefficients with NASA-LeRC Data on Fixed Reference Nozzles

A comparison of the variable-nozzle system used in the AEDC testing of TFE731 Variable-Cycle Engine Serial No. 7399-2 and the reference fixed-nozzle system used in the NASA-LeRC testing of TFE731-2 Engine Serial No. 7306-2 previously presented in 4.4.3 is repeated in Figure 680 for convenience to the reader. A comparison of the combined exhaust-nozzle thrust coefficients of the two nozzle systems at 40,000 feet, Mach 0.8, standard atmosphere, also presented in 4.4.3, is repeated in Figure 681. The combined nozzle thrust coefficient, CFGISEN, is defined as:

$$CFGISEN = \frac{FG}{\frac{WG8}{g}\,V8ISEN + \frac{WG18}{g}\,V18ISEN}$$

where FG = total measured gross thrust, lbf. Other terms have been defined in Paragraph 4.4.14.3.

The data presented in Figure 681 indicates that the combined nozzle thrust coefficients of the variable nozzles were approximately 2 percent lower than those of the fixed reference nozzles. This accounts for approximately 4 percent lower net thrust of the variable-cycle engine at the fixed-cycle engine aerodynamic design condition because the gross-to-net thrust ratio is approximately 2:1 at this condition. Figure 681 includes, in addition, variable-nozzle data points corrected for the lower fan nozzle plug performance. These adjusted combined thrust coefficients indicate that, if the fan nozzle plug performance were improved by the change in design of the fan nozzle as illustrated in Figure 679, the performance of the variable nozzles would be equal to that of the reference fixed nozzles used in the NASA-LeRC testing.

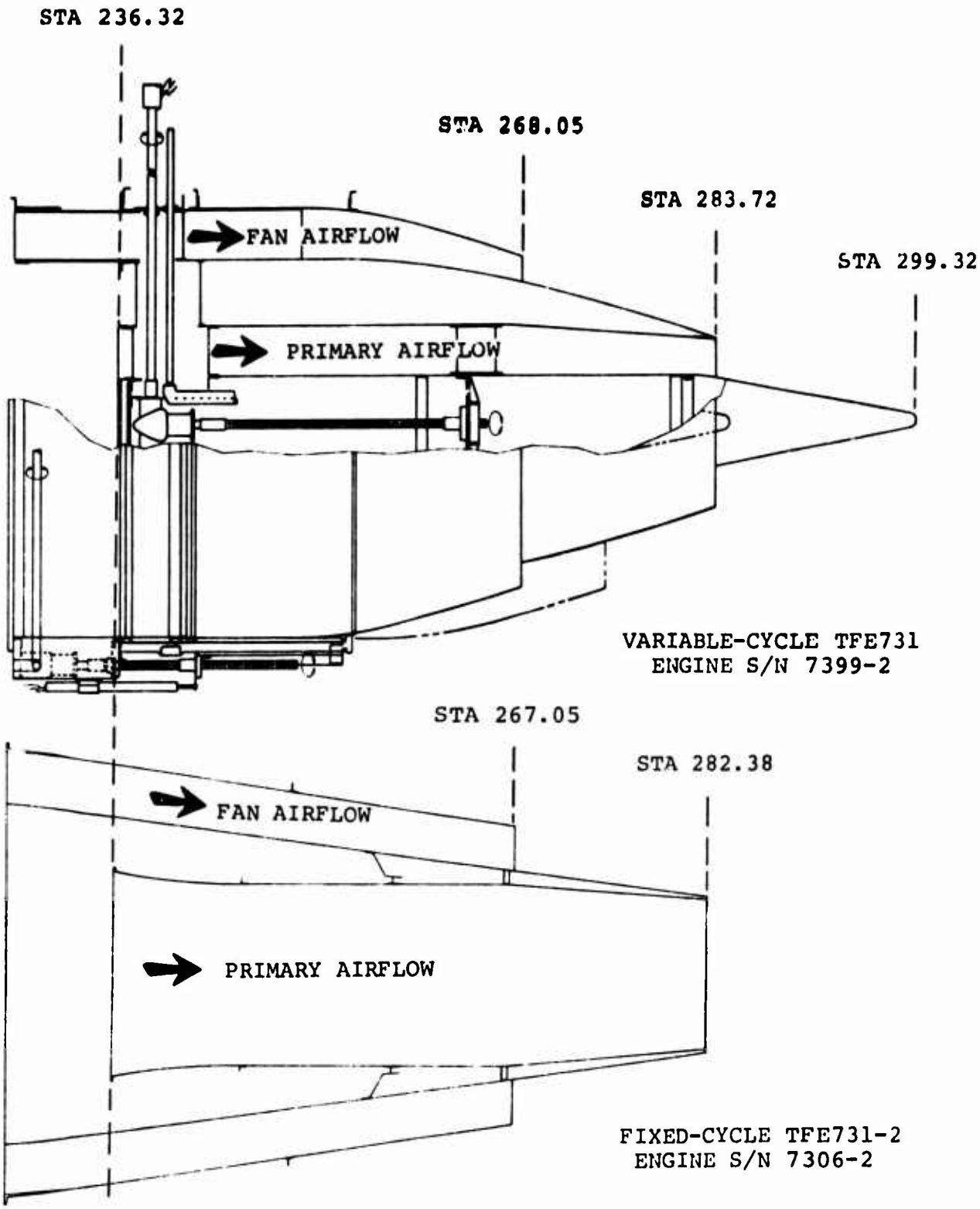

Figure 680. Comparison of Exhaust Nozzle Systems of Variable- and Fixed-Cycle Engines.

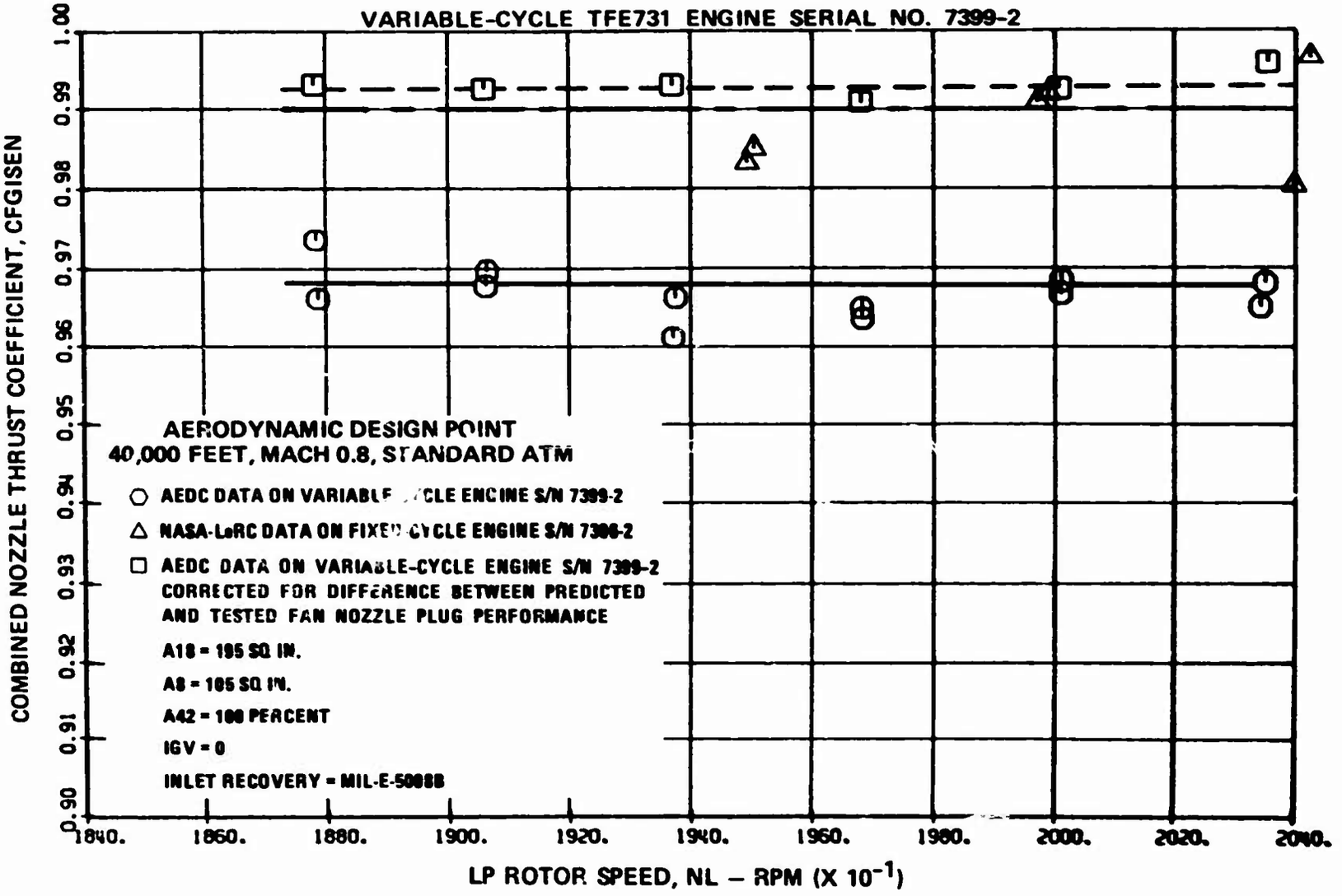

Figure 681. Fixed-and Variable-Nozzle Comparison at Aerodynamic Design Point, Combined Nozzle Thrust Coefficient Versus LP Rotor Speed.

4.4.14.6 Overall Variable-Area Exhaust-Nozzle Data Correlation

Exhaust-nozzle component performance in terms of combined nozzle thrust coefficients, CFGISEN, primary exhaust-nozzle flow coefficients, CD8, and fan nozzle flow coefficients, CD18, are presented for individual test conditions throughout Section 4.4 of this report as an aid in analyzing the overall engine performance test results. For purposes of record, the nozzle data from this test for the particular exhaust-nozzle area combination where a significant amount of data was accumulated is presented versus exhaust-nozzle pressure ratios in Figures 682 through 685. A median line has been drawn through the data on these figures and a ±1 percent tolerance band has been shown for reference. The parameters presented in these curves are listed in Table 85.

TABLE 85. EXHAUST-NOZZLE PERFORMANCE

Figure No.	Parameters Presented
682	Primary Nozzle Flow Coefficient Versus Primary Nozzle Pressure Ratio
683	Combined Nozzle Thrust Coefficient Versus Primary Nozzle Pressure Ratio
684	Fan Nozzle Flow Coefficient Versus Fan Nozzle Pressure Ratio
685	Combined Nozzle Thrust Coefficient Versus Fan Nozzle Pressure Ratio

The data presented in these figures fall within an acceptable tolerance band, and, except for fan nozzle flow coefficients exhibit expected trends. The fan nozzle flow coefficient correlation (see Figure 684) shows two trends that were not expected. These anomalies are: (a) flow coefficients are not constant above the choking pressure ratio of approximately 2:1 as would be expected, and (b) the flow coefficients become greater than 1.0. Possible causes for these trends are thermal and pressure growth of the nozzle material and leakage through the sliding seal on the outer fan duct. Both of these effects tend to increase the effective nozzle flow area. Therefore, in addition to the design changes discussed in 4.4.14.4, the nozzle performance would probably be enhanced by an improved fan outer duct seal.

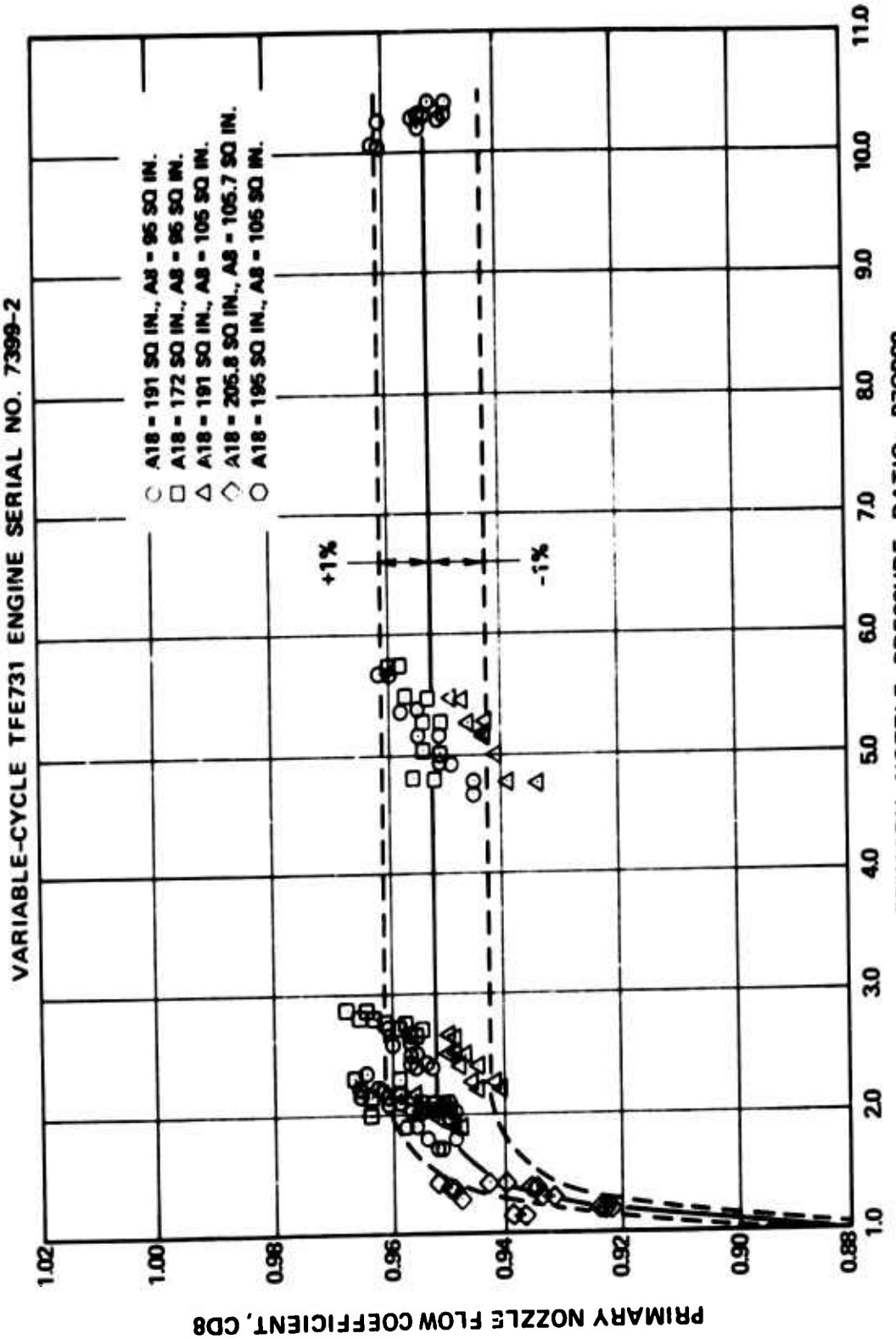

Figure 682. Tested Variable Exhaust Nozzle Performance, Primary Nozzle Flow Coefficient Versus Primary Nozzle Pressure Ratio.

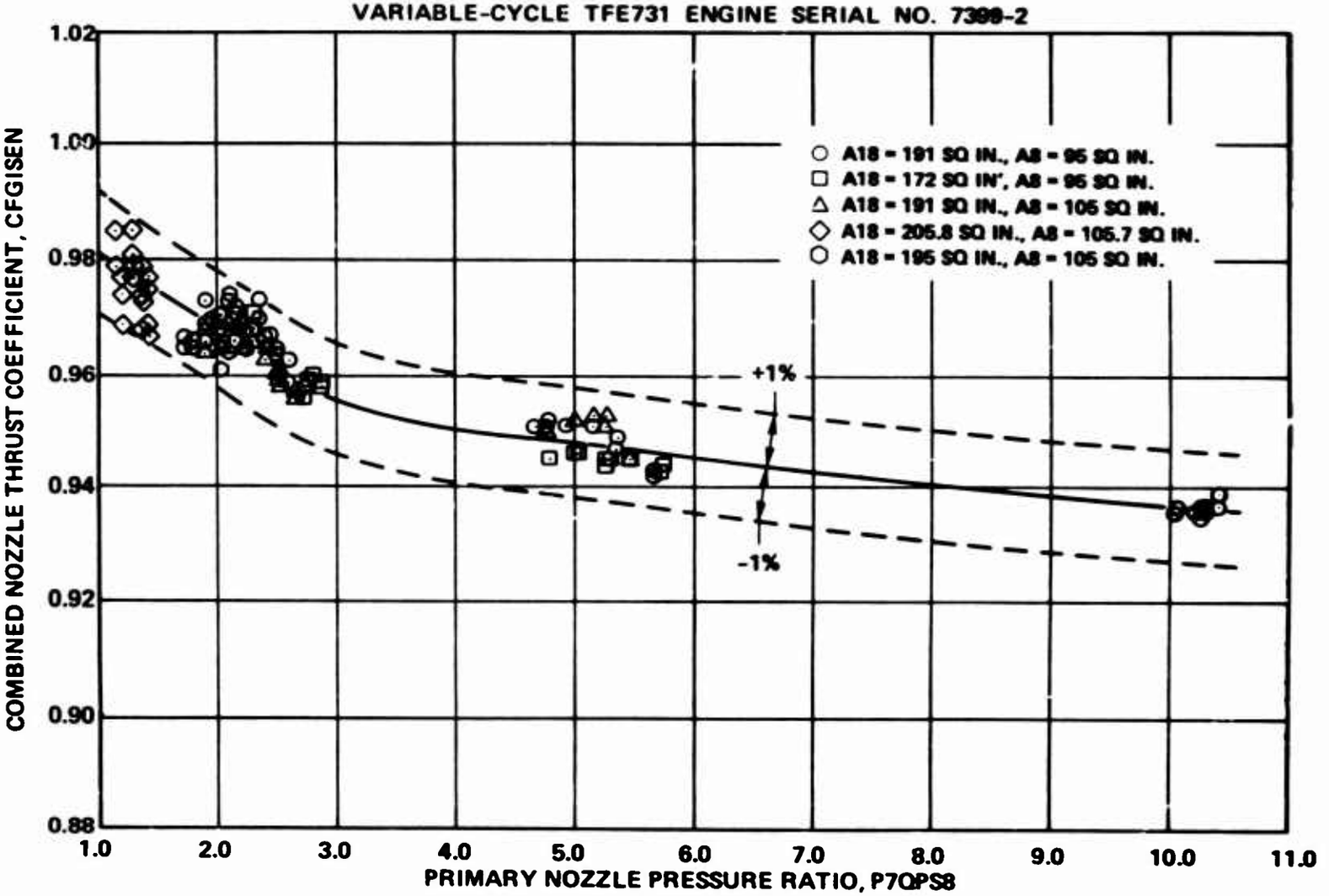

Figure 683. Tested Variable Exhaust Nozzle Performance, Combined Nozzle Thrust Coefficient Versus Primary Nozzle Pressure Ratio.

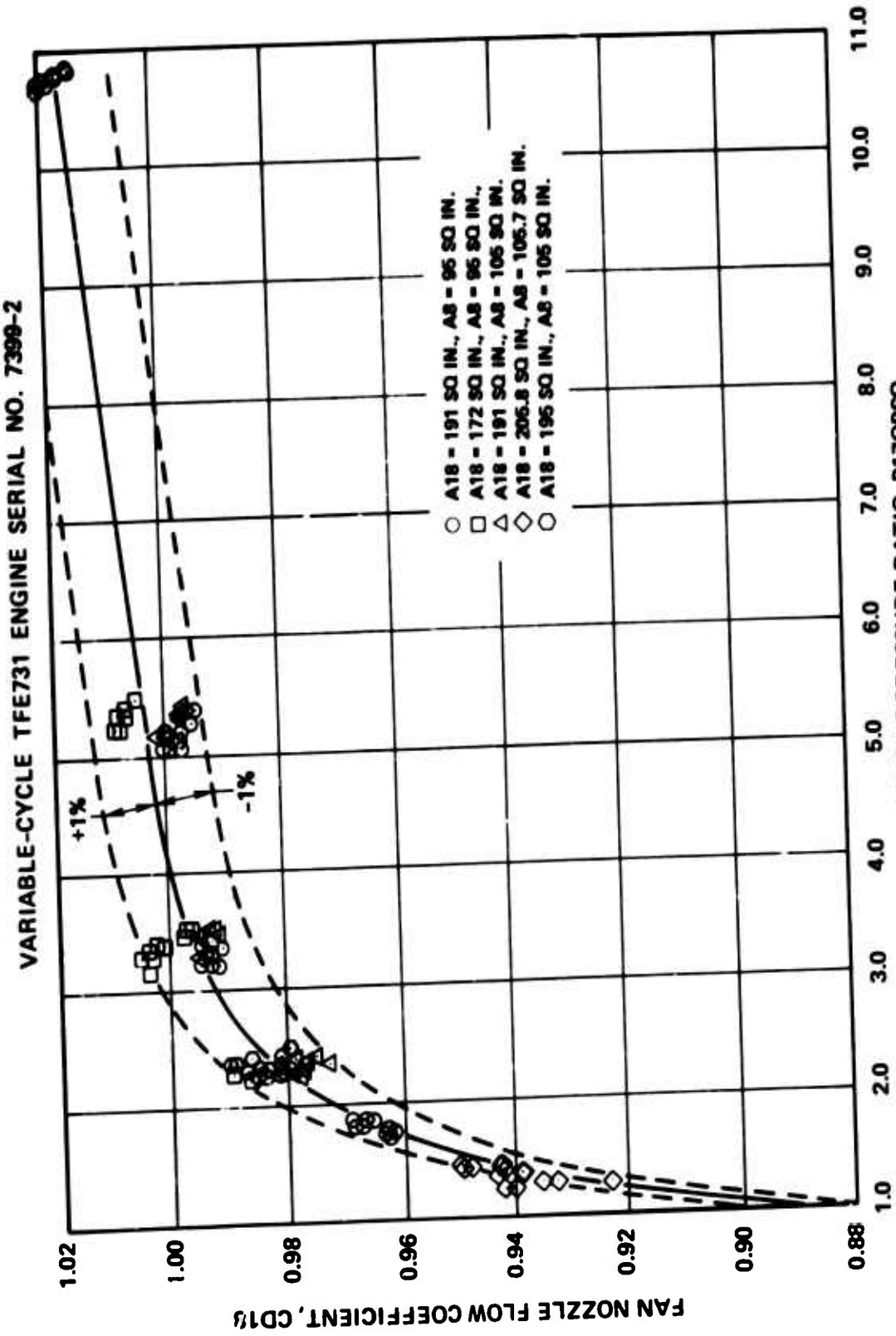

Figure 684. Tested Variable Exhaust Nozzle Performance, Fan Nozzle Flow Coefficient Versus Primary Nozzle Pressure Ratio.

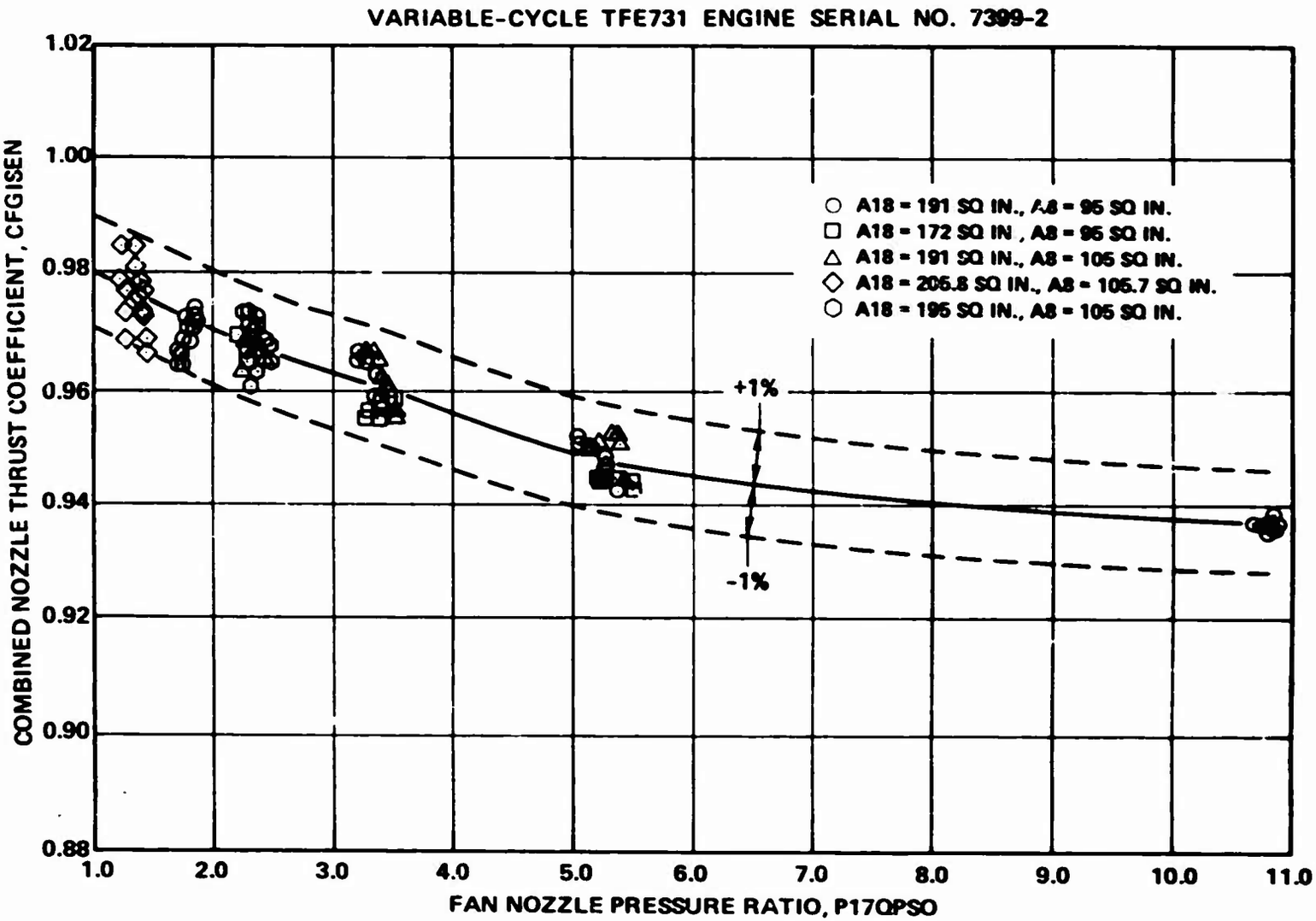

Figure 685. Tested Variable Exhaust Nozzle Performance, Combined Nozzle Thrust Coefficient Versus Fan Nozzle Pressure Ratio.

4.4.15 Variable-Cycle Engine Analytical Model

Early in the AEDC testing it was recognized that, although the February 1974 Variable-Cycle TFE731 Engine Analytical Model gave reasonable predictions of engine performance at sea-level static conditions, its predictions were generally optimistic at altitude conditons. In fact, its predictions at 40,000 feet, Mach 0.8, standard atmosphere were approximately 3 percent better on specific fuel consumption at a given net thrust than the values demonstrated on a fixed-geometry engine in a previous test at NASA-LeRC. Relative to the variable-cycle engine data at 40,000 feet, Mach 0.8, the analytical model was approximately 7 percent optimistic on specific fuel consumption. Similar discrepancies were found at other flight conditons--for example, in the exhaust-nozzle rematching tests at 50,000 feet.

The component maps requiring revision to correct the above performance predictions were, primarily, the exhaust-nozzle thrust coefficients, and the fan map performance characteristics, especially at high referred speeds. The fan map changes were necessary to bring the analytical model more in line with the performance levels previously demonstrated at NASA-LeRC. The exhaust-nozzle thrust coefficient changes were necessary to account for the difference (approximately 4 percent) in specific fuel consumption between the NASA-LeRC and AEDC test data.

A second problem with the original model was that it calculated an incorrect trend of performance parameters as a function of the LP turbine nozzle area as discussed in 4.4.5. It had been analytically predicted that the LP turbine efficiency would decrease as the LP turbine nozzle area was varied in either the open or the closed direction from the nominal value and the LP turbine maps in the model reflected this predicted trend. The test data, however, indicates that LP turbine efficiency did not fall off as predicted when the turbine area was

increased from the nominal value. The data also indicated a more rapid decrease than predicted in LP turbine efficiency as the turbine nozzle area was reduced below the nominal value. A comparison of the LP turbine efficiency trend predicted by the February 1974 model with the tested trend is presented in Figure 686.

A third problem was encountered with the February 1974 model--namely, it did not correctly predict the magnitude of an observed decrease of HP rotor speed for altitudes above 50,000 feet or the decrease in LP compressor surge margin at high altitudes. The data indicated that at altitudes above 50,000 feet, the Reynolds number corrections required revision to correctly reflect the tested trends.

Other changes necessary included adjustment of the component maps to agree with the results of the flow-path measurements. For example, LP compressor maps for IGV angles of zero and 30 degrees were tabulated in the February 1974 analytical model. For other IGV angles, the program interpolated between or extrapolated beyond these maps. Test data indicated that these interpolations and extrapolations were not adequate. Maps for IGV angles of 15 and minus 10 degrees should be added to the program. The burner map needed to be revised to reflect tested burner efficiencies, and the relationship of measured inter-turbine temperature to the thermodynamic average value needed to be correlated and inserted into the program. These are some examples of revisions required for the analytical model and do not represent a complete list.

Some revisions to the February 1974 analytical model have been made to reflect the above analysis. These changes are preliminary and have been accomplished within the limitations of the schedule for the final report. Further refinements are needed to make the model better fit the data under all conditions. However, this model, identified as the August 1974

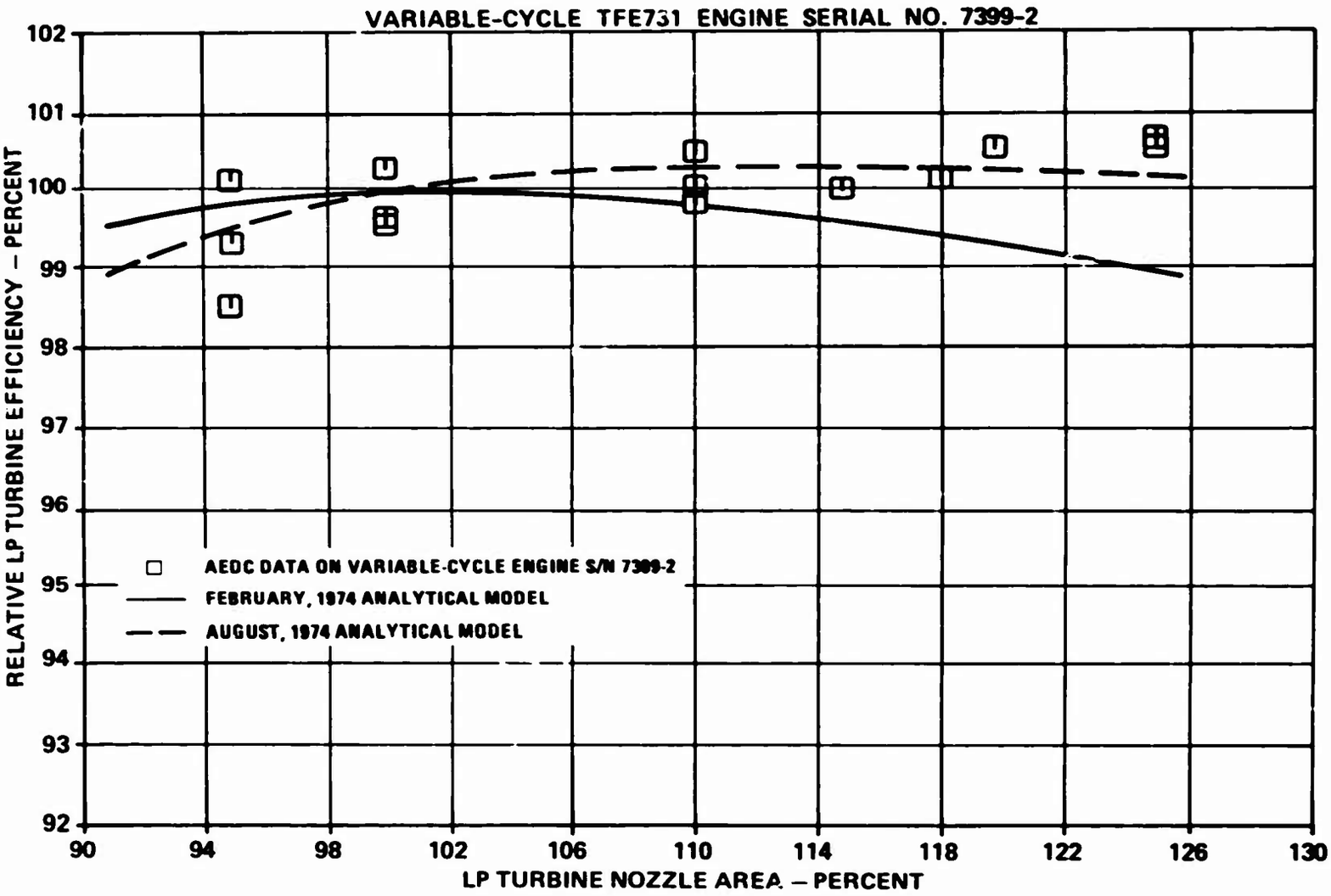

Figure 686. LP Turbine Efficiency Comparison.

model, appears to fit the test results better under most conditions than the February 1974 model. A comparison of various performance parameters predicted by both analytical models with corresponding tested values for the 40,000-foot, Mach 0.8 design point is presented in Figures 687 through 698. The parameters presented in these figures are listed in Table 86. A comparison of the February 1974 and August 1974 model predicted thrust and SFC with the tested values for other flight conditions at one LP rotor speed is presented in Table 87.

TABLE 86. ANALYTICAL MODEL COMPARISONS, AERODYNAMIC DESIGN POINT, 40,000 FEET, MACH 0.8, STANDARD ATM.

Figure No.	Parameter Presented
687	Thrust specific fuel consumption versus net thrust
688	Interturbine temperature versus net thrust
689	Net thrust versus LP rotor speed
690	Fuel flow versus LP rotor speed
691	Interturbine temperature versus LP rotor speed
692	HP rotor speed versus LP rotor speed
693	Cycle pressure ratio versus LP rotor speed
694	Engine total airflow versus LP rotor speed
695	Fan tip pressure ratio versus LP rotor speed
696	Engine pressure ratio versus LP rotor speed
697	Fan hub pressure ratio versus LP rotor speed
698	Bypass ratio versus LP rotor speed

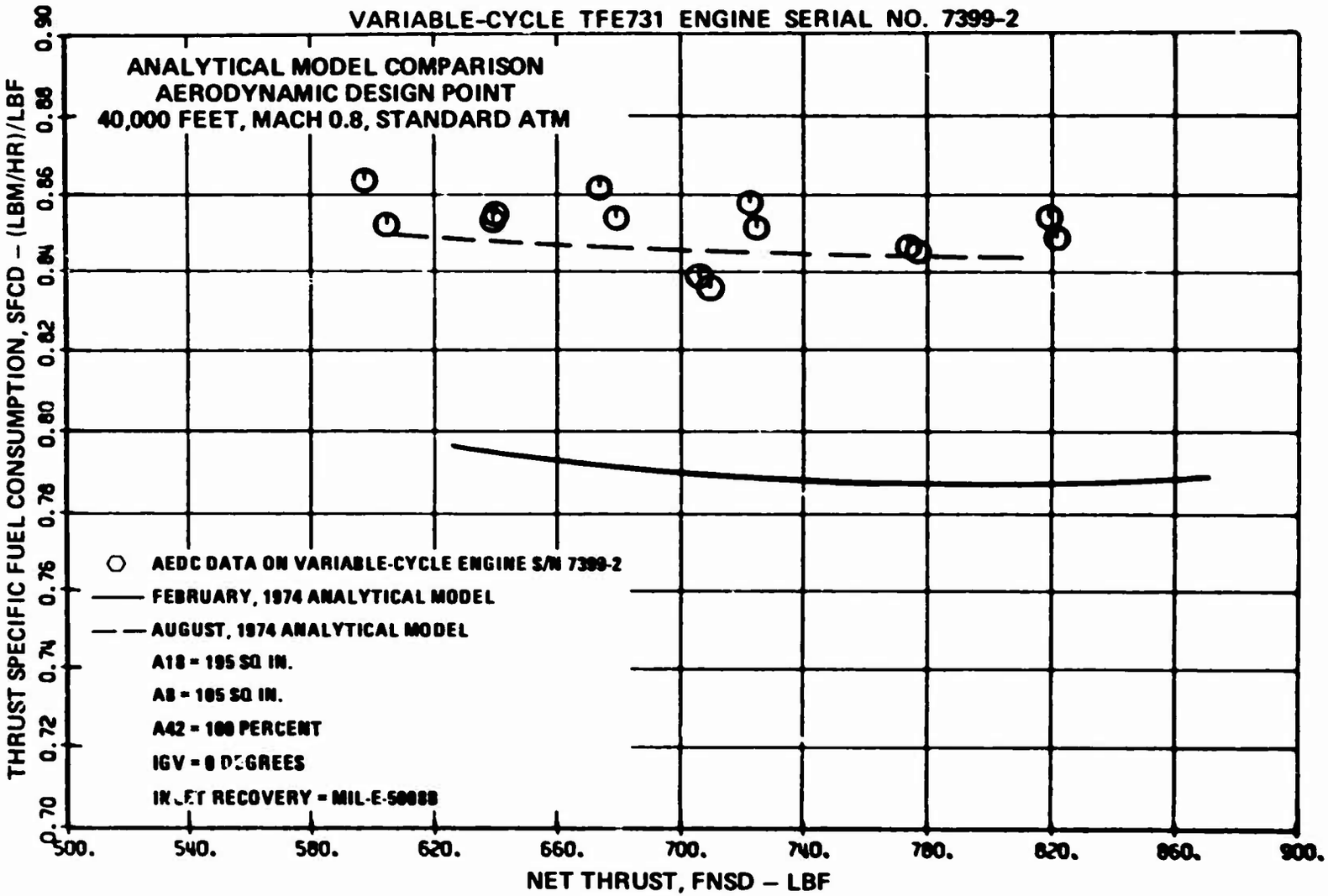

Figure 687. Comparison of Predicted and Tested Performance at Mach 0.8, 40,000 Feet, Thrust Specific Fuel Consumption Versus Net Thrust.

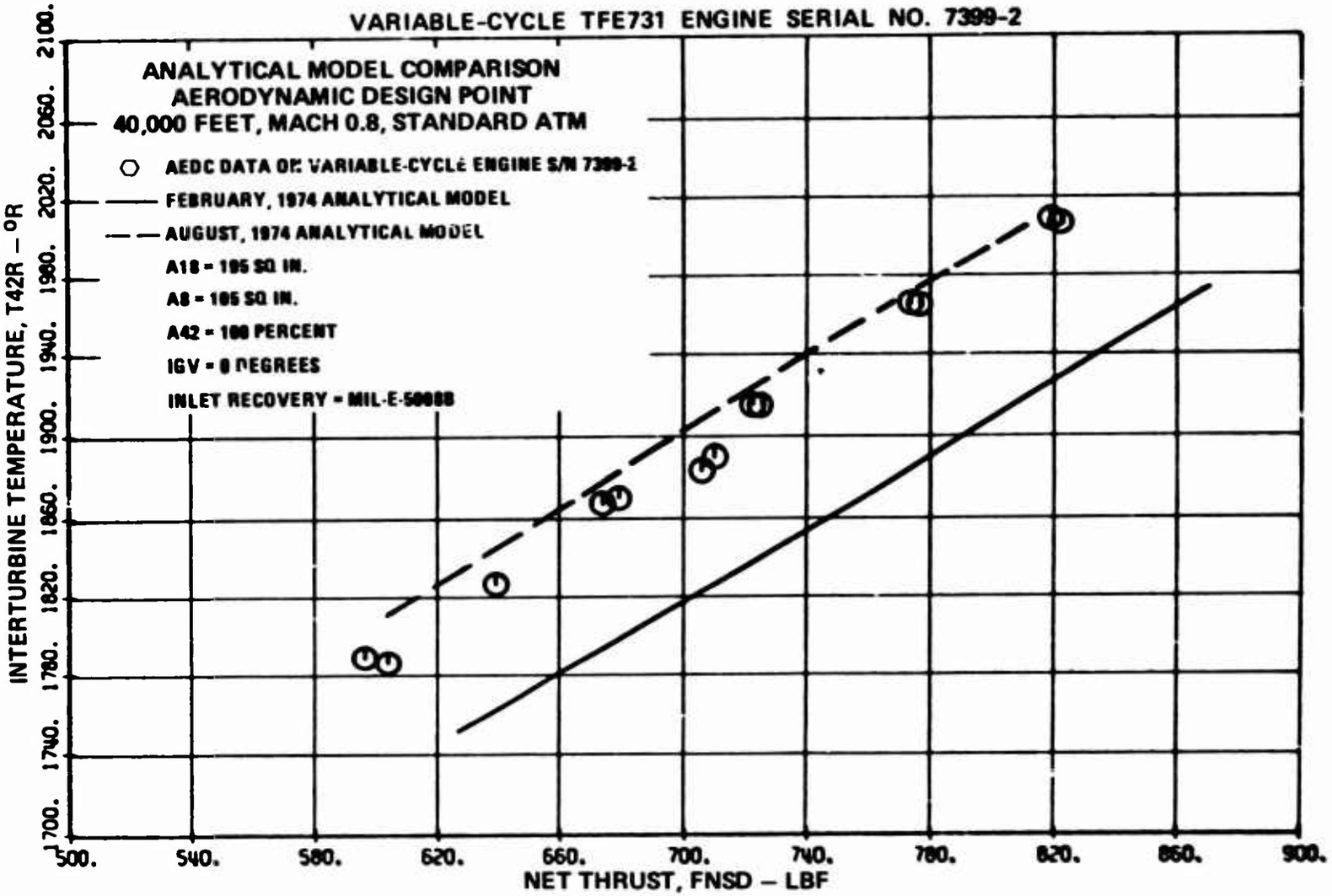

Figure 688. Comparison of Predicted and Tested Performance at Mach 0.8, 40,000 Feet, Interturbine Temperature Versus Net Thrust.

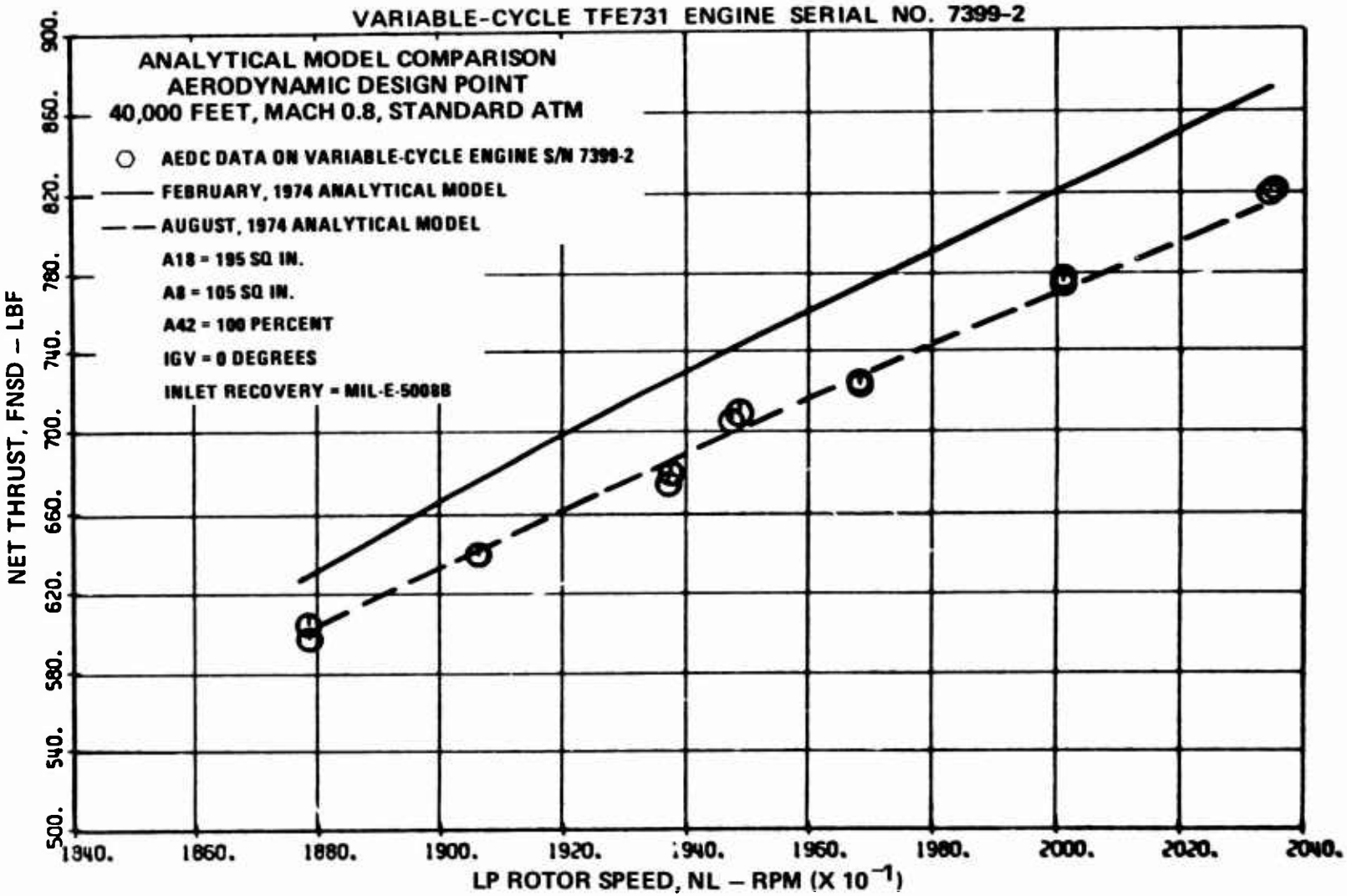

Figure 689. Comparison of Predicted and Tested Performance at Mach 0.8, 40,000 Feet, Net Thrust Versus LP Rotor Speed.

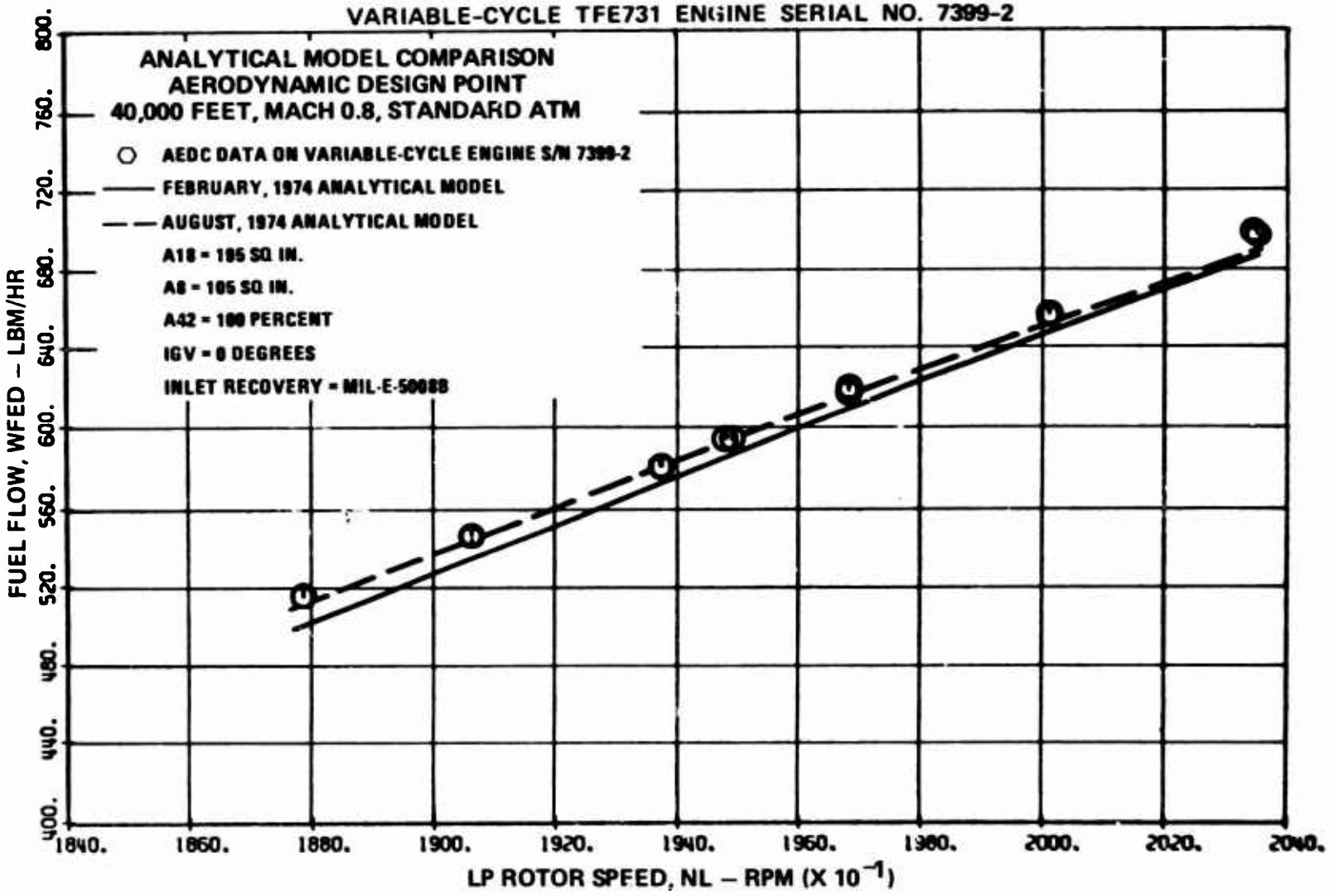

Figure 690. Comparison of Predicted and Tested Performance at Mach 0.8, 40,000 Feet, Fuel Flow Versus LP Rotor Speed.

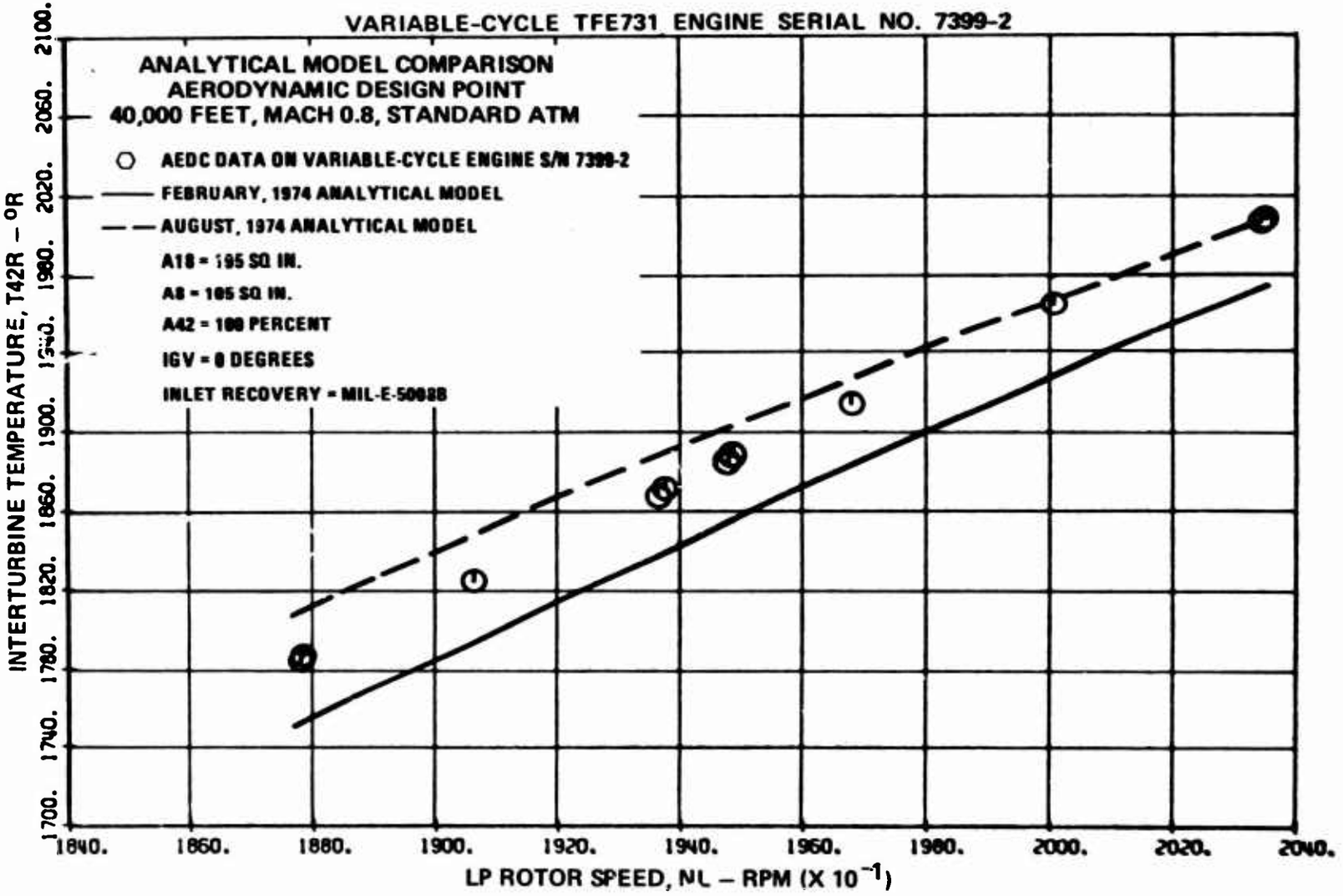

Figure 691. Comparison of Predicted and Tested Performance at Mach 0.8, 40,000 Feet, Interturbine Temperature Versus LP Rotor Speed.

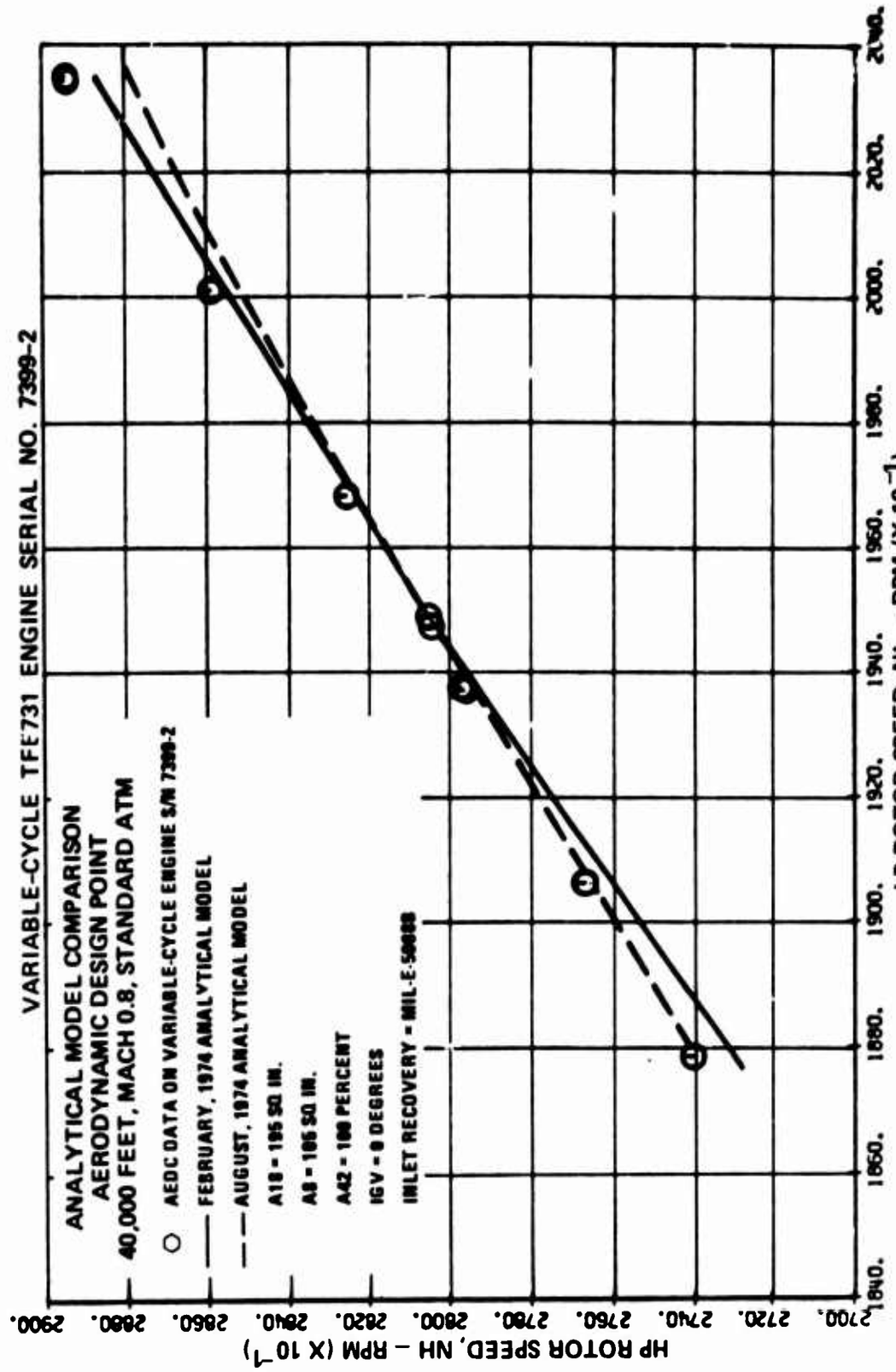

Figure 692. Comparison of Predicted and Tested Performance at Mach 0.8, 40,000 Feet, HP Rotor Speed Versus LP Rotor Speed.

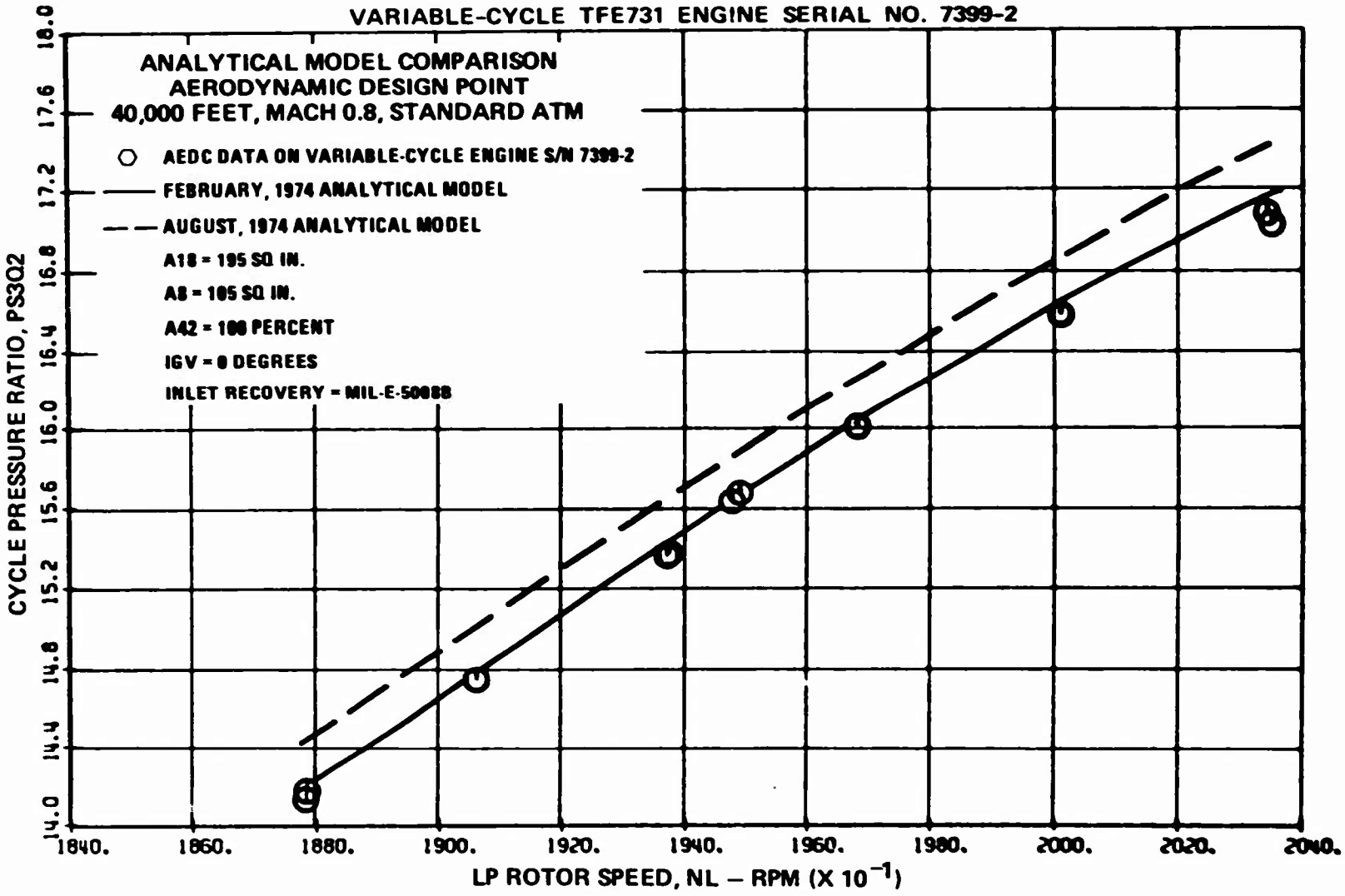

Figure 693. Comparison of Predicted and Tested Performance at Mach 0.8, 40,000 Feet, Cycle Pressure Ratio Versus LP Rotor Speed.

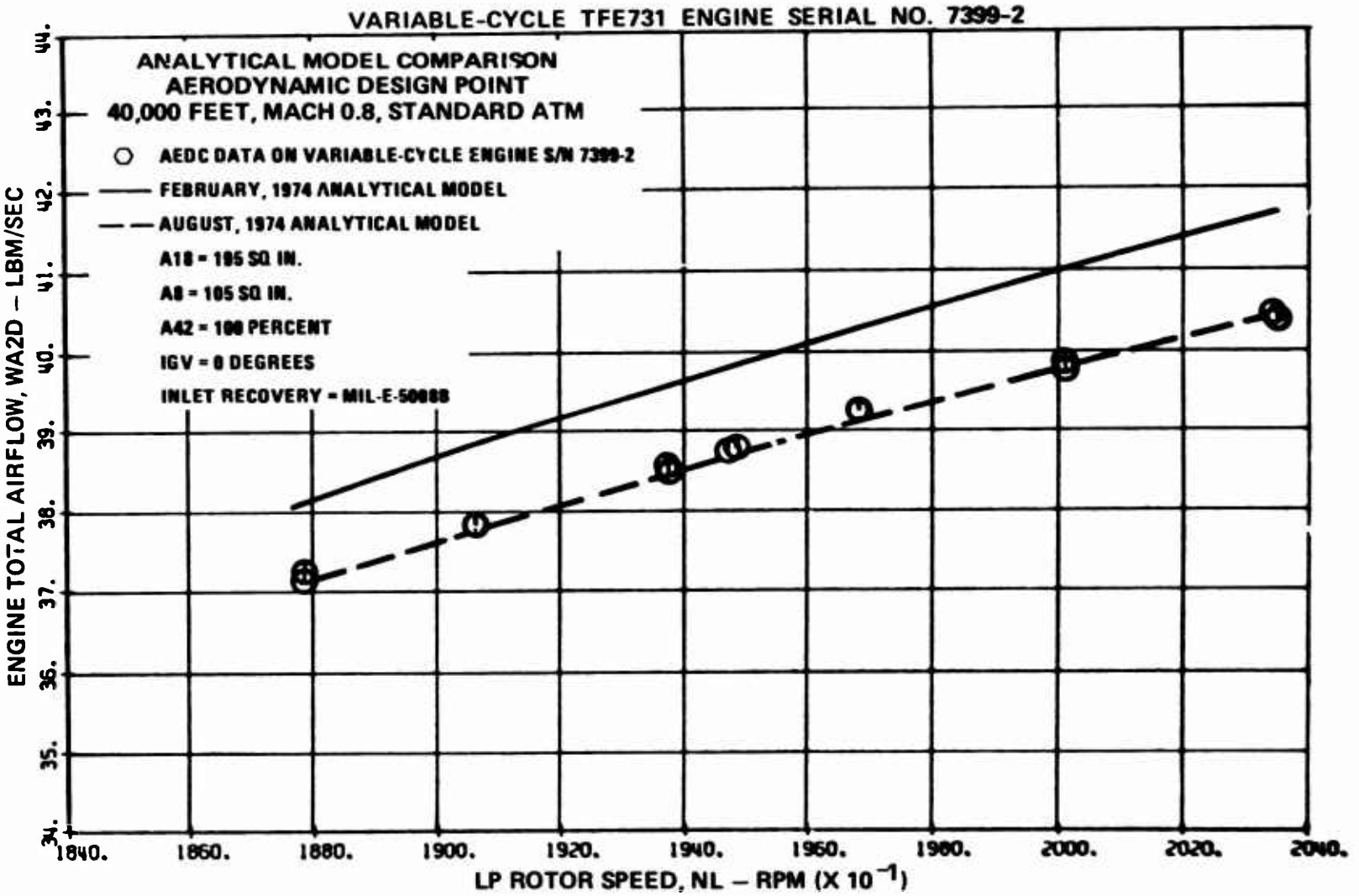

Figure 694. Comparison of Predicted and Tested Performance at Mach 0.8, 40,000 Feet, Engine Total Airflow Versus LP Rotor Speed.

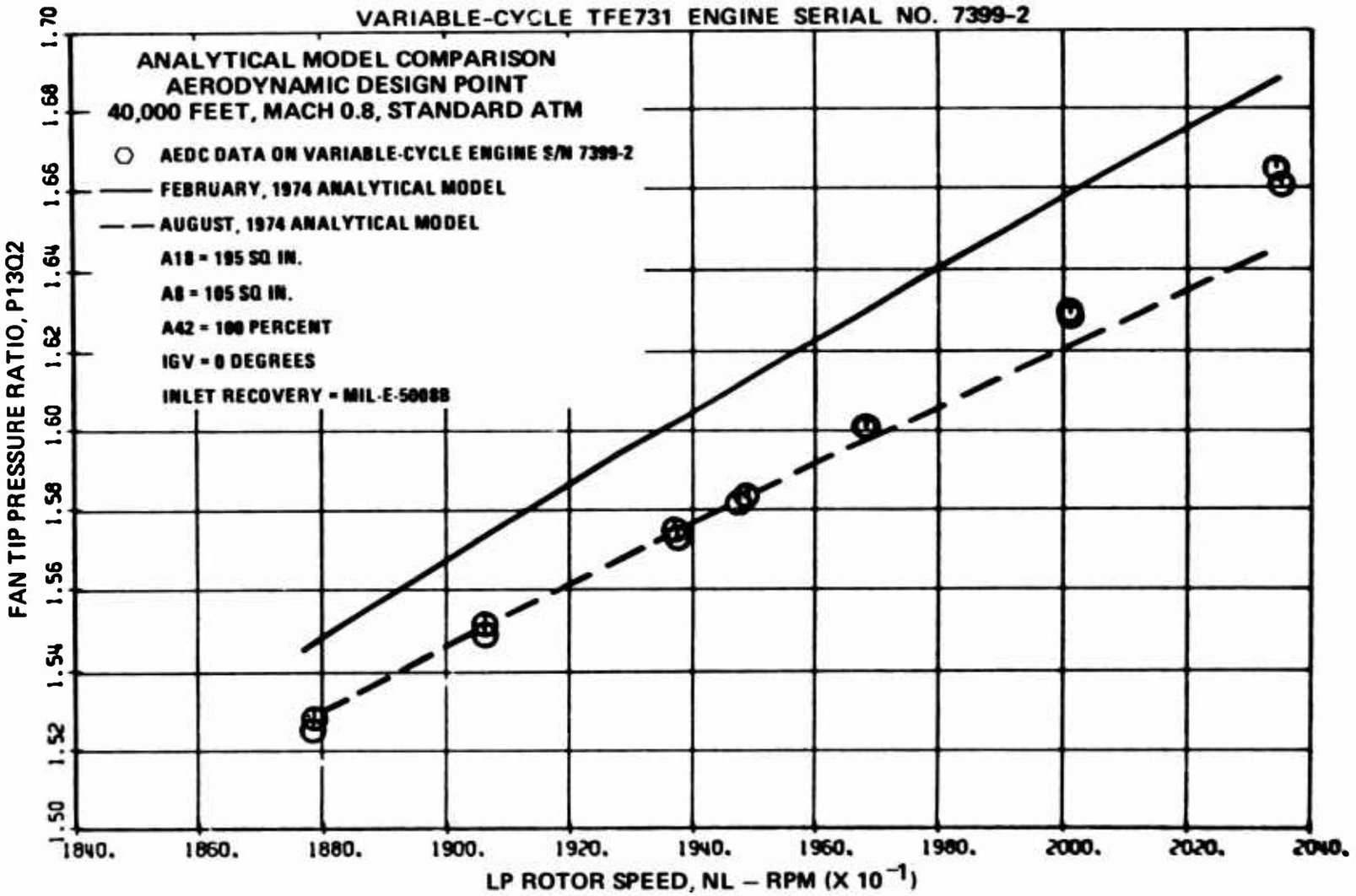

Figure 695. Comparison of Predicted and Tested Performance at Mach 0.8, 40,000 Feet, Fan Tip Pressure Ratio Versus LP Rotor Speed.

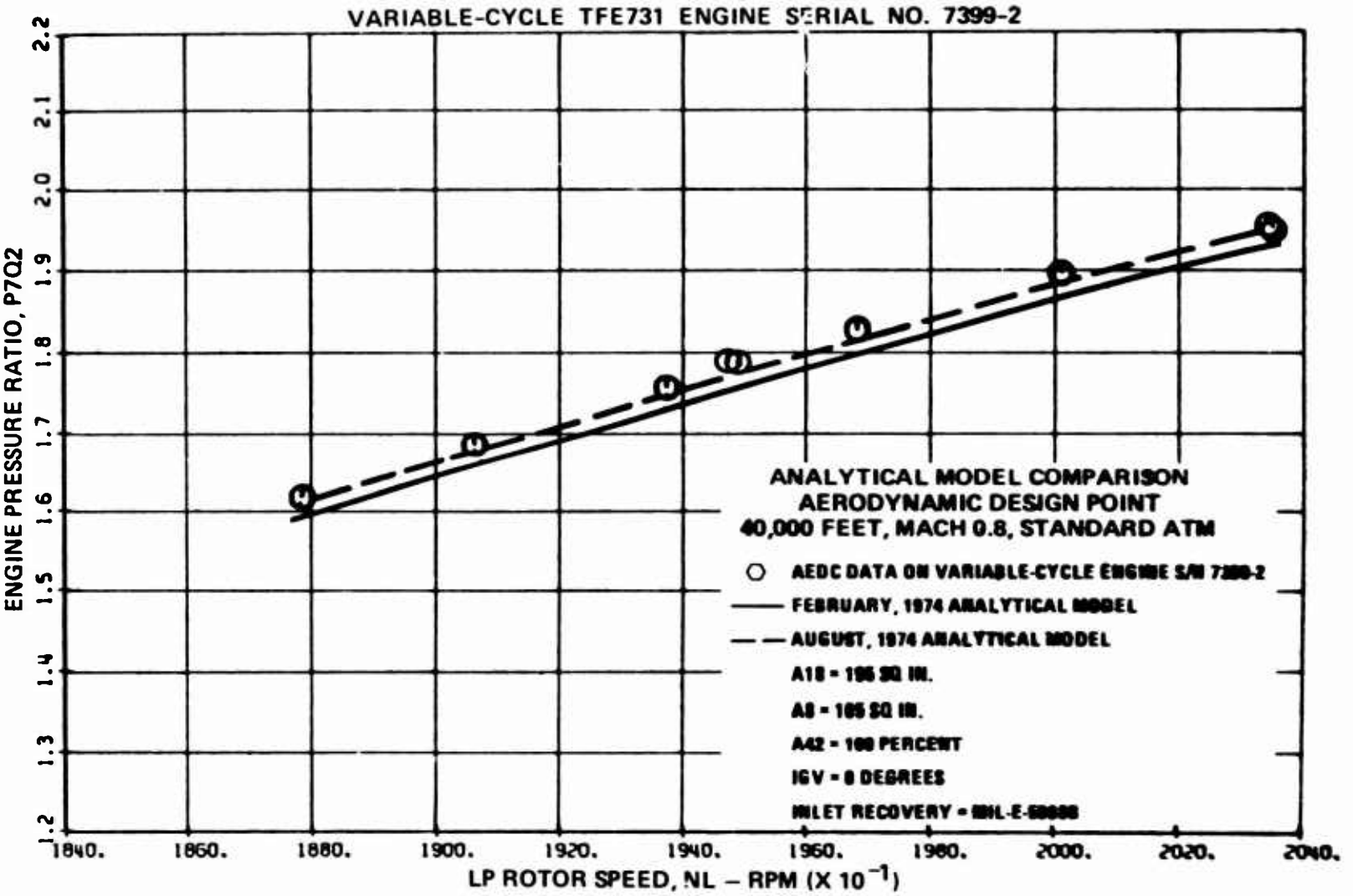

Figure 696. Comparison of Predicted and Tested Performance at Mach 0.8, 40,000 Feet, Engine Pressure Ratio Versus LP Rotor Speed.

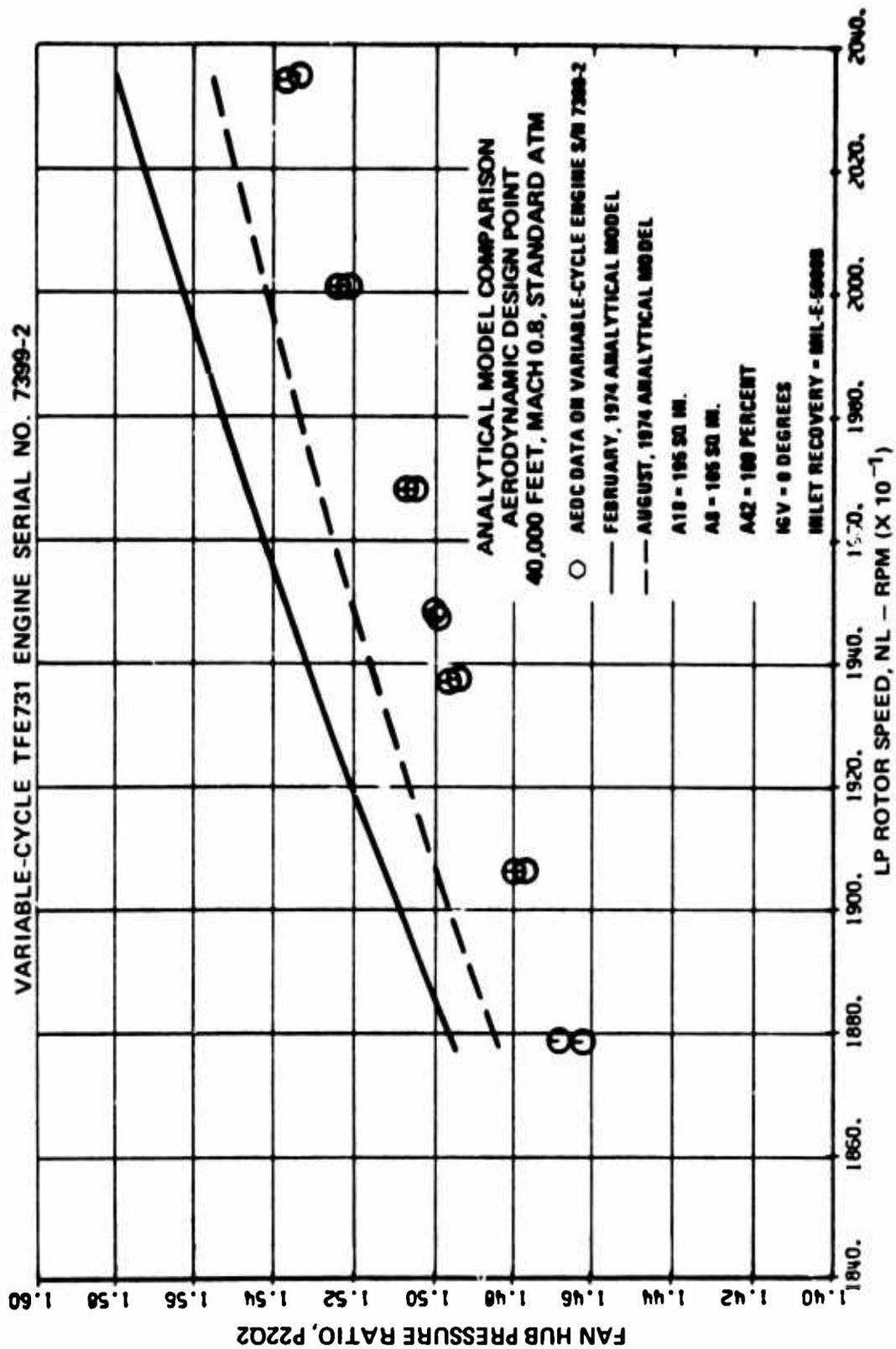

Figure 697. Comparison of Predicted and Tested Performance at Mach 0.8, 40,000 Feet, Fan Hub Pressure Ratio Versus LP Rotor Speed.

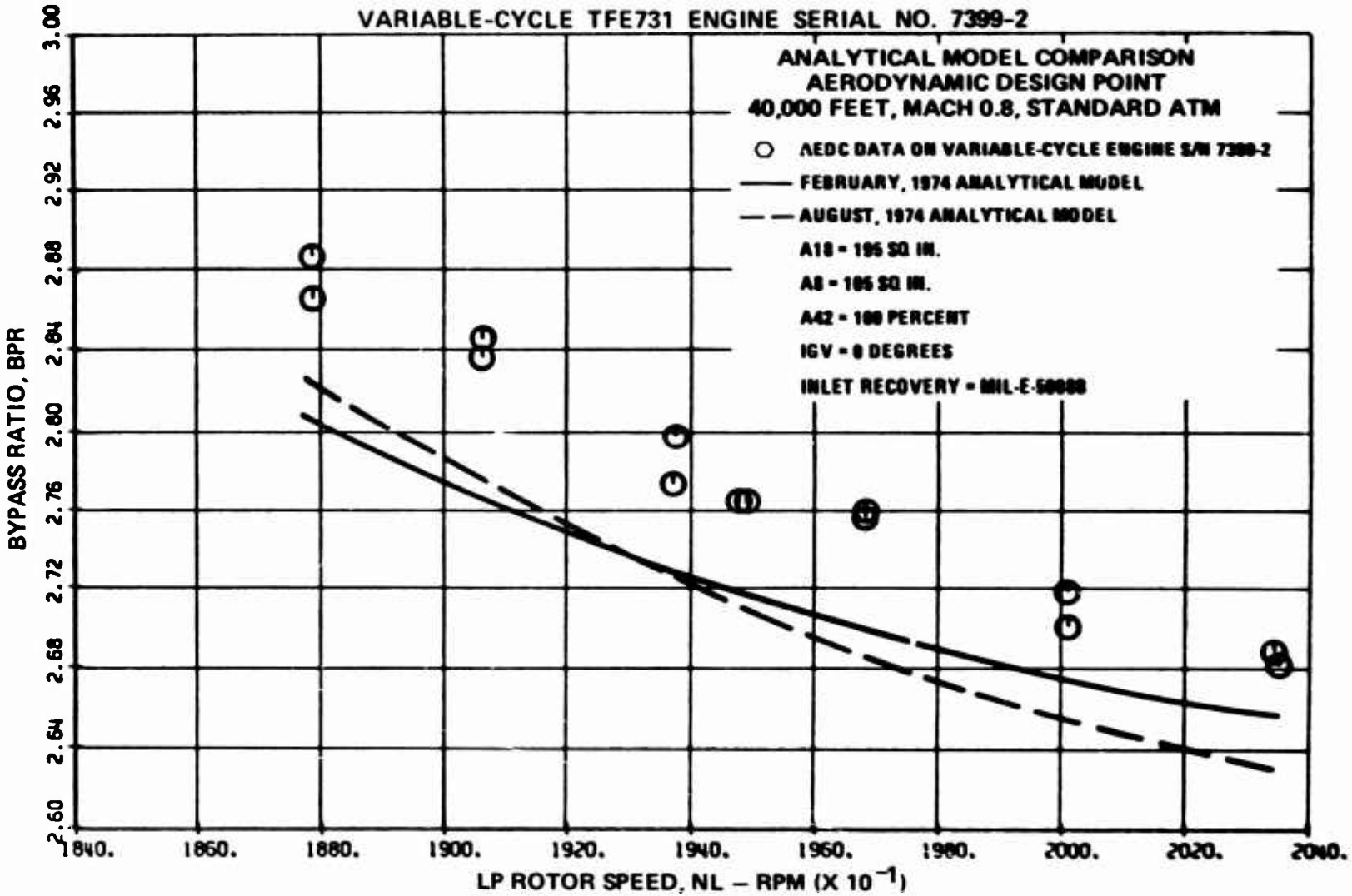

Figure 698. Compariso . of Predicted and Tested Performance at Mach 0.8, 40,000 Feet, Bypass Ratio Versus LP Rotor Speed.

TABLE 37. COMPARISON OF FEBRUARY 1974 AND AUGUST 1974 ANALYTICAL MODELS TO AEDC TEST DATA FOR LOW ROTOR SPEED OF 19,000 RPM

Flight Condition	Test Data		February, 1974 Model				August, 1974 Model				Notes
	Net Thrust (lbf)	SFC [(lbm/hr)/lbf]	Net Thrust (lbf)	Diff. (%)	SFC [(lbm/hr)/lbf]	Diff. (%)	Net Thrust (lbf)	Diff. (%)	SFC [(lbm/hr)/lbf]	Diff. (%)	
SL, Static Standard Day	3320	0.483	3260	-1.81	0.482	-0.21	3280	-1.20	0.482	-0.21	A18 = 205.8 sq in. A8 = 105.7 sq in.
20,000 feet XMOD = 0.6, Standard Day	1350	0.784	1362	+0.89	0.771	-1.66	1342	-0.59	0.794	+1.28	
40,000 feet XMOD = 0.8 Standard Day	631	0.854	665	+5.39	0.791	-7.38	634	+0.48	0.849	-0.59	
50,000 feet XMOD = 0.5 Standard Day	456	0.743	466	+2.19	0.736	-0.94	449	-1.54	0.768	+3.36	
50,000 feet XMOD = 0.8 Standard Day	393	0.897	417	+6.11	0.940	-6.35	396	+0.76	0.895	-0.22	
50,000 feet XMOD = 1.2 Standard Day	412	1.095	430	+4.37	0.988	-9.77	403	-2.18	1.089	-0.55	
50,000 feet XMOD = 1.6 Standard Day	369	1.490	403	+9.21	1.295	-13.09	363	-1.63	1.512	+1.48	IGV = 15 degrees
50,000 feet XMOD = 2.2 Cold Day	95	7.000	419	+341.05	1.578	-77.46	140	+47.37	4.818	-31.17	IGV = 30 degrees A8 = 95 sq in. NL = 17,192 rpm
65,000 feet XMOD = 0.62 Standard Day	162	0.901	157	-3.09	0.917	+1.78	154	-4.94	0.941	+4.44	A42 = 105 percent NL = 18,000 rpm A8 = 105 sq in.

Except where noted, geometry settings were A18 = 191 sq in., A8 = 105 sq in., A42 = 100 percent, and IGV = 0 degrees.

SECTION III

CONCLUSIONS AND RECOMMENDATIONS

plant through the Mach 2.2 regime. The then-current level of variable geometry incorporated in the LP compressor and turbine was shown by analysis to be a valuable tool in rematching the LP compressor, providing for adequate component stability throughout the operating range. LP-spool modulation was predicted to be required above Mach 1.8 in order to provide adequate surge margin while incurring no significant performance penalty.

(d) The Phase I study program indicated the desirability of having particular component flexibility associated with a specific off-design condition. For example, the current level of variable geometry in conjunction with a variable fan nozzle provides for a predicted 12-percent reduction in TSFC at 30 percent maximum power at a sea-level static condition. The predicted advantages of LP rotor modulation for specific fuel consumption are maximized at a low-power, low-airspeed condition typical of loiter, and diminish as engine power and aircraft speed are increased. However, as noted above, it was predicted that variable geometry provides an effective means of furnishing the required surge margin at high flight speeds.

1.2 Phase II, Fabrication and Rig Tests

The Phase II variable-cycle engine activities, including the fabrication and rig testing of three compressor configurations, fabrication and rig testing of the variable-cycle engine combustor, fabrication and instrumentation of all the variable-cycle engine components, and design and fabrication of all of the test support equipment for the variable-cycle engine performance test, were successfully completed on schedule. The following conclusions were drawn from the Phase II activities:

(a) There were no assembly problems, and the operation of the variable-geometry compressor was trouble-free throughout the rig tests. Therefore, the variable geometry compressor was considered to represent a good mechanical design.

(b) The variable-geometry compressor rig tests were both mechanically and aerodynamically successful. The compressor rig test showed that the variable inlet guide vanes and first-stage stator vanes accomplished the intended variability in compressor performance. The expected improvements in surge margin and efficiency were met or exceeded. The increase in surge margin was shown by analysis to be adequate for surge-free operation at Mach 2.2 at an altitude of 40,000 feet.

(c) The combustor rig tests showed that the combustor met or exceeded design objectives and was useable, as designed, in the variable-cycle engine.

1.3 Phase III, Engine Modification and Sea-Level Test

The following conclusions were derived both from the results of 56 hours and 50 minutes of variable-cycle TFE731 Engine testing conducted in Phoenix from July 21 to November 29, 1972, and from the results of calculations made with the analytical model that was developed to simulate the variable-cycle engine:

(a) The variable and fixed-geometry components designed and fabricated in Phases I and II experienced no mechanical problems throughout the sea-level performance testing. Upon completion of the tests, the engine was disassembled and thoroughly inspected. The inspection showed no hardware discrepancies. This phase of the program proved the feasibility of using

developed, production-type hardware to build and test a variable-cycle engine.

(b) The performance penalty in TSFC and interturbine temperature due to incorporating the variable compressor and turbine geometry at their nominal settings is approximately a 1-percent TSFC increase and a negligible increase in interturbine temperature at a constant thrust.

(c) The combined effects of increased fan exhaust nozzle area, increased bypass ratio, and more efficient LP compressor surge protection afforded by the variable IGV and interturbine temperature were shown to decrease the TSFC up to 10 percent relative to that obtained with nominal settings and base-line exhaust nozzles. The 10-percent reduction in TSFC occurred at 1200 pounds of net thrust, which is approximately 34 percent of maximum available net thrust.

(d) The tested fan exhaust-nozzle area increase of 11.5 percent relative to the base-line nozzles demonstrated an effective method of controlling the fan operating line and bypass ratio with minor rematching of the LP compressor.

(e) The tested primary nozzle area increase of 7.6 percent relative to the base-line nozzles demonstrated a method of increasing takeoff thrust by approximately 5 percent at sea-level static, standard-day conditions, at a constant interturbine temperature. In addition, the primary exhaust nozzle area variation demonstrated a method of modulating the LP rotor speed.

(f) Setting the variable IGV and first-stage stator on the LP compressor in a positive preswirl direction

of plus 30 degrees and plus 10 degrees, respectively, provided an effective method of significantly increasing the LP compressor surge margin. For example, at 50 percent LP compressor referred speed, the surge margin was increased from essentially zero to 23 percent. This increased surge margin would permit surge-free operation of augmented versions of the variable-cycle TFE731 Engine to flight speeds beyond Mach 2.2.

(g) The negative preswirl testing at an IGV setting of minus 5 degrees on the LP compressor did not show an increase in net thrust at a constant HP turbine inlet temperature. Furthermore, testing at a minus 10-degree IGV setting resulted in a loss in net thrust at a constant HP turbine inlet temperature.

(h) Effective rematching of the gas generator components was attained by the modulation of LP turbine nozzle area. The results of the testing indicated that LP turbine nozzle area variation is very effective in modulating HP rotor speed and in controlling the LP compressor surge margin at a constant LP rotor speed. At constant HP turbine inlet temperature, variation in interturbine temperature increased net thrust with little penalty in TSFC.

(i) The range of LP turbine nozzle area variations was shown to be limited by the LP compressor surge margin requirements, HP turbine inlet temperature limits, and HP rotor speed limits.

(j) The analytical model represented a good simulation of the variable-cycle TFE731 Engine in the nominal configuration at sea-level static conditions. Variable fan nozzle area, primary nozzle area, and LP

compressor geometry were also closely simulated. Further work was required to improve the simulation of the effects of LP turbine nozzle area variation.

(k) The variable LP turbine nozzle effects on engine performance were the same at sea-level static conditions with the three nozzle configurations and the nominal and minus 5-degree IGV settings. The effects of LP turbine nozzle area modulation were similar in trend but different in magnitude for the 30-degree IGV setting because of the change in LP compressor characteristics.

1.4 Phase IV, Additional Hardware Design and Fabrication, Engine Modification, and Altitude Test

The following conclusions were drawn from the Phase IV activities:

(a) The agreement in measured performance of the variable-cycle TFE731 Engine between AEDC and AiResearch sea-level static, pretest calibrations on all parameters compared at a constant net thrust of 3300 pounds was within 1.6 percent.

(b) A comparison of the measured performance of the variable-cycle TFE731 Engine with nominal geometry settings and a fixed-cycle TFE731-2 Engine, previously tested at NASA-LeRC, at the TFE731-2 design point of 40,000 feet, Mach 0.8, standard atmosphere, indicated lower performance for the variable-cycle engine due to lower thrust coefficients for the variable exhaust nozzles. No base-line performance loss was attributed to the variable turbine and compressor; and when corrected for differences in nozzle thrust coefficients, the performance of the two engines agreed within 1 percent.

(c) Analysis of the measured exhaust-nozzle component data indicated that the lower performance of the variable exhaust nozzles at the 40,000-foot, Mach-0.8 design point is due to a lower than predicted integrated pressure area force on the fan exhaust-nozzle afterbody. Analysis indicates that the variable exhaust nozzles could be redesigned to obtain exhaust-nozzle thrust coefficients similar to those of the TFE731-2 fixed-reference exhaust nozzles.

(d) The results of the exhaust nozzle rematching flexibility tests indicated that the main effect of fan nozzle area is to position the operating line on the fan map. The main effect of primary exhaust-nozzle area is to determine the LP rotor speed at a given turbine inlet temperature.

(d) A near-optimum fan exhaust-nozzle area is one that positions the fan operating line through the center of the efficiency islands. This area is essentially constant once the fan nozzle becomes choked. Below choking, which occurs at reduced flight Mach numbers, the fan exhaust-nozzle area should be increased for optimum performance.

(f) For optimum performance, the primary exhaust-nozzle area should be increased to increase LP rotor speed, when the LP rotor referred speed is below 100 percent. Up to 6 percent increase in net thrust at a constant turbine inlet temperature was demonstrated for a 10-percent increase in primary exhaust-nozzle area.

(g) The variable-area LP turbine nozzle was effective in controlling the power split between the HP and LP turbines, in controlling the HP rotor speed, and in gaining LP compressor surge margin without any penalty in engine performance.

(h) The ability to modulate net thrust while maintaining a constant engine inlet airflow and a constant operating point on the LP compressor was demonstrated at two flight conditions, with two LP rotor speeds and two fan exhaust-nozzle areas at one of the operating conditions. Approximately 20 percent net thrust modulation was demonstrated at each combination.

(i) Increases of approximately 5 percent in airflow and 7 percent in climb net thrust, at a constant turbine inlet temperature, were demonstrated at Mach 0.6, 20,000 feet, standard atmosphere by the use of a combination of increased primary exhaust nozzle area and increased LP turbine nozzle area.

(j) The bleed effects testing confirmed the ability to recover part of the net thrust loss due to bleed-air extraction by the use of variable geometry. From 28 to 47 percent of the net thrust loss due to bleed-air extraction was recovered at the four test conditions.

(k) The results of the high-altitude testing demonstrated the effectiveness of LP turbine nozzle modulation on LP compressor surge margin control. The surge-free altitude at an interturbine temperature of 1500°F was

increased from 65,000 to 75,000 feet by an increase of approximately 10 percent in LP turbine nozzle area.

(l) The results of the surge margin check verified the AiResearch rig-tested LP compressor surge lines within a tolerance of ±2.5 percent.

(m) The engine operated satisfactorily at Mach 2.2, 50,000 feet, MIL-STD-210 Cold Atmosphere, and the effectiveness of LP turbine nozzle area modulation on the LP compressor surge margin at this operating condition was demonstrated.

(n) A comparison of the AEDC pre- and post-test calibrations at a constant net thrust indicated that the specific fuel consumption on the post-test calibration had increased by 1.2 percent and the interturbine temperature had increased by 23°F, relative to those measured on the pretest calibration.

(o) Comparisons of tested performance with predictions by the February 1974 analytical model indicated that performance predictions were satisfactory at sea-level static, but were generally optimistic at altitude conditions. Analysis of the test data indicated a need to revise certain component maps and Reynolds number corrections.

(p) The variable LP compressor, LP turbine and exhaust nozzles experienced no mechanical difficulties throughout the expanded flight envelope testing, and provided a convenient means of adjusting the engine cycle conditions and acquiring test data.

Upon completion of the 94.22 hours of Phase IV testing, 74.5 hours of which were conducted at the AEDC test facility, the engine was completely disassembled and inspected. No mechanical discrepancies were observed, which confirmed the integrity of the variable geometry components employed in the test and the basic Model TFE731-2 Engine as well.

1.5 Overall Program Results

The overall program results verified the general performance effects predicted for variable-geometry modulation in the LP compressor, LP turbine, fan exhaust nozzle, and primary exhaust nozzle of a two-spool turbofan engine. These demonstrated benefits offer potential performance improvements (References 10 and 11) to the following problem areas in future multimission aircraft at off-design conditions:

- Inlet spillage and exhaust system drag losses.
- Compressor surge margin control.
- Airframe bleed-air extraction effects on engine performance.
- Performance at engine rotor speed or turbine temperature limits.

Reference 10. Davenport, W. R., and G. J. Dixon, "The Garrett-AiResearch Variable-Cycle TFE731 Turbofan Engine," SAE Paper No. 730918, October 1973.

Reference 11. Stephenson, D. W., W. R. Davenport, and R. F. Topping, "Altitude Evaluation of a Variable-Cycle Turbofan Engine," SAE Paper No. 740806, October 1974.

2. RECOMMENDATIONS

Based on the results of this program, the following activities are recommended as logical steps for further investigation of the advantages of variable-cycle engines:

(a) Analytical study of variable compressor, turbine and exhaust-nozzle geometry in engines representative of those required for current and future generation multimission aircraft, including preparation of off-design computer analytical models and mission analyses to evaluate their advantages in terms of installed performance and aircraft performance.

(b) Design, build, rig test, analytical study, and engine test of a variable-area HP turbine.

(c) Design, build, and test of variable geometry control and actuation systems for variable-cycle engines that meet the requirements of advanced, high-performance engines.

(d) Investigation of differences between analytically predicted and engine-test derived effects of turbine nozzle area variation on turbine efficiency.

REFERENCES

(1) Okiishi, T. H., G. H. Junkhan, and G. K. Serovy, "Experimental Performance in Annular Cascade of Variable Trailing Edge Flap, Axial-Flow Compressor Inlet Guide Vanes," ASME 70-GT-106, May 1970.

(2) Schlichting, H., "Boundary-Layer Theory," p. 647, McGraw-Hill, Sixth Edition, 1968.

(3) Brimelow, B., "Performance Matching of the Propulsion System," SAE Paper No. 680712, 1968.

(4) Jones, B. A., "Single-Stage Experimental Evaluation of Variable Geometry Inlet Guide Vanes and Stator Blading, Part VI," NASA CR-54559, September 1967.

(5) Jones, B. A., "Single-Stage Experimental Evaluation of Slotted Rotor and Stator Blading, Part VII," - NASA CR-54550, September 1967.

(6) TEST FACILITIES HANDBOOK (Tenth Edition), Arnold Engineering Development Center, Air Force Systems Command, USAF, May 1974.

(7) AiResearch Report 73-210158-C, "Altitude Test Plan for Variable-Cycle TFE731 Engine," March 4, 1974.

(8) Ramsey, J. W., and G. C. Oates, "Potential Operating Advantages of a Variable Area Turbine Turbojet," ASME Paper 72 WA/AERO-4, 1972.

(9) May, R. J. Jr., and W. F. Zavatsky, "Influence of Variable Turbine Geometry on Engine Installation Losses and Cycle Selection," Proc. of 1972 JANNAF Propulsion Meeting (Aircraft Propulsion Session), 1972.

(10) Davenport, W. R., and G. J. Dixon, "The Garrett-AiResearch Variable-Cycle TFE731 Turbofan Engine," SAE Paper No. 730918, October 1973.

(11) Stephenson, D. W., W. R. Davenport, and R. F. Topping, "Altitude Evaluation of a Variable-Cycle Turbofan Engine," SAE Paper No. 740806, October 1974.

APPENDIX A

DATA-REDUCTION EQUATIONS

General methods and equations employed to compute the steady-state parameters presented in the TFE731 Variable-Cycle Engine final report are given below. When applicable, arithmetic averages of the pressures and indicated temperatures were used.

SPECIFIC HEATS

The specific heat at constant pressure (CP) was computed from the empirical equation:

$$CP = \frac{(a_1 + b_1T + c_1T^2) + f(a_2 + b_2T + c_2T^2)}{1 + f} \qquad (1)$$

where f is the fuel-air ratio; a_1, b_1, and c_1 are constants based on the specific heats of the constituents of air; and a_2, b_2, and c_2 are the constants based on a fuel hydrogen-carbon ratio of 0.16 and the specific heats of water vapor, oxygen, and carbon dioxide. The equation was derived for the two temperature ranges shown below:

Temperature Range, °R	a_1	b_1	c_1	a_2	b_2	c_2
400 to 1700	0.2318	0.1040×10^{-4}	0.7166×10^{-8}	0.2655	3.7265×10^{-4}	-6.6353×10^{-8}
1701 to 4500	0.2214	0.3521×10^{-4}	-0.3776×10^{-8}	0.3397	2.7182×10^{-4}	-2.9044×10^{-8}

RATIO OF SPECIFIC HEATS

The ratio of specific heats (γ) of air was calculated from the expression:

$$\gamma = \frac{CP}{CP - \frac{R}{J}} \tag{2}$$

For a fuel-air mixture, the gas constant was expressed as

$$R = \frac{53.342 + 55.121f}{1 + f} \tag{3}$$

TOTAL TEMPERATURE

Total temperatures were obtained by applying a recovery ratio (RR_n)--a function of stream Mach number and probe geometry--to the indicated temperature in the following relationship:

$$T_n = \frac{Tind}{RR_n} \tag{4}$$

where n denotes the station number.

The venturi inlet thermocouples (TOO) were mounted on the grid upstream of the venturi, and the engine inlet thermocouples (T2P) were mounted on a grid in the test cell plenum chamber upstream of the engine inlet. The fan inlet temperature (T2) was assumed to be equal to the engine inlet temperature (T2P).

The following recovery ratios were used in the calculation of total temperatures at the indicated instrumentation stations:

Station	RR
00, 2P, 3	1.00
22	0.9985
24	0.9988
42	0.9975
7	0.9984
13	0.9981
17	0.9988

MACH NUMBER

Mach number was obtained from the equation:

$$M = \sqrt{\frac{2}{\gamma-1}\left[\left(\frac{P}{PS}\right)^{\frac{\gamma-1}{\gamma}} - 1\right]} \qquad (5)$$

VELOCITY

Velocity was determined from the relation:

$$V = \sqrt{\frac{2\gamma gRT}{\gamma-1}\left[1 - \left(\frac{PS}{P}\right)^{\frac{\gamma-1}{\gamma}}\right]} \qquad (6)$$

GAS FLOW

Airflow at Station 1n (venturi throat) was calculated from the following equation for critical venturi flow (critical flow was established for all testing above idle power) as follows:

$$WA1N = (P00)(A1N)(CF1N)\left(\frac{2}{\gamma+1}\right)^{\frac{\gamma+1}{2(\gamma-1)}}\sqrt{\frac{\gamma g}{R(T00)}} \qquad (7)$$

For windmill and idle power, where the venturi was unchoked, airflow was calculated with use of the relation:

$$WA1N = \sqrt{\frac{2\gamma g}{R(\gamma-1)}} \frac{(PSIN)(A1N)(CF1N)\sqrt{1 - \left(\frac{PS1N}{P00}\right)^{\frac{\gamma-1}{\gamma}}}}{\sqrt{T00}\left(\frac{PS1N}{T00}\right)^{\frac{\gamma-1}{\gamma}}} \qquad (8)$$

where CF1N is an empirically determined flow coefficient based on the venturi wall curvature, area ratio, and boundary-layer development. The flow coefficient was evaluated and expressed as a function of Mach number (MIN) and venturi throat Reynolds number (Re1N) as follows:

$$CF1N = 0.9861 + 0.0012 \log RE1N - 0.055 (1 - MIN)$$

Airflow at Station 2.2 (LP compressor inlet) was calculated from the following equation:

$$WA22 = \sqrt{\frac{2\gamma g}{R(\gamma-1)}} \frac{(PS22)(AE22)\sqrt{1 - \left(\frac{PS22}{P22}\right)^{\frac{\gamma-1}{\gamma}}}}{\sqrt{T22}\left(\frac{PS22}{P22}\right)^{\frac{\gamma-1}{\gamma}}} \qquad (9)$$

For all testing except for the special high-altitude test, air or gas flows at other stations were obtained by adding or subtracting from the venturi and Station 2.2 measured airflows as follows:

$$WA2 = WA1N$$
$$WA13 = WA2 - WA22$$
$$WA24 = WA22 - WL1 - WBLP$$
$$WA3 = WA24 - WTC1 - WTC2$$
$$WG4 = WA3 + WFE$$
$$WG42 = WG4 + WTC1$$
$$WG7 = WG42 + WTC2$$
$$WA18 = WA13 + WBLP$$

where the parasitic flow rates were determined as follows (values of parasitic flow constants supplied by AiResearch):

$$WL1 = 0.0011\ WA22$$
$$WTC1 = 0.011\ WA24$$
$$WTC2 = 0.020\ WA24$$

LP compressor discharge bleed flow (WBLP) was calculated from the following critical flow relationship:

$$WBLP = (PBLP)(AEBLP)\left(\frac{2}{\gamma+1}\right)^{\frac{\gamma+1}{2(\gamma-1)}}\sqrt{\frac{\gamma g}{R\ T24}} \qquad (10)$$

where PBLP = P24(1 - DELPB) and DELPB is an AiResearch empirically determined total pressure relationship:

$$DELPB = 0.1142236\ [WBLP\sqrt{T24/518.7}/(PBLP/14.696)]^2 \qquad (11)$$

For the special high-altitude test, the HP turbine inlet flow rate was calculated by iteration to satisfy the HP turbine choked flow equation:

$$WG4 = P4X\ (AE4)\left(\frac{2}{\gamma+1}\right)^{\frac{\gamma+1}{2(\gamma-1)}}\sqrt{\frac{\gamma g}{R(T4X7W)}} \qquad (12)$$

A value of AE4 = 14.343 square inches empirically determined from prior testing was used in this equation. The other flow rates were then determined by use of the previously defined relationships.

CALCULATED TOTAL PRESSURES

The total pressures at several stations were determined by application of AiResearch empirically determined pressure-loss relationships as follows:

LP Compressor Discharge

The LP compressor discharge total pressure was determined as follows:

$$P23X = P24(1 + DP24) \tag{13}$$

where $$DP24 = 0.2875 \times 10^{-3} \left[(WA24) \frac{\sqrt{T24/518.7}}{P24/14.696}\right]^2$$

HP Compressor Discharge

The HP compressor discharge total pressure was determined by iteration of the following relationship:

$$P3X = \frac{PS3}{1 - 0.001649\left[(WA3)\frac{\sqrt{T3/518.7}}{P3X/14.696}\right]^2} \tag{14}$$

HP Turbine Inlet

The HP turbine inlet total pressure was obtained as follows:

$$P4X = P3X(1 - DP3) \tag{15}$$

where $$DP3 = 0.4424 \times 10^{-3}\left(6.027 + \frac{T4X}{T3}\right)\left(\frac{WA3\sqrt{T3/518.7}}{P3X/14.696}\right)^2$$

HP Turbine Discharge

The HP turbine discharge total pressure was determined as follows:

$$P41X = P42(1 + DP24) \tag{16}$$

where $$DP42 = 0.2262 \times 10^{-3}\left[\frac{WG42\sqrt{T42/518.7}}{P42/14.696}\right]^2$$

LP Turbine Discharge

The LP turbine discharge total pressure was calculated by the following relationship:

$$' = P7(1 + DP7) \tag{17}$$

where $$DP7 = 0.12415 \times 10^{-4}\left[\frac{WG7\sqrt{T7/518.7}}{P7/14.696}\right]^2$$

ENTHALPY

Enthalpy at all stations where the necessary temperature and fuel-flow measurements were available was obtained by integration of the empirical specific heat formula:

$$H = \int_{400°}^{T} CPdT \tag{18}$$

Enthalpy at all other stations was calculated with use of the method of conservation of energy, with the assumption of no heat transfer.

HIGH-PRESSURE TURBINE INLET ENTHALPY

The enthalpy at Station 4 was obtained as a function of primary nozzle inlet temperature and compressor work from the following equation:

$$H4X7W = \frac{(H7)WG7 - H3(WTC1 + WTC2)}{WG4}$$

$$+ \frac{\left(\begin{matrix}\text{Fan}\\\text{Work}\end{matrix}\right) + \left(\begin{matrix}\text{LPC}\\\text{Work}\end{matrix}\right) + \left(\begin{matrix}\text{HPC}\\\text{Work}\end{matrix}\right) + \left(\begin{matrix}\text{LP}\\\text{Loss}\end{matrix}\right) + \left(\begin{matrix}\text{HP}\\\text{Loss}\end{matrix}\right)}{WG4} \qquad (19)$$

where fan work = WA13 (H13 - H2) + WA22 (H22 - H2)
LPC work = WA22 (H23 - H22)
HPC work = WA24 (H3 - H24)

LPLOSS and HPLOSS are AiResearch-supplied LP and HP rotor bearing and seal losses.

TURBINE INLET TEMPERATURE

The calculated turbine inlet temperature T4X7W was obtained from an iteration of the equation:

$$\int_{400}^{T4X7W} CPdT = H4XTW \qquad (20)$$

COMPONENT EFFICIENCIES

Fan Hub

The fan hub adiabatic efficiency was determined from the relationship:

$$ETAHUB = \frac{H22_{isen} - H2}{H22 - H2} \qquad (21)$$

Fan Tip

The fan tip adiabatic efficiency was determined from the following:

$$ETATIP = \frac{H22_{isen} - H2}{H13 - H2} \tag{22}$$

Overall Fan

The overall fan adiabatic efficiency was calculated as follows:

$$ETAFAN = \frac{WA22\left(H22_{isen} - H2\right) + WA13\left(H13_{isen} - H2\right)}{WA22\ (H22 - H2) + WA13\ (H13 - H2)} \tag{23}$$

LP Compressor

The LP compressor adiabatic efficiency was determined from the relationship:

$$ETALPC = \frac{H23_{isen} - H22}{H23 - H22} \tag{24}$$

HP Compressor

The HP compressor adiabatic efficiency was determined from the following:

$$ETAHPC = \frac{H3_{isen} - H24}{H3 - H24} \tag{25}$$

COMBUSTOR

The combustor efficiency was calculated from the equation:

$$ETABX = \frac{(H17)WA18 + (H7)WG7 + (H24)WL1 - (H2)WA2}{(LHV)\ WFE} + \frac{DHWOC - WFE\left[59.62 + \int_{540°}^{TF} CPdT\right]}{(LHV)\ WFE} \quad (26)$$

where LHV is the lower heating value of the fuel and the quantity 59.62 (Btu/lbm fuel) accounts for the differences between the enthalpy of carbon dioxide and water vapor formed during combustion and enthalpy of the oxygen removed from the air by their formation in the temperature range from 400°R (base of the enthalpy equation) to 540°R (reference temperature for determination of LHV).

The quantity DHWOC is the energy removed from the engine oil by the auxiliary water-oil heat exchanger, calculated as follows:

$$DHWOC = WWOC \times CP(TWOCO - TWOCI) \quad (27)$$

HP Turbine

The HP turbine efficiency was determined as follows:

$$ETAHPT = \frac{H4 - H41}{H4 - H41_{isen}} \quad (28)$$

LP Turbine

The LP turbine efficiency was calculated as follows:

$$\text{ETALPT} = \frac{\text{H42} - \text{H5}}{\text{H42} - \text{H5}_{\text{isen}}} \tag{29}$$

THRUST

Jet Thrust

Jet thrust was calculated from the following expression:

$$\text{FGS} = \text{FS} + \left(\frac{\text{WA2}}{g}\right) \text{V1} + \text{A1ODC} \ (\text{PS1} - \text{PS0}) \tag{30}$$

where A1ODC is the effective labyrinth air seal area and PS1 = PS0.5.

Net Thrust

Net thrust was calculated by the use of the following equation:

$$\text{FNS} = \text{FGS} - \left(\frac{\text{WA2}}{g}\right) \text{VO} \tag{31}$$

where VO is calculated from the relation:

$$\text{VO} = \sqrt{\frac{2\gamma g R}{\gamma - 1} \left(\text{T2} - \text{TO}\right)}$$

$$\text{and} \quad \text{TO} = \frac{\text{T2}}{\left(\frac{\text{P1NF}}{\text{PSO}}\right)^{\frac{\gamma-1}{\gamma}}} \tag{32}$$

where PINF is the free-stream stagnation pressure.

Isentropic Thrust

Isentropic thrust was calculated from the equation:

$$FGISEN = \left(\frac{WG8}{g}\right) V8ISEN + \left(\frac{WA18}{g}\right) V18ISEN \quad (33)$$

where isentropic exit velocity was determined from the relation:

$$VISEN = \sqrt{2gJ\left(H - HS_{isen}\right)} \quad (34)$$

and HS_{isen} is obtained from an isentropic expansion from the exhaust-nozzle total pressure to the ambient pressure (PSO).

NOZZLE THRUST COEFFICIENT

The exhaust-nozzle thrust coefficient was defined as the ratio of measured jet thrust to calculated ideal thrust as follows:

$$CFGISEN = \frac{FGS}{FGISEN} \quad (35)$$

INLET AND TEST CELL AMBIENT PRESSURE CORRECTION

Since the test cell pressure could not always be maintained at the desired altitude pressure, a correction to the measured values of jet and net thrust was applied if the data were obtained at operating conditions that satisfied the following:

a. The actual exhaust-nozzle pressure ratios P7/PSO and P17/PSO were greater than the critical pressure ratio and

b. The desired exhaust-nozzle pressure ratios P7/PSOM and P17/PSOM were greater than the critical pressure ratio where

$$PSOM = P2 \left(\frac{PSO}{P2}\right)_{desired} \tag{36}$$

It was also necessary to apply a correction to engine airflow, fuel flow, jet thrust, and net thrust because of slight deviations of actual inlet setting pressure from the desired pressure corresponding to the desired Mach number. No attempt was made to correct for off-temperature conditions. The adjusted engine airflow and fuel flow were then obtained from

$$WA2D = \frac{WA2}{DELTA2A}$$

$$WFED = \frac{WFE \quad \left(LHV/LHV_{ref.}\right)}{DELTA2A} \tag{37}$$

where DELTA2A is defined as the ratio of the actual engine inlet total pressure to the desired engine inlet total pressure corresponding to the desired flight condition ($P2/P2_{desired}$). The term LHV/LHV_{ref} is the ratio of the actual to the specified (18,400 Btu/lbm) lower heating value of the fuel.

The adjusted jet thrust is obtained from

$$FGSD = \frac{FGS + (PSO - POM)A8 + (PSO - POM)A18}{DELTA2A} \tag{38}$$

The adjusted net thrust is obtained from the following:

$$FNSD = FGSD - \left(\frac{WA2D}{g}\right)VOD \tag{39}$$

where VOD is based on the static temperature determined from the isentropic pressure ratio for the desired Mach number and the measured engine inlet temperature (T2).

SPECIFIC FUEL CONSUMPTION

The engine specific fuel consumption was calculated as follows:

$$SFCD = \frac{WFED}{FNSD} \tag{40}$$

REYNOLDS NUMBER INDEX

Reynolds number index was obtained from the relationship:

$$REI = \frac{\delta}{\phi \sqrt{\theta}} \tag{41}$$

where

$$\phi = \frac{718.2 \quad \theta^{3/2}}{T2 + 199.5}$$

and

$$\theta = \frac{T2}{518.7}$$

APPENDIX B

DATA UNCERTAINTY CALCULATIONS

The following pages contain the equations and calculations for the data uncertainty analysis presented in 4.2.5.3. The equations are presented in the following order: net thrust, fuel flow, and specific fuel consumption. Each flight condition is then presented with the parameters in the same order as presented in the equations. Flight conditions presented are: sea-level static; 40,000 feet, Mach 0.8; 65,000 feet, Mach 0.62; and 50,000 feet, Mach 1.6.

Following the uncertainty calculations, the uncertainties of the measured parameters as determined by Arnold Engineering Development Center, Tullahoma, Tennessee, are presented.

DATA UNCERTAINTY EQUATIONS

I. Net Thrust

$$\left(\frac{\delta FNSD}{FNSD}\right)^2 = \frac{1}{(FNSD)^2}\left[\left(\frac{\partial FNSD}{\partial FS}\,\delta FS\right)^2 + \left(\frac{\partial FNSD}{\partial P00}\,\delta P00\right)^2 + \left(\frac{\partial FNSD}{\partial T00}\,\delta T00\right)^2 + \right.$$

$$\left.\left(\frac{\partial FNSD}{\partial T2}\,\delta T2\right)^2 + \left(\frac{\partial FNSD}{\partial PSO5}\,\delta PSO5\right)^2 + \left(\frac{\partial FNSD}{\partial PSO}\,\delta PSO\right)^2 + \left(\frac{\partial FNSD}{\partial PTO5}\,\delta PTO5\right)^2\right]$$

II. Fuel Flow

$$\left(\frac{\delta WFED}{WFED}\right)^2 = \frac{1}{(WFED)^2}\left[\left(\frac{\partial WFED}{\partial WF}\,\delta WF\right)^2 + \left(\frac{\partial WFED}{\partial T_{FUEL}}\,\delta T_{FUEL}\right)^2 + \left(\frac{\partial WFED}{\partial PTO5}\,\delta PTO5\right)^2\right]$$

III. Specific Fuel Consumption

$$\left(\frac{\delta SFCD}{SFCD}\right)^2 = \frac{1}{(SFCD)^2}\left[\left(\frac{\partial SFCD}{\partial FS}\,\delta FS\right)^2 + \left(\frac{\partial SFCD}{\partial P00}\,\delta P00\right)^2 + \left(\frac{\partial SFCD}{\partial T00}\,\delta T00\right)^2 + \right.$$

$$\left(\frac{\partial SFCD}{\partial T2}\,\delta T2\right)^2 + \left(\frac{\partial SFCD}{\partial PSO5}\,\delta PSO5\right)^2 + \left(\frac{\partial SFCD}{\partial PSO}\,\delta PSO\right)^2 + \left(\frac{\partial SFCD}{\partial PTO5}\,\delta PTO5\right)^2 +$$

$$\left.\left(\frac{\partial SFCD}{\partial WF}\,\delta WF\right)^2 + \left(\frac{\partial SFCD}{\partial T_{FUEL}}\,\delta T_{FUEL}\right)^2\right]$$

SEA-LEVEL STATIC DATA POINT 17-48

$$\left(\frac{\Delta FNSD}{FNSD}\right)^2 = \frac{1}{(3462.9)^2}\left[\underset{(FS)}{(29.425 \times 0.4)^2} + \underset{(P00)}{(13.015 \times 0.4)^2} + \underset{(T00)}{(1.247 \times 2.3)^2} + \underset{(T2)}{(1.23 \times 2.3)^2}\right.$$

$$\left. + \underset{(PSO5)}{(5.076 \times 0.55)^2} + \underset{(PSO)}{(93.94 \times 0.4)^2} + \underset{(PTO5)}{(53.148 \times 0.5)^2}\right]$$

$\Delta FNSD$ = 48.04 lbs, uncertainty = $\pm$1.39%

$$\left(\frac{\Delta WFED}{WFED}\right)^2 = \frac{1}{(1703.6)^2}\left[\underset{(WF)}{(17.211 \times 0.6)^2} + \underset{(T_{FUEL})}{(0.906 \times 2.3)^2} + \underset{(PTO5)}{(16.963 \times 0.5)^2}\right]$$

$\Delta WFED$ = 13.52 lbm/hr, uncertainty = $\pm$0.79%

$$\left(\frac{\Delta SFCD}{SFCD}\right)^2 = \frac{1}{(0.49195)^2}\left[\underset{(FS)}{(0.00421 \times 0.4)^2} + \underset{(P00)}{(0.00185 \times 0.4)^2} + \underset{(T00)}{(0.00018 \times 2.3)^2}\right.$$

$$+ \underset{(T2)}{(0.00017 \times 2.3)^2} + \underset{(PSO5)}{(0.00072 \times 0.55)^2} + \underset{(PSO)}{(0.01299 \times 0.4)^2} + \underset{(PTO5)}{(0.01264 \times 0.5)^2}$$

$$\left. + \underset{(WF)}{(0.00497 \times 0.6)^2} + \underset{(T_{FUEL})}{(0.00026 \times 2.3)^2}\right]$$

$\Delta SFCD$ = 0.00895, uncertainty = $\pm$1.82%

40,000 FT, MACH 0.8 DATA POINT 5-23

$$\left(\frac{\Delta FNSD}{FNSD}\right)^2 = \frac{1}{(821.6)^2}\left[\underset{(FS)}{(3.991 \times 1)^2} + \underset{(P00)}{(4.767 \times 0.4)^2} + \underset{(T00)}{(0.531 \times 2.3)^2} + \underset{(T2)}{(0.542 \times 2.3)^2}\right.$$

$$\left. + \underset{(PSO5)}{(1.444 \times 0.55)^2} + \underset{(PSO)}{(3.291 \times 2.0)^2} + \underset{(PTO5)}{(7.174 \times 0.5)^2}\right]$$

$\Delta FNSD$ = 8.91 lbs, uncertainty = $\pm$1.08%

$$\left(\frac{\Delta WFED}{WFED}\right)^2 = \frac{1}{(697.4)^2}\left[\underset{(WF)}{(6.95 \times 0.9)^2} + \underset{(T_{FUEL})}{(0.39 \times 2.3)^2} + \underset{(PTO5)}{(7.10 \times 0.5)^2}\right]$$

$\Delta WFED$ = 7.25, uncertainty = $\pm$1.04%

$$\left(\frac{\Delta SFCD}{SFCD}\right)^2 = \frac{1}{(0.84887)^2}\left[\underset{(FS)}{(0.00414 \times 1)^2} + \underset{(P00)}{(0.0049 \times 0.4)^2} + \underset{(T00)}{(0.00055 \times 2.3)^2}\right.$$

$$+ \underset{(T2)}{(0.00056 \times 2.3)^2} + \underset{(PSO5)}{(0.00149 \times 0.55)^2} + \underset{(PSO)}{(0.00339 \times 2.0)^2} + \underset{(PTO5)}{(0.01616 \times 0.5)^2}$$

$$\left. + \underset{(WF)}{(0.00849 \times 0.9)^2} + \underset{(T_{FUEL})}{(0.00044 \times 2.3)^2}\right]$$

$\Delta SFCD$ = 0.01398 (lbm/hr)/lbf, uncertainty = $\pm$1.65%

65,000 FT, MACH 0.62 DATA POINT 14-46

$$\left(\frac{\Delta FNSD}{FNSD}\right)^2 = \frac{1}{(176.3)^2}\left[\underset{(FS)}{(4.09 \times 1)^2} + \underset{(P00)}{(0.769 \times 0.4)^2} + \underset{(T00)}{(0.096 \times 2.3)^2} + \underset{(T2)}{(0.089 \times 2.3)^2}\right.$$

$$\left. + \underset{(PS05)}{(0.341 \times 0.6)^2} + \underset{(PS0)}{(5.190 \times 0.75)^2} + \underset{(PT05)}{(4.571 \times 0.5)^2}\right]$$

$\Delta FNSD$ = 6.11 lbs, uncertainty = $\underline{\pm 3.48\%}$

$$\left(\frac{\Delta WFED}{WFED}\right)^2 = \frac{1}{(157.2)^2}\left[\underset{(WF)}{(-1.62 \times 0.9)^2} + \underset{(T_{FUEL})}{(0.05 \times 2.3)^2} + \underset{(PT05)}{(1.54 \times 0.5)^2}\right]$$

$\Delta WFED$ = 1.652 lbm/hr, uncertainty = $\underline{\pm 1.05\%}$

$$\left(\frac{\Delta SFCD}{SFCD}\right)^2 = \frac{1}{(0.89137)^2}\left[\underset{(FS)}{(0.02118 \times 1)^2} + \underset{(P00)}{(0.00386 \times 0.4)^2} + \underset{(T00)}{(0.00049 \times 2.3)^2}\right.$$

$$+ \underset{(T2)}{(0.00044 \times 2.3)^2} + \underset{(PS05)}{(0.00174 \times 0.6)^2} + \underset{(PS0)}{(0.02549 \times 0.75)^2}$$

$$\left. + \underset{(PT05)}{(0.03291 \times 0.5)^2} + \underset{(WF)}{(0.00899 \times 0.9)^2} + \underset{(T_{FUEL})}{(0.00047 \times 2.3)^2}\right]$$

$\Delta SFCD$ = 0.0340 (lbm/hr)/lbf, uncertainty = $\underline{\pm 3.02\%}$

50,000 FT, MACH 1.6 DATA POINT 13-41

$$\left(\frac{\Delta FNSD}{FNSD}\right)^2 = \frac{1}{(374.0)^2}\left[\underset{(FS)}{(3.98 \times 1)^2} + \underset{(P00)}{(17.33 \times 0.4)^2} + \underset{(T00)}{(1.41 \times 2.3)^2} + \underset{(T2)}{(1.41 \times 2.3)^2}\right.$$

$$\left. + \underset{(PS05)}{(2.6 \times 0.35)^2} + \underset{(PS0)}{(6.0 \times 0.6)^2} + \underset{(PT05)}{(34.16 \quad 0.5)^2}\right]$$

$\Delta FNSD$ = 19.76 lbs, uncertainty = $\pm$5.28%

$$\left(\frac{\Delta WFED}{WFED}\right)^2 = \frac{1}{(572.4)^2}\left[\underset{(WF)}{(5.76 \times 0.9)^2} + \underset{(T_{FUEL})}{(0.31 \times 2.3)^2} + \underset{(PT05)}{(5.78 \times 0.5)^2}\right]$$

$\Delta WFED$ = 5.98 lbm/hr, uncertainty = $\pm$1.04%

$$\left(\frac{\Delta SFCD}{SFCD}\right)^2 = \frac{1}{(1.5303)^2}\left[\underset{(FS)}{(0.01661 \times 1)^2} + \underset{(P00)}{(0.06762 \times 0.4)^2} + \underset{(T00)}{(0.00595 \times 2.3)^2}\right.$$

$$+ \underset{(T2)}{(0.00558 \times 2.3)^2} + \underset{(PS05)}{(0.01085 \times 0.35)^2} + \underset{(PS0)}{(0.02401 \times 0.6)^2} + \underset{(PT05)}{(0.17098 \times 0.5)^2}$$

$$\left. + \underset{(WF)}{(0.01540 \times 0.9)^2} + \underset{(T_{FUEL})}{(0.00082 \times 2.3)^2}\right]$$

$\Delta SFCD$ = 0.09532 (lbm/hr)/lbf, uncertainty = $\pm$6.23%

PROJECT R41B-01A
PREPARED BY DEH
APPROVED BY WMS

MEASUREMENT UNCERTAINTY

SHEET NO. 1 OF 6

TESTING COMPLETED 6/24/74
TABLE COMPLETED 9/3/74
TABLE REVISED

Parameter Designation	STEADY-STATE ESTIMATED MEASUREMENT* Precision Index (S) Percent of Reading	Precision Index (S) Unit of Measurement	Precision Index (S) Degree of Freedom	Bias (B) Percent of Reading	Bias (B) Unit of Measurement	Uncertainty ±(B + t95S) Percent of Reading	Uncertainty ±(B + t95S) Unit of Measurement	Range	Type of Measuring Device	Type of Recording Device	Method of System Calibration
Venturi Inlet Static Pressure, Sta. 00, PS00	±0.10	----	31	±0.2	----	±0.4	----	1.7 to 32 psia	Bonded Strain-Gage-Type Pressure Transducers	Automatic Multiple Pressure Scanning System onto Sequential Sampling, Millivolt-to-Digital Converter, and Magnetic Tape Storage Data Acquisition System	In-Place Application of Multiple Pressure Levels Measured with a Pressure-Measuring Device Calibrated in the Standards Laboratory
Venturi Throat Static Pressure, Sta. 1N, PS1N	±0.22	----	31	±0.3	----	±0.75	----	0.75 to 30 psia			
Engine Inlet Plenum Static Pressure, Sta. 2P, PS2P	±0.1	----	3	±0.30	----	±0.6	----	0.8 to 1.0psia			
	±0.1	----	31	±0.25	----	±0.45	----	2 to 17 psia			
Bellmouth Total Pressure, Sta. 0.5, PT0.5	±0.10	----	31	±0.30	----	±0.50	----	0.8 to 17 psia			
Bellmouth Static Pressure, Sta. 0.5, PS0.5W	±0.1	----	3	±0.30	----	±0.6 Note 1	----	0.75 to 0.02 psia			
	±0.05	----	66	±0.25	----	±0.35 Note 2	----	2 to 7 psia			
	±0.15	----	31	±0.25	----	±0.55 Note 3	----	3 to 16 psia			
Low-Pressure Compressor Inlet Total Pressure, Sta. 2.2, PT2.2	±0.10	----	31	±0.30	----	±0.50	----	1 to 20 psia			
Low-Pressure Compressor Inlet Static Pressure, Sta. 2.2, PS2.2	±0.10	----	31	±0.30	----	±0.50	----	1 to 20 psia			
High-Pressure Compressor Discharge Total Pressure, Sta. 2.4, PT4.2	±0.1	----	31	±0.2	----	±0.4	----	4 to 80 psia			

*REFERENCE: Abernethy, R. B. and Thompson, J. W. Jr. "Handbook, Uncertainty in Gas Turbine Measurements." AEDC TR-73-5 (AD755356), February 1973.

NOTES:
1. Run 19 only.
2. Runs 8, 9, 10, 12, 13, 14, 16, 18 only.
3. Runs 4, 5, 17 only.
4. Runs 8, 9, 10, 12, 13, 14 only.
5. Runs 4, 5, 16, 17, 18 only.

PROJECT R41B-01A

PREPARED BY DEH

APPROVED BY WMS

MEASUREMENT UNCERTAINTY

SHEET NO. 2 OF 8

TESTING COMPLETED 8/24/74

TABLE COMPLETED 9/3/74

TABLE REVISED

Parameter Designation	STEADY-STATE ESTIMATED MEASUREMENT[a]							Range	Type of Measuring Device	Type of Recording Device	Method of System Calibration
	Precision Index (S)			Bias (B)		Uncertainty ±(B + t95S)					
	Percent of Reading	Unit of Measurement	Degree of Freedom	Percent of Reading	Unit of Measurement	Percent of Reading	Unit of Measurement				
High-Pressure Compressor Inlet Total Pressure, Sta. 2.4, PT2.4	±0.12	----	3	±0.2	----	±0.55 Note 1	----	2.7 to 5.7 psia	Bonded Strain-Gage-Type Pressure Transducers	Automatic Multiple Pressure Scanning System onto Sequential Sampling, Millivolt-to-Digital Converter, and Magnetic Tape Storage Data Acquisition System	In-Place Application of Multiple Pressure Levels Measured with a Pressure-Measuring Device Calibrated in the Standards Laboratory
	±0.10	----	31	±0.2	----	±0.4 Note 4	----	11 to 28 psia			
	----	±0.02 psi	31	----	±0.04 psi	----	±0.08 psi Note 5	9 to 20 psia			
	±0.10	----	31	±0.2	----	±0.4 Note 5	----	20 to 63 psia			
Primary Nozzle Inlet Total Pressure, Sta. 7, PT7	±0.1	----	31	±0.3	----	±0.5	----	1 to 19 psia			
Engine PT7 Probe Pressure, PT7E	±0.1	----	31	±0.3	----	±0.5	----	1 to 19 psia			
Primary Nozzle Discharge Static Pressure, Sta.8,PS8	±0.15	----	31	±0.25	----	±0.55	----	0.6 to 13 psia			
Fan Duct Inlet Static Pressure, Sta. 13, PS13	±0.15	----	31	±0.25	----	±0.55	----	0.9 to 17 psia			
Fan Duct Inlet Total Pressure, Sta. 13, PT13	±0.15	----	31	±0.25	----	±0.55	----	1.1 to 19 psia			
Fan Nozzle Inlet Total Pressure, Sta. 17, PT17	±0.12	----	31	±0.26	----	±0.5	----	1 to 19 psia			

[a]REFERENCE:

NOTES:

PROJECT R41B-01A
PREPARED BY DEN
APPROVED BY WMS

MEASUREMENT UNCERTAINTY

SHEET NO. 3 OF 5

TESTING COMPLETED 6/24/74
TABLE COMPLETED 9/3/74
TABLE REVISED

Parameter Designation	STEADY-STATE ESTIMATED MEASUREMENT* Precision Index (S) Percent of Reading	Precision Index (S) Unit of Measurement	Precision Index (S) Degree of Freedom	Bias (B) Percent of Reading	Bias (B) Unit of Measurement	Uncertainty ±(B + t95S) Percent of Reading	Uncertainty ±(B + t95S) Unit of Measurement	Range	Type of Measuring Device	Type of Recording Device	Method of System Calibration
Fan Nozzle Discharge Static Pressure, Sta. 18, PS18	±0.15	----	3	±0.40	----	±0.9 Note 1	----	0.5 to 0.9 psia	Bonded Strain-Gage-Type Pressure Transducers	Automatic Multiple Pressure Scanning System onto Sequential Sampling, Millivolt-to-Digital Converter, and Magnetic Tape Storage Data Acquisition System	In-Place Application of Multiple Pressure Levels Measured with a Pressure Measuring Device Calibrated in the Standards Laboratory
	±0.14	----	83	±0.28	----	±0.55 Note 4	----	1 to 3 psia			
	----	±0.005 psi	31	----	±0.01 psi	----	±0.02psi Note 5	1.6 to 5 psia			
	±0.10	----	31	±0.2	----	±0.4 Note 5	----	5 to 12 psia			
Altitude Ambient Static Pressure, PS0	±0.12	----	3	±0.35	----	±0.75 Note 1	----	0.5 to 0.9 psia			
	±0.18	----	83	±0.22	----	±0.6 Note 2	----	1.0 to 3 psia			
	----	±0.005 psi	31	----	±0.01 psi	----	±0.02psi Note 3	2 to 5 psia			
	±0.10	----	31	±0.2	----	±0.4 Note 3	----	5 to 12 psia			
High-Pressure Compressor Discharge Static Pressure, Sta.3, PS3	±0.10	----	31	±0.2	----	±0.4	----	7 to 160 psia		Sequential Sampling, Millivolt-to-Digital Converter, and Magnetic Tape Storage Data Acquisition System	Resistance Shunt Based on the Standards Laboratory Determination of Transducer Applied Pressure versus Resistance Shunt Equivalent Pressure Relationship
Venturi Inlet Total Temperature, Sta 00, T00	----	±0.25°F	100	----	±1.8°F	----	±2.3°F	-70 to 225°F	Copper-Constantan Temperature Transducers		Millivolt Substitution Based on the NBS Temperature versus Millivolt Tables
Engine Inlet Plenum Total Temperature, Sta 2P, T2P	----	±0.25°F	100	----	±1.8°F	----	±2.3°F	-22 to 206°F			
Low-Pressure Compressor, Inlet Total Temperature, Sta 2.2, T2.2	----	±0.25°F	100	----	±2.2°F	----	±2.7°F	50 to 260°F	Chromel-Alumel Temperature Transducers		

*REFERENCE:
NOTES:

PROJECT R41B-01A
PREPARED BY DEH
APPROVED BY WMS

MEASUREMENT UNCERTAINTY

SHEET NO. 4 OF 5

TESTING COMPLETED 6/24/74
TABLE COMPLETED 9/3/74
TABLE REVISED

Parameter Designation	STEADY-STATE ESTIMATED MEASUREMENT* Precision Index (S) Percent of Reading	Precision Index (S) Unit of Measurement	Precision Index (S) Degree of Freedom	Bias (B) Percent of Reading	Bias (B) Unit of Measurement	Uncertainty ±(B + t_{95}S) Percent of Reading	Uncertainty ±(B + t_{95}S) Unit of Measurement	Range	Type of Measuring Device	Type of Recording Device	Method of System Calibration
High-Pressure Compressor, Inlet Total Temperature, Sta. 2.4, T2.4	----	±0.25°F	100	----	±2.2°F	----	±2.7°F	115 to 500°F	Chromel-Alumel Temperature Transducers	Sequential Sampling, Millivolt-to-Digital Converter, and Magnetic Tape Storage Data Acquisition System	Millivolt Substitution Based on the NBS Temperature versus Millivolt Tables
High-Pressure Compressor Discharge Total Temperature, Sta 3, T3	----	±0.25°F	100	----	±2.2°F	----	±2.7°F	100 to 530°F			
	----	±0.25°F	100	±(0.25% + 0.9°F)		±(0.25% + 1.4°F)		530 to 800°F			
High-Pressure Turbine Discharge Total Temperature, Sta 4.2, T4.2	----	±0.25°F	100	----	±2.2°F	----	±2.7°F	140 to 530°F			
				±(0.25% + 0.9°F)		±(0.25% + 1.4°F)		530 to 1550°F			
Fan Nozzle Inlet Total Temperature, Sta 17, T17	----	±0.25°F	100	----	±2.2°F	----	±2.7°F	40 to 255°F			
Primary Nozzle Inlet Total Temperature, Sta. 7, T7	----	±0.25°F	100	±(0.25% + 0.9°F)		±(0.25% + 1.4°F)		620 to 1080°F			
Fan Duct Inlet Total Temperature, Sta. 13, T13	----	±0.25°F	100	----	±2.2°F	----	±2.7°F	40 to 255°F			
Fuel Temperature at Flowmeter, TFH,TFL	----	±0.25°F	100	----	±1.8°F	----	±2.3°F	55 to 90°F	Copper-Constantan Temperature Transducers		
Engine Fuel Flow Low-Range, WFL	±0.22	----	9	±0.53	----	±1.0	----	65 to 155 PPH	Turbine Volumetric Flow Transducers	Frequency-to-Voltage Converter onto Sequential Sampling, Millivolt-to-Digital Converter, and Magnetic Tape Storage Data Acquisition System	Frequency Substitution Based on the Standards Laboratory Determination of Transducer Water Volumetric Flow versus Frequency Output Relationship
	±0.28	----	100	±0.35	----	±0.9	----	280 to 910 PPH			
Engine Fuel Flow High-Range, WFH	±0.18	----	31	±0.22	----	±0.6	----	600 to 1830 PPH			

*REFERENCE:
NOTES:

PROJECT R41B-0[illegible]

PREPARED BY DEH JHB

APPROVED BY WMS

MEASUREMENT UNCERTAINTY

SHEET NO. 5 OF 5

TESTING COMPLETED 8/24/74

TABLE COMPLETED 9/3/74

TABLE REVISED

Parameter Designation	STEADY-STATE ESTIMATED MEASUREMENT* Precision Index (S) Percent of Reading	Precision Index (S) Unit of Measurement	Degree of Freedom	Bias (B) Percent of Reading	Bias (B) Unit of Measurement	Uncertainty ±(B + t95S) Percent of Reading	Uncertainty ±(B + t95S) Unit of Measurement	Range	Type of Measuring Device	Type of Recording Device	Method of System Calibration
Scale Force, FS	±0.13	----	31	±0.15	----	±0.4	----	-4600 to -1000 lbf	Bonded Strain-Gage-Type Force Transducers	Sequential Sampling, Millivolt-to-Digital Converter, and Magnetic Tape Storage Data Acquisition System	In-Place Application of Multiple Force Levels Measured with Force Transducers in the Standards Laboratory
	----	±1.3 lbf		----	±1.5 lbf	----	±4 lbf	-1000 to +1000 lbf			
	±0.13	----		±0.15	----	±0.4	----	1000 to 24001bf			
Low-Pressure Rotor Speed, NL	±0.1	----	31	±0.1	----	±0.3	----	9800 to 20,350 rpm	Electro-mechanical Transducers	Frequency-to-Voltage Converter onto Sequential Sampling, Millivolt-to-Digital Converter, and Magnetic Tape Storage Data Acquisition System	Frequency Substitution Based on the Transducer and Transducer-to-Engine Rotor Coupling Characteristics
High-Pressure Rotor Speed, NH	±0.1	----	31	±0.1	----	±0.3	----	22,500 to 29,650 fps			
Low-Pressure Compressor Inlet Guide Vane Angle, IGV	----	±0.01°	39	----	±0.3°	----	±0.3° Note 6	-10 to +30°	Rectilinear Potentiometer	Sequential Sampling, Millivolt-to-Digital Converter, and Magnetic Tape Storage Data Acquisition System	In-Place Measurement of Physical Dimensions versus Transducer Output
Low-Pressure Compressor 1st Stage Stator Angle	----	±0.01°	39	----	±0.1°	----	±0.1° Note 6	0 to 10°			
Low-Pressure Turbine Nozzle Area, A4.2	±0.03	----	39	±0.75	----	±0.8 Note 6	----	84 to 130%	Rotary Potentiometer		
Primary Exhaust Nozzle Area, A8	±0.02	----	39	±0.75	----	±0.8 Note 6	----	87.5 to 110.5 in^2			
Fan Exhaust Nozzle Area, A18	±0.03	----	39	±0.75	----	±0.8 Note 6	----	172 to 210 in^2			

*REFERENCE:

NOTES: 6. Uncertainty Estimate Based on Experience with Systems Similar to those Furnished by User.

ABBREVIATIONS AND SYMBOLS

PARTS I AND II

Engineering Symbol	Units	Description
A_N/A_{ND}	dimensionless	LP Turbine Nozzle Area Ratio, Actual/ Design Value
$A_{4.2}$	percent	LP Turbine Nozzle Area
$A_{E4.2}$	percent	Effective LP Turbine Nozzle Area
A_8	sq in.	Primary Exhaust-Nozzle Area
A_{E8}	sq in.	Primary Exhaust-Nozzle Effective Area
A_{18}	sq in.	Fan Exhaust-Nozzle Area
A_{E18}	sq in.	Bypass Exhaust-Nozzle Throat Effective Area
$A_{18.1...10}$	sq in.	Fan Nozzle Afterbody
Alt	feet	Pressure Altitude
BPR	dimensionless	Engine Bypass Ratio
C_{D8}	dimensionless	Primary Nozzle Flow Coefficient
C_{D18}	dimensionless	Bypass Nozzle Flow Coefficient
C_{f8}	dimensionless	Primary Nozzle Thrust Coefficient
C_{f18}	dimensionless	Bypass Nozzle Thrust Coefficient
F_{ram}	lbf	Ram Drag
$F_{g'}$	lbf	Ideal Gross Thrust
F_{g19}	lbf	Bypass Stream Gross Thrust
$F_{g19'}$	lbf	Bypass Stream Ideal Gross Thrust
F_n	lbf	Net Thrust in Pounds
F_n/W_1	lbf/lbm/sec	Engine Specific Thrust
F_g	lbf	Gross Thrust
HP_{ext}	horsepower	Customer HP Power Extraction
LHV	Btu/lbm	Fuel Lower Heating Value
M_n	dimensionless	Flight Mach Number
N_F	rpm	Fan Compressor Rotor Speed
$N_F/\sqrt{\theta_{t2}}/(N_F/\sqrt{\theta_{t2}})_{design}$	percent	Fan Rotor Speed Referred to Station 2
N_H	rpm	HP Rotor Speed

(Continued)

ABBREVIATIONS AND SYMBOLS (CONTD)

PARTS I AND II

Engineering Symbol	Units	Description
$N_H/\sqrt{\theta_{t2}}$	rpm	HP Rotor Speed Referred to Station 2
$N_H/\sqrt{\theta_{t2.4}}/(N_H/\sqrt{\theta_{t2.4}})_{design}$	percent	HPC Rotor Speed Referred to Station 2.4
$N_H/\sqrt{\theta_{t4}}/(N_H/\sqrt{\theta_{t4}})_{design}$	percent	HPT Rotor Speed Referred to Station 4
N_L	rpm	LP Rotor Speed
$N_L/\sqrt{\theta_{t2}}$	rpm	LP Rotor Speed Referred to Station 2
$N_L/\sqrt{\theta_{t2.2}}/(N_L/\sqrt{\theta_{t2.2}})_{design}$	percent	LPC Rotor Speed Referred to Station 2.2
$N_L/\sqrt{\theta_{t4.2}}/(N_L/\sqrt{\theta_{t4.2}})_{design}$	percent	LPT Rotor Speed Referred to Station 4.2
P_{amb}	lbf/in^2	Free-Stream Static Pressure
$P_{b2.2}$	lbf/in^2	LPC Discharge Bleed Flow Total Pressure
P_{b3}	lbf/in^2	HPC Discharge Bleed Flow Total Pressure
PLA	degree	Power Lever Angle
P_{S3}	lbf/in^2	Burner Plenum Static Pressure
P_{S3}/P_{t2}	dimensionless	Cycle Pressure Ratio
$P_{S18.1...10}$	lbf/in^2	Fan Nozzle Afterbody Static
P_{t1}	lbf/in^2	Engine Inlet Total Pressure
$P_{t2.3}/P_{t2.2}$	dimensionless	LPC pressure Ratio
$P_{t3}/P_{t2.4}$	dimensionless	HPC Pressure Ratio
$P_{t4}/P_{t4.1}$	dimensionless	HPT Expansion Ratio
$P_{t4.2}/P_{t5}$	dimensionless	LPT Expansion Ratio
P_{t7}	lbf/in^2	Primary Exhaust Flow Total Pressure
P_{t7}/P_{amb}	dimensionless	Primary Nozzle Pressure Ratio
P_{t7}/P_{t2}	dimensionless	Engine Pressure Ratio
P_{t13}/P_{t12}	dimensionless	Fan Tip Pressure Ratio
P_{t17}	lbf/in^2	Bypass Exhaust Flow Total Pressure
P_{t17}/P_{amb}	dimensionless	Bypass Nozzle Pressure Ratio
RNI	dimensionless	Engine Inlet Reynolds Number Index
SHP	horsepower	Shaft Power Extraction
T_{amb}	°R	Free-Stream Static Temperature Used in Computation of Flight Mach Number

(Continued)

ABBREVIATIONS AND SYMBOLS (CONTD)

PARTS I AND II

Engineering Symbol	Units	Description
TSFC	lbm/hr/lbf	Thrust Specific Fuel Consumption
T_{t1}	°R	Engine Inlet Total Temperature
T_{t4}	°R	HP Turbine Inlet Temperature
$T_{t4.2}$	°R	Cockpit Display Temperature (Interturbine Temperature)
T_{t7}	°R	Primary Exhaust Flow Total Temperature
T_{t17}	°R	Bypass Exhaust Flow Total Temperature
$T_{tb2.2}$	°R	LPC Discharge Bleed Flow Total Temperature
T_{tb3}	°R	HPC Discharge Bleed Flow Total Temperature
T_{to}	°R	Free-Stream Total Temperature
V_8	ft/sec	Primary Nozzle Exhaust Velocity
V_{18}	ft/sec	Bypass Nozzle Exhaust Velocity
V_{18}/V_8	dimensionless	Exhaust Velocity Ratio ($V_{bypass}/V_{primary}$)
W_1	lbm/sec	Total Engine Airflow
$W_1\sqrt{\theta_{t2}}/\delta_{t2}$	lbm/sec	Engine Total Airflow Referred to Station 2
W_2	lbm/sec	Engine Core Airflow
$W_{2.2}\sqrt{\theta_{t2.2}}/\delta_{t2.2}$	lbm/sec	LPC Airflow Referred to Station 2.2
$W_{2.4}\sqrt{\theta_{t2.4}}/\delta_{t2.4}$	lbm/sec	HPC Airflow Referred to Station 2.4
$W_4\sqrt{\theta_{t4}}/\delta_{t2.4}$	lbm/sec	HPT Gas Flow Referred to Station 4
$W_{4.2}\sqrt{\theta_{t4.2}}/\delta_{t4.2}$	lbm/sec	LPT Gas Flow Referred to Station 4.2
W_7	lbm/sec	Primary Exhaust Flow
W_{17}	lbm/sec	Bypass Exhaust Flow Rate
W_{24}	lbm/sec	HPC Inlet Flow Rate
W_{b3}	lbm/sec	HPC Discharge Bleed Flow Rate
$W_{b3}/W_{a2.2}$	dimensionless	HPC Bleed Flow Ratio
W_{b22}	lbm/sec	LPC Bleed Flow Rate
$W_{b22}/W_{a2.2}$	dimensionless	LPC Bleed Flow Ratio
W_{fe}	lbm/hr	Engine Fuel Flow Rate
W_{ft}	lbm/hr	Total Fuel Flow Rate
W_{fe}/P_{s3}	lbm/hr/lbf/in^2	Fuel Control Parameter

ABBREVIATIONS AND SYMBOLS (CONCLUDED)

PARTS I AND II

Engineering Symbol	Units	Description
$\beta_{B.T.}$	degrees	Boat-Tail Angle
$\beta_{1ST\ STG}$	degrees	LPC First-Stage Stator
β_{IGV}	degrees	LPC Inlet Guide Vane
ΔT_{amb}	°F	Ambient Temperature Minus Standard Atmospheric Pressure
η_{ram}	dimensionless	Inlet Ram Recovery

ABBREVIATIONS

Fan	Fan Compressor
HPC	High Pressure Compressor
HPT	High Pressure Turbine
LPC	Low Pressure Compressor
LPT	Low Pressure Turbine

$$\left\{\left[\frac{W\sqrt{\theta_t}/\delta_t}{(P_t/P_t)}\ \text{Operating point} \Big/ \frac{W\sqrt{\theta_t}/\delta_t}{(P_t/P_t)}\ \text{Surge point}\right] - 1\right\} \times 100 \quad \text{at constant referred speed}$$

Surge margin is computed for each compressor using the appropriate flows and pressure ratios.

ABBREVIATIONS AND SYMBOLS

PART III

Engineering Symbol	Units	Description
A42	percent	LP Turbine Nozzle Area
A8	sq in.	Primary Exhaust Nozzle Area
A8E	sq in.	Projected Flow Area at Nozzle (Plug) Exit
A18	sq in.	Fan Exhaust Nozzle Area
A18E	sq in.	Projected Flow Area at Fan Plug Exit
A1N	sq in.	Venturi Throat Area
A1ODC	sq in.	Effective Area of Labyrinth Air Seal
AE4	sq in.	Effective Area of Station 4
AEBLP	sq in.	Effective Area of Bleed Valve
ALTD	feet	Pressure Altitude
CD6	dimensionless	Primary Nozzle Flow Coefficient
CD18	dimensionless	Bypass/Fan Nozzle Flow Coefficient
CF1N	dimensionless	Venturi Flow Coefficient
CFG8	dimensionless	Primary Nozzle Thrust Coefficient
CFG18	dimensionless	Fan Nozzle Thrust Coefficient
CFGT18	dimensionless	Fan Nozzle Throat Thrust Coefficient
CFPLUG	dimensionless	Fan Plug Thrust Coefficient
CP	Btu/lbm/°F	Specific Heat at Constant Pressure
CS8	dimensionless	Primary Nozzle Vacuum Thrust Coefficient
CS18	dimensionless	Fan Nozzle Vacuum Thrust Coefficient
DELPB	decimal percent	Pressure Drop (at LP Bleed Valve)
DP	decimal percent	Pressure Drop (at Indicated Station)
DHWOC	Btu/sec	Energy Removed from Engine Oil by Auxiliary Water-Oil Heat Exchanger
ERAM	dimensionless	Ram Recovery
ETABX	percent	Combustor Efficiency
ETAFAN	percent	Overall Fan Adiabatic Efficiency
ETAHPC	percent	HP Compressor Adiabatic Efficiency

ABBREVIATIONS AND SYMBOLS (CONTD)

PART III

Engineering Symbol	Units	Description
ETAHPT	percent	HP Turbine Efficiency
ETAHUB	percent	Fan Hub Adiabatic Efficiency
ETALPC	percent	LP Compressor Adiabatic Efficiency
ETALPT	percent	LP Turbine Efficiency
ETATIP	percent	Fan Tip Adiabatic Efficiency
FG	lbf	Gross Thrust
FGCN18	lbf	Bypass/Fan Stream Gross Thrust
FGISEN	lbf	Ideal Gross Thrust
FGISEN18	lbf	Bypass/Fan Stream Ideal Gross Thrust
FN	lbf	Net Thrust
FNSQWA2	lbf/lbm/sec	Engine Specific Thrust
FS	lbf	Measured Scale Force
H	Btu/lbm	Enthalpy (at Indicated Station)
LHV	Btu/lbm	Lower Heating Value of Fuel
M1N	dimensionless	Venturi Throat Mach Number
M	dimensionless	Mach Number (at Station Indicated)
NF	rpm	Fan Compressor Rotor Speed
NFK2	rpm	Fan Rotor Speed Referred to Station 2
NH	rpm	HP Rotor Speed
NHK2	rpm	HP Rotor Speed Referred to Station 2
NHK4	rpm	HPT Rotor Speed Referred to Station 4
NHK24	rpm	HPC Rotor Speed Referred to Station 2.4
NL	rpm	LP Rotor Speed
NLK2	rpm	LP Rotor Speed Referred to Station 2
NLK22	rpm	LPC Rotor Speed Referred to Station 2.2
NLK42	rpm	LPT Rotor Speed Referred to Station 4.2
P2	lbf/in^2	Engine Inlet Total Pressure
P22	lbf/in^2	LP Compressor Inlet Total Pressure

ABBREVIATIONS AND SYMBOLS (CONTD)

PART III

Engineering Symbol	Units	Description
P23X	lbf/in^2	LP Compressor Discharge Total Pressure
P23XQ22	dimensionless	LP Compressor Pressure Ratio
P24	lbf/in^2	HP Compressor Inlet Total Pressure
P3X	lbf/in^2	HP Compressor Discharge Total Pressure
P3XQ24	dimensionless	HP Compressor Pressure Ratio
P4X	lbf/in^2	HP Turbine Inlet Total Pressure
P41X	lbf/in^2	HP Turbine Discharge Total Pressure
P4XQ41X	dimensionless	HP Turbine Expansion Ratio
P42	lbf/in^2	LP Turbine Inlet Total Pressure
P5X	lbf/in^2	LP Turbine Discharge Total Pressure
P42Q5X	dimensionless	LP Turbine Expansion Ratio
P7	lbf/in^2	Primary Exhaust Flow Total Pressure
P7QPSO	dimensionless	Primary Nozzle Pressure Ratio
P7Q2	dimensionless	Engine Pressure Ratio
P13	lbf/in^2	Fan Duct Inlet Total Pressure
P13Q2	dimensionless	Fan Tip Pressure Ratio
P17	lbf/in^2	Bypass/Fan Nozzle Inlet Total Pressure
P17QPSO	dimensionless	Bypass/Fan Nozzle Pressure Ratio
PBLP	lbf/in^2	LP Bleed Pressure
PSO	lbf/in^2	Free-Stream Static Pressure
PS1N	lbf/in^2	Venturi Throat Wall Static Pressure
PS22	lbf/in^2	LP Compressor Inlet Wall Static
PS3	lbf/in^2	Burner Plenum Static Pressure
PS3QP2	dimensionless	Cycle Pressure Ratio
PS8E	lbf/in^2	Static Pressure at Nozzle (Plug) Exit
PS18T	lbf/in^2	Static Pressure at Fan Nozzle Throat
R	ft-lbf/lbm °R	Gas Constant
RR	dimensionless	Thermocouple Recovery Ratio

ABBREVIATIONS AND SYMBOLS (CONTD)

PART III

Engineering Symbol	Units	Description
RE1N	dimensionless	Venturi Throat Reynolds Number
REI2	dimensionless	Engine Inlet Reynolds Number Index
TAMD	°R	Free-Stream Static Temperature Used in Computation of Flight Mach Number
T00	°R	Venturi Inlet Total Temperature
T2	°R	Engine Inlet Total Temperature
T22	°R	LP Compressor Inlet Total Temperature
T24	°R	HP Compressor Inlet Total Temperature
T3	°R	HP Compressor Discharge Total Temperature
T4X	°R	HP Turbine Inlet Temperature
T4X7W	°R	HP Turbine Inlet Temperature (Based on Measured T7 and Energy Balance Between Compressors and Turbines)
T42R	°R	Measured Interturbine Temperature (average)
T7	°R	Primary Exhaust Flow Total Temperature
T13	°R	Fan Duct Inlet Total Temperature
T17	°R	Bypass/Fan Exhaust Flow Total Temperature
TO	°R	Free-Stream Total Temperature
TF	°R	Temperature of Fuel
TWOCI	°R	Auxiliary Oil Cooler Water Inlet Temperature
TWOCD	°R	Auxiliary Oil Cooler Water Discharge Temperature
VO	ft/sec	Free-Stream Velocity
V1	ft/sec	Inlet Duct Velocity
V8	ft/sec	Primary Nozzle Exhaust Velocity
V8ISEN	ft/sec	Isentropic Velocity for Full Expansion of Primary Stream to Ambient Pressure
V18	ft/sec	Bypass/Fan Nozzle Exhaust Velocity
V18ISEN	ft/sec	Isentropic Velocity for Full Expansion of Fan Nozzle Stream to Ambient Pressure
V18QV8	dimensionless	Exhaust Velocity Ratio ($V_{bypass}/V_{primary}$)

ABBREVIATIONS AND SYMBOLS (CONTD)

PART III

Engineering Symbol	Units	Description
WA1M	lbm/sec	Venturi Airflow
WA2	lbm/sec	Total Engine Airflow
WA2K2	lbm/sec	Engine Total Airflow Referred to Station 2
WA22	lbm/sec	Engine Core Airflow
WA22K22	lbm/sec	LPC Airflow Referred to Station 2.2
WA24	lbm/sec	HPC Inlet Airflow
WA24K24	lbm/sec	HPC Airflow Referred to Station 2.4
WA3	lbm/sec	HPC Exit Airflow
WA18	lbm/sec	Fan Exhaust Flow Rate
WBLP	lbm/sec	LP Compressor Bleed Flow Rate
WFE	lbm/hr	Engine Fuel Flow Rate
WFEQPS3	$lbm/hr/lbf/in^2$	Fuel Control Parameter
WG4	lbm/sec	HPT Inlet Gas Flow
WG4K4	lbm/sec	HPT Gas Flow Referred to Station 4
WG42	lbm/sec	LPT Inlet Gas Flow
WG42K42	lbm/sec	LPT Gas Flow Referred to Station 4.2
WG7	lbm/sec	Primary Exhaust Flow
WL1	lbm/sec	LPC Leakage Overboard Airflow
WTC1	lbm/sec	LP Turbine Inlet Cooling Airflow
WTC2	lbm/sec	LP Turbine Discharge Cooling Airflow

ABBREVIATIONS AND SYMBOLS (CONCLUDED)

PART III

Engineering Symbol	Description
γ	Ratio of Specific Heats
η	Component Efficiency
ηDES	Component Design Efficiency
ηREF	"Reference Efficiency"--A parameter used to indicate relative efficiency differences rather than absolute levels, in decimal units; for example, if ηREF = 0.85, ηREF -0.01 = 0.84.
ηREL	"Relative Efficiency"--A parameter used to denote a component efficiency relative to the design efficiency in decimal units, or, when indicated, as a percent; for example, when η = 0.85 and ηDES = 0.90, ηREL = 0.95.

NOTES:

The use of an "S" following the thrust symbol on the plots appearing in Part III indicates that the thrust presented was based on the measured scale force.

The use of a "D" following any symbol on the plots appearing in Part III indicates that the parameter has been referred to the desired flight condition.

LP Compressor Surge Margin

$$\left\{\left[\frac{(WA22K22/P23XQ22)\ \text{OPERATING}}{(WA22K22/P23XQ22)\ \text{SURGE}}\right] - 1\right\} \begin{matrix} \text{X100} \\ \text{NLK22} = \text{CONSTANT} \end{matrix}$$

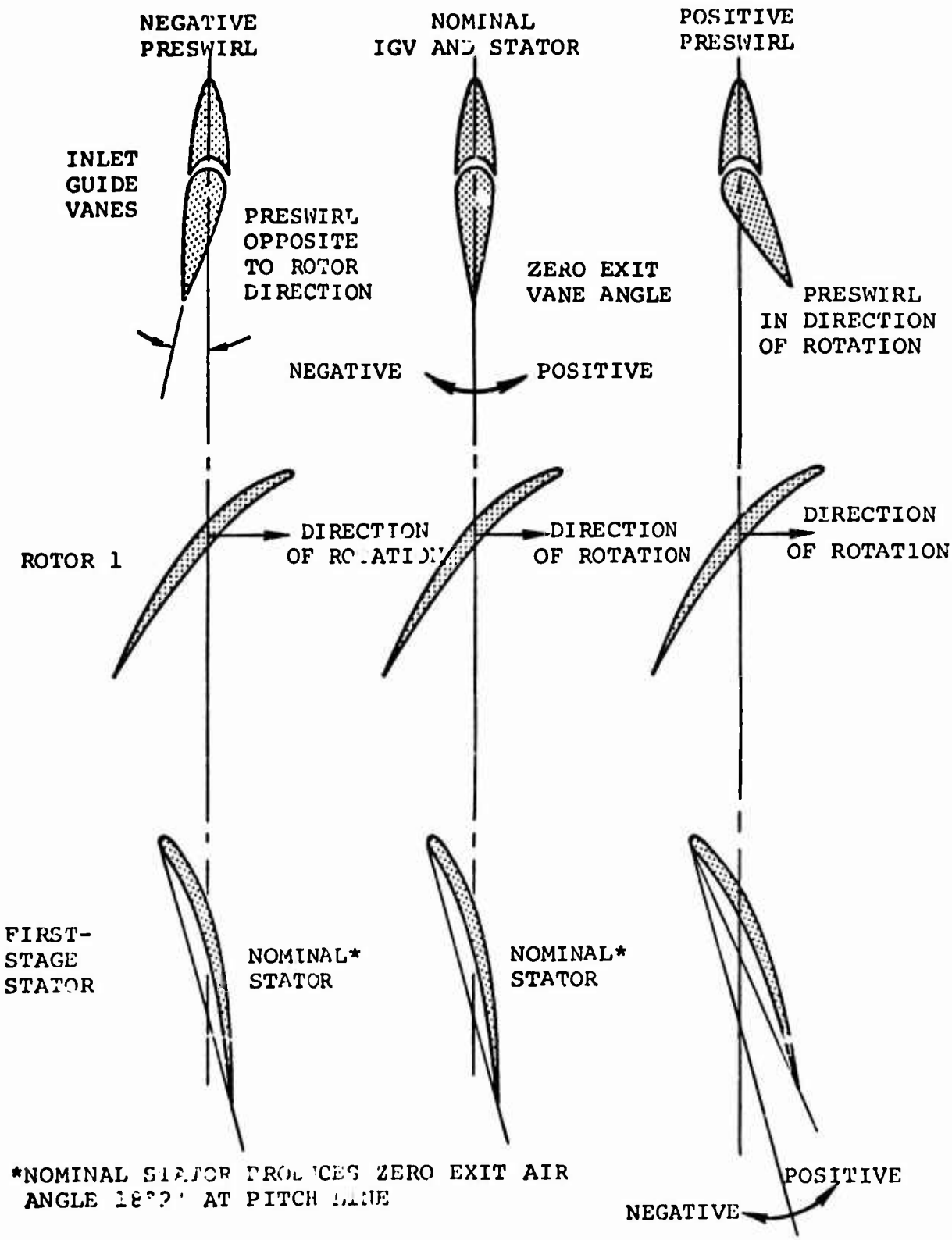

Figure 699. Variable IGV and Stator Sign Convention Diagram.